Contents:

Preview

Bis-phenols are well known for their host-guest chemistry. *Bis*-phenolic compounds have hydroxy groups prone towards the formation of host-guest assemblies through hydrogen bonds. Various hydrogen bonded motifs such as dimer, cyclic-oligomer and linear polymeric chain are formed through self-assemblies of *bis*-phenols which are guided by strong and directional O-H···O interactions. Apart from the strong O-H···O interactions, weak interactions such as C-H···O, C-H···π, π -π, O-H···π interactions also play vital role in the assembling of *bis*-phenols. Thus, *bis*-phenols are useful to construct various supramolecular architectures. There is a necessity to systematically study and identify the role of weak interactions in various host-guest systems of *bis*-phenols. This thesis narrates the host-guest chemistry of imidazole, fluoro-benzene and dimethylaminobenzene containing *bis*-phenols as well as the coordination chemistry of functionalized *bis*-phenols to dicaroxylic acids through functionalization of the hydroxy groups. While doing so various desolvates, polymorphs and coordination complexes were prepared and characterised. There are six chapters in the thesis based on the results on the analysis of the experimental observations obtained during the reseach period.

Chapter 1: Introduction

A general introduction to *bis*-phenols and some related V-shaped molecules are brought forward in this chapter. This includes a brief discussion on the structural features and inclusion properties of *bis*-phenols and other V-shaped molecules. This chapter also features discussions on several *bis*-phenol based macromolecular architectures and their preferential binding to different guest. The polymorphism in *bis*-phenols and their related compounds are narrated. The pharmaceutical applications of some *bis*-phenol derivatives are also discussed. Various coordination complexes derived from *bis*-phenols and functionalized *bis*-phenols are also included. The catalytic activities of metal complexes derived from *bis*-phenols towards various organic reactions are included in this chapter.

Chapter 2: Quasi-isostructural solvates of *bis*(4-hydroxy-3,5-dimethylphenyl)(4-N,N-dimethylaminophenyl)methane

This chapter deals with the structural studies on solvates of *bis*(4-hydroxy-3,5-dimethylphenyl)(4-N,N-dimethylaminophenyl)methane **(Ambp, 2.1).** A series of solvates illustrated in Scheme **1** were structurally characterised.

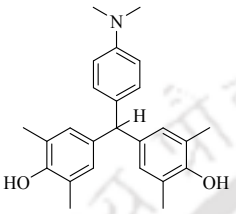

Ambp (2.1)

Solvent (S)

x **Ambp**. yS. zH_2O

x= y=1, z=0 for **2.2-2.6**, **2.9**

x= y=2, z=3 for **2.7**

x= y= z=1 for **2.8**

Scheme 1: Formation of different solvates of **Ambp (2.1)**.

The solvates **2.2-2.5** are isostructural and belongs to space group $P2_1/c$. From the structural study it is seen that solvate **2.2-2.6** form chain-like structures through O-H···O interactions. The O-H···O distances in these solvates are comparable except for the dimethylacetamide solvate **(2.4)**. Based on the similarities observed among the hydrogen bonded motifs, three different types of H-bonded motifs between the solvent molecules and the host *bis*-phenol **2.1** were identified. They are namely, the motifs having **(a)** single point contact of solvent molecules to the bridging O-H···O unit with additional weak interactions, or **(b)** single point contact of the solvent molecules forming $R_2^2(6)$ type hydrogen-bonded motifs or **(c)** two point contact leading to $R_3^3(7)$ type hydrogen bonded motifs. The donor-acceptor distances in **2.2** (Acetone solvate) and **2.3** (DMSO solvate) are similar and the structures belong to the first type; whereas the solvates **2.5** (Morpholine solvate) and **2.6** (Piperidine solvate) have similar structures which belong to the third type. The dimethylacetamide solvate **2.4** possesses the second type of structure.

The solvates **2.2-2.5** are isostructural with similar arrangements of the host molecules in their respective unit cells, and the solvent molecules are located in the channels running along the [010] direction formed by the molecular framework of the host

Ambp as shown in the Figure **1a**. Although the piperidine solvate (**2.6)** have a similar unit cell parameters with that of the solvates **2.2-2.6**; it has a different structure and

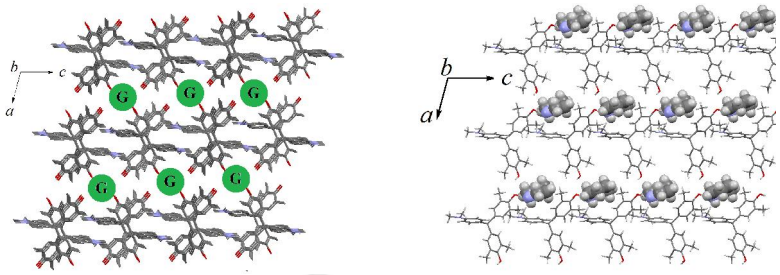

(a) **(b)**

Figure 1: (a) Packing of the solvates **2.2-2.5** showing the guest inclusion in the channels, **(b)** 2D net formation by the **Ambp** molecules in the solvate **2.6**.

it forms 2D net through O-H···O interactions and the piperidine molecules attached to the net through O-H···N, C-H···O and N-H···π interactions (Figure **1b**). The disruption of the O-H···O interactions between the host molecules occurs in the structure of the DABCO solvate **(2.7)** and dioxane solvate **(2.8)**.

Chapter 3: Polymorphs, solvates, polymorphs of solvate and Cs^+-π interactions of fluorine-substituted *bis*-phenols

In this chapter the self-assemblies of 4-[(2-fluorophenyl)(4-hydroxy-3,5-dimethylphenyl)methyl]-2,6-dimethylphenol (*bis*-phenol **3.1**) and 2-[(2-fluorophenyl)(2-hydroxy-3,5-dimethylphenyl)methyl]-4,6-dimethylphenol (*bis*-phenol **3.2**) leading to different polymorphs and polymorphs of solvate as well as cation-π interactions are discussed.

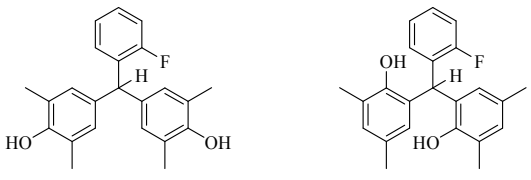

Bis-phenol **3.1** *Bis*-phenol **3.2**

Figure 2: Structures of *bis*-phenol **3.1** and *bis*-phenol **3.2**.

We observed two polymorphs of *bis*-phenol **3.1**, namely, **3.1a** having porous structure (Figure **3**) and another **3.1b** having non-porous structure. The porous form transforms to the non porous form on heating. The packing pattern of the two polymorphs are distinguished by O-H···O and C-H···F-C interactions. The porous polymorph **3.1a** and dimethylformamide solvate **(3.1c)** of *bis*-phenol **3.1** converted to the non porous polymorphic form on heating upto 140°C. All the thermal conversions were established by PXRD.

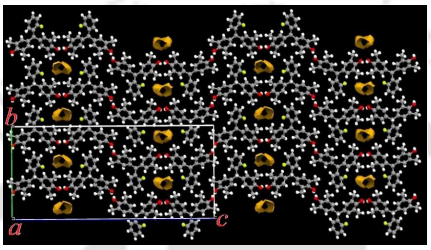

Figure 3: Packing of the porous polymorph **3.1a.**

In case of the *bis*-phenol **3.2** we did not obtained polymorphs. However, it forms two DMSO solvates with diffenet host-guest ratios under two diffenet conditions. At room temperature it forms 1:0.5 solvate **(3.2b)**, whereas at high temperature it forms 1:1 DMSO solvate **(3.2c)** (Scheme **2**).

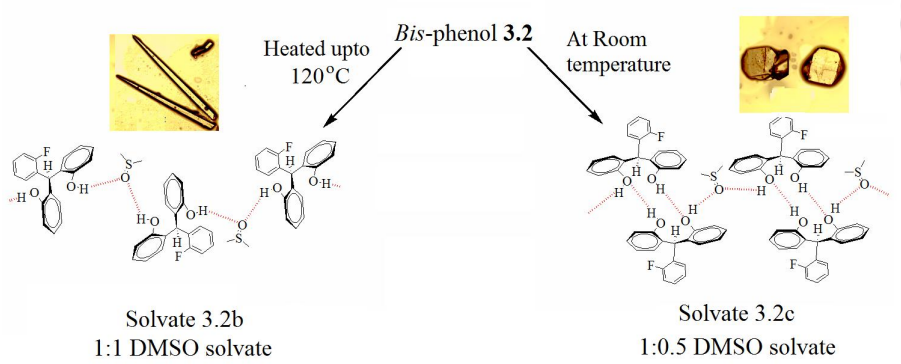

Scheme 2: Formation of DMSO solvates of different host-guest ratios under two different conditions.

The *bis*-phenol **3.2** forms two concomitant dioxane solvates with same host-guest ratios. One of the dioxane solvate has sheet-like structure (**3.2d**), whereas the other

has 3D cahnnel structure **(3.2e)**. The O-H···O interactions are similar in the two polymorphs of dioxane solvate. But, the diffenece between them arises due to the difference in C-H···F-C and C-H···π interactions. The *bis*-phenol **3.2** forms a one dimensonal coordination polymer **3.2f** with caesium cation in which intersting η^2- and η^4-type of cation-π interactions are oberved. The cation-π interactions are evident in the ^{1}H-NMR spectra of the caesium complex. The structures are discussed to show the desolvation process and the role of the fluoro-group in self-assemblies of these molecules.

Chapter 4: Polymorphs, solvates and anion assisted assemblies of imidazole based *bis*-phenols

This chapter deals with the polymorphs, solvates and anion assisted assemblies of two imidazole based *bis*-phenols, 4-[(4-hydroxy-3,5-dimethylphenyl)(5-methyl-1H-imidazol-4-yl)methyl]-2,6-dimethylphenol (**4.1**) and 2-((2-Hydroxy-3,5-dimethylphenyl)(imidazol-4-yl)methyl)-4,6-dimethylphenol (**4.2**).

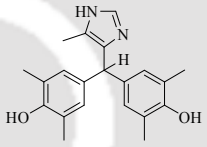

***Bis*-phenol 4.1**

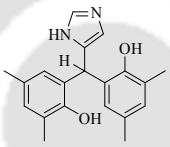

***Bis*-phenol 4.2**

Figure 4: Structures of *bis*-phenols **4.1** and *bis*-phenol **4.2**.

The crystallization of **4.1** from a methanolic solution led to the formation two concomitant polymorphs, namely, polymorph **4.1a** and polymorph **4.1b.** The *bis*-phenol also forms 1:0.5 solvate with acetone and 1:1 monohydrated solvates with DMSO (Scheme **3**).

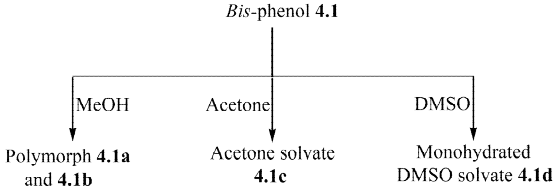

Scheme 3: Formation of polymorphs and solvates of *bis*-phenol **4.1**.

The polymorph **41.b** has a porous structure that contains voids with a radius of 1.2 Å running parallel to the crystallographic [010] plane (Figure **5a**) and it is confirmed by nitrogen adsorption-desorption experiment (Figure **5b**). The acetone solvate **4.1c** of *bis*-phenol **4.1** is isostructural with the porous polymorph **4.1b**. The polymorph **4.1b** reverssibily adsorbs acetone solvents and it is established with PXRD.

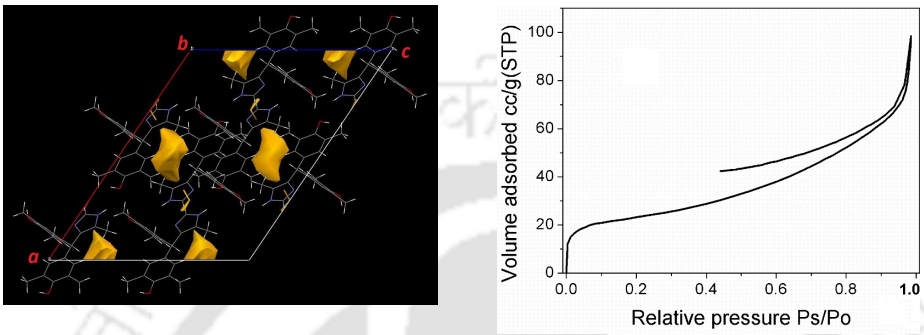

(a) **(b)**

Figure 5: (a) Packing of the porous polymorph **4.1b** showing the voids, **(b)** Nitrogen adsorption-desorption isotherm of polymorph **4.1b**.

On the other hand, we did not observe any polymorph of the *bis*-phenol **4.2**. However, we were able to obtain unsolvated and one methanol solvate of the *bis*-phenol **4.2**. The *bis*-phenol **4.2** forms crystalline salts with varius organic acids and inorganic acids. For example, treatment of *bis*-phenol **4.2** with sulphuric acid forms 1:0.5 salt where one of the hydroxy group of *bis*-phenol **4.2** involves in $R_3^3(6)$-type of cyclic

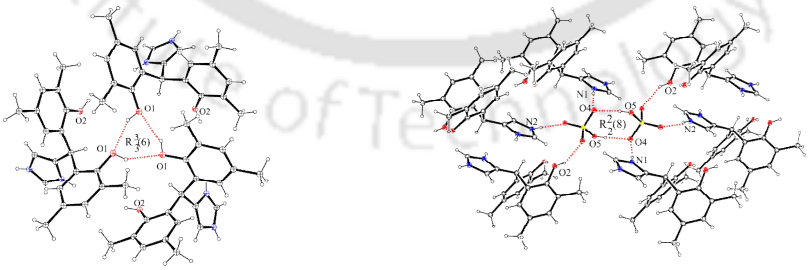

(a) **(b)**

Figure 6: (a) $R_3^3(6)$ type of cyclic hydrogen bonding in sulphate salt of *bis*-phenol **4.2**, **(b)** $R_2^2(8)$ type of cyclic hydrogen bonding in bisulpahte salt of the *bis*-phenol **4.2.**

hydrogen bond to form trimeric assembly (Figure **6a**). On the other hand treatment of *bis*-phenol **4.2** with sulphuric acid in presence of $MgSO_4$ forms 1:1 bisulphate salt (Figure **6b**). Similarly, the *bis*-phenol **4.2** also forms 1:1 salt with perchlorate and nitrate anions; and 1:1 monohydrated salt with tetrafluoroborate ion. In this chapter the role of the imidazole in guiding various anions assisted assemblies and mainly some of the important features on desolvation could be revealed.

Chapter 5: Alkali metal complexes of *bis*-phenol based flexible dicarboxylic acids

This chapter deals with the synthesis of sodium, potassium and caesium complexes of V-shaped flexible dicarbxylic acids H_2L^1 **(5.1)**, H_2L^2 **(5.2)**, H_2L^3 **(5.3)** and H_2L^4 **(5.4)** derived form *bis*-phenol (Figure **6**).

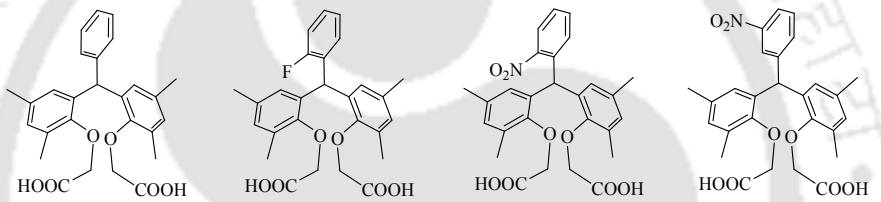

H_2L^1(5.1) H_2L^2(5.2) H_2L^3 (5.3) H_2L^4(5.4)

Figure 7: Structures of the ligands used.

The reaction of H_2L^1 with sodium acetate (or sodium hydroxide) and potassium acetate (or potassium hydroxide) at ambient condition result in the formation of disodium salt $\{[Na_2L^1(\mu\text{-}H_2O)(H_2O)_3].H_2O\}_n$ **(5.1c)** and $[K_4(L^1)_2(\mu\text{-}H_2O)_2(H_2O)_2](H_2O)_n$ **(5.1d)** respectively**,** whereas a similar reaction caesium acetate (or caesium carbonate) lead to mono deprotonated salt $[Cs(HL^1)(\mu\text{-}H_2O)(H_2O)]_n$ **(5.1e)**. We were able to crystallize the complexes **5.1c**, **5.1d** and **5.1e** and determined their crystal structures. In case of the ligand H_2L^2 we obtained single crystal of sodium complex $[\{Na_2L^2(\mu\text{-}H_2O)(H_2O)_3\}.H_2O]_n$. (**5.2c**) and caesium complex $[\{(H_2O)Cs(\mu\text{-}H_2O)_2(\mu\text{-}L^2)Cs(H_2O)_2\}]_n$ (**5.2d**). But we did not obtained any single crystal of the potassium salt of the ligand H_2L^2 (**5.2).** The interesting feature of the coordination polymer **5.2d** is the presence of Cs···F-C coordination bond. In case of the ligand H_2L^3 **(5.3)**, we did not obtain suitable single crystal of the sodium and caesium complex. However, we

obtained single crystals of the potassium salt (**5.3c**) of the ligand **5.3** having compositions $[K_2L^3(H_2O)]_n$ and it is a two dimensional (2D) coordination polymer. In the coordination polymer **5.3c**, the nitro group at the ortho position coodinates to two potassium ions (Figure **8**). We did not obtain any alkali metal complex using the ligand H_2L^4 **(5.4)**.

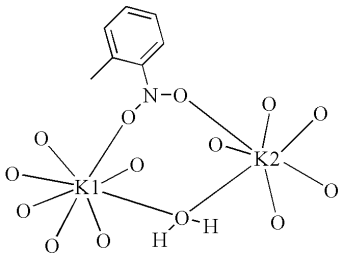

Figure 8: The bridging two potassium ions by nitro group in complex **5.3c**.

In this chapter the coordination effect of nitro group and fluoro group to change the composition and the coordination modes in alkali metal ions are being shown.

Chapter 6: Synthesis of Cadmium (II) and Mercury (II) metallacycles using *bis*-phenol based dicarboxylic acids:

In this chapter we have used the same ligands used in the chapter 5 to prepare cadmium and mercury complexes.

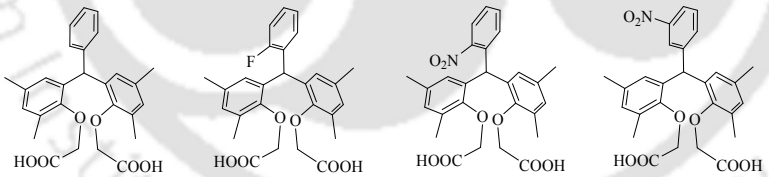

H_2L^1(5.1) H_2L^2(5.2) H_2L^3 (5.3) H_2L^4(5.4)

Figure 9: Structures of the ligands used.

An interesting structural variation from the one dimensional coordination polymer to mononuclear complex or metallacycle were observed depending upon the ligands and solvents used in the reactions. The ligand H_2L^1 forms 1D coordination polymer $[CdL^1(py)_3]n{\cdot}3nH_2O$ **(6.1a)** with cadmium in methanol solvent. The ligand H_2L^2 (**5.2**) either formed mononuclear complex $[CdL^2(py)_2H_2O]$ (**6.2a**), dinuclear complex $[CdL^2(py)(DMSO)]_2$ (**6.2b**) or metallacycle $\{[Cd(py)_2H_2O].(py).CH_3OH\}$ (**6.2c**)

depending on the solvent used in the reaction. On the other hand, ligand H_2L^3 (**5.3**) forms dinuclear complex $[CdL^3(py)(CH_3OH)]_2 \cdot CH_3OH$ (**6.3a**) and metallacycle $\{[CdL^3(py)_2(H_2O)]_2 \cdot H_2O\}$ (**6.3b**) when the reaction was carried out in methanol and dimethylformamide respectively. The ligand H_2L^4 **(5.4)** formed a metallacycle $[CdL^4(py)_2(H_2O)]_2 \cdot 3H_2O$ **(6.4a)** in dimethylformamide solvent. The whole results are summerised in the scheme **4**.

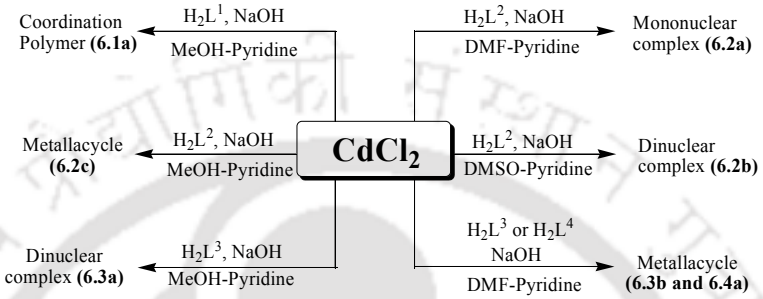

Scheme 4: Formation of various coordination complexes of cadmium with H_2L^1, H_2L^2, H_2L^3 and H_2L^4 in different solvents.

The metallacycle **6.2c** formed in MeOH-pyridine converts to dinuclear complex **6.2b** in presence of DMSO. Similarly, the dinuclear complex **6.3a** formed in methanol-pyridine solvent converts to the metallacyle **6.3b** in presence of dimethylformamide and pyridine (Scheme **5**).

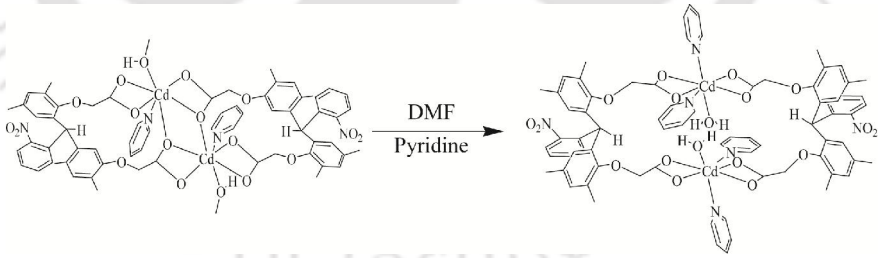

Scheme 5: Coversion of dinuclear complex **6.3a** to the metallacycle **6.3b** in DMF and pyridine mixture.

The coordination chemistry of cadmium complexes with V-shaped flexible dicarboxylic acids have been discussed here. The role of solvent as well as substituent in prepartion of specific compounds and conversion between dinuclear Cd_2O_2 core to macrocyclic compounds have been established.

CHAPTER 6

Synthesis of Cadmium (II) and Mercury (II) metallacycles using *bis*-phenol based dicarboxylic acids

There is a growing trend of using flexible ligands for the construction of coordination polymers with intriguing network structures.[1] V-shaped molecules with carboxylic acid functionality at the two ends are most appealing for the construction of various metal-organic frameworks because of two different metal binding sites with a large spacer.[2] The use of a flexible or less-rigid spacer for the construction of a coordination complex has an added advantage as they have many degrees of freedom and a few conformational restraints, which can give various topologies. These types of conformational flexible ligands give unique opportunities to construct novel structures with desirable characteristics. Complicacy in predicting the architecture of the coordination complexes derived from these types of flexible ligands arises due to different coordination modes of carboxylate ligands, which are further complicated by

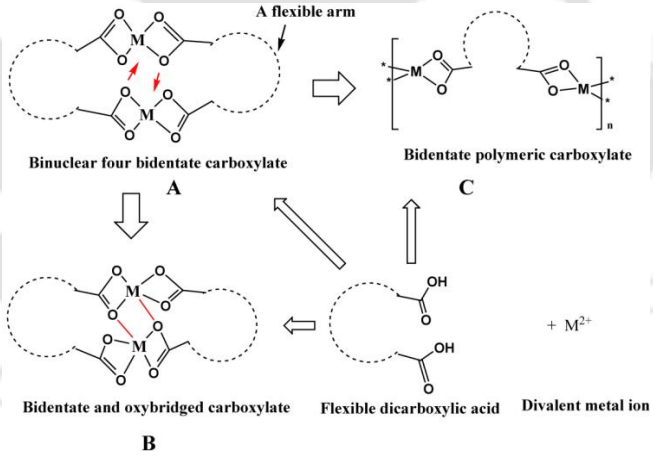

Scheme 6.1: Formation of metallacycle **(A)** (red arrows show the possible path for metallacycle converted to dinuclear complex); Dinuclear complex **(B)**; linear coordination polymer **(C)** from flexible V-shaped ligand.

factors such as the variation of crystallization conditions. However, one may simplify this by restricting to one, or two binding modes of carboxylates[3] leading to a coordination polymer, metallacycle and dinuclear complex, as shown in Scheme **6.1.**

The metallacycle 'A' may be coverted to form the dinuclear complex 'B' on slight change in reaction conditions. It was earlier shown that cadmium mononuclear complex can self assembles to form polymeric structure.[4] These polymers were characterized crystallographically and the existance of the mononuclear units were established by mass spectroscopy. On the other hand, solvent is one of the important factors which often influences the coordination behavior of the metal ions.[5] Solvents can coordinate to metal or it may influences the overall frameworks of the coordination complex without participating in coordination. There are many examples where the coordination complexes of carboxylic acids transform to different forms on changing the solvents.[6]

Moreover, d^{10} metal ions containing dicarboxylate coordination polymers, those with cadmium[7] or mercury[8] ions are especially of great importance. The cadmium dicarboxylate polymers show interesting optical properties[7] and mercury dicarboxylates have medical applications,[9] such as their role in the treatment of renal failure. In addition to these, dicarboxylic acids in ionic liquids bind mercury ions and have the property to absorb gases.[10] The mercury can have relatively stable variable valences[11] and can be easily functionalised to organometallics. Moreover, cadmium[12a,b] and mercury[12c,d] compounds are hazardous, thus their extraction would depend upon the binding ability with various lignds.

In chapter **5** we have seeen that *bis*-phenol based dicarboxylic acid lignds **5.1** (H_2L^1), **5.2** (H_2L^2), **5.3** (H_2L^3) and **5.4** (H_2L^4) can coordinate to alkali metal to give metal complexes of various dimensions. In this chapter we discuss the synthesis and characterization of some cadmium and mercury complexes of these ligands (Figure **6.1**). Flexibility associated with $-CH_2COOH$ parts and the shape and rigidity associated with the *bis*-phenol part makes this class of ligands unique, as cyclic structures may be anticipated when these ligands are attached to appropriate connections.

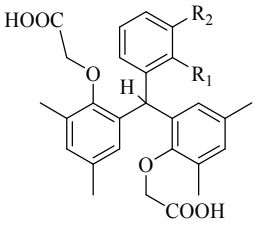

Where R_1= H, R_2= H **(H_2L^1, 5.1)**
R_1= F, R_2= H **(H_2L^2, 5.2)**
R_1= NO_2, R_2= H **(H_2L^3, 5.3)**
R_1= H, R_2= NO_2 **(H_2L^4, 5.4)**

Figure 6.1: Dicarboxylic acid ligands used in the study.

6.1 Cadmium and mercury complexes of H_2L^1, H_2L^2, H_2L^3 and H_2L^4:

The coordination complexes reported in this chapter were synthesised under identical ambient conditions in methanol or dimethyl formamide or dimethylsulphoxide. An interesting structural variation from the one dimensional coordination polymer **(6.1a)** to mononuclear complex (**6.2a**) or metallacycle (**6.2c**, **6.3b** and **6.4a**) were observed depending upon the ligands and solvents used in the reactions. It was observed that on changing the solvent from methanol to dimethyl formamide, the dinuclear complex (**6.3a**) was converted to a metallacycle (**6.3b**). The whole results are summerized in the Scheme **6.2**.

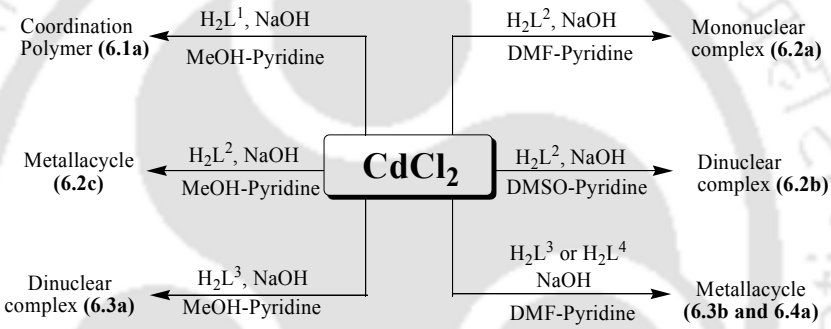

Scheme 6.2: Formation of various coordination complexes of cadmium with H_2L^1, H_2L^2, H_2L^3 and H_2L^4 in different solvents.

The cadmium complex of the ligand H_2L^1 (**5.1**), $[CdL^1(py)_3]n{\cdot}3nH_2O$ (**6.1a**) is a coordination polymer. The ligand H_2L^2 (**5.2**) either formed mononuclear complex $[CdL^2(py)_2H_2O]$ (**6.2a**), dinuclear complex $[CdL^2(py)(DMSO)]_2$ (**6.2b**) or metallacycle $\{[Cd(py)_2H_2O].(py).CH_3OH\}$ (**6.2c**) depending on the solvent used in the reaction. On the other hand, ligand H_2L^3 (**5.3**) forms dinuclear complex $[CdL^3(py)(CH_3OH)]_2{\cdot}CH_3OH$ (**6.3a**) and metallacycle $\{[CdL^3(py)_2(H_2O)]_2{\cdot}H_2O\}$ (**6.3b**) when the reaction was carried out in methanol and dimethylformamide respectively. The ligand **H_2L^4 (5.4)** formed a metallacycle $[CdL^4(py)_2(H_2O)]_2{\cdot}3H_2O$ **(6.4a)** in dimethylformamide solvent. In all of the complexes, the metal ions are linked by carboxylate functional groups present at two ends of the ligands. A similar reaction of H_2L^3 with mercury (II) chloride in DMF in presence of NaOH gave

metallacycle $[HgL^3(py)_2]_2 \cdot DMF$ (**6.3c**). The crystal structures of all of these complexes were determined.

6.1.1 Cadmium complex of H_2L^1 (5.1):

The coordination polymer **6.1a** has seven coordinated cadmium ions, each having a pentagonal bipyramidal geometry. These geometries are constructed by three monodentate pyridine ligands and two chelating carboxylate groups from two independent ligands. The crystal structure of the coordination polymer contains three water molecules of crystllization. The coordination polymer has a spiral structure (Figure **6.2a and 6.2c**). Each pentagonal bipyramid has two pyridine ligands at its axial positions. The equatorial positions are occupied by four oxygen atoms of carboxylate ligands and a nitrogen atom of a pyridine ligand. The metal- ligand bond

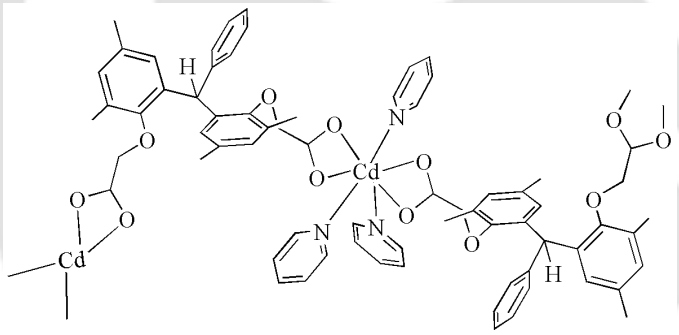

(a)

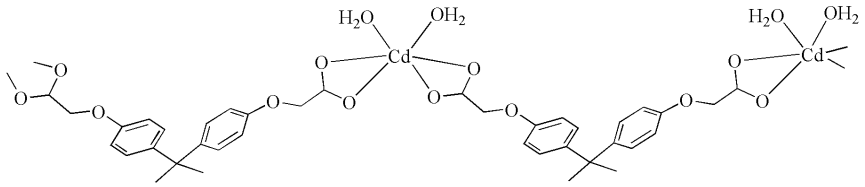

(b)

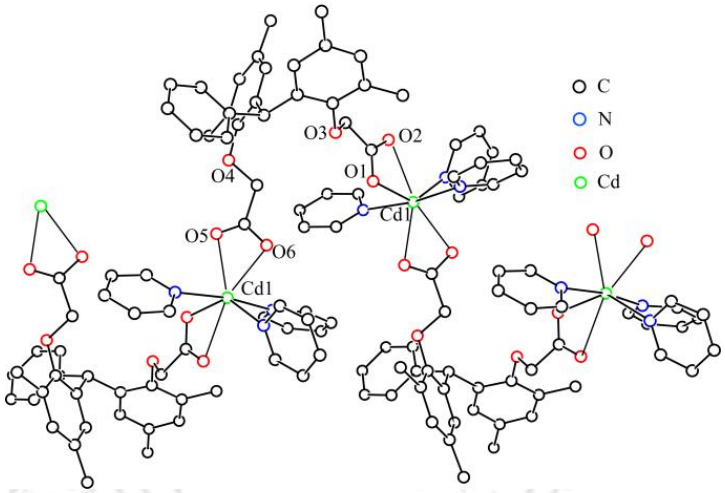

(c)

Figure 6.2: (**a**) and (**c**) The structure of the coordination polymer **6.1a** (Hydrogen atoms are omitted for clearity), **(b)** Structure of a 1D Cd-coordination polymer formded by 4,4'-[isopropylidenebis(p-phenyleneoxy)]diacetic acid.

parameters are listed in Table **6.1**. The V-shaped carboxylic acid ligands along with less flexible ligands were used in the synthesis of cadmium metal-organic frameworks of different dimensions.[2,7,8] For example, a V-shaped *bis*-phenol based flexible dicarboxylic acid, 4,4'-[isopropylidenebis(p-phenyleneoxy)]diacetic acid forms a similar type of spiral one dimensional coordination polymer with cadmium as shown in the Figure **6.1b**.[13]

From the TG analysis **(Figure 6.3a)** it was seen that the coordination polymer losses 34.45% (theoretical weight loss 34.5%) weight in the temperature range of 40-280 °C due to the loss of three lattice water and three coordinated pyridine molecules. The Experimental and simulated PXRD of **6.1a** shows a quite good agreement which indicates the homogeneousity of the sample (Figure **6.3b**). The ^{1}H-NMR spectra of coordination polymer **6.1a** is shown in Figure **6.4**. There are three singlets at 2.11 ppm, 2.14 ppm and 4.01 ppm; the former two signals are for two different types of methyl groups on the aromatic rings and the latter is for -CH_2O- groups. Again, the singlet peaks at 6.37 ppm, 6.43 ppm and 6.85 ppm appear for the methine proton and aromatic protons of methyl group-containing ring, respectively. The peaks for the coordinated pyridine molecule appear at 7.39 (triplet), 7.79 (doublet) and 8.58 ppm (singlet), as illustrated in Figure **6.4**.

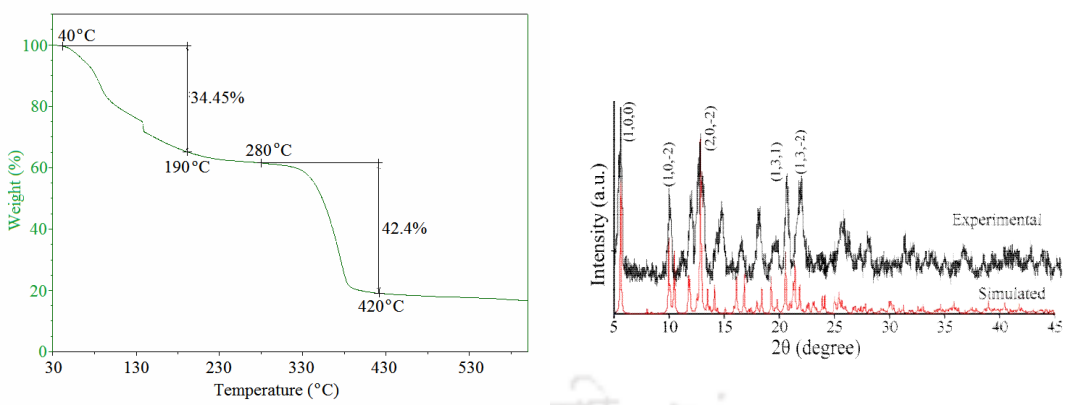

(a) **(b)**

Figure 6.3: (a) The TG of the coordination polymer **6.1a** (5°C/ minute heating rate) **(b)** Comparison of the simulated and the experimental PXRD of the coordination polymer **6.1a**.

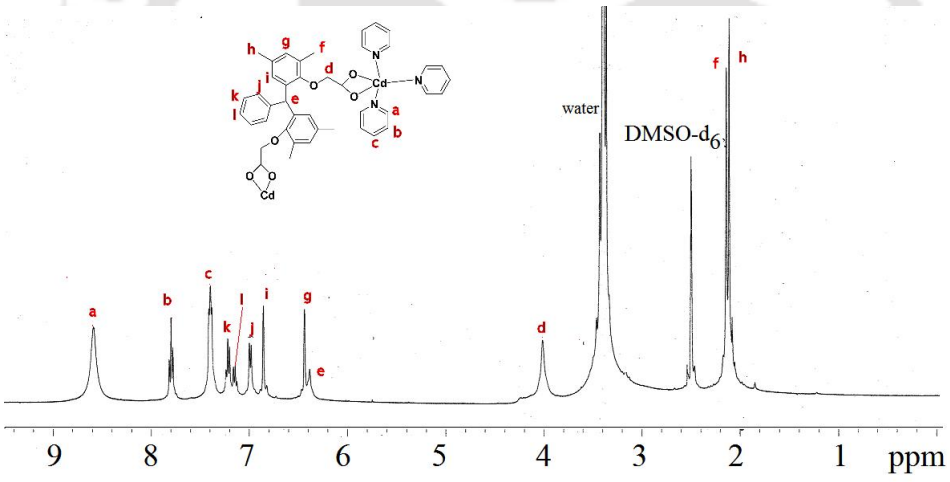

Figure **6.4**: ^{1}H-NMR of the coordination polymer **6.1a** (DMSO-d_6, 400MHz).

Table 6.1: The bond lengths and angles of coordination polymer **6.1a.**

M-L	d_{M-L} (Å)	<L-M-L	Angle (°)	<L-M-L	Angle (°)	<L-M-L	Angle(°)
Cd1-N3	2.333(3)	N3-Cd1-N2	95.27(11)	N2 -Cd1- O5	129.82(10)	O5- Cd1- O6	51.12(9)
Cd1-N2	2.344(3)	N3 -Cd1- O1	84.24(10)	O1- Cd1- O5	93.83(9)	N3- Cd1 -O2	82.01(10)
Cd1-O1	2.360(2)	N2- Cd1- O1	136.16(10)	N1- Cd1- O5	100.54(11)	N2- Cd1- O2	82.98(9)
Cd1-N1	2.375(3)	N3 -Cd1 -N1	170.04(10)	N3- Cd1 -O6	107.21(11)	O1- Cd1- O2	53.44(8)
Cd1-O5	2.474(3)	N2- Cd1- N1	88.85(11)	N2- Cd1- O6	82.30(10)	N1- Cd1- O2	89.52(10)
Cd1-O6	2.478(3)	O1- Cd1- N1	86.51(10)	O1- Cd1- O6	139.73(10)	O5- Cd1 -O2	145.35(9)
Cd1-O2	2.548(3)	N3- Cd1- O5	83.78(11)	N1- Cd1- O6	82.30(11)	O6- Cd1- O2	163.28(10)

6.1.2 Cadmium complexes of H_2L^2 (5.2):

The cadmium complexes **6.2a**, **6.2b** and **6.2c** are synthesised by a common procedure but in different solvents as shown in the scheme **6.3**. we obtained mononuclear complex $[CdL^2(py)_2(H_2O)]$ **(6.2a)** from DMF, dinuclear complex $[CdL^2(py)(DMSO)]_2$ **(6.2b)** and the metallacycle $[CdL(py)_2(H_2O)]_2$.MeOH.py (**6.2c)** from methanol solvent.

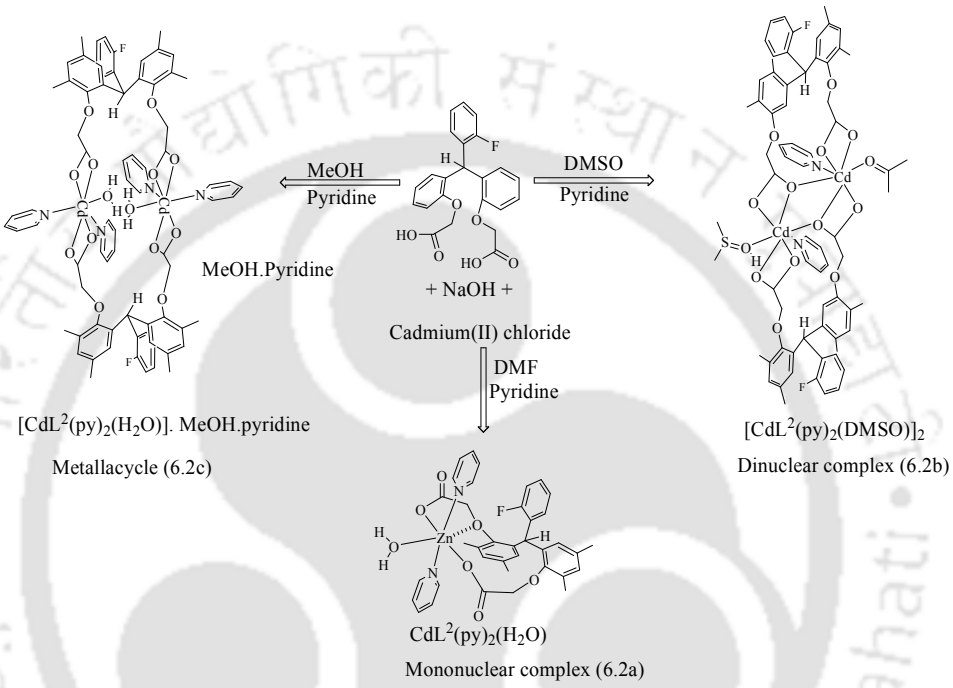

Scheme 6.3: Reaction of H_2L^2 with Cadmium chloride.

In the mononuclear complex $[CdL^2(py)_2(H_2O)]$ **(6.2a)** the cadmium atom has trigonal-bipyramidal geometry (Figure **6.5a**). The equatorial positions of the cadmium atom are occupied by two carboxylate O-atom and a water molecule and the axial position is occupied by two pyridine molecules. One of the ethereal oxygen of the ligand is relatively close to the cadmium ion suggesting very weak interaction. This coordination bond is relatively weak with respect to the other cadmium-oxygen bonds. The distance of Cd1⋯O4 bond is 2.677 Å, which is much longer than other three Cd-O bonds that are observed to be in the range 2.198-2.256Å (Table **6.2)**. This type of five-coordinated mononuclear complex was earlier observed in case of the unsubstituted ligand H_2L^1 with Zinc (II) and it was obtained from methanol as solvent

(Figure **6.5b**).[14] The crystal structure of the Zn (II) complex contains lattice water and a pyridine molecule. However in the present case, although DMF is used as solvent it was neither observed as solvent of crystallization nor as ligand. The coordinated water molecule and one of the carboxylate O- atoms involves in H-bonding to give two different types of $R_2^2(12)$ cyclic H-bonding and finally it forms one dimensional polymeric hydrogen bonded chain (Figure **6.5c**). The selected H-bond parameters of complex **6.2a** are given in the Table **6.3**. We did not observe hydrogen bond interactions involving the C-F bond and neither the cadmium-fluorine interactions in solid state structure. The ligand H_2L^2 shows IR stretching band at 1720 cm^{-1}, but in

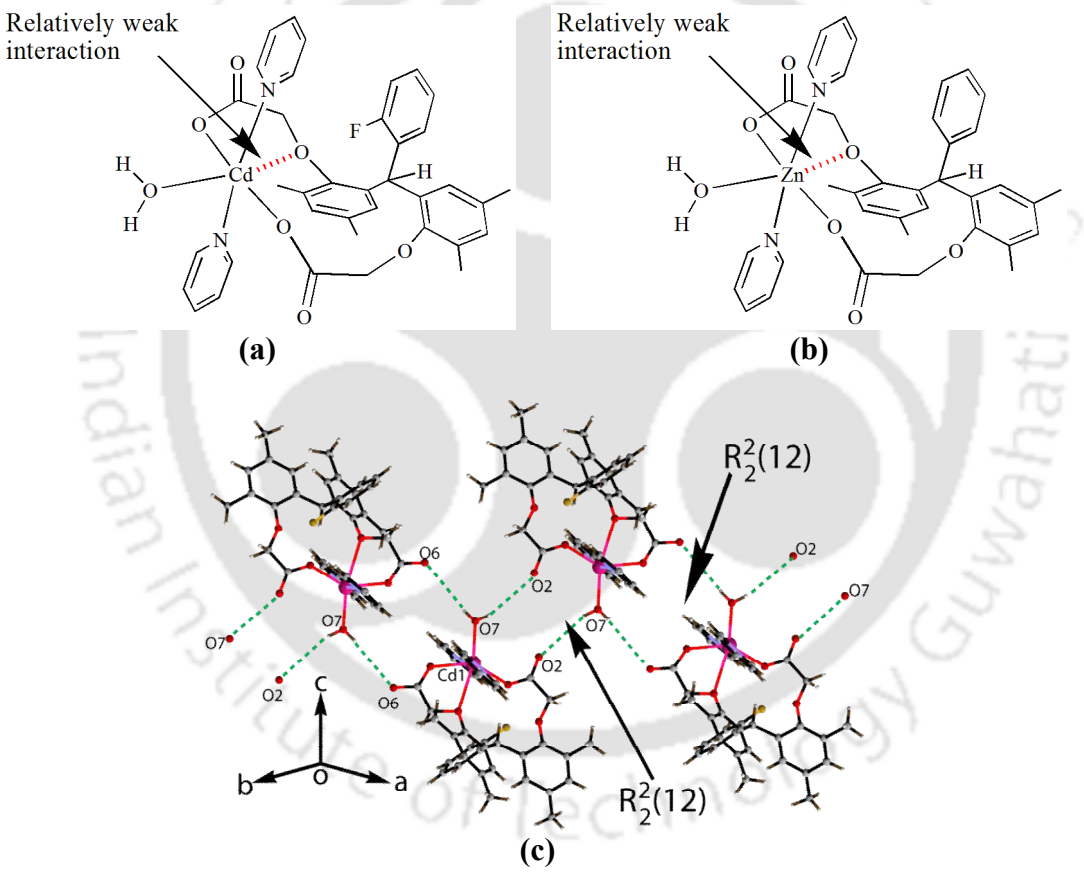

Figure 6.5: **(a)** Structure of the Cd-mononuclear complex **6.2a** showing the weak Cd···O interaction, **(b)** Structure of the Zn-mononuclear complex formed by the unsubstituted ligand H_2L^1, **(c)** Different types of cyclic H-bonding of the mononuclear complex **6.2a,** leading to polymeric H-bonded chain.

the complex **6.2a** it appears at 1667 cm^{-1}. This shows the mono-dentate carboxylate binding mode in the complex, as the C=O stretching of mono-dentate carboxylate shifts to lower frequency than the corresponding acid.[15]

The dinuclear complex $[CdL^2(py)(DMSO)]_2$ **(6.2b)** has a Cd_2O_2-core where both the cadmium atom have same coordination environment (Figure **6.6a**). Here, we observed two different binding modes of the caboxylate groups. One of the oxygen atoms of a carboxylate group involves in μ^1-bridge with two cadmium ions to form the Cd_2O_2-core. Each of the cadmium atoms has one pyridine and one dimethylsulphoxide molecule in its coordination site and they project away from each other in the dimeric structure (Figure **6.6a**). The coordinated DMSO molecules help in providing appropriate geometry to the carboxylate ligand to form the bridged structure. The complex has one pyridine molecule per cadmium ion and the metal are in close proximity to form six coordinated binuclear complex where the Cadmium-Cadmium distance is found to be 3.65Å. This separation is less than the cadmium-cadmium separation 3.97 Å found in dinuclear complex reported earlier.[4] Generally, the Cadmium-Cadmium separation in Cd_2O_2 core with η^1 and η^3-carboxylate is found to be in the range of 3.8 to 4.15 Å.[16] The selected bond length and bond angle parameter are given in the Table **6.2**.

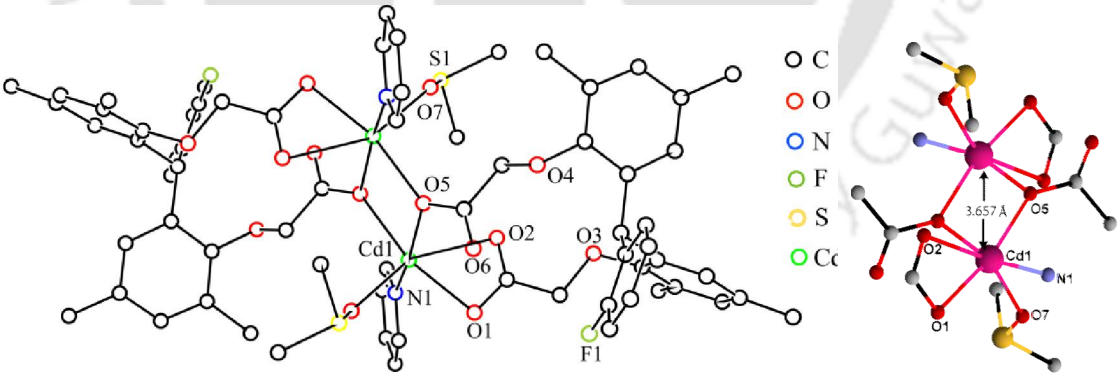

(a) **(b)**

Figure 6.6: **(a)** Structure of the dinuclear complex **6.2b** showing the coordinated dimethylsulphoxide molecules, **(b)** Coordination environment of the two Cadmium atoms in the dinuclear complex **6.2b**.

Table 6.2: The selected bond lengths and bond angles of the complexes **6.2a-6.2c:**

Compd. No.	M-L	d_{M-L} (Å)	<L-M-L	Angle (°)	<L-M-L	Angle (°)
6.2a	Cd1-O1	2.198(3)	O1-Cd1-O5	143.89(13)	O7- Cd1 N2	93.70(16)
	Cd1-O5	2.253(3)	O1-Cd1-O7	118.18(15)	O1-Cd1-N1	88.94(15)
	Cd1-O7	2.256(4)	O5-Cd1-O7	97.83(14)	O5-Cd1-N1	88.56(14)
	Cd1-N1	2.319(4)	O1-Cd1-N2	92.54(15)	O7-Cd1-N1	89.90(16)
	Cd1-N2	2.308(4)	O5-Cd1-N2	87.36(14)	N2-Cd1-N1	174.89(16)
6.2b	Cd1-O1	2.278(3)	O7-Cd1-O5	99.11(11)	O5-Cd1-O2	78.38(9)
	Cd1-O7	2.250(3)	O7-Cd1-O1	95.26(11)	O5-Cd1-O5	74.31(11)
	Cd1 O5	2.265(3)	O5-Cd1-O1	165.16(10)	O1-Cd1-O5	99.59(10)
	Cd1-O1	2.278(3)	O7-Cd1-N1	92.14(12)	N1-Cd1-O5	163.35(11)
	Cd1-N1	2.308(3)	O5-Cd1-N1	92.80(11)	O7-Cd1-O2	148.87(11)
	Cd1-O5	2.323(3)	O1 Cd1-N1	90.32(12)	O5-Cd1-O2	110.11(9)
	Cd1-O2	2.483(3)	O7-Cd1-O5	100.16(11)	N1-Cd1-O2	96.82(11)
6.2c	Cd1-O1	2.320(2)	N1-Cd1-O5	133.35(8)	N2-Cd1-O6	85.23(10)
	Cd1-N1	2.287(2)	N1-Cd1-O1	139.27(8)	N1-Cd1-O2	86.14(8)
	Cd1-O5	2.301(2)	O5-Cd1-O1	86.97(8)	O5-Cd1-O2	138.60(8)
	Cd1-O1	2.320(2)	N1-Cd1-O7	86.59(9)	O7-Cd1-O2	83.63(9)
	Cd1-O7	2.339(2)	O5-Cd1-O7	86.65(8)	N2-Cd1-O2	93.59(9)
	Cd1-N2	2.377(3)	O1-Cd1-O7	91.23(9)	N1-Cd1-O6	83.68(8)
	Cd1-O2	2.547(2)	N1-Cd1-N2	96.70(10)	O1-Cd1-O6	136.70(7)
	Cd1-O6	2.649(2)	O5-Cd1-N2	93.21(10)	O7-Cd1-O6	98.13(9)
			O1-Cd1-N2	84.32(9)	N2-Cd1-O6	85.23(10)
			O7-Cd1-N2	175.56(9)		

Table 6.3: Seleced hydrogen parameters of complex **6.2a** and **6.2c**:

Compound No.	D-H···A	d_{D-H}(Å)	$d_{H\cdots A}$(Å)	$d_{D\cdots A}$(Å)	< D-H···A(°)
6.2a	O(7)-H(7M)···O(6) [-x,1-y,-z]	0.85(5)	1.88(4)	2.705(6)	164(5)
	O(7)-H(7N)···O(2) [1-x,-y,-z]	0.84(5)	1.84(5)	2.680(7)	178(9)
6.2c	O(8)-H(8)···O(6) [x,1+y,z]	0.82	2.12	2.860(6)	151
	C(41) -H(41) ···O(8)	0.93	2.55	3.471(13)	171

In the metallacycle {[CdL^2 $(py)_2(H_2O)]_2$.Py.MeOH} **(6.2c),** the cadmium ions are seven coordinated having pentagonal bi-pyramidal geometry. There are two chelating carboxylate and a water molecule along with two pyridine molecules binding to the cadmium ion (Figure **6.7**). One of the coordinated and the lattice pyridine molecule

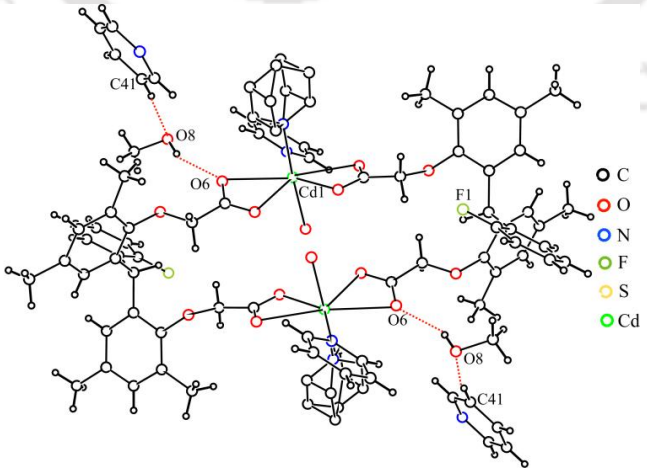

Figure 6.7: Structure of the metallocycle **6.2c** of cadmium showing the Selected hydrogen C-H···**O** and O-H···**O** interactions.

are disordered in the crystal structure. The coordinated disordered pyridine molecules are disposed in the lattice such that the two carbon atoms at each **2** and **3** position of the pyridine ring are shared with half occupancies. Apart from these the unit cell contains one methanol molecule and one disordered pyridine molecule. The methanol molecule out side the of coordination sphere are held by the O-H···O interaction to the oxygen atom of carboxylate groups (Figure **6.7**). Beside this, the uncoordinated pyridine molecules are also held in the lattice through C-H···O interactions as shown in the Figure **6.7**. The selected hydrogen parameters for metallacycle **6.2c** given in Table **6.3** have suitable bond parameters to support the presence of such interactions.[17]

Thermogram of the complex **6.2a** (Figure **6.19**) shows 22.8 % weight loss in the region 70-230°C which corresponds to loss of two pyridine and one water molecule (calculated loss 21.8 %). On the other hand, complex **6.2b** losses 25.0 % of its weight in the range of 70-300 °C (Figure **6.20b**) is due to loss of the DMSO and the pyridine molecules (theoretical loss 21.3 %). The complex **6.2c** loses the solvated methanol and pyridine below 150 °C (theoretical weight loss 6.2%, experimental weight loss 6.4 %) (Figure **6.21b**). It loses 27.1% of its weight in the range of 150-230 °C due to loss of all the pyridine molecules and the solvent molecules (theoretical weight loss 26.4%)

In the solution state ^{1}H-NMR spectra of the complexes **6.2a**-**6.2c** show characteristic signals of the parent ligand H_2L^2, but the signals appears at slightly different chemical shift with respect to the parent ligand. The ^{1}H-NMR of the mononuclear complex (Figure **6.8**) shows singlets at 2.12 ppm, 2.16 ppm corresponds to methyl protons attached to the aromatic rings. A singlet observed at 4.03 ppm corresponds to -CH_2O- protons. Besides these, singlet at 6.30 ppm corresponds to the central methine proton of *bis*-phenol whereas a singlets at 6.39 ppm and 6.92 ppm corresponds to the aromatic protons of the methyl group containing aromatic ring. The peaks for the coordinated pyridines appear at 7.54 ppm, 7.99 ppm and 8.65 ppm. The presence of coordinated dimethylsulphoxide as ancillary ligands in the dinuclear complex **6.2b** is confirmed by ^{1}H-NMR where the protons of DMSO appear at 2.53 ppm (Figure **6.20c**). The ^{1}H-NMR of **6.2b** shows signal for the methine proton at 6.40 ppm and the aromatic protons of the methyl containing rings appears at 6.38 ppm and 6.90 ppm. The peaks for coordinated pyridine molecules in **6.2c** appear at 7.37 ppm

(triplet), 7.77 ppm (triplet) and 8.58 ppm (broad). The ^{1}H-NMR of the metallacycle **6.2c** (Figure **6.21c**) shows the peak for the central methine proton of the *bis*-phenol at 6.28 ppm. The peaks for the coordinated pyridine appear at 7.30 ppm (triplet), 7.72 ppm (triplet) and 8.43 ppm (doublet). Thus, comparing the chemical shift of the respective protons in the complexes **6.2a-c,** it was observed that they were distinguishable in solution. The LC-mass spectra of the complex **6.2a** shows m/e peak at 735.2925, which corresponds to the mass of the [CdL(py)$_2$] ion, whereas the complex **6.2b** and **6.2c** degrades in formic acid matrix and showed common peak of the ligand as the base peak at 489.1681 (L+ Na^+).

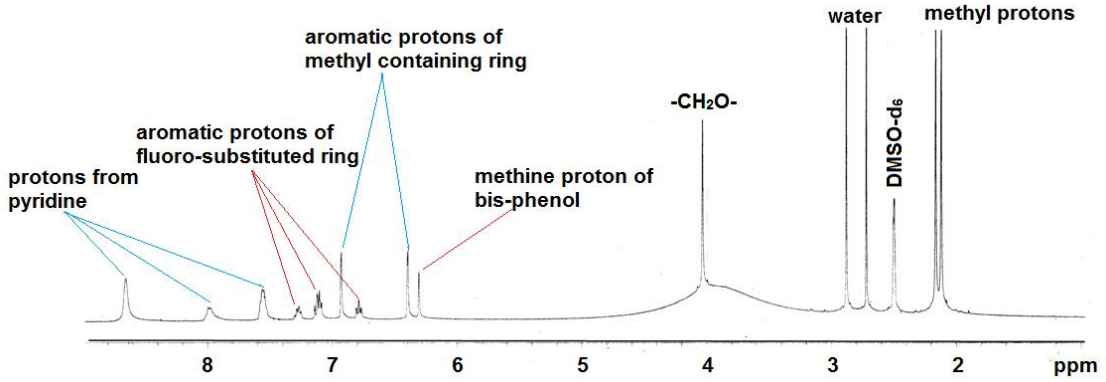

Figure 6.8: ^{1}H-NMR of the mononuclear complex **6.2a** (DMSO-d_6, 400MHz).

The predictability of weak interactions rendered by a covalently linked fluorine atom in crystal lattice is still in question,[18] nonetheless we have not observed any of the often encountered weak interactions such as F···F or C-H···F interactions[18,19] in the present case. There are certain differences in the preferential formation of different architecture by the non-fluorinated analogous of H_2L^2. The non fluorinated ligand H_2L^1 forms 1D coordination polymer in methanol, which is in contrast to the formation of metallacycle by fluorinated ligand H_2L^2 in methanol. Further to this, when we consider complexes **6.2a**, **6.2b** and **6.2c** formed by the ligand H_2L^2, it was seen that there are two pyridine per cadmium in complexes **6.2a** and **6.2c**. But, in case of **6.2b** there is only one pyridine per cadmium ion. ^{19}F-NMR can be use as a tool to distinguish between different fluoro-carboxylate complexes.[20] The ^{19}F-NMR of the ligand H_2L^2, complexes **6.2a**, **6.2b** and **6.2c** are compared in the Figure **6.9**. However, we did not observed much difference between the chemical shift of the ligand **5.2** and the complex **6.2a** as both shows signals at -118.1 ppm. The complexes **6.2b** and **6.2c**

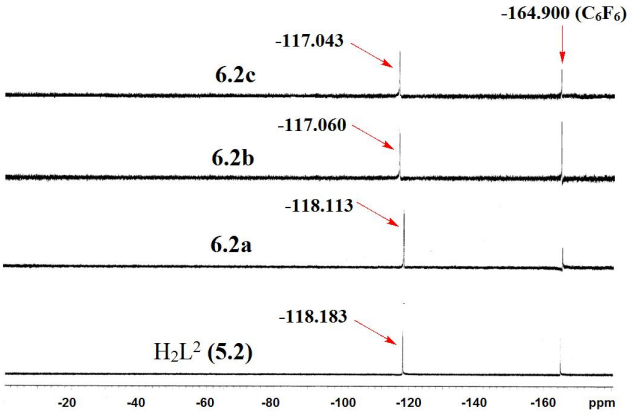

Figure 6.9: ^{19}F-NMR of the ligand H_2L^2 **(5.2)**, complex **6.2a**, **6.2b** and **6.2c**. (400 MHz, DMSO- d_6, using C_6F_6 as internal reference).

show chemical shift at -117.0 ppm in their respective ^{19}F-NMR spectra. Thus complexes **6.2b** and **6.2c** can be distinguished from the mono nuclear complex **6.2a**, but it is difficult to distinguish **6.2b** and **6.2c** from ^{19}F-NMR.

The complex **6.2c** is soluble in DMSO as well as methanol, whereas the complex **6.2b** is soluble in DMSO but not in methanol. The crystallization of **6.2c** from a solution of DMSO with or without pyridine yielded the dinuclear complex **6.2b**.

$$\underset{\textbf{6.2c}}{[CdL^2(py)(H_2O)]_2.\ MeOH.py} \xrightarrow{DMSO} \underset{\textbf{6.2b}}{[CdL(py)(DMSO)]_2}$$

Equation 6.1: Solvent assisted conversion of complex **6.2c** to **6.2b.**

6.1.3 Cadmium complexes of H_2L^3 (5.3):

The reaction of cadmium(II) chloride with H_2L^3 in presence of sodium hydroxide in MeOH-pyridine forms a dinuclear complex $[CdL^3(py)(CH_3OH)]_2{\cdot}CH_3OH$ **(6.3a)**, where both of the cadmium ions are in identical environments (Figure **6.10a)**. Each cadmium ion has one pyridine and one methanol molecule in its coordination sphere and the methanol ligands are independently attached to two cadmium ions. They

project away from each other at two ends of the dimeric structure. The presence of methanol molecules as ligands at the terminal ends inhibits the formation of a polymeric structure. The crystal structure of the dinuclear complex **6.3c** cotains one lattice methanol and one water molecules. The nitro group present at the ortho position of the aromatic ring also plays a role by providing the adequate twist to the carboxylate group to form the Cd_2O_2-type core. Such effects were earlier observed in 2-nitrobenzoate complexes with metal ions, such as zinc, manganese and cadmium.[4, 21] The 2-nitro benzoate provides the appropriate orientation to two carboxylate groups

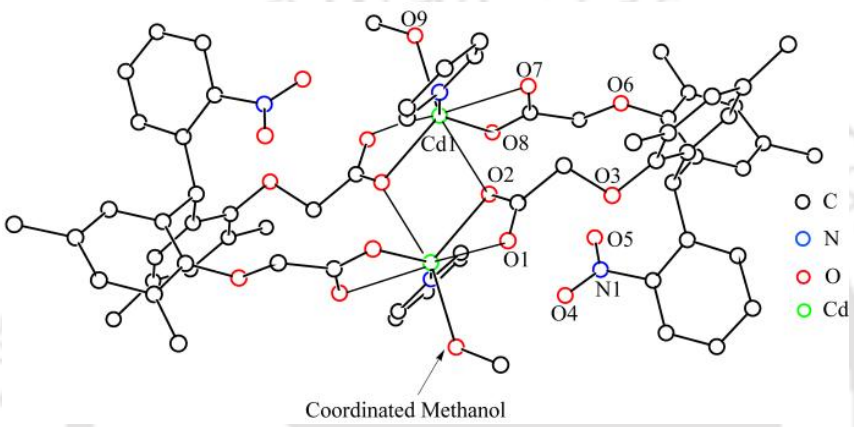

(a)

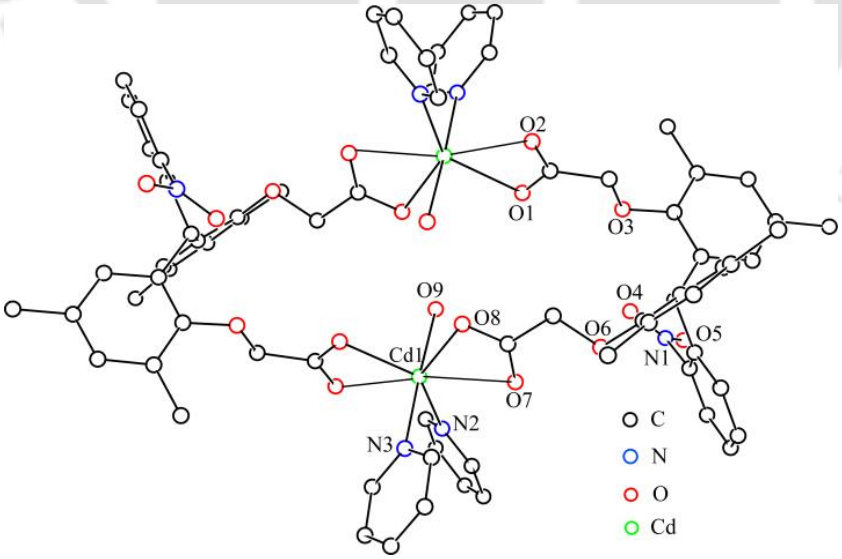

(b)

Figure 6.10: (a) The structure of the dinuclear complex **6.3a** showing the Cd_2O_2-core, **(b)** structure of the metallacycle **6.3b**.

to form the Cd_2O_2 core.[4] Complex **6.3a** has one pyridine ligand per cadmium ion and the two metal ions in close proximity form the seven coordinate dinuclear complex where the metal-metal distance is found to be 3.97 Å. The selected bond angles and bond distances are listed in Table **6.4**.

A similar reaction of cadmium (II) chloride with H_2L^3 in DMF-pyridine under basic condition form metallacycle $[CdL^3(py)_2(H_2O)]_2 \cdot H_2O$ **(6.3b)**. This metallacycle may be attributed to the opening of a Cd_2O_2-core in the dinuclear complex **6.3a**. Each cadmium ion has a coordination number of seven, comprised of two chelating carboxylates and a water molecule along with two pyridine ligands. Although the DMF was used as the solvent, we did not observe DMF molecules in its crystal lattice as the solvent of crystallization or as a ligand. However, DMF can easily interact with different functional groups (in this case either nitro or carboxylic acid) during the course of the reaction, to guide the carboxylate to form a metallacycle. The structure of the complex determined by X-ray single crystal diffraction is shown in Figure **6.10b**. The very weak bonds Cd1-O7 and Cd1-O2 are 2.501(6) and 2.555(5) Å, whereas the Cd1-O8 and Cd1-O1 are 2.327(5) and 2.308(5) Å, respectively, supporting that the carboxylates are ligated as bidentate chelate. The metal-ligand bond distances and bond angles are listed in Table **6.4**. The cadmium ions have

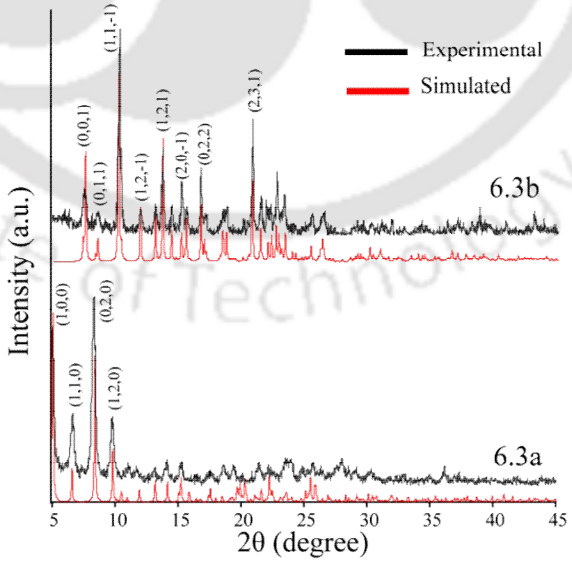

Figure 6.11: Comparison of the simulated and the experimental PXRD of the dinuclear complex **6.3a** and **6.3b**.

pentagonal bipyramid structures, in which one pyridine and two carboxylate groups occupy the equatorial positions; a water molecule and a pyridine molecule occupy the axial positions. The PXRD patterns of complexes **6.3a** and **6.3b** are distinguishable (Figure **6.11**). The experimental PXRD pattern of complexes **6.3a** and **6.3b** have excellent agreement with the theoretical pattern obtained form single crystal data. The IR spectra of complexes **6.3a** and **6.3b** are distinguishable, as the carbonyl stretching of complex **6.3a** appears at 1599 cm^{-1}, whereas the carbonyl stretching of complex **6.3b** appears at 1679 cm^{-1}, which is shown in the Figure **6.12**.

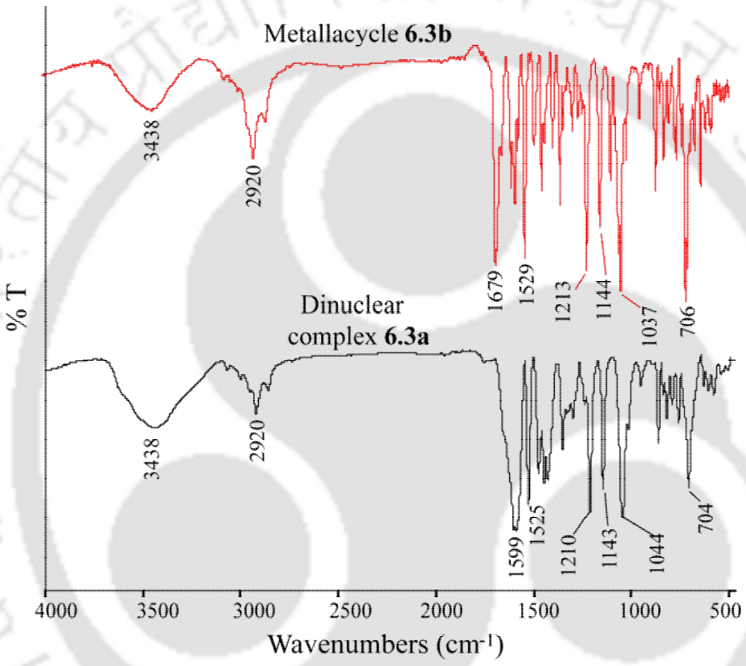

Figure 6.12: Overlay of the FT-IR spectra of the dinuclear complex **6.3a** and metallacycle **6.3b**.

The ^{1}H-NMR spectra of dinuclear complex **6.3a** is shown in Figure **6.13a**. From the spectra, it is seen that there are three singlets at 2.10 ppm, 2.15 ppm and 4.10 ppm for two types of methyl protons and -CH_2O-, respectively. Again, the singlets at 6.23 ppm, 6.90 ppm and 6.65 ppm are due to the aromatic protons of the methyl group-containing aromatic ring and methine proton of the parent *bis*-phenol molecule, respectively. The signals for the protons of the coordinated pyridine molecules appear at 7.39 ppm (triplet), 7.79 ppm (triplet) and 8.58 ppm (doublet). On the other hand, in the ^{1}H-NMR spectra of the metallacycle **6.3b** (Figure **6.13b**) there are three singlets

at 2.09 ppm, 2.15 ppm and 4.12 ppm for two types of methyl protons of aromatic rings and -CH_2O-, respectively. Again, the singlets at 6.24 ppm, 6.90 ppm and 6.65 ppm are due to the aromatic protons of methyl groups containing aromatic rings and methine proton of the parent *bis*-phenol molecule respectively. The signals for the protons of the coordinated pyridine molecules appear at 7.39 ppm (triplet), 7.81 ppm (triplet) and 8.59 ppm (doublet). From the ^{1}H-NMR spectra of **6.3a** and **6.3b**, it is seen that the position of the peaks are almost similar, however, the splitting pattern and coupling constant values are different, suggesting that in solution they retain their identity. The coupling scheme interpreted from ^{1}H-NMR is confirmed by recording HOMO-COSY spectra of the complex **6.3a** and **6.3b** (Figure **6.22a and 6.22b**).

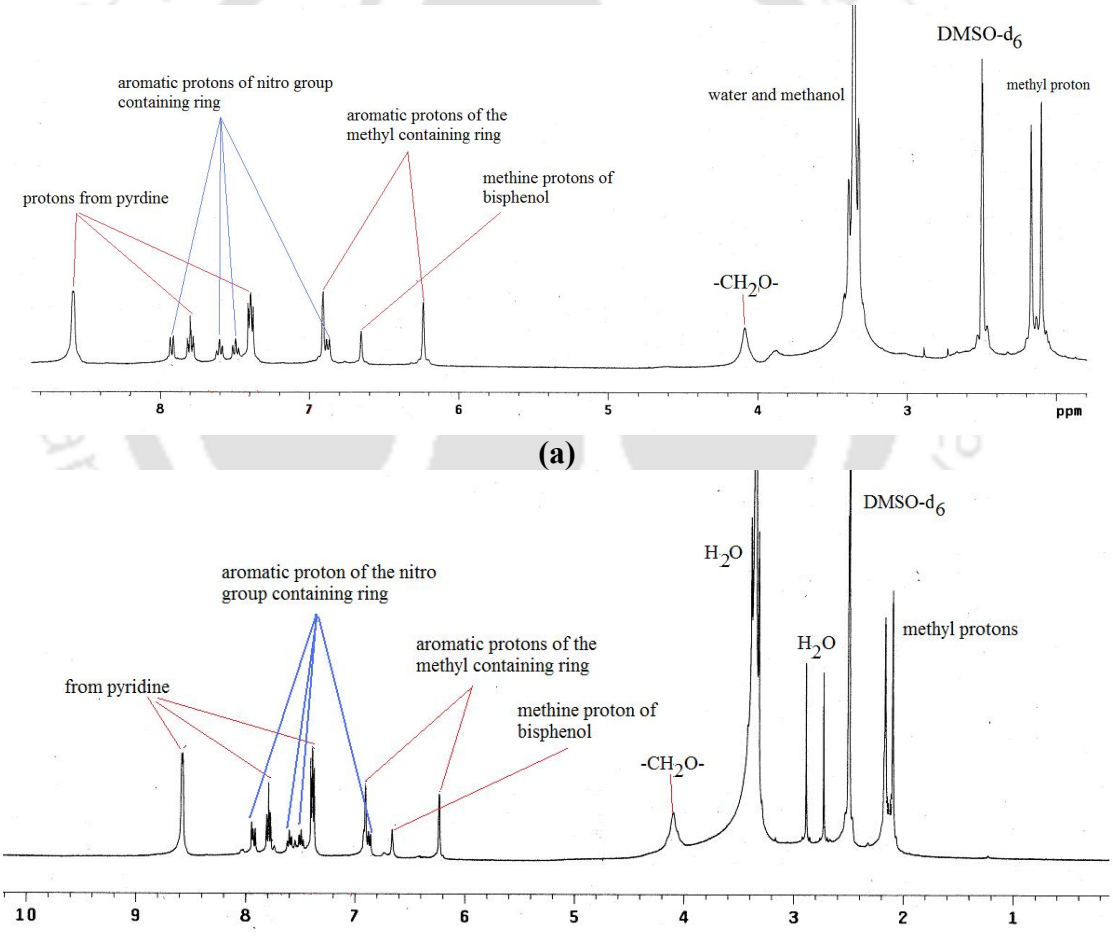

Figure 6.13: **(a)** ^{1}H-NMR of the dinuclear complex **6.3a** and **(b)** ^{1}H-NMR of the metallacycle **6.3b** in DMSO-d_6 (400MHz).

From the TG of dinuclear complex **6.3a** (Figure **6.14a**), it was seen that it losses one lattice water and three (two coordinated and one lattice) methanol molecules in the temperature range of 40-280°C (experimental weight loss 16.5%, theoretical weight loss 17.84%). On the other hand, when the metallacycle **6.3b** was heated up to 220° C it losses four coordinated pyridine and three water molecules (experimental weight loss 23.5%, theoretical weight loss 23.24%) (Figure **6.14b**).

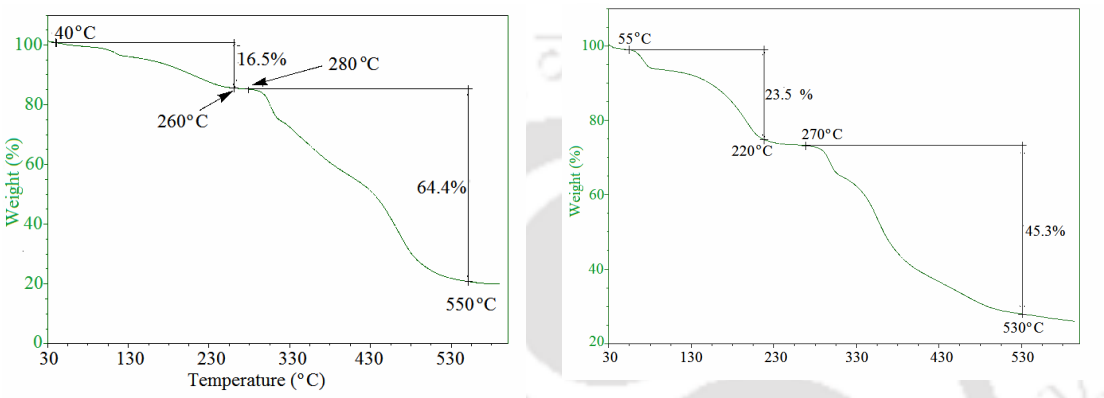

(a) **(b)**

Figure 6.14: TG of the **(a)** dinuclear complex **6.3a** and **(b)** metallacycle **6.3b**.

Table 6.4: The Bond lengths and angles of the dinuclear complex **6.3a** and metallacycle **6.3b**:

Compd No.	M-L	d_{M-L} (Å)	<L-M-L	angle (°)	<L-M-L	Angle (°)	<L-M-L	Angle(°)
6.3a	Cd1-N3	2.333(3)	O9-Cd1-O7	87.85(18)	N2-Cd1-O7	89.14(18)	O1-Cd1-O2	113.83(18)
	Cd1-N2	2.344(3)	O2-Cd1-O8	112.39(17)	O2- Cd1-O7	148.80(18)	O7-Cd1-O2	78.47(16)
	Cd1-O5	2.474(3)	N2-Cd1-O8	142.6(2)	O8-Cd1-O7	55.56(16)	O8-Cd1-O2	81.05(16)
	Cd1-O2	2.548(3)	O9 Cd1-O8	98.20(18)	O9-Cd1-O1	82.1(2)	O2-Cd1-O2	70.9(2)
	Cd- O6	2.478(3)	N2-Cd1-O2	91.20(19)	N2-Cd1-O1	128.9(2)	N2-Cd1-O2	80.01(18)
	Cd1-O1	2.360(2)	O9- Cd1-O2	123.32(19)	O2-Cd1-O1	53.94(18)	O9-Cd1-O2	163.95(18)
	Cd1-N1	2.375(3)	O9-Cd1-N2	91.54(19)	O8-Cd1-O1	88.27(18)	O7-Cd1-O1	140.63(17)
6.3b	Cd1-O1	2.308(5)	O1- Cd1- N3	136.38(19)	N3-Cd1-N2	91.7(3)	O1- Cd1- O2	53.46(16)
	Cd1-N3	2.312(6)	O1- Cd1- O9	82.17(19)	O9-Cd1-N2	178.0(2)	N3- Cd1- O2	84.6(2)
	Cd1-O9	2.322(5)	N3- Cd1- O9	87.7(2)	O8-Cd1-N2	89.6(3)	O9- Cd1 -O2	90.7(2)
	Cd1-O8	2.327(5)	O1- Cd1- O8	89.98(17)	N3-Cd1-O8	132.9(2)	O8- Cd1- O2	142.51(18)
	Cd1-N2	2.334(6)	O1-Cd1- N2	97.0(2)	O9 -Cd1- O7	88.2(2)	N2 -Cd1- O2	87.3(2)
	Cd1-O7	2.501(6)	O1- Cd1- O7	141.39(17)	O8- Cd1- O7	52.96(19)	O7- Cd1- O2	164.53(18)
	Cd1-O2	2.555(5)	N3- Cd1- O7	80.0(2)	N2-Cd1- O7	93.5(2)		

6.1.4 Cadmium complex of H_2L^4(5.4):

Metallacycle $[CdL^4(py)_2(H_2O)]_2 \cdot 3H_2O$ **(6.4a)** was obtained from the reaction of cadmium (II) chloride with H_2L^4 **(5.4)** in methanol and pyridine in presence of sodium hydroxide, where both of the cadmium ions are in identical environments (Figure **6.15**). The other coordination sites of the metal atoms are occupied by two pyridine molecules and a water molecule. It is evident from the Cd-O bond distances that the carboxylate groups in this complex are a combination of a monodentate and another bidentate with distorted chelate structure, where Cd1-O2, Cd1-O7 and Cd1-O9 bond distances are 2.346 Å, 2.263 Å and 2.341 Å respectively. These distances are within the limit of generally observed Cd-O bond distances in related compounds. Whereas the Cd1-O1 separation at 2.524 Å and Cd1-O8 separations at 2.677 Å are long for the

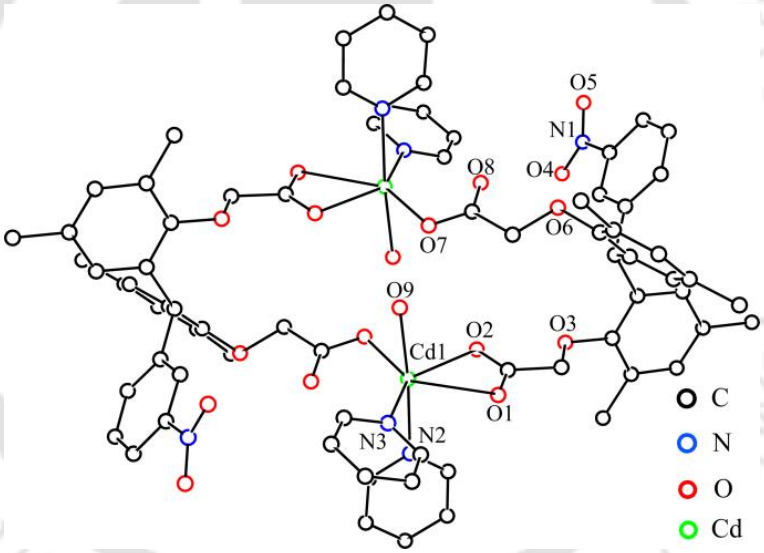

Figure 6.15: Structure of the cadmium metallacycle **6.4a.**

formation of a bond, but the Cd1-O1 can be suggested as weakly interacting.[4, 22] This makes the two slightly different coordination modes of the two carboxylate attached to a cadmium ion. The Cd1-N2 and Cd1-N3 distances in the complex are 2.361 Å and 2.332 Å, respectively. Thus, the molecule adopts distorted pentagonal bipyramid geometry, in which one pyridine and two carboxylates connected to Cd1 make the five-member geometry and the axial bonds are Cd1-N2 and Cd1-O9 bonds. The bond angles ∠N3-Cd1-O2, ∠N3-Cd-O7 and ∠O2-Cd1-O7 are 134.32°, 139.46° and 85.07°,

respectively. If the two weak contacts are not taken into consideration, then each of the cadmium ions in the complex can be described as a distorted trigonal bipyramid. Nonetheless, the overall structure of the metallacycle is highly symmetric and contains a mirror plane that bisects it into two halves. Each equivalent half contains one cadmium ion with one carboxylate, two pyridine and one water molecules. The simulated and the experimental powder X-ray diffraction patterns of **6.4a** are shown in Figure **6.16b**. All of the principal peaks for different Miller indices are observed, confirming the phase purity and homogeneity of the samples. The TG (Figure **6.16a**) shows that **6.4a** losses four lattice water and four coordinated pyridine molecules when heated at around 50-215°C (theoretical weight loss 23.24% experimental weight loss 25.80%).

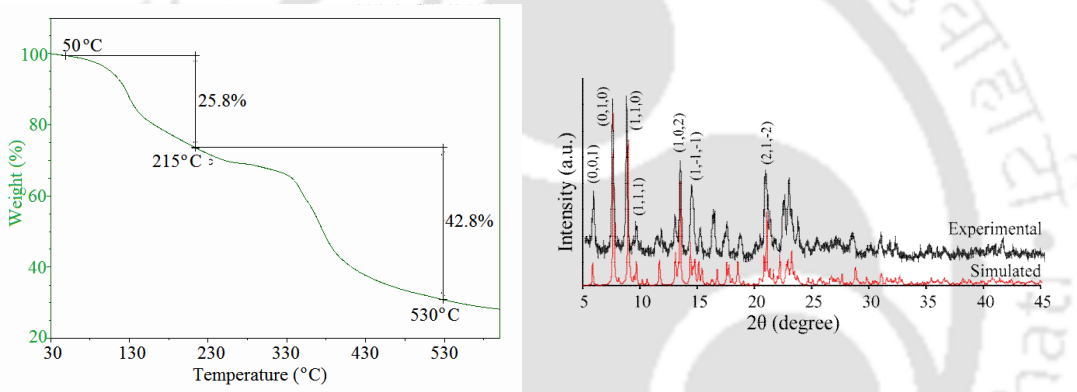

(a) **(b)**

Figure 6.16: (a) TG of the metallacycle **6.4a** (heating rate 5 °C/minute). **(b)** PXRD of the metallacycle **6.4a.**

6.1.5 Mercury complex of H_2L^3 (5.3):

Since both metallacycles as well as a binuclear complex of cadmium with the H_2L^3 are observed, we have examined the effect of size of the metal ions in deciding their formation. Thus, mercury metallacycle $[HgL^3(py)_2]_2 \cdot DMF$ **(6.3c)** was prepared by reacting H_2L^3 with mercury(II) chloride in DMF in presence of sodium hydroxide, followed by treatment with pyridine (Figure **6.17a**). In this case, we were not successful in obtaining crystals from the reaction carried out in methanol. The size of mercury being bigger than cadmium, it accommodates two pyridine ligands and retained a cyclic structure, where each mercuric ion has a distorted tetrahedral

geometry. The metal-ligand bond parameters are listed in Table **6.5**. The Hg1-O2 and Hg1-O7 separations are 2.91 Å and 2.68 Å, respectively, suggesting that there is no Hg-O bond between these atoms. This shows that the carboxylates are coordinated in a monodentate fashion to the mercury (II). From the ^{1}H-NMR spectrum of the mercury-containing metallacycle **6.3c**, it is seen that signals from the protons of coordinated pyridine molecules appear at 7.52 ppm, 7.91 ppm and 8.69 ppm (Figure **6.24b**). The packing pattern of the mercury complex suggests that the solvent molecules are held between the interstitial spaces of the metallacycles. The coordinating carboxylate groups on the cyclic part have no interactions with the DMF

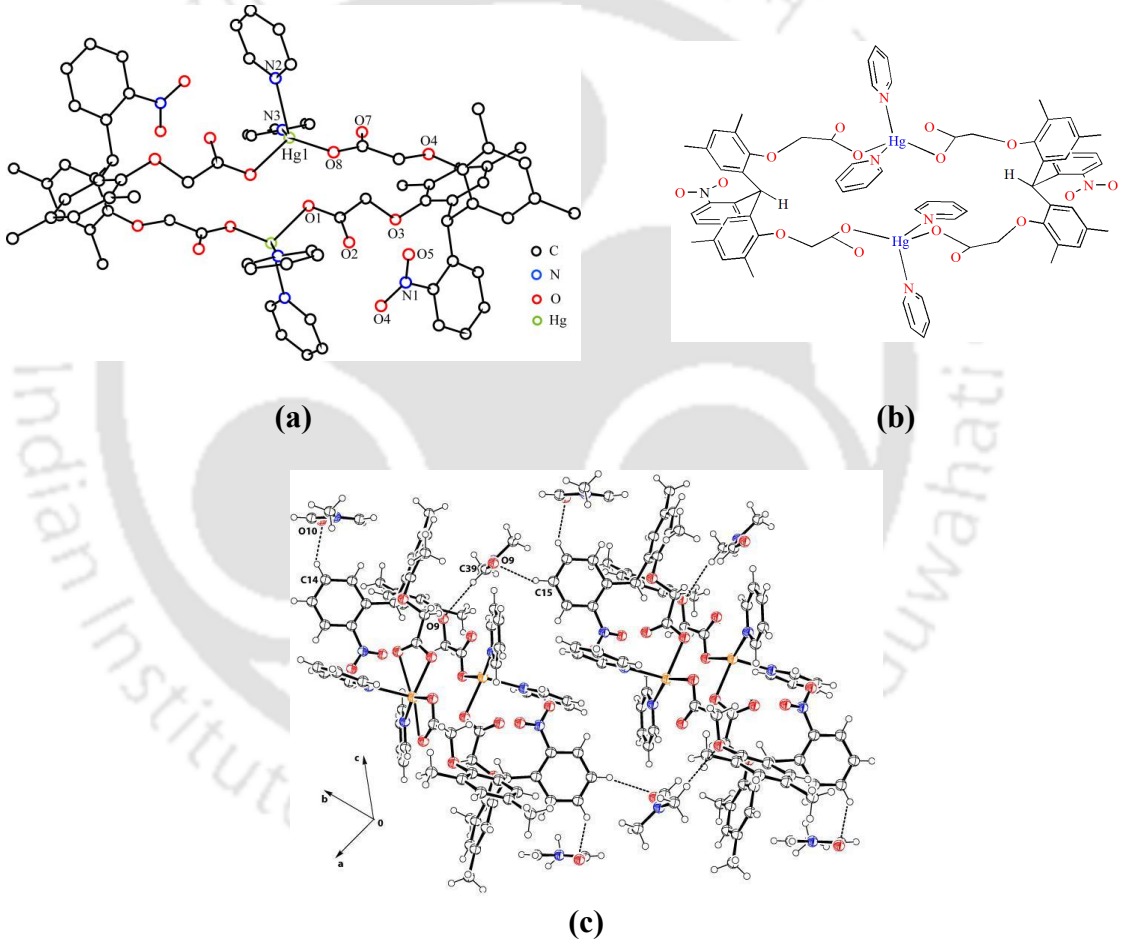

Figure **6.17**: **(a)** and **(b)** structure of the mercury metallacycle **6.3c**. **(c)** Weak interactions of DMF molecules in the crystal lattice of **6.3c**.

molecules of the lattice. The carbonyl oxygen of DMF and a C-H bond of the aromatic ring of the ligand provide C15-H···O9 interactions ($d_{D\text{-}H}$=0.929 Å; $d_{D\text{-}A}$=

3.295 Å; ∠D-H···A=140.6°) to hold the DMF in the interstices, as shown in Figure **6.17c**. The metallacycle **6.3c**, losses two lattice DMF molecules and four coordinated pyridine molecules at around 75-145°C (theoretical weight loss 24.29%, experimental weight loss 22.0%) (Figure **6.25a**).

Table 6.5: The metal-ligand bond lengths and bond angles of complex **6.3c.**

M-L	d_{M-L} (Å)	<L-M-L	angle (°)
Hg1- N3	2.227(3)	N3- Hg1- O1	119.95(13)
Hg1- O1	2.233(3)	N3- Hg1- O8	142.46(13)
Hg1- O8	2.291(3)	O1- Hg1- O8	87.03(13)
Hg1- N2	2.381(4)	N3- Hg1-N2	103.76(13)
		O1- Hg1- N2	101.88(13)
		O8-Hg1-N2	94.40(14)

6.2. Discussion:

The formation of different types of structures in different solvents by H_2L^2 and H_2L^3, shows that the solvent guides the coordination of pyridine into the coordination spheres of the metal ions in these complexes. Conversely, the numbers of pyridine molecules also decide the formation of a dinuclear metal complex or metallacycle. On the other hand, the dinuclear

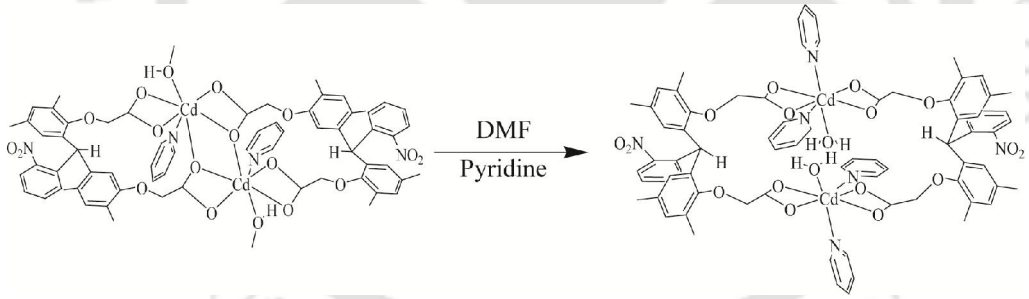

Scheme 6.4: Coversion of dinuclear complex **6.3a** to the metallacycle **6.3b** in DMF and pyridine mixture.

complex **6.3a** converted to metallacyle **6.3b** in presene of DMF and pyridine (Scheme **6.4**). These result demonstrates a process that has close analogy to the off-on of a metallacycle through the coordination effect. This important observation has relevance and analogy with tunable on-off responses for select guest molecules[23,24] by metal-organic frameworks, in which molecules may come close to self-assemble or get dis-assembled by solvent molecules or by an external ligands. Furthermore, there

are examples of cyclic molecules adopting different polymorphic structures to controls pores in transport processes.[25]

The formation different structure of the Cadmium (II) complexes with the ligands H_2L^1, H_2L^2, H_2L^3 and H_2L^4 on changing the solvent are summerized in the Table **6.6.** All the skeletal parameters, other than the substituent on the aromatic ring of the ligands are similar and the syntheses of these complexes were carried out at ambient conditions. However, the number of pyridine molecules per cadmium ion in these complexes varies. This suggests that the substituent present at the remote site of the aromatic ring also guides the incoming pyridine molecules to the coordination sphere of cadmium ions. Although dicarboxylic acids were extensively used for the designing of various metal-orgnic framework,[26] this types of metallacycle formation by flexible dicarboxylic acid is very rare. Generlly, N-containg polydentate ligands are employeed for the construction of metallacycle.[27] Some of the examples of

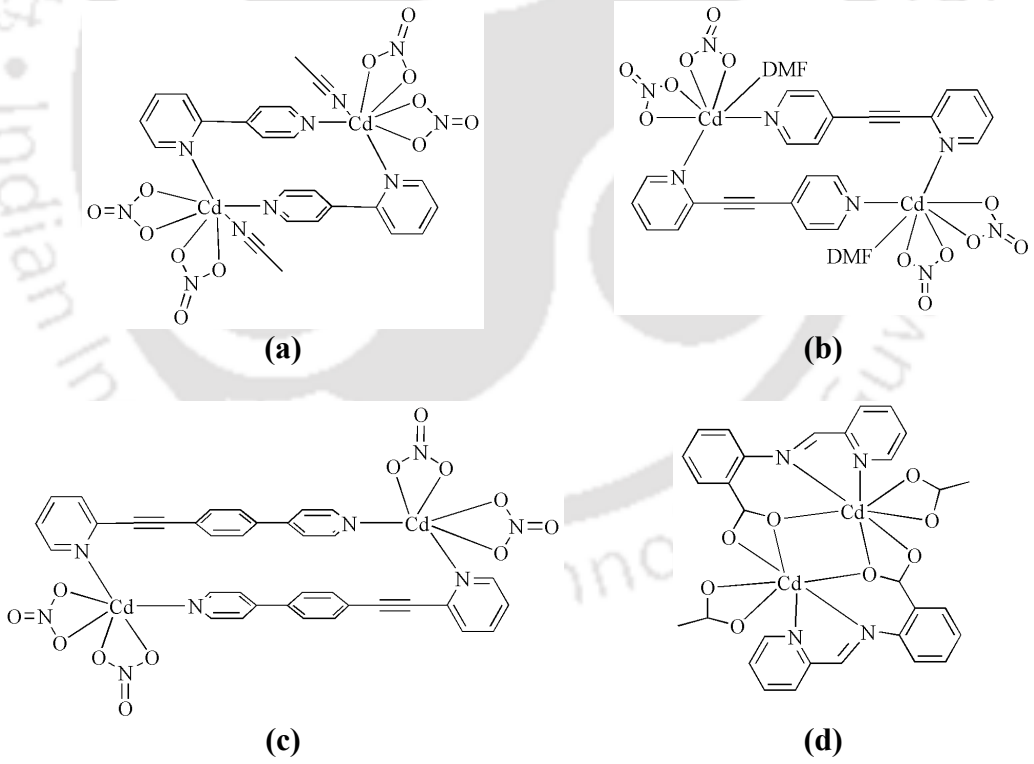

Figure 6.18: **(a)**, **(b)** and **(c)** are the examples of cadmium metallacycle formed by N-donor ligands, **(d)** Formation of Cd_2O_2-core through bridging carboxylate group in cadmium dinuclear complex formed by mixed donor ligand.

cadmium metllacycles based on N-donor ligands are shown in the Figure **6.18a, 6.1b and 6.18c.** On the other hand, nitrogen containg flexible monocarboxylic acid ligand can form dinucllear complex having Cd_2O_2 core as shown in the figure **6.18d**.[28]

Table 6.6: Formation of diffenet cadmium complexes by the ligands H_2L^1, H_2L^2, H_2L^3 and H_2L^4 in diffenet solvents:

Ligands	Solvents		
	DMF	DMSO	MeOH
H_2L^1 **(5.1)**	-	-	Coordination polymer **6.1a**
H_2L^2 **(5.2)**	Mononuclear complex **6.2a**	Dinuclear complex **6.2b**	Metallacycle **6.2c**
H_2L^3 **(5.3)**	Metallacycle **6.3b**	-	Dinuclear complex **6.3a**
H_2L^4 **(5.4)**	Metallacycle **6.4a**	-	-

6.3. Conclusion:

In conclusion, we have shown the formation of cadmium and mercury complexes with different architecture from four flexible *bis*-phenol based dicarboxylate ligands. The unsubstituted ligand H_2L^1 forms 1D coordination polymer of cadmium. In some cases, we have found the formation of a mononuclear complex, dinuclear complex, as well as the cadmium metallacycle of ligand H_2L^2 and H_2L^3 by changing the solvent. Again, the inter conversion between the metallacycle and the dinuclear complexs are possible through Cd_2O_2 core closing or opening. For example, the dinuclear complex **6.3a** converts to the metallacycle **6.3b** in presence of DMF and pyridine mixture.

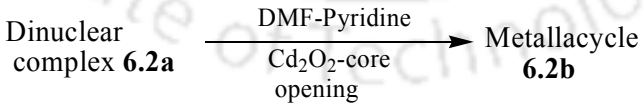

This type of inter-conversion by solvent may have applications in solvent mediated crystal to crystal transformations.

Again, this series of complexes also clearly demonstrates the role of the fluoro and nitro group on the ligand; it is shown that even when it doesn't coordinate to the cadmium or mercury ions, its presence has a striking effect on the structure of cadmium complexes. These types of substituent effect in controlling and tuning the

molecular architecture of the coordination polymers would be a potentially effective approach. We have demonstrated that a flexible tether (-CH_2CO_2) with rigid directing functionality (in this case the *bis*-phenol part) makes it possible to obtain metallacycles in ambient conditions.

6.4. Experimental section:

Complex $[CdL^1(py)_3]_n \cdot 3nH_2O$ (6.1a).To a well-stirred solution of H_2L^1 (0.224 g, 0.5 mmol) and sodium hydroxide (0.02 g) dissolved in methanol (10 ml), $CdCl_2.H_2O$ (0.093 g, 0.5 mmol) was added. The white precipitate obtained was dissolved by the addition of the minimum amount of pyridine. The reaction mixture was filtered and the transparent liquid was kept for crystallization. After one week colorless needle-like crystals were obtained. Isolated yield: 50%. IR (KBr, cm^{-1}): 3426 (bs), 2924 (s), 2855 (w), 1600 (s), 1447 (s), 1415 (m), 1327 (w), 1245 (w), 1208 (m), 1141 (m), 1036 (s), 760 (w), 702 (s). ^{1}H-NMR (DMSO-d_6): 8.58 (s, 6H), 7.79 (7.6 Hz, t, 6H), 7.21 (5.3 Hz, t, 3H), 7.18 (t, 7.0 Hz, 1H), 6.98 (d, 6.2 Hz, 2H), 6.85 (s, 2H), 6.43 (s, 2H), 6.37 (s, 1H), 4.01 (s, 4H), 2.14 (s, 6H), 2.11 (s, 6H).

Complex $[Cd\ L^2(py)_2(H_2O)]$ (6.2a): To a well-stirred solution of H_2L^2 (0.233 g, 0.5 mmol) in DMF (10 ml), 0.4 g of NaOH (1 mmol) was added and allowed to stir about 10 minutes. After 10 mintues cadmium (II) chloride monohydrate (0.090 g, 0.5 mmol) was added to the reaction mixture. The white precipitate obtained was dissolved by the addition of the minimum amount of pyridine. The reaction mixture was filtered and the transparent liquid was kept for crystallization. After one week colorless needle-like crystals were obtained. Isolated yield: 45%. IR (KBr, cm^{-1}) 3407 (s), 2923 (m), 1667 (s), 1599 (s), 1487 (s), 1447 (s), 1417 (s), 1321 (m), 1243 (w), 1213 (s), 1142 (m), 1095 (m), 1036 (s), 940 (w), 863 (w), 829 (w), 756 (m), 690 (m), 628 (w): ^{1}H-NMR (DMSO-d_6): 8.65 (*s*, 2H), 7.99 (*d*, J= 1.6Hz, 1H), 7.54 (*t*, J=4.4 Hz, 2H), 7.27 (*dd*, J= 4.4 Hz, 6.4 Hz 1H), 7.12 (*d*, J= 8Hz, 1H), 7.10 (*d*, J=7.6Hz, 1H), 6.92 (*s*, 2H), 6.78 (*t*, J= 8 Hz), 6.39 (*s*, 2H), 6.30 (*s*, 1H), 4.03 (*s*, 4H), 2.16 (*s*, 6H), 2.12 (*s*, 6H), ^{19}F-NMR (DMSO-d_6): -118.11 (using C_6F_6 as internal reference).

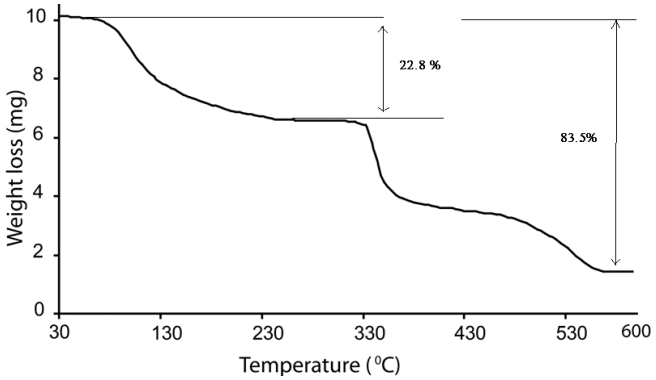

Figure 6.19: TG of mononuclear complex **6.2a.**

Complex $[CdL^2(py)(DMSO)]_2$ (6.2b): To a well-stirred solution of H_2L (0.233 g, 0.5 mmol) in DMSO (10 ml), 0.4 g of NaOH (1 mmol) was added and allowed to stir about 10 minutes. After 10 mintues cadmium (II) chloride monohydrate (0.090 g, 0.5 mmol) was added to the reaction mixture. The white precipitate obtained was dissolved by the addition of the minimum amount of pyridine. The reaction mixture was filtered and the transparent liquid was kept for crystallization. After 10-12 days colorless needle-like crystals were obtained. Isolated yield: 40%. IR (KBr, cm^{-1}) : 3409 (s), 3000 (w), 2916 (w), 2862 (w), 1599 (s), 1485 (m), 1446 (s), 1426 (s), 1320 (s), 1297 (w), 1212 (s), 1143 (s), 1094 (w), 1037 (s), 948 (m), 861 (w), 830 (w), 756 (m), 702 (m), 628 (w), 604 (w), 578 (w). ^{1}H-NMR (DMSO-d_6): 8.58 (*s*, 2H), 7.79 (*t*, 6.4 Hz, 1H), 7.38 (*t*, 6 Hz, 2H), 7.26 (*dd*, 5.6 Hz, 5.4 Hz, 1H), 7.09 (*s*, 1H), 7.07 (*d*, 6.4 Hz, 1H), 6.90 (*s*, 2H), 6.68 (*t*, 6.8, 1H), 6.40 (*s*, 1H), 6.38 (*s*, 2H), 4.09 (*s*, 4H), 2.53 (*s*, 6H), 2.16 (*s*, 6H), 2.12 (*s*, 6H). ^{19}F-NMR (DMSO-d_6): -117.06 (using C_6F_6 as internal reference).

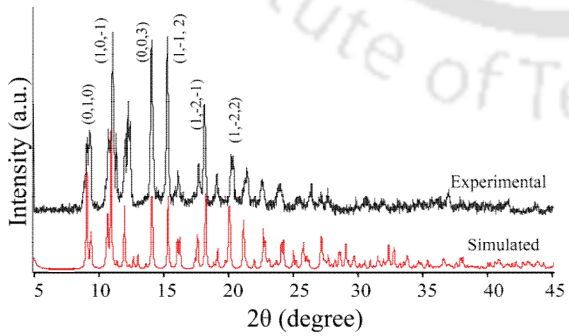

(a)

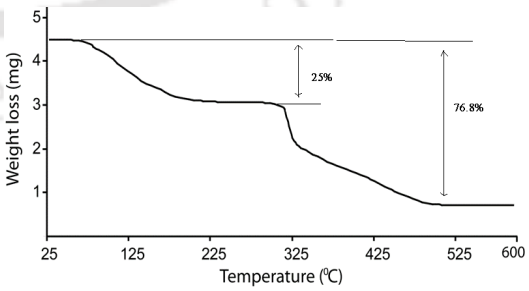

(b)

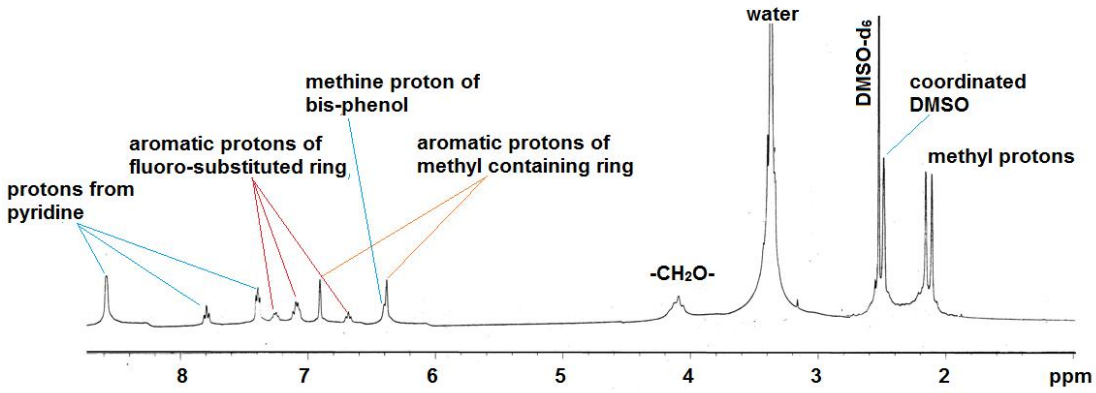

(c)

Figure 6.20: **(a)** Comparison of the simulated and the experimental PXRD of **6.2b. (b)** TG of the dinuclear complex **6.2b**. **(c)** ^{1}H-NMR of the dinuclear complex **6.2b** (DMSO-d_6, 400 MHz).

Complex {[CdL^2(py)(H$_2$O)]$_2$}.py. MeOH (6.2c): To a well-stirred solution of H_2L (0.233 g, 0.5 mmol) in methanol (10 ml), 0.4 g of NaOH (1 mmol) was added and allowed to stir about 10 minutes. After 10 mintues cadmium (II) chloride monohydrate (0.090 g, 0.5 mmol) was added to the reaction mixture. The white precipitate obtained was dissolved by the addition of the minimum amount of pyridine. The reaction mixture was filtered and the transparent liquid was kept for crystallization. After 2-3 days colorless block crystals appeared which are suitable for single crystal analysis. Isolated yield: 55%. IR (KBr, cm^{-1}): 3432 (m), 3065 (w), 2920 (m), 2862 (w), 1599 (s), 1475 (m), 1447 (s), 1426 (s), 1322 (m), 1297 (w), 1212 (s), 1142 (s), 1037 (s), 1009 (w), 945 (w), 859 (w), 835 (w), 756 (s), 701 (s), 627 (w). ^{1}H-NMR (MeOH-d_4): 8.43 (*s*, 2H), 7.72 (*t*, J=7.6 Hz, 1H), 7.72 (*t*, J= 6Hz, 2H), 7.07 (*dd*, J=6.0 Hz, J=4.2 Hz), 6.90 (*t*, J= 7.2 Hz), 6.82 (*d*, J= 9.2 Hz), 6.78 (*s*, 2H), 6.39 (*s*, 2H), 6.28 (*s*, 1H), 3.92 (*s*, 4H), 2.07 (*s*, 6H), 2.00 (*s*, 6H). ^{19}F-NMR (DMSO-d_6): -117.04 (using C_6F_6 as internal reference).

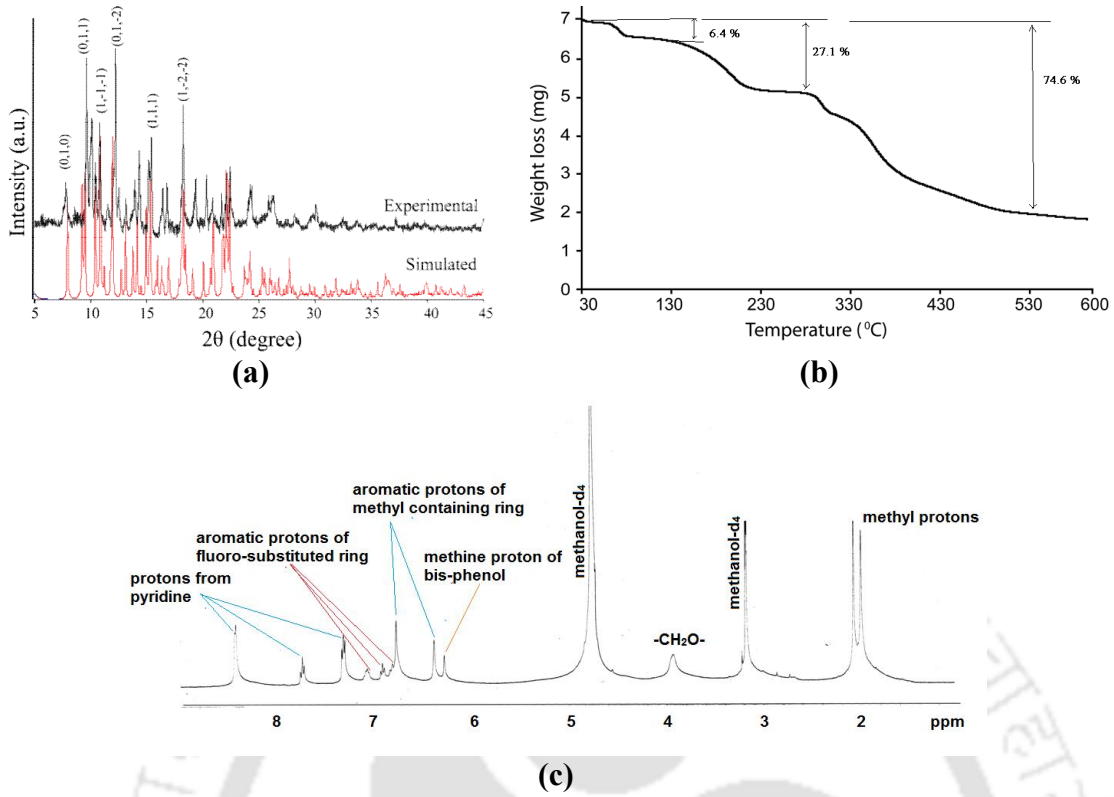

Figure **6.21**: (a) Comparison of the simulated and the experimental PXRD of **6.2c. (b)** TG of the dinuclear complex **6.2c**. **(c)** ^{1}H-NMR of the dinuclear complex **6.2c** (DMSO-d_6, 400 MHz).

Complex $[CdL^{3}(py)(CH_3OH)]_2 \cdot CH_3OH$ (6.3a): To a well-stirred solution of H_2L^{3} (0.246 g, 0.5 mmol) and sodium hydroxide (0.02 g) dissolved in methanol (10 ml), cadmium (II) chloride monohydrate $CdCl_2.H_2O$ (0.093 g, 0.5 mmol) was added. A white precipitate was obtained, which was dissolved by the addition of the minimum amount of pyridine. The reaction mixture was filtered and the transparent liquid was kept for crystallization. After one week light yellow needle-like crystals were obtained. Isolated yield: 60%. IR (KBr, cm^{-1}): 3438 (bs), 2953 (w), 2920 (w), 2859 (w), 1599 (s), 1525 (s), 1473 (m), 1445 (m), 1427 (m), 1351 (m), 1296 (w), 1210 (s), 1143 (s), 1044 (s), 860 (m), 817 (w), 704 (s). ^{1}H-NMR (DMSO-d_6): 8.58 (d, 6.2 Hz, 2H). 7.93 (d, 8 Hz, 1H), 7.79 (t, 6.4, 1H), 7.60 (t, 7.6 Hz, 1H), 7.49 (t, 7.6 Hz, 1H), 7.39 (t, 5.6 Hz, 2H), 6.90 (s, 2H), 6.88 (d, 8 Hz, 1H), 6.65 (s, 1H), 6.25 (s, 2H), 4.10 (s, 4H), 2.15 (s, 6H), 2.10 (s, 1H).

Complex $[CdL^{3}(py)_2(H_2O)]_2 \cdot H_2O$ (6.3b): This was prepared by exactly the same procedure as for **6.3a**, but instead of methanol, dimethylformamide was used as the

solvent. After one week colorless block crystals were obtained. Isolated yield: 80%. IR (KBr, cm^{-1}): 3438 (bs), 2920 (w), 1679 (s), 1578 (m), 1529 (s), 1443 (m), 1347 (m), 1213 (s), 1144 (s), 1037 (s), 706 (s).^{1}H-NMR (DMSO-d_6): 8.58 (d, 4.0 Hz, 4H), 7.93 (t, 5.6 Hz, 1H), 7.79 (t, 1.6 Hz, 2H), 7.59 (t, 6 Hz, 1H), 7.51 (t, 7.6 Hz, 1H), 7.39 (t, 1.6 Hz, 4H), 6.90 (d, 6.4 Hz, 2H), 6.87 (d, 8.0 Hz, 1H), 6.66 (s, 1H), 6.23 (s, 2H), 4.09 (s, 4H), 2.16 (s, 6H), 2.10 (s, 6H).

Alternatively, complex **6.3b** can be prepared by dissolving complex **6.3a** in a DMF-pyridine solvent and slow evaporation of the solvent at room temperature for several days.

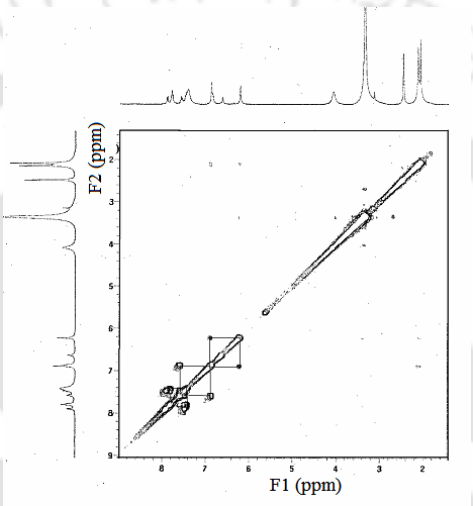

(a)

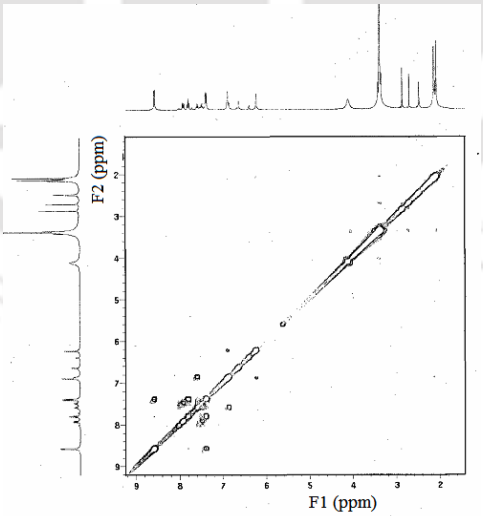

(b)

Figure **6.22**: **(a)** ^{1}H-HOMO-COSY spectra of **6.3a** (DMSO-d_6, 400 MHz). **(b)** ^{1}H-HOMO-COSY spectra of **6.3b** (DMSO-d_6, 400 MHz).

Complex $[CdL^4(py)_2(H_2O)]_2 \cdot 3H_2O$ (6.4a): To a well-stirred solution of H_2L^4 (0.25 g, 0.5 mmol) and sodium hydroxide (0.02 g) dissolved in methanol (10 ml), cadmium(II) chloride monohydrate (0.09 g, 0.5 mmol) was added. A white precipitate was obtained, which was dissolved by the addition of the minimum amount of pyridine. The reaction mixture was filtered and the transparent liquid was kept for crystallization. After one week colorless needle-like crystals were obtained. Isolated yield: 55%. IR (KBr, cm^{-1}): 3433 (bs), 2923 (m), 1633 (s), 1525 (w), 1446 (w), 1348 (w), 1213 (m), 1143 (m), 1055 (w), 864 (w), 698 (m). ^{1}H-NMR (DMSO-d_6): 8.58 (s, 2H), 8.02 (d, 6.8 Hz, 1H), 7.77 (t, 7.6 Hz, 2H), 7.74 (s, 1H), 7.50 (t, 6.8 Hz, 1H), 7.37 (t, 5.6 Hz, 2H), 6.91 (s, 2H), 6.74 (s, 1H), 6.39 (s, 2H), 4.08 (d, 14.4 Hz, 4H), 4.02 (d, 14.4 Hz, 4H), 2.16 (s, 6H), 2.12 (s, 6H).

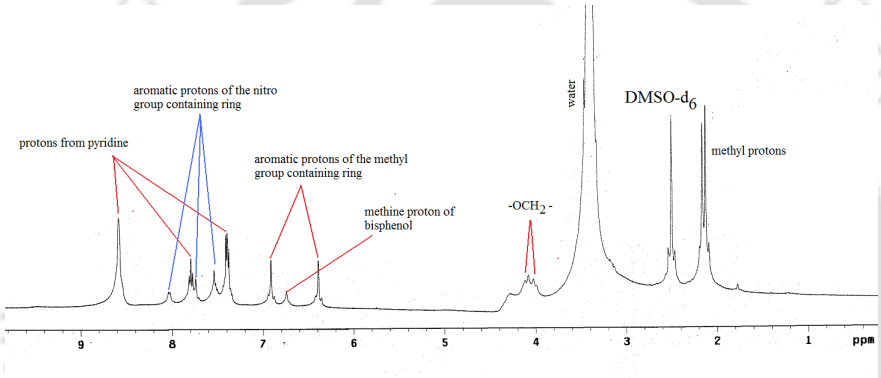

Figure **6.23**: ^{1}H-NMR of the metallacycle **6.4a** (DMSO-d_6, 400 MHz).

Complex $[HgL^3(py)_2]_2 \cdot DMF$ (6.3c): To a well-stirred solution of H_2L^3 (0.25 g, 0.5 mmol) and sodium hydroxide (0.02 g) dissolved in dimethylformamide (10 ml), mercury (II) chloride (0.135 g, 0.5 mmol) was added. A white precipitate was obtained, which was dissolved in the minimum amount of pyridine. Any residue at this stage was filtered and the transparent liquid was kept for crystallization. After one week crystals were obtained. Isolated yield: 55%. IR (KBr, cm^{-1}): 3432 (bs), 1609 (s), 1537 (m), 1474 (w), 1415 (m), 1363 (w), 1321 (w), 1299 (w), 1239 (w), 1214 (w), 1142 (m), 1031 (m), 860 (w), 713 (m). ^{1}H-NMR (DMSO-d_6): 8.69 (d, 4.4 Hz, 4H), 7.97 (s, 1H), 7.94 (s, 2H), 7.89 (t, 1.6 Hz, 1H), 7.60 (t, 7.2 Hz, 1H), 7.52 (t, 7.6 Hz, 4H), 6.92 (s, 2H), 6.87 (d, 7.6 Hz, 1H), 6.75 (s, 1H), 6.26 (s, 2H), 4.45 (d, 14 Hz, 2H), 4.24 (d, 15.2 Hz, 2H), 2.17 (s, 6H), 2.11 (s, 6H).

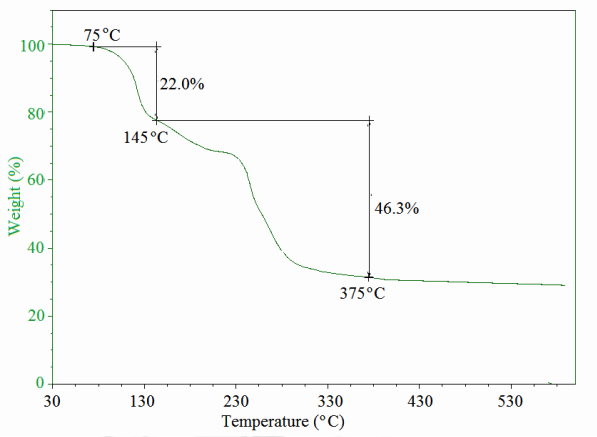

(a)

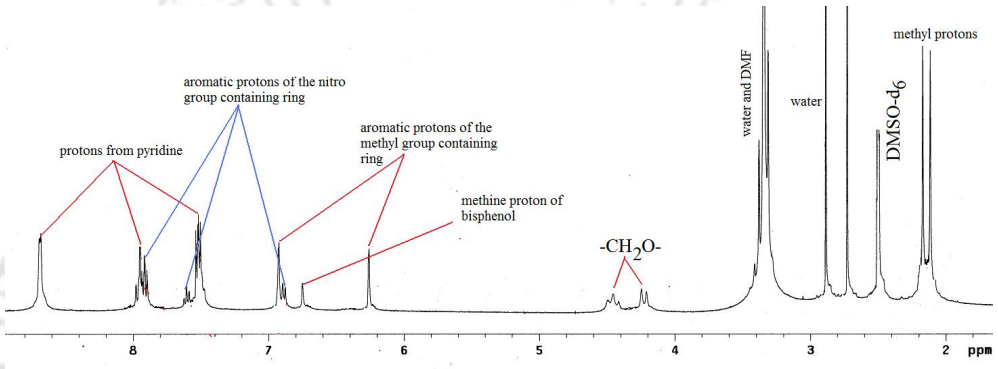

(b)

Figure **6.24 (a)** TG of the metallacycle **6.3c** (heating rate 5°C/ minutes), **(b)** ^{1}H-NMR of the metallacycle **6.3c** (DMSO-d_6, 400 MHz).

References:

1. (a) S. Samai, K. Biradha, *Cryst. Growth Des.*, 2011, **11**, 5723-5732; (b) P. Cui, J. Dou, D. Sun, F. Dai, S. Wang, D. Sun, Q. Wu, *CrystEngComm*, 2011, **13**, 6968-6971; (c) G. -Q. Kong, C. -D. Wu, *Cryst. Growth Des.*, 2010, **10**, 4590-4595; (d) B. Ding, Y. -Y. Liu, Y. -Q. Huang, W. Shi, P. Cheng, D. -Z. Liao, S. -P. Yan, *Cryst. Growth Des.*, 2009, **9**, 593-601.
2. (a) Z. Dong, Y. Y. Wang, R. T. Liu, J. Q. Liu, L. Cui, Q. Z. Shi, *Cryst. Growth Des.*, 2010, **10**, 3311-3314; (b) H. Wang, D. Zhang, D. Sun, Y. Chen, L. F. Zhang, L. Tian, J. Jiang, Z. H. Ni, *Cryst. Growth Des.*, 2009, **9**, 5273-5282; (c) L. Carlucci, G. Ciani, D. M. Proserpio, *Coord. Chem. Rev.*, 2003, **246**, 247-289; (d) X. Shi, G. Zhu, X. Wang, G. Li, Q. Fang, G. Wu, G. Tain,

M. Xue, X. Zhao, R. Wang, S. Qiu, *Cryst. Growth Des.*, 2005, **5**, 207-213; (e) C. D. Wu, W. Lin, *Angew. Chem., Int. Ed.*, 2007, **46**, 1075-1078; (f) R. -Q. Zou, H. Sakurai, S. Han, R. -Q. Zhong, Q. Xu, *J. Am. Chem. Soc.*, 2007, **129**, 8402-8403; (g) H. -L. Jiang, B. Liu, Q. Xu, *Cryst. Growth Des.*, 2010, **10**, 806-811; (h) J. Hu, L. Huang, X. Yao, L. Qin, Y. Li, Z. Guo, H. Zheng, Z. Xue, *Inorg. Chem.*, 2011, **50**, 2404-2414.

3. (a) C. Mellot-Draznieks, G. Ferey, *Prog. Solid State Chem.*, 2005, **33**, 187-197; (b) O. M. Yaghi, M. Keeffe, N. W. Ockwig, H. K. Chae, M. Eddaoudi, J. Kim, *Nature*, 2003, **423**, 705-714; (c) B. Moulton, M. J. Zaworotko, *Chem. Rev.*, 2001, **101**, 1629-1658.
4. A. M. Baruah, A. Karmakar, J. B. Baruah, *Open Inorg. Chem. J.*, 2008, **2**, 62-68.
5. (a) D. Banerjee, J. Finkelstein, A. Smirnov, P. M. Forster, L. A. Borkowski, S. J. Teat, J. B. Parise, *Cryst. Growth Des.*, 2011, **11**, 2572-2579; (b) S. C. Chen, Z. H. Zhang, K. L. Huang, Q. Chen, M. Y. He, A. J. Cui, C. Li, Q. Liu, M. Du, *Cryst. Growth Des.*, 2008, **8**, 3437-3445; (c) X. C. Huang, D. Li, X. M. Chen, *CrystEngComm*, 2006, **8**, 351-357; (d) W. M. Singh, J. B. Baruah, *Dalton Trans.*, 2009, 2352-2358.
6. (a) L. Li, S. Wang, T. Chen, Z. Sun, J. Luo, M. Hong, *Cryst. Growth Des.*, 2012, **12**, 4109-4115; (b) J. Xiao, B. -Y. Liu, G. Wei, X. -C. Huang, *Inorg. Chem.*, 2011, **50**, 11032-11038; (c) K. Davies, S. A. Bourne, C. L. Oliver, *Cryst. Growth Des.*, 2012, **12**, 1999-2003; (d) L. Cui, G. -P. Yang, W. -P. Wu, H. -H. Miao, Q. Shi, Y. -Y. Wang, *Dalton Trans.***,** 2014, DOI: 10.1039/C3DT53342E; (e) X. Zhou, P. Liu, W. -H. Huang, M. Kang, Y. -Y. Wang, Q. -Z. Shi, *CrystEngComm*, 2013, **15**, 8125-8132.
7. (a) L. -Y. Zhang, J. -P. Zhang, Y. -Y. Lin, X. -M. Chen, *Cryst. Growth Des.*, 2006, **6**, 1684-1689; (b) C. -S. Liu, J. -J. Wang, Z. Chang, L. -F. Yan X. -H. Bu, *CrystEngComm*, 2010, **12**, 1833-1841; (c) M. A. Braverman, R. M. Supkowski, R. L. LaDuca, *J. Solid State Chem.*, 2007, **180**, 1852-1862; (d) D. P. Martin, M. R. Montney, R. M. Supkowski, R. L. LaDuca, *Cryst. Growth Des.*, 2008, **8**, 3091-3097; (e) E. M. Lyons, M. A. Braverman, R. M. Supkowski, R. L. LaDuca, *Inorg. Chem. Commun.*, 2008, **11**, 855-858.

8. Z. Chen, X. Wu, S. Qin, C. Lei, F. Liang, *CrystEngComm*, 2011, **13**, 2029-2038.
9. B. C. Burckhardt, B. Drinkuth, C. Menzel, A. Konig, J. Steffgen, S. H. Wright, G. Burckhardt, *J. Am. Nephrol.*, 2002, **13**, 2628-2638.
10. O. Peise, L. Ji, S. W. Theil, N. G. Pinto, *Main Group Chem.*, 2008, **7**, 181-189.
11. T. Yamane, N. Davidson, *J. Am. Chem. Soc.*, 1960, **82**, 2123-2129.
12. L. Friberg, C. G. Elinder, T. Kjellstrom, *Cadmium*; World Health Organization: Geneva, Switzerland, 1992; (b) M. P. Waalkes, *J. Inorg. Biochem.*, 2000, **79**, 241-244; (c) H. H. Harris, I. J. Pickering, G. N. George, *Science*, 2003, **301**, 1203-1203; (d) P. Grandjean, P. Weihe, R. F. White, F. Debes, *Environ. Res.*, 1998, **77**, 165-172.
13. Z. -B. Zheng, R. -T. Wu, J. -K. Li, Y. -F. Sun, Y. -F. Han, *J. Mol. Struct.*, 2010, **964**, 109-118.
14. B. Nath, D. Kalita, J. B. Baruah, J. Coord. Chem., 2011, **64**, 2545-2553.
15. D. N. Styanaryana, *Vibrational Spectrocopy: Theory and applications*. New-age International, New-Delhi, India, 2007.
16. M. Nishio, Y. *Phys. Chem. Chem. Phys.*, 2011, **13**, 13873-13900.
17. M. Nisho, Y. Umezawa, H. Suezaa, S. Tsuboyama, in *The importance of π-interactions in crystal engineering: Frontiers in crystal engineering.* Eds E. R. T. Tiekink and Zukerman-Schpector. Ch. 1; 2012 John Wiley & Sons, Ltd.
18. M. D. Prasnna, T. N. Guru Row, *CrystEngComm*, 2000, **3**, 134-140.
19. (a) D. Chopra, *Cryst. Growth Des.*, 2012, **12**, 541-546; (b) K. Reichenbacher, H. I. Suss, J. Hulliger, *Chem. Soc. Rev.*, 2005, **34**, 22-30.
20. (a) T. Gueden-Silber, K. Klein, M. Allouchi, *Dalton Trans.*, 2013, **42**, 13882-13888; (b) N. R. Rhodes, K. Belmore, C. J. Cssady, J. B. Vincent, Polyhedron, 2013, **64**, 136-141.
21. (a) A. Karmakar, K. Bania, A. M. Baruah, J. B. Baruah, *Inorg. Chem. Commun.*, 2007, **10**, 959-964; (b) A. M. Baruah, A. Karmakar, J. B. Baruah, *Inorg. Chim. Acta*, 2008, **361**, 2777-2784.
22. (a) F. Dai, S. Gong, P. Cui, G. Zhang, X. Qiu, F. Ye, D. Sun, Z. Pang, G. L. Zhang, C. D. Zhang, *New J. Chem.*, 2010, **34**, 2496-2501.
23. P. A. Write, *Science*, 2010, **329**, 1025-1026.

24. (a) C. Serre, C. Mellot-Draznieks, S. Surble, N. Audebrand, Y. Filinchuk, G. Férey, *Science*, 2007, **315**, 1828-1831; (b) S. Horike, S. Shimomura, S. Kitagawa, *Nat. Chem.*, 2009, **1**, 695-704; (c) D. Bradshaw, J. E. Warren, M. J. Rosseinsky, *Science*, 2007, **315**, 977-980.
25. J. T. A. Jones, D. Holden, T. Mitra, T. Hasell, D. J. Adams, K. E. Jelfs, A. Trewin, D. J. Willock, G. M. Day, J. Bacsa, A. Steiner, A. I. Cooper, *Angew. Chem. Int. Ed.*, 2011, **50**, 749-753.
26. (a) Z. -M. Sun, J. -G. Mao, Y. -Q. Sun, H. -Y. Zeng, A. Clearfield, *Inorg. Chem.*, 2004, **43**, 336-341; (b) R. Wang, J. Zhang, L. Li, *Inorg. Chem.*, 2009, **48**, 7194-7200; (c) L. Wang, M. Yang, G. Li, Z. Shi, S. Feng, *Inorg. Chem.*, 2006, **45**, 2474-2478; (d) O. R. Evans, W. Lin, *Inorg. Chem.*, 2000, **39**, 2189-2198.
27. A. N. Khlobystov, M. T. Brett, A. J. Blake, N. R. Champness, P. M. W. Gill, D. P. O'Neill, S. J. Teat, C. Wilson, M. Schroder, *J. Am. Chem. Soc.*, 2003, **125**, 6753-6761; (b) D. L. Reger, A. E. Pascui, P. J. Pellechia, M. D. Smith, *Inorg. Chem.*, 2013, **52**, 11638-11649.
28. S. Shit, J. Chakraborty, B. Samanta, G. Pilet, S. Mitra, *J. Mol. Struct.*, 2009, **919**, 361-365.

CHAPTER 1

Introduction

1.1 General introduction on hydrogen bond and their assemblies:

Hydrogen bond is one of the principal weak interaction which helps in the construction of various supramolecular assemblies.[1] Hydrogen bond is defined as a form of association between an electronegative atom and a hydrogen atom attached to a second, relatively electronegative atom.[1e,f] It is a particular kind of dipole-dipole interaction in which the hydrogen atom attached to an electronegative atom (or electron withdrawing group) is attracted towards neighbouring electronegative atom. Hydrogen bonds are typically written as D-H···A which involve a hydrogen atom attached to an electronegative atom, for example, O or N as the donor (D) and similarly electronegative atom bearing a lone pair as an acceptor (A). There is also significant hydrogen bond interactions where carbon acts as donor rather than nitrogen or oxygen.[2] Hydrogen bonds have a wide spread of bond lengths and angles and accordingly hydrogen bond interactions between hydrogen bond donor D and acceptor A (D-H···A), may be classified as strong, moderate and weak.[3] Different parameters that are used to define the strength of the hydrogen bond can be depicted with the help of Figure **1.1**. A strong hydrogen bond is somewhat similar in character

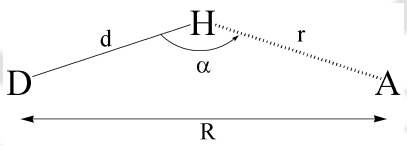

Figure 1.1: Schematic representation of hydrogen bond.

Table 1.1: Donor acceptor distances and angles in hydrogen bonds

Parameters	Strong	Moderate	Weak
Bond energy ($kJmol^{-1}$)	60-120	16-60	Less than 12
H···A (r Å)	1.2-1.5	1.5-2.2	2.2-3.2
D···A (R Å)	2.2-2.5	2.5-3.2	3.2-4.0
<D-H···A (α°)	175-180	130-180	90-150

to a covalent bond and generally forms between strong acid and good hydrogen bond acceptor whereas the moderate hydrogen bonds form between neutral donor and neutral acceptor via lone pairs of electron and do not have linear geometry but are slightly bent. The parameters that tentatively decide the classification of hydrogen bonded system in terms of its strength are listed in the Table **1.1.**

Various functional groups that have hydrogen atom attached to an electronegative element can behave as hydrogen bond donors and an electron rich element within the compound or from a different one may behave as hydrogen bond acceptor leading to intra and intermolecular hydrogen bonds. The complementary nature of hydrogen bonds in different functional groups show clear preferences for specific hydrogen bond patterns in their solid state structures, despite the presence of other unpredictable and non specific lattice forces.[4] Although hydrogen bonds are form between many types of components, amide and carboxylic acid groups are most studied, because, both of them can act as hydrogen bond donor as well as acceptor. Some of the common hydrogen bonded structures from acid and amide are depicted in the Figure **1.2.**[5]

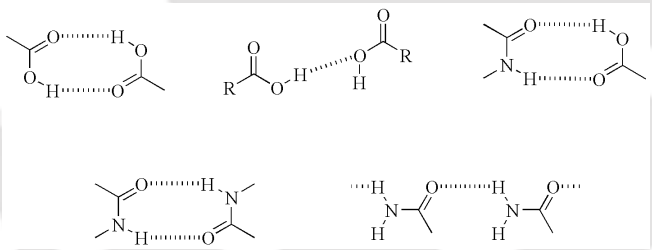

Figure 1.2: Some commonly observed hydrogen bonded motifs from acid-acid, acid-amide and amide-amide interactions.

Due to directional properties of hydrogen bonds, the assemblies formed by such interactions are generally ordered. Such orderliness has helped in many natural processes and in making different hydrogen bonded assemblies of molecules with novel properties. Different hydrogen bonded motifs namely linear, infinite chain, cyclic type are present in different possible ways and these are generally termed as synthons.[6] The non covalent bond between two molecules in supramolecular assemblies can be thought as supramolecular synthon. The hydrogen bonded rings are

among the most beautiful and most versatile supramolecular synthons in crystal engineering.[7] In general, some functional groups have strong tendency towards the formation of these types of cyclic hydrogen bonded synthons and some examples are depicted in the Figure **1.3**

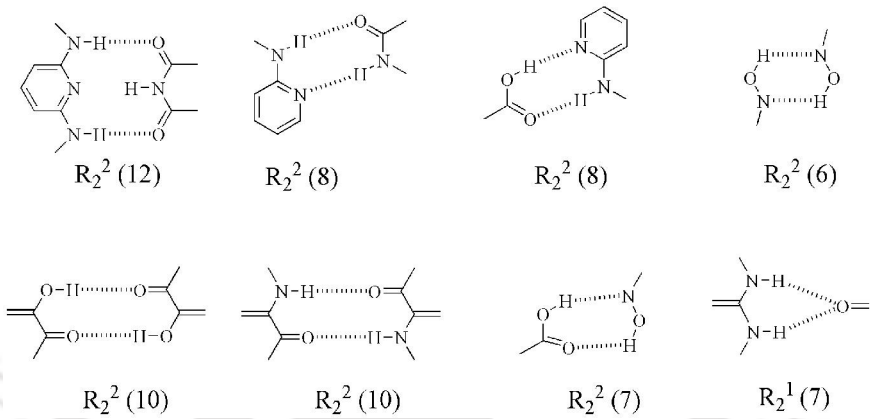

Figure 1.3: Some cyclic hydrogen bonded synthons.

1.2 Hydrogen bonded assemblies of V-shaped molecules:

Development of novel building blocks with appropriate hydrogen-bond sites is an essence of various supramolecular architectures. Among various structures, linear and tetrahedral molecules are commonly used for the construction of various network structures.[8] Irrespective of shape of the molecules, a hydrogen bonded system can be made by self-assembling or assemblies mediated by guest molecules. Among the molecules having bent geometry, V-shaped molecules have attracted significant attention in the supramolecular chemistry in last few decades.[9] Water is the simplest V-shaped molecule which can acts as donor or acceptor.[10] The different types of assemblies of water in the form of water clusters (Figure **1.4**) or solvent of crystallisation have generated extensive chemistry and plays a major role in biological systems.[11] Complicacy in self-assembled structures of water arises from its multiple donor as well as acceptor hydrogen bond sites. These can be manipulated in an organic V-shaped molecule, which has two sites as hydrogen bond acceptors, or two sites as hydrogen bond donor or combination of an acceptor and a donor. Further to

such wide range of possibilities to generate assemblies and host-guest systems, the V-shaped molecules have advantage of having the shapes of cleft and scissor which

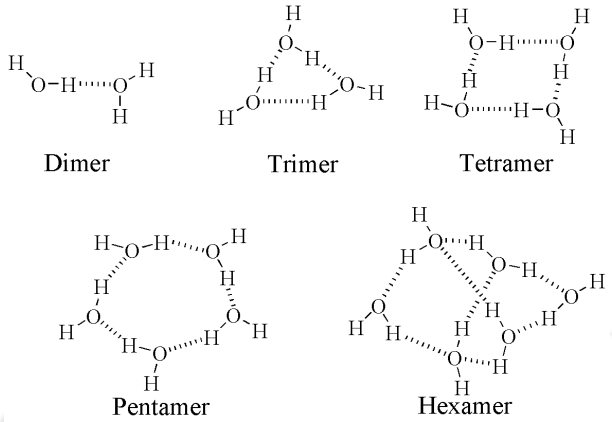

Figure 1.4: Formation of different self-assembling by water molecules.

are commonly used in molecular recognition. Moreover, the recognition of anions by non covalent interaction is a major interest in supramolecular chemistry. The molecular properties in such systems occur due to preorganised structures that complements with the guest geometry. V-shaped molecules also possess voids and pores in their solid state structures. Such voids may be occupied with guest molecules which controls the supramolecular architecture of the host. For example, 1,2-bis(3-hydroxyphenylethynyl)benzene **(1.1)** is a V-shaped molecule which has screw type packing arrangement. The solid state structure has tetrahedral cavities occupied by

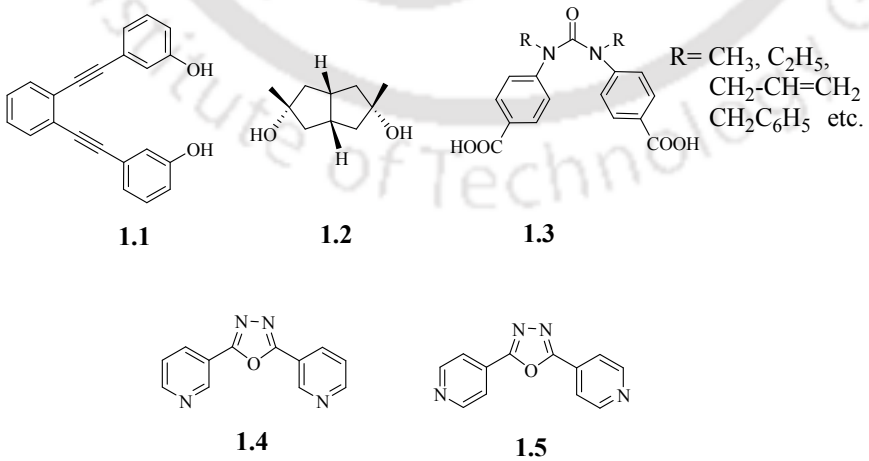

1.1 **1.2** **1.3**

1.4 **1.5**

Figure 1.5: Example of some V-shaped molecule **1.1**-**1.5**.

water molecules.[12] Another similar example is the packing of 3,7-dimethylbicyclo [3.3.0] octane-endo-3-endo-7-diol **(1.2).** It has V-shaped geometry and is capable of forming hemi-hydrates, hydrates and clathrates.[13]

Urea is a V-shaped molecule and its derivatives have different types of structures.[14] Substituted urea molecules are broadly classified from structural point of view as symmetric and non-symmetric. A tetra N-substituted urea skeleton **1.3** (Figure **1.5**) self-assembles to give ladder type and zig-zag packing pattern, and such packing patterns depend on the substituents **R** on the urea nitrogen atoms.[15] V-shaped bipyridines **1.4** and **1.5** form binary co-crystals with trimesic and pyromellitic acid, each of them has independent network structures at ambient conditions.[16]

Due to the pre-organised structure of 2,7-bis(1H-pyrrol-2-yl)ethynyl-1,8-naphthyridine **(1.6, BPN)**[17] has complementing hydrogen bonds with octylglucopyranoside (OGU) and it selectively binds to OGU (Figure **1.6**). This selective binding has helped it to be an ultra sensitive fluorescent probe for octylglucopyranoside.

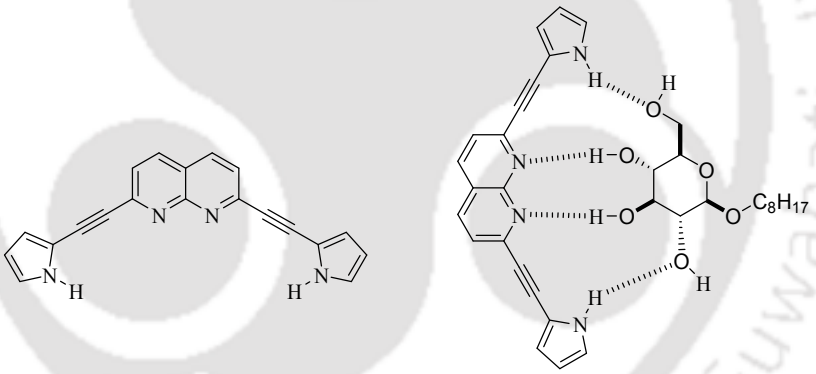

1.6 **1.7**

Figure 1.6: The structure of **1.6** and host-guest complex of OGU with octylglucopyranoside **(1.7)**.

Small solvent molecules such as dichloromethane, tetrahydrofuran, chloroform, and benzene form inclusion compound with 1,4,8,11-Tetrabromo-5bα,6,12bα,13-tetrahydropentaleno[1,2-b:4,5-b']diquinoline **(1.8a)** and its analogue **1.8b, 1.9a** and **1.9b** (Figure **1.3**).[18a-b] The sulphur bridged diquinoline derivative 6,7,14,15-tetrahydro-6,14-thiacycloocta[1,2-b:5,6-b']diquinoline **1.10a**[18c] and **1.10b**[18d] have V-shaped geometries and they are capable of forming solvate with various solvents.

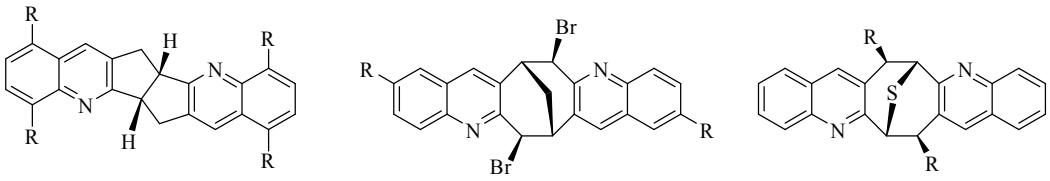

R= Br, **1.8a**
I, **1.8b**

R= H, **1.9a**
Cl,**1.9b**

R= H, **1.10a**
Br,**1.10b**

Figure 1.7: Some V-shaped diquinoline derivatives.

Troger base has been used to generate various rigid structural motifs with V-shaped molecular scaffolds where two aryl rings are almost perpendicular to each other. This important shape has considerable role to recognise guest molecules and numbers of receptors were developed based on this structural motif. For example, the compound **1.11** is used as colorimetric sensor for fluoride ion.[19] The naphthalimide based V-shaped receptor **1.12** is a AIE (Aggregation Induced Emission) active molecule. It forms fluorescent nanoaggregates and used for mercury detection via chemodosimetric approach.[20]

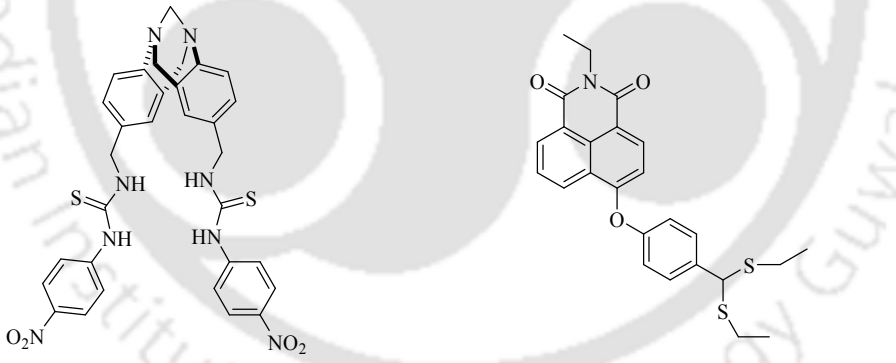

1. 11 **1. 12**

Figure 1.8: The structure of **1.11** and **1.12**.

The molecule **1.13** has a rigid V-shaped geometry and it contains an active carboxylic acid group, that helps it to act as an efficient receptor for adenine.[21] It binds adenine through N-H···O and O-H···N interactions **(1.13a** and **1.13b)** as illustrated in Figure **1.9**. The tetrathiafulvalene based molecule **1.14** is an efficient receptor for

fullerene.[22a] Based on similar principle V-shaped anthracene derivative **1.15** acts as a receptor for fullerene. The compound **1.15** shows high selectivity for C_{70} over C_{60}.[22b]

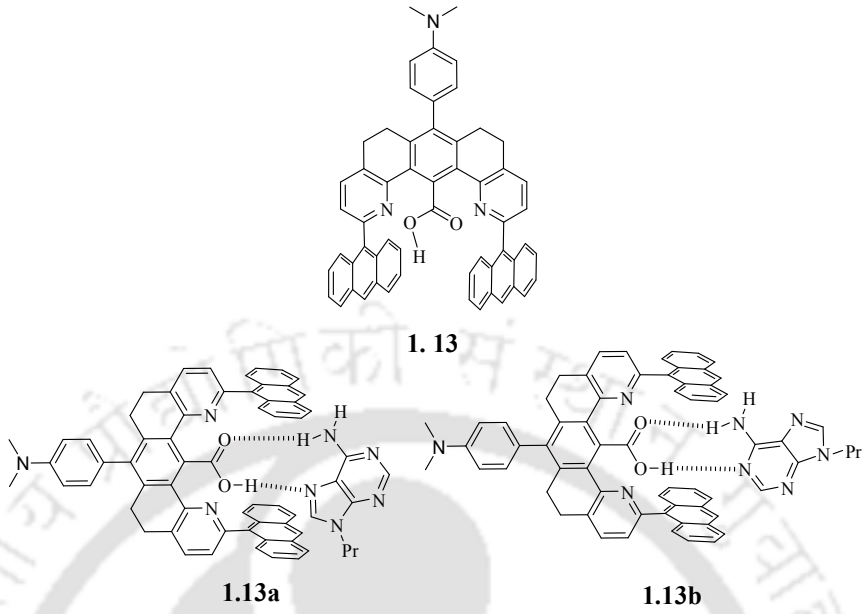

1. 13

1.13a **1.13b**

Figure 1.9: The compound **1.13** and host-guest binding with adenine.

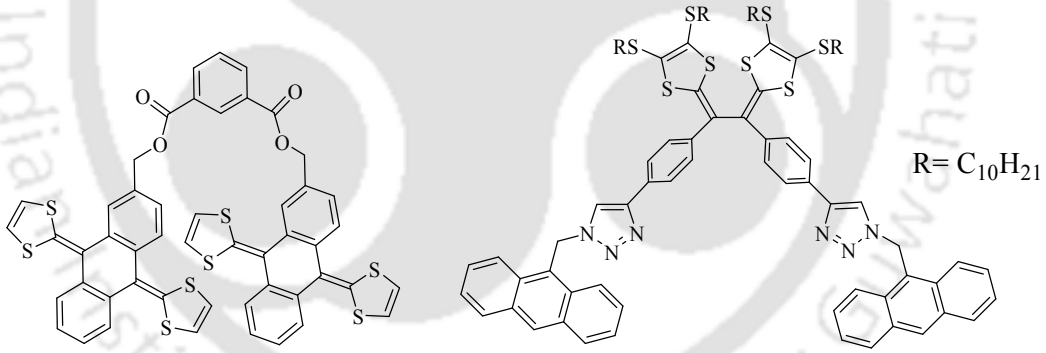

1.14 **1.15**

Figure 1.10: The molecules **1.14** and **1.15**.

Apart from these, various V-shaped ligands are designed to construct coordination complex with diverse molecular structures. The conformation of the ligand, especially the angle between the two coordinating sites is the key factor to generate helical coordination polymers. In that sense, one of the fruitful approaches for the generation of helical coordination polymer is the use of V-shaped flexible ligands. A large number of helical coordination polymers were reported from V-shaped

polycarboxylic acids.[23] The use of multidentate O-donor ligands with two or more carboxylic acid groups attached to a semi rigid V-shaped cental molecular framework usually generate coordination polymers of different dimensions with discrete metal ions as nodes. For example, 4,4'-sulfonyldibenzoicacid **(1.16)**[24] (Figure **1.11**) forms a 3D microporous metal organic framework **1.16a** (Figure **1.12a**) with cadmium (II); which selectively absorbs CO_2. The higher selectivity is attributed to the interactions of CO_2 with two phenyl ring of the V-shaped linker. On the other hand, the 3,3',4,4'-diphenylsulfonetetracarboxylic acid **(1.17)** forms coordination polymers with Co(II) and Mn(II) ions.[25] Another V-shaped symmetrical dicarboxylic acid 4,4'-dicarboxy-diphenylamine **(1.18)** generates different metal organic frameworks in different solvents.[26]

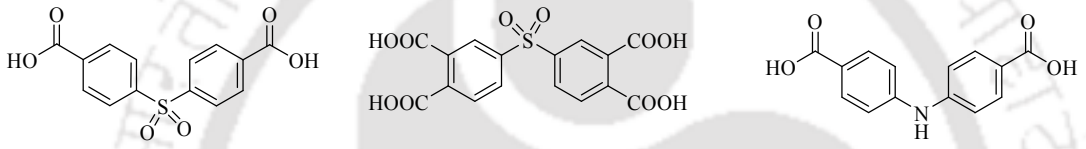

1.16 **1.17** **1.18**

Figure 1.11: The structure of V-shaped dicarboxylic acids **1.16-1.18**.

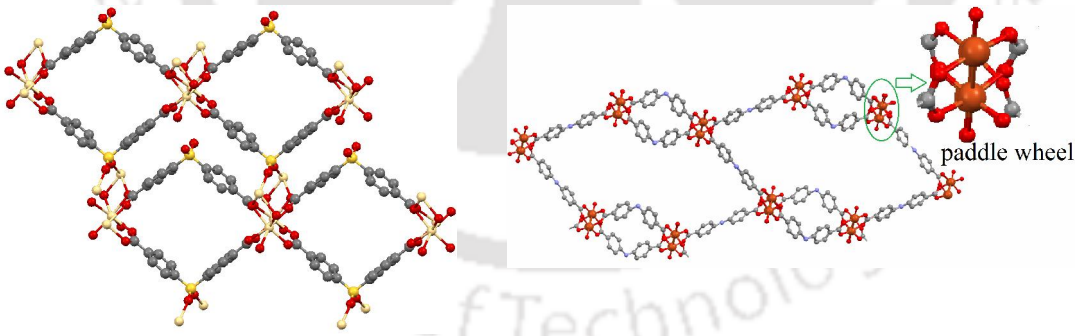

(a) **(b)**

Figure 1.12: (a) The 3D framework 4, 4'-sulfonyldibenzoic **(1.16)** acid with cadmium (II) on (**1.16a**), **(b)** A single net of 4, 4'-dicarboxydiphenylamine **(1.18)** with paddle wheel secondary building blocks of copper (II).

Phthalic acid derivatives such as 4-(2-carboxyphenoxy)phthalic acid **(1.19)**, 3-(2-carboxyphenoxy)phthalic acid **(1.20)**, 3-(4-carboxyphenoxy)phthalic acid **(1.21)** and 4-(4-carboxyphenoxy)phthalic acid **(1.22)** lead to coordination polymers with different dimensionalities.[27] Polycarboxylic acids with two benzene rings bridged by oxygen atom increases flexibility in phthalic acid derivatives. Such ligands are used to generate complexes with diverse structures. The free rotation of the two benzene rings around the bridged oxygen atom helps to provide specific orientation to corresponding coordination polymer.

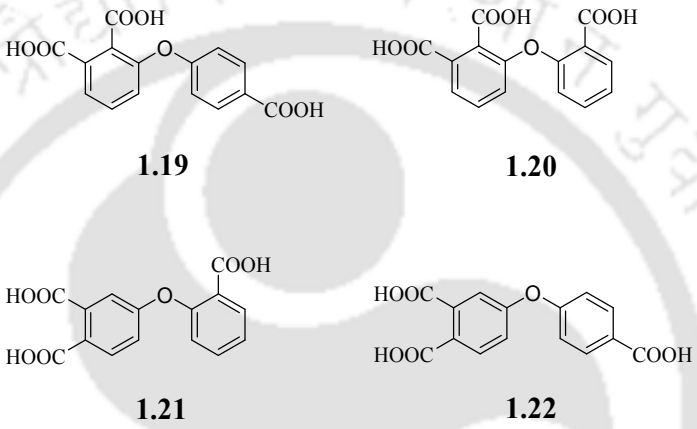

Figure 1.13: The structure of unsymmetrical dicarboxylic acids **1.19-1.22**.

Apart from the poly-carboxylic acids, various N-donor V-shaped ligands are designed to construct coordination complexes of various dimensions. Due to their strong coordination ability, many pyridyl-containing bidentate ligands are extensively studied.[28] For example, the *bis*-pyridyl ligand **1.23** reacts with group **IIB** transition

Figure 1.14: Structure of V-shaped N-donor ligands **1.23-1.24**.

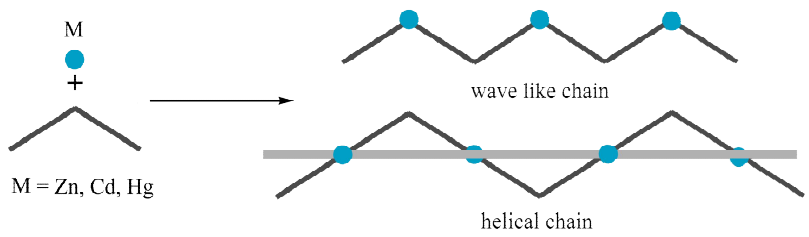

Figure 1.15: The wave-like or helical chain from bis-pyridyl ligands **1.23** and 1.**24**.

metal ions to give isostructural one dimensional coordination polymers with wave-like structures; whereas bis-pyridyl ligand **1.24** gives one dimensional helical chains (Figure **1.15**).[29]

Thus these discussions have clarified the extensive use of V-shaped molecules to make varieties of molecular scaffolds which in turn have selectivity to bind or to make new well defined architectures.

1.3 *Bis*-phenol and their scaffolds:

Bis-phenols are aromatic molecules in which at least two hydroxy groups containing aromatic rings are connected by an appropriate spacer (Figure **1.16**).[30] There are several ways to connect two phenyl rings to construct *bis*-phenols. However, the term *bis*-phenol is used to represent those where methylene group is present as a spacer between two aromatic rings bearing hydroxy groups as described by structure **1.26**. Many *bis*-phenolic molecules have V-shaped geometry. Some examples of *bis*-phenols are *bis*-phenol A (**1.27**, prepared from acetone), *bis*-phenol F (**1.28**, prepared from formaldehyde) and *bis*-phenol C (**1.29**, prepared from dichloroketene). *Bis*-phenol molecules with a methylene group as a spacer have V-shaped geometry and they are versatile candidate for the construction of infinite 1D chain. This is because of their rigid skeleton and geometrically directional H-bonding sites.

Some of the *bis*-phenols and other related phenolic compounds (Figure **1.17**) show various biological activities.[31] For example, 3,4',5-trihydroxy-trans-stilbene commonly known as resveratrol (**1.30**) is an endocrine modulator that recognizes estrogen receptors alpha and beta (ERα and ERβ)[32] as well as, it is a free radical scavenger.[33] The *bis*-phenol based compound (E)-3,4-(bis)(4′-hydroxyphenyl)-3-

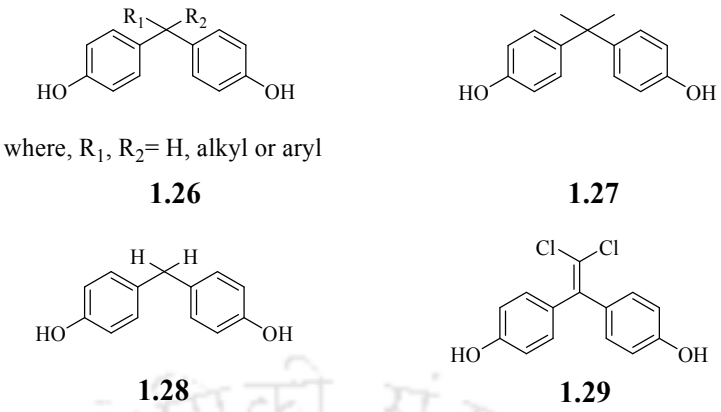

Figure 1.16: Example of some *bis*-phenols.

hexene commonly known as diethylstilbestrol (**1.31**, DES)[34] acts as a powerful estrogen, this compound was earlier clinically prescribed for the prevention of pregnancy complications. But subsequently it was prohibited due to its side effects such as carcinogenicity and teratogenicity.[35] 1,1-bis(4′-hydroxyphenyl)-2-phenylbut-1-ene (**1.32**) is an synthetic *bis*-phenol which shows estrogenic effects.[36] The organometallic *bis*-phenolic compound 1,1-bis(4′-hydroxyphenyl)-2-ferrocenyl-but-1-

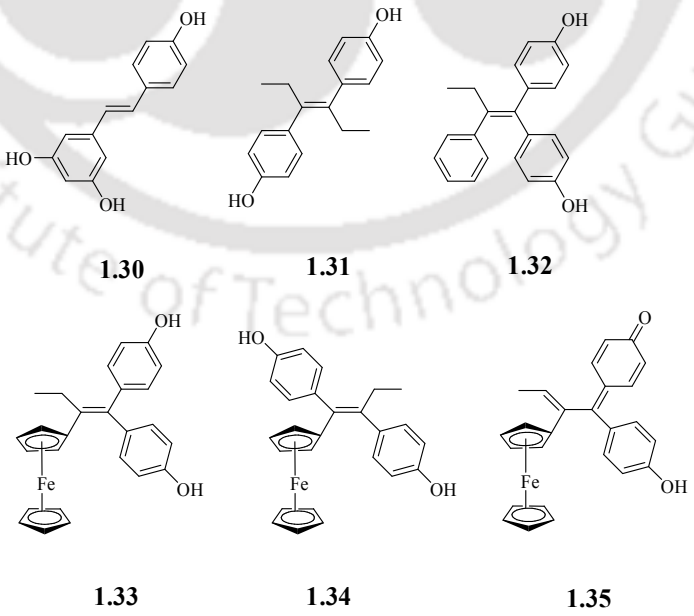

Figure 1.17: Structure of some biologically active *bis*-phenols.

ene (**1.33**) shows strong antiproliferative effect in breast cancer cell lines.[31b] On the other hand its regioisomer 1,2-bis(4′-hydroxyphenyl)-2-ferrocenyl-but-1-ene **(1.34)** shows only modest effect on these cell lines.[31b] The cytotoxicity of the compound **1.33** is due to the conversion of phenol to quinoid (quinine methide, **1.35**) via ferrocene oxidation.

Bis-phenols having V-shaped geometry can be modified to give different macromolecular architectures[37] and polymers.[38] For example, *bis*-phenol **A** based mixed donor types macrocyclic Schiff base **1.36** can be use for the extraction of trivalent iron and gallium.[39] The phenolic hydroxy groups in the Schiff base moiety

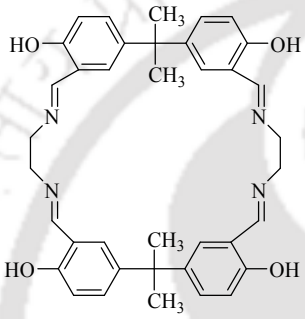

1.36

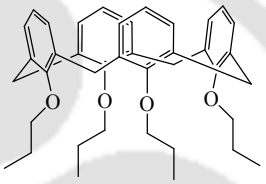

1.37

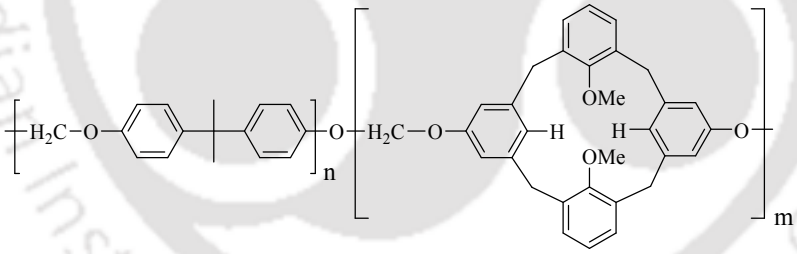

1.38

Figure 1.18: The structure of *bis*-phenol base macrocycle **1.36** and copolymer **1.38**.

additionally contribute to the complexation and extraction of iron (III) and gallium (III). Another example of *bis*-phenol **A** based receptor is the calixarene containing co-polyether **1.38** (Figure **1.18**), which has Ag^{+}- binding properties. The Ag^{+}- binding property of **1.38** is found to be more than hundred fold that of the tetra-propoxy derivative calix [4] arene tetrapropyl ether **1.37.**[40]

Bauer et al. reported a series of isomeric phosphorous-containing cryptands starting from *bis*-phenol A and PCl_3 (equation **1.1**).[41] The condensation of dichlorophosphite

(**1.39**) with different *bis*-phenols lead to macrocyclic phosphite of different size depending on the geometry of the *bis*-phenol employed.[42] The use of the flexible trinuclear *bis*-phenol **1.40**, results in the formation of dimeric macrocycle **1.41** in moderate yield through [2+2] type of macrocyclocondensation reaction (Equation **1.1**), whereas the use of binuclear *bis*-phenol **1.42** leads to the formation of both dimeric **1.43** and trimeric macrocycle **1.45** in equal amounts. On the other hand the use of linear 1,1-biphenyl-4,4-diol **(1.43)** led to a tetrameric, square, macrocyclic phosphite **1.46** (Figure **1.19**)**.**

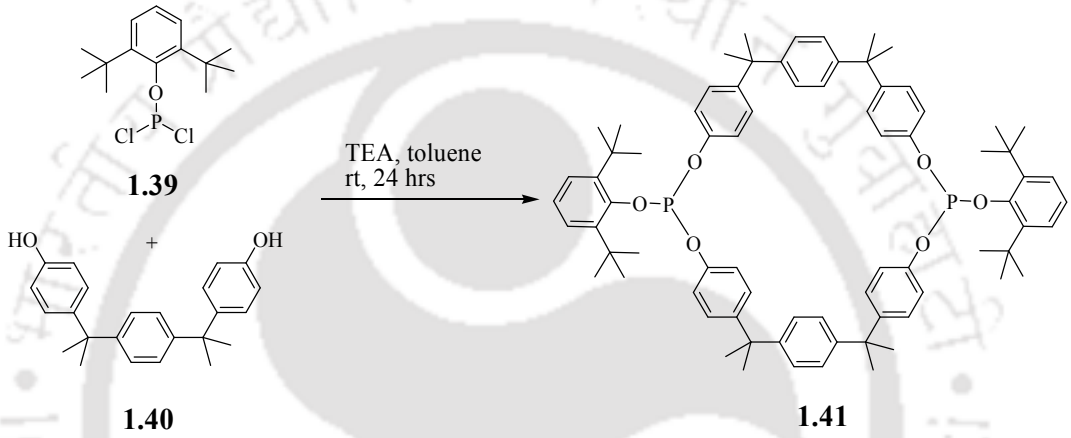

1.39 + **1.40** → **1.41**

Equation 1.1: Condensation of dichlorophosphite with *bis*-phenol **1.40**.

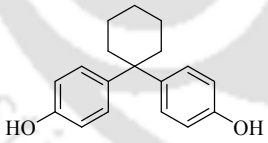

1.42

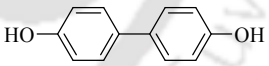

1.43

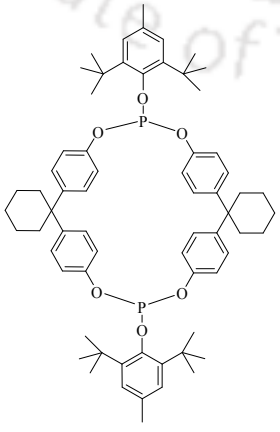

1.44

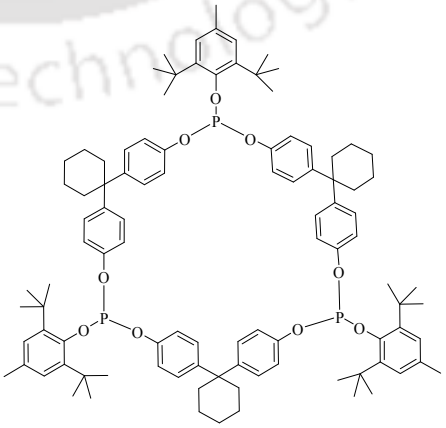

1.45

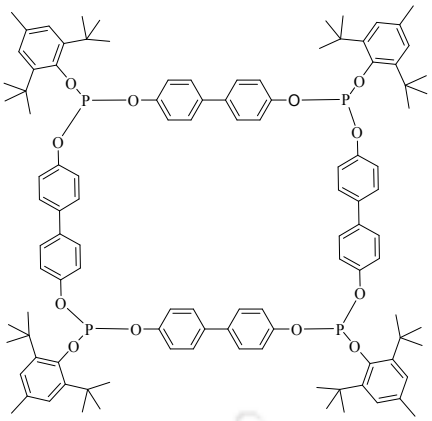

1.46

Figure 1.19: Example of some phosphorous-containing cryptands derived from *bis*-phenol.

Bis-phenols are the raw materials for the synthesis of various polycarbonates.[43] Brunelle et al. described an efficient route (Equation **1.2**) for the synthesis of macrocyclic aromatic carbonates which provides a mixture of cyclic oligomers (from dimer to docsamer).[44] The cyclic oligomeric carbonates based on *bis*-phenol A (**1.47**) are anionic in nature. The ring opening polymerization of these cyclic oligomers leads polymers (**1.48**) with molecular weight significantly higher than possible with conventional procedures.

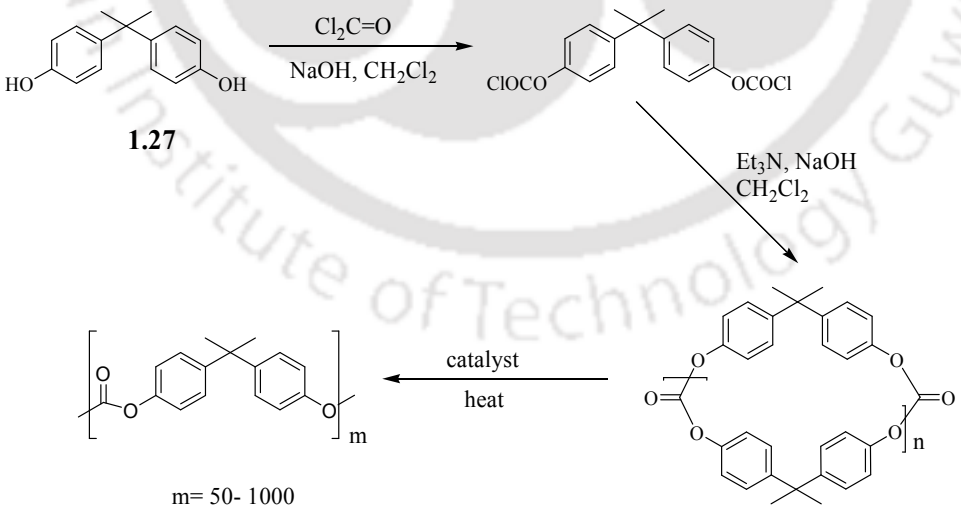

1.27 **1.48** **1.47**

Equation 1.2: Synthesis of polycarbonate **(1.48)** from *bis*-phenol A.

1.4 Supramolecular chemistry of *bis*-phenols:

The assembling of *bis*-phenols are generally guided by various strong and weak interactions such O-H···O, C-H···O, C-H···π interactions.[1, 2] Besides these, in many *bis*-phenols π-π, N-H···π, O-H···π interactions plays crucial roles.[45] Strong directional O-H···O interactions are generally characteristics of *bis*-phenolic compounds to form various hydrogen-bonded motifs such as dimer, cyclic oligomers, linear chains etc as shown in the Figure **1.18**.[46] The hydroxy groups of phenolic derivatives are more acidic than that of alcohols, and hence they can act as hydrogen bond donors towards suitable hydrogen-bonding acceptors. However, in certain cases, the oxygen atom of the hydroxy group of the phenol can also appear as an efficient hydrogen bond acceptor. Thus, it is reasonable to expect that the presence of two such O-H groups would impart intrinsic molecular and supramolecular dimensions to *bis*-phenols. In this regard, the hydrogen-bonded assemblies of *bis*-phenols are interesting because they lead to the formation of various network structures.

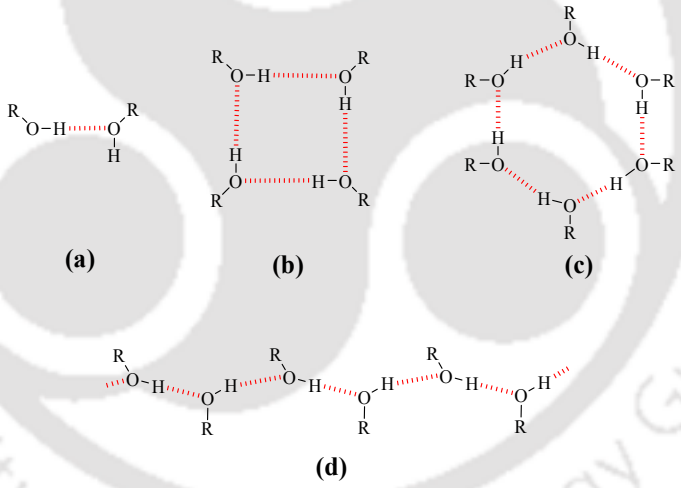

Figure 1.20: Some representative typical weak interactions observed in the self assemblies of hydroxy group containing compounds **(a)** dimer, **(b)** tetrameric ring, **(c)** hexameric ring and **(d)** infinite 1D chain.

The *bis*-phenol, *bis*(4-hydroxyphenyl)(phenyl)-methane **(1.48)** has T-shaped geometry and one of the hydroxyl groups of six *bis*-phenol molecules are H-bonded via a single water molecule to form cyclic hexameric network (Figure **1.22**).[47] The remaining OH groups of each *bis*-phenols participate in the formation of triangular type of arrangement. On the other hand the unsolvated form of methyl substituted analogue of

1.48, *bis* (4-hydroxy-3, 5- dimethylphenyl)(phenyl) methane **(1.49)** forms infinite zig-zag chain through O-H···O interactions.[48] The H-bonding pattern of **1.49** is different

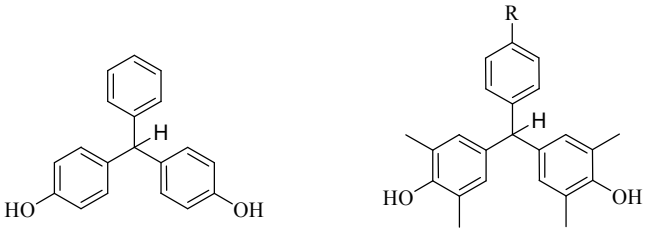

1.48

Where, R = H (**1.49**), OH (**1.50**), NO_2 (**1.51**)

CHO (**1.52**), NH_2 (**1.53**), NMe_2 (**1.54**)

Figure1.21: Structure of *bis*-phenols **1.48-1.54**.

from **1.48**, indicating that the presence of methyl substituent ortho- to the hydroxy group restricts the orientation of the O-H···O bonds along with a concomitant reduction of the hydrogen bond strengths.

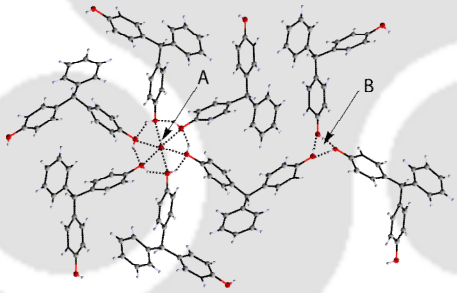

Figure 1.22: Hexameric network **'A'** and triangular network **'B'** in self-assembly of *bis*-(4-hydroxyphenyl)(phenyl)-methane (**1.48**).

Bis-phenols and its related poly-phenols also have tendency to form inclusion compounds with aromatic guest molecules. For example, the *tris*-phenol **1.50** form 1:1 inclusion compound with toluene[47] where the hydroxy groups of the host molecule (**1.50)** forms a cyclic hexamer through O-H···O interactions (Figure **1.23**). The toluene guest molecules are included between the molecules of **1.50** and this lead to column-like structures. On the other hand, nitro substituted *bis*-phenol **1.51** forms 1:1 inclusion compound with benzene. In this case, the *bis*-phenol molecules self-assemble via intermolecular hydrogen bonds that involves the hydroxy groups of the

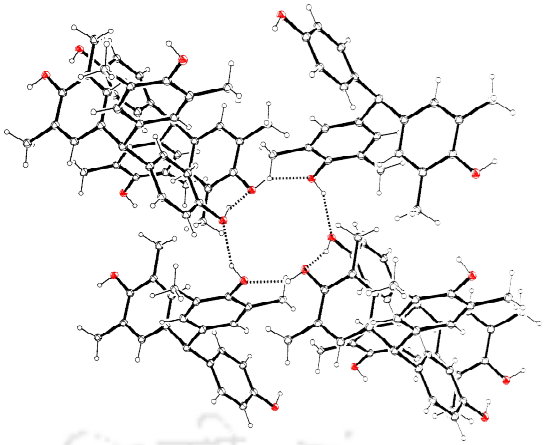

Figure 1.23: Cyclic hexamer generated by O-H···O hydrogen-bonding interactions in **1.50**•Toluene inclusion complex.

phenol as donors and the nitro groups as acceptors resulting in two-dimensional network structure. Each of the two-dimensional networks contains cavities, which are occupied by the benzene molecules.

Similarly, *bis*-(4-hydroxy-3,5-dimethylphenyl)(4-formylphenyl)-methane (**1.52**) from 1:1 molecular complex[47] with benzene where O-H···O interaction between the hydroxy groups of the phenol and the carbonyl group generates a molecular ladders that extend parallel to the [010] plane (Figure **1.24a**). Each of these ladders assembles

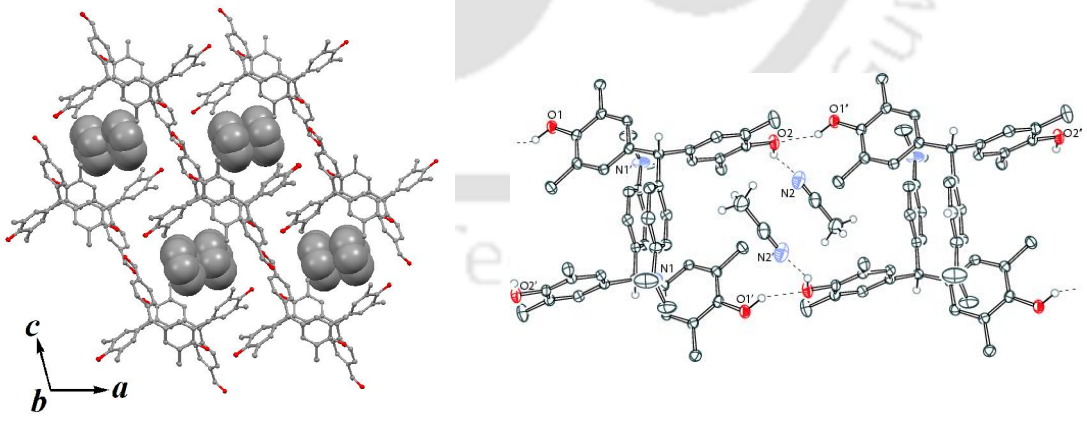

(a) **(b)**

Figure 1.24: (a) Formation of molecular ladders by **1.52**, which accommodates benzene molecules, **(b)** Intermolecular hydrogen bonding between the acetonitrile molecules and *bis*-phenol (**1.54**).

anti-parallel to each other generating cavities of dimension ~7.0×8.2 Å, which are large enough to accommodate the benzene molecules. *Bis*(4-hydroxy-3,5-dimethylphenyl)(4-aminophenyl) methane **(1.53)** forms 1:1 inclusion complex with toluene.

Bis-phenols form inclusion compounds with polar guest molecules such as methanol and acetonitrile. For instance, bis(4-hydroxy-3,5-dimethylphenyl)(4-N,N-dimethyl-aminophenyl) methane (**1.54)** forms 1:1 inclusion complex with acetonitrile.[49] In the acetonitrile solvate **1.54,** the *bis*-phenol molecules are linked by intermolecular O-H···O hydrogen bonds to form one-dimensional chains (Figure **1.24b**).

The self-assemblies keto *bis*-phenols 4,4'-*bis*-(4-hydroxyphenyl)cyclohexanone (**1.55**) and 4,4'-*bis*-(3-methyl-4-hydroxyphenyl)cyclohexanone (**1.56**)[50] consist of hydrogen bonded network and both the structures have two symmetry independent molecules in their respective unit cells. The compound **1.55** forms self host-guest complex where one set of molecules form square network through strong O-H···O interactions, having channel like structure and the other set of molecules are incorporated in to these channels (Figure **1.26a**).

1,1-bis-(3,4-dihydroxyphenyl)cyclohexane **(1.56)** forms a novel replica as organic zeolite structure upon spontaneous self aggregation.[51] The molecule **1.56** forms inclusion complexes with benzene and *p*-xylene, where the host molecules self

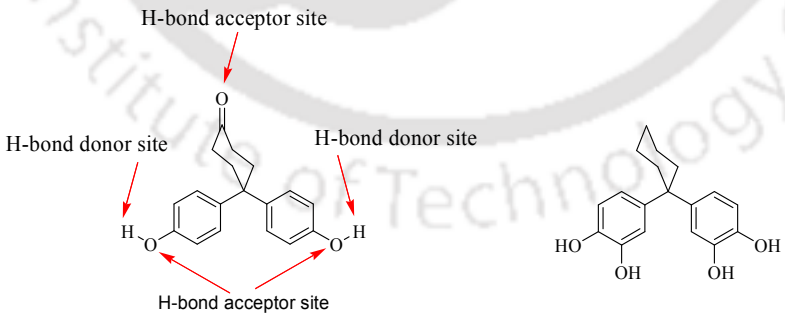

1.55 **1.56**

Figure 1.25: Structure of *bis*-phenol **1.55** and **1.56**.

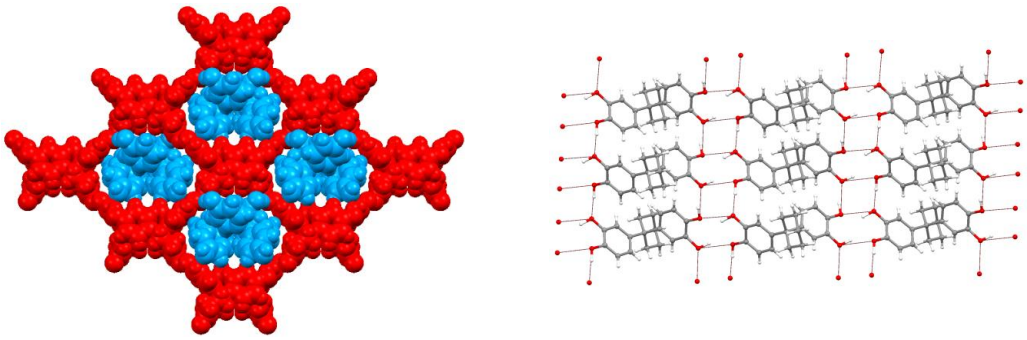

(a) **(b)**

Figure 1.26: (a) Self host-guest complex formed by *bis*-phenol **1.55**, **(b)** Fused H-bonded ring to form a sheet-like structure of the host molecules in the crystal structure of benzene and *p*-xylene complex of **1.56**.

assembles through intermolecular $R_4^4(8)$ and $R_4^4(10)$ types of cyclic O-H···O interactions (Figure **1.24b**).[52,53]

Bis-phenol A **(1.2)** and its derivatives 2,2′-bis(4-hydroxy-phenyl)hexafluoropropane (**1.58**) and 4,4′-methylenediphenol (**1.59**) forms charge transfer complexes with electron acceptors such as *p*-benzoquinone (**1.60**).[54] Thus *p*-benzoquinone can be used as visible indicator for these *bis*-phenol derivatives as different *bis*-phenols give different color with *p*-benzoquinone in solid state.

R = Me (**1.27**), R = CF_3(**1.58**),
R = H(**1.59**)

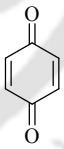

Benzoquinone(**1.60**)

Figure 1.27: Structure of *bis*-phenol **1.27, 1.58, 1.59** and benzoquinone **(1.60)**.

Bis-phenols and its related poly-phenolic compounds are known to form ladder like structures which are comparable with the metal organic frameworks. The first deliberate attempt to construct a purly organic ladder was by Desiraju et. al.[55] and they designed an organic T-shaped molecule 4,4-bis(4′-hydroxyphenyl)-1-cyclohexanol (**1.61**), which self assemble via three intermolecular O-H···O hydrogen

bonds to form a ladder with two alternating cavities (rung-to-rung distance 5.6 Å and 7.5 Å, Figure **1. 29**). This was the first example of organic ladder which provides a direct comparison between metal organic framework and purely organic ladder framework.

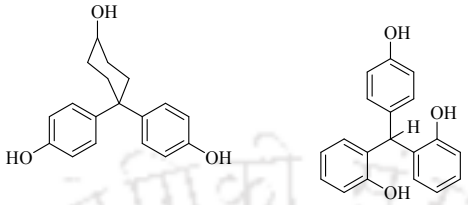

1.61 **1.62**

Figure 1.28: Structure of *bis*-phenol **1.61** and **1.62**.

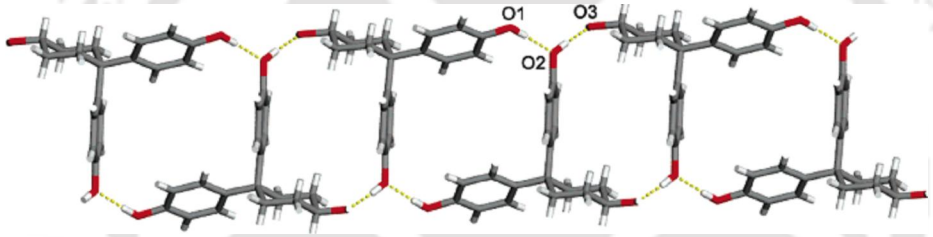

Figure 1.29: The purely organic ladder based on 4,4-bis(4′-hydroxyphenyl)-1-cyclohexanol (**1.61**).

T-shape molecule **1.55** also forms **1D** ladder host-guest framework in solid state.[56] The ladder accommodates aniline, phenol, o-cresol, m-cresol, o-chlorophenol and m-bromophenol and demonstrates its utility as versatile substrate for tecton formation (Figure **1.30**). On the other hand the assembling of this T-shaped compound changes to **2D** brick type structure when *o*-fluorophenol or *m*-fluorophenol is employed as guest. It exhibit high selectivity for aniline, as well as they are capable of accommodating both aniline and phenol within separate cavities by disrupting the strong aniline···phenol hydrogen bonds.

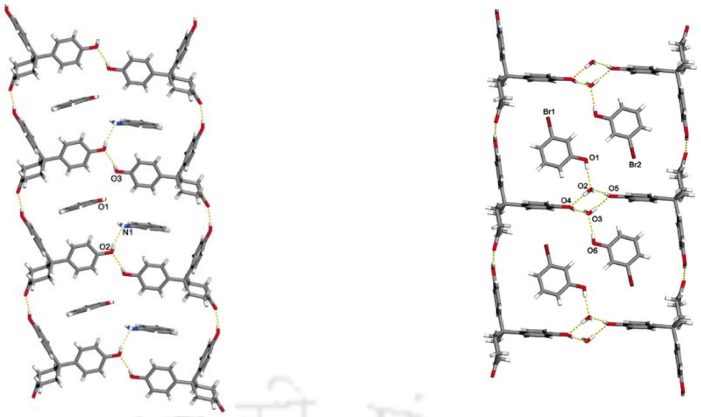

(a) **(b)**

Figure 1.30: Formation of 1D ladder by 4, 4-bis (4′-hydroxyphenyl)-1-cyclohexanone **(1.55)** on (a) simultaneous inclusion of aniline and phenol, **(b)** inclusion of *m*-bromophenol.

The triphenol **1.62** (Figure **1.28**) forms a distorted 1D ladder like structure through O-H···O interaction from the neighboring chains of the host molecules.[57] The triphenol **1.62** also forms ladder type assemblies with pyrazine,[58] where pyrazine molecules acts as a rung between two hydrogen bonded rod like structure of the host molecules through O-H···**N** interactions (Figure **1.31**). On the other hand, the molecules of **1.62** also form 1:1.5 host-guest complex with 4, 4'-bipyridine where the host molecules form H-bonds with the 4,4' -bipyridine molecules through O-H···**N** interactions. These results in formation of **2D** sheets and these sheets undergo 4-fold interpenetration to give a 3D network structure.

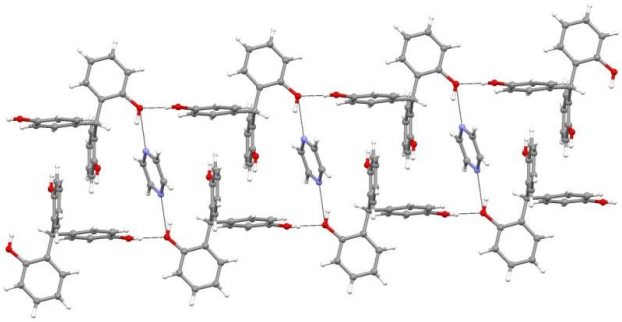

Figure 1.31: Formation of the ladder type arrangement of the **1.62•** pyrazene complex.

The sterically hindered and rigid C_3-symmetric molecular tectons **1.63** and **1.64,** self-assembles through O-H···O interaction to give eight fold interpenetrated hexagonal (6, 3) and two fold interpenetrated square (4, 4) networks (Figure **1.33a**) respectively.[59] Such interpenetrated structure get destroyed in the presence of [18]-crown-6 as guests. The guest [18]-crown-6 molecules are found to nicely fit in these hexagonal voids formed by **1.63**. The empty spaces in the crown ethers are further occupied by neutral (methanol/water, methanol/acetonitrile) or ionic guest species such as KI/ KAcAc (where AcAc is acetylacetone) (Figure **1.33b**) to generate novel multi-component assemblies in a host ⊂ guest ⊂ guest manner. On the other hand the triphenol host **1.64** also forms analogous multi-component molecular complexes where crown-K^+ acts as s spacer in the hydrogen bonded self assembly leading to wire-like networks.

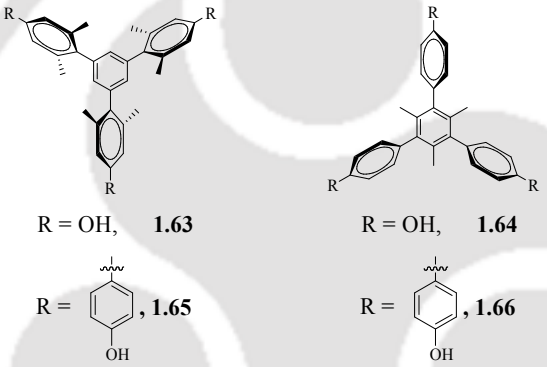

Figure 1.32: The structure of trisphenol **1.63-1.66**.

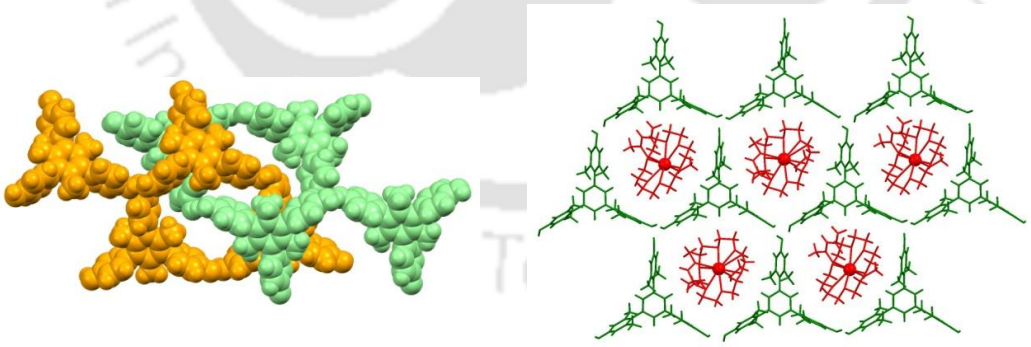

(a) **(b)**

Figure 1.33: (a) Doubly interpenetrated square (4, 4) net formation by host molecules in ethylacetate solvate of trisphenol **1.64**, **(b)** The honeycomb pattern of **1.63** which includes 18-crown-6•K-AcAc in the hexagonal voids in a guest ⊂ guest ⊂ host manner.

The extended triphenol **1.65** also forms multi-component molecular complex with [18]-crown-6; which includes benzene and acetonitrile as second set of guest molecules.[60] In this case the crown ether acts as spacer to form hexameric assembly and the assembly is highly porous to undergo interpenetration. Whereas the compound **1.66** self-assembles with [18]-crown-6 as a spacer to afford self-interpenetrated pseudohexagonal (6, 3) net.[60]

The cooperative effect helps in the formation of self-assembly of tetraphenol **1.67**. In the assembly of **1.67**, each molecule of tetraphenol involves in total eight O-H···O bonds with four symmetrically orientated neighbours.[57] This leads to the formation of an eight member finite ring type of O-H···O hydrogen bonds (Figure **1.34**). The tetraphenol **1.67** forms 1:2 and 1:1.5 complex with 4,4'-bipyridine and 1,2-bis(4-pyridyl)ethylene respectively.[61]

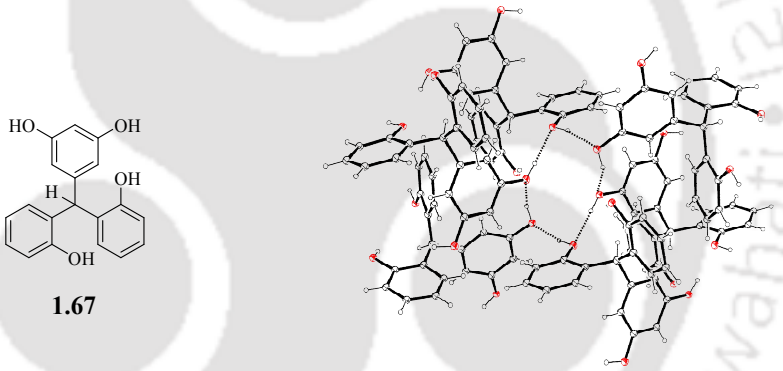

1.67

Figure 1.34: Formation of eight member ring of O-H···O interactions in the crystal structure of the tetraphenol **1.67.**

Bis-phenol based compound 1,1,2,2-tetrakis(4-hydroxyphenyl)ethane (**1.68**, TEP) forms inclusion compound with N-donor compounds. It was used as a complexing agent for the separation of N-donor guest molecule. [62a, 62b] The TEP molecule forms 1: 2 inclusion complex with 5-chloro-2-methyl-4-isothiazolin-3-one **(1.69)**.[62c]

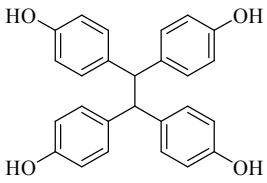

1.68

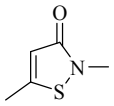

1.69

Figure 1.35: Structure of tetra-phenol **1.68** and 5-chloro-2-methyl-4-isothiazolin-3-one **(1.69)**.

Nangia et al. reported a series of compounds where the two *bis*-phenol molecules are connected by a covalent linker to adopt H-shape.[63,64] These H-shaped tetra-phenols self-assembles to give various architectures such as 1D ladders, interpenetrated ladders, 2D hexagonal sheets or poly-catenated 3D frameworks. In the guest-free form of **1.70**, the molecules form a 1D→1D interpenetrated ladder structure (Figure **1.37a-b**). In ethyl acetate and DMSO solvate of **1.70**, the host molecules form 1D ladder through phenol O-H···O interactions. However, the difference between the two solvate is that, in case of the ethyl acetate solvate, the solvent molecules are connected to the sides of the ladder whereas, in case of the DMSO solvate the solvent molecules act as a connector between the OH groups through O-H···O interactions (Figure **1.38a** and **1.38b**). The difference in the O-H···O bonds of the two structure is attributed to the stronger H-bond accepting ability of DMSO compared to ethyl acetate. Hence the hydrogen bonds between the host molecules[65] can be disrupted easily by DMSO.

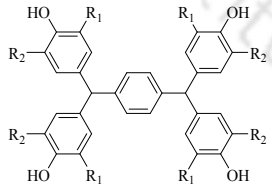

$R_1 = R_2 = H$ **(1.70)**
$R_1 = H$, $R_2 = Me$ **(1.71)**
$R_1 = R_2 = Me$ **(1.72)**

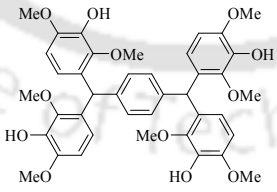

1.73

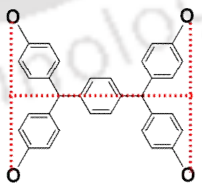

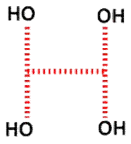

H-shape of **1.70-1.72**

Figure 1.36: Structure of tetra-phenol **1.70-1.72**.

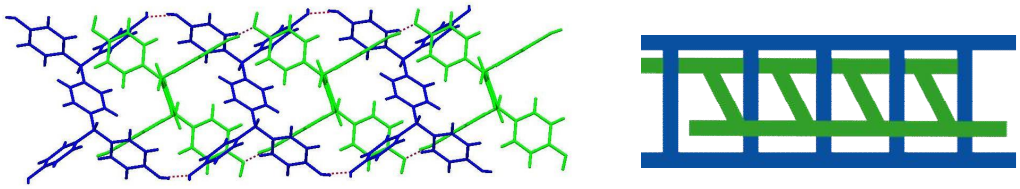

(a) **(b)**

Figure 1.37: (a) and **(b)** Double interpenetration of inclined ladders in the guest-free form of **1.70**. Symmetry-independent molecules are shown in different colour.

Similar types of 1D ladder of the host molecules was observed in the isopropanol, dioxane and acetonitrile solvate of **1.70**; acetonitrile solvate of **1.71** and acetonitrile, DMSO, toluene, nitromethane solvate of **1.72**; dioxane and DMSO solvate of **1.73.**[64] In the DMF solvate of **1.72,** the host molecules form 2D→2D interpenetrated honeycomb nets. In this case the hexagonal net expands in 2D and another (6, 3) net intertwines in a parallel fashion which is an example of interpenetration through Hopf link (Figure **1.39**). This can also be simply defined as two interlocked rings that can only be separated by cutting open one ring.[64]

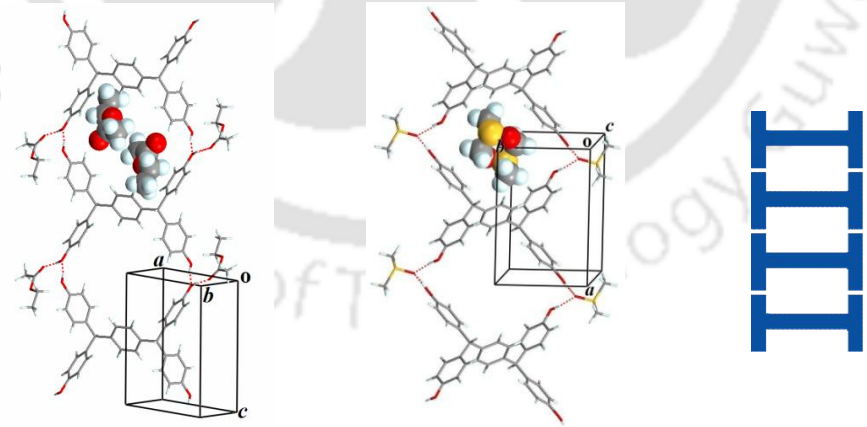

(a) **(b)** **(c)**

Figure 1.38: The ladder like network of **(a)** ethylacetate and **(b)** DMSO solvate of **1.70**, **(c)** Schematic presentation of a ladder network.

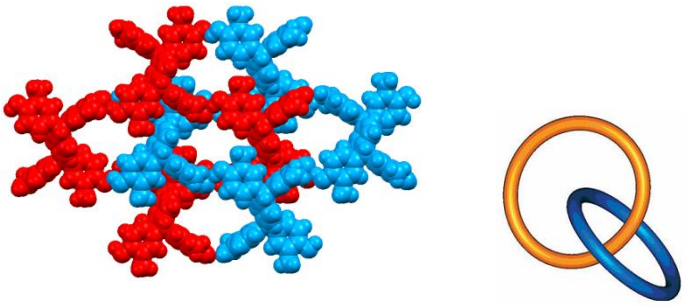

(a) **(b)**

Figure 1.39: **(a)** Parallel 2D→2D 2-fold interpenetration of **1.72** in its DMF solvate, **(b)** A Hopf link.

Introduction of a bipyridine spacer to the H-shaped tecton[66] also leads to the formation of a 1D ladder **1.70•**2(4,4'-bpy), which self-assembled through O-H···N interactions between the bipyridines and the H-shaped units (Figure **1.40**). The introduction of the linear spacer increased the rung-to-rung distance from 11.3 Å to 20.2 Å.

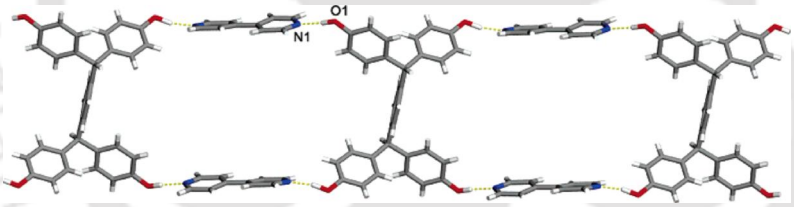

Figure 1.40: The self-assembly of **1.70•** (4, 4'-bpy) into a 1D ladder.

Aoyama et al**.** reported another H-shaped molecules 9,10-bis-(2,5-dihydroxy-1-phenyl)anthracene **(1.74)**[67] that forms a **1D** ladder like structure, which is a multi-dimensional host system that incorporates solvents molecules as guest. Specifically, the diol functionality of **1.74** self-assembled through intermolecular O-H···O interactions to give a ladder like structure where the anthracene units act as rung. The guest ketone molecules incorporate in between the rung of the ladder through O-H···O=C interaction (Figure **1.41**). The framework exhibited selectivity for smaller ketones that provided a better fit for smaller cavities.

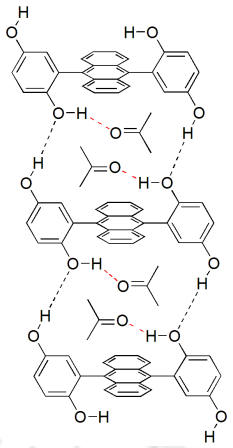

Figure 1.41: Acetone recognition by 9, 10-bis-(2, 5-dihydroxy-1-phenyl) anthracene **(1.74)**.

The guest inclusion behaviour of **1.75** and **1.76** were studied by Moorthy et al.[68] with various aromatic guest such as benzene **(B)**, nitrobenzene **(NB)**, benzonitrile **(BN)**, o-dichlorobenzene **(C)** and pyridine **(P)**. The pyrene based tetra-phenol **1.75** self-assembles through O-H···O interaction and has an inherent property for the inclusion of two or more guest molecules simultaneously. For example, tetra-phenol **1.75** can simultaneously incorporate benzene and nitrobenzene or pyridine and o-dichlorobenzene to give **1.84**•B•NB and **1.84**•C•P. Like tetra-phenol **1.75**, its half component *bis*-phenol **1.76** also undergoes O-H···O hydrogen-bonded self-assembly, but the formation of these types of ternary complexes was not observed in case of **1.76**. Indeed, the inclusion compounds of **1.76** with benzene (**1.76•B**), benzonitrile (**1.76•BN**), nitrobenzene (**1.76•NB**) and o-dichlorobenzene (**1.76•C**) exhibit packing equivalence despite the fact that the crystals of **1.76•C** correspond to *P-1*, while those of all others correspond to $P2_1/c$.

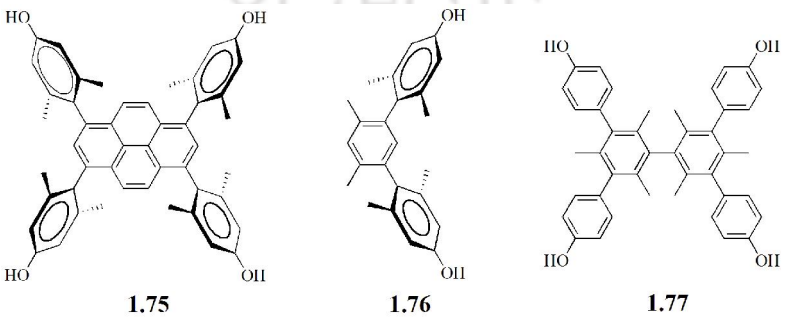

1.75 **1.76** **1.77**

Figure 1.42: Structure of tetra-phenol **1.75** and **1.77** and *bis*-phenol **1.76**.

Moorthy et al. reported another tetra-phenol molecule **1.77,**[69] which includes guest molecules such as ethyl formate, ethyl acetate and ethanol etc in its crystal lattice. The tetraphenol **1.77** forms a helical self-assembly based on O-H···O interactions in all the three dimension which results in the creation of channels in the lattice (Figure **1.43**).

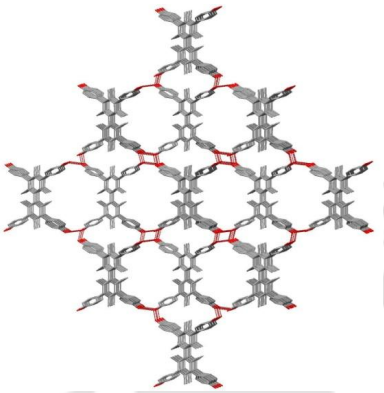

Figure 1.43: The crystal packing of the tetraphenol **1.77** showing the formation of the channels.

1.5 Polymorphism in *bis*-phenols:

McCrone[70] defined polymorphism as "the existence of a solid crystalline phase of a given compound resulting from the possibility of at least two different arrangements of molecules of that compound in the solid state". Polymorphism is a common phenomenon in organic solids.[71] Versatility in packing patterns arising from conformational flexibility or due to the presence of more than one molecule in the unit cell to give higher Z′ value causes polymorphism in *bis*-phenols.[72] For example, 1,1-bis(4-hydroxyphenyl)cyclohexane **(1.78)** has two polymorphs, and it arises due the difference in Z'-values in their respective unit cells. [73]

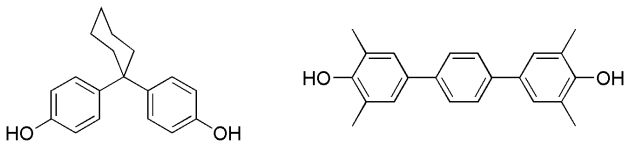

1.78 **1.79**

Figure 1.44: Structure of *bis*-phenol **1.78** and **1.79**.

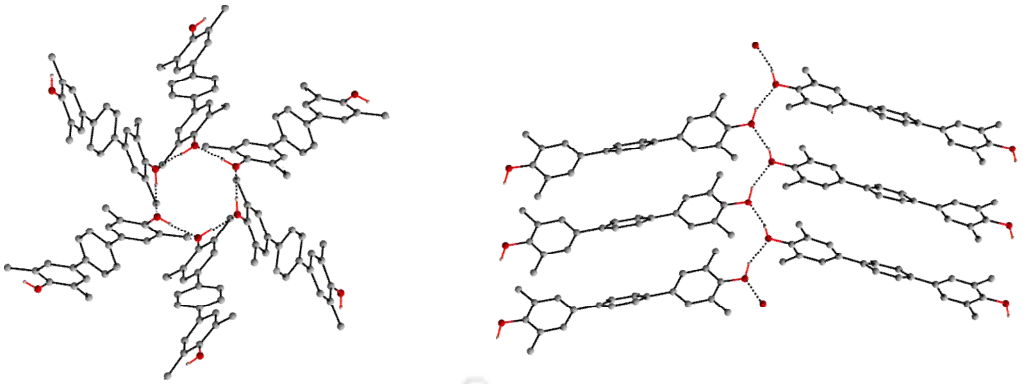

(a) **(b)**

Figure 1.45: The two polymorphs of **1.79**, (a) Chair cyclohexane rings of O-H···O interactions in the polymorph **1.79a,** (b) Infinite H-bonded chain in the polymorph **1.79b**.

2,2′,6,6′-tetramethyl-4,4′-terphenyldiol (**1.79**) has two polymorphic forms. In one polymorph one of the hydroxy group of **1.79** forms cyclohexane ring through O-H···O interactions, whereas in the other polymorph the hydroxy groups form infinite hydrogen bonded chain through O-H···O interactions (Figure **1.45**).

1.5 Anion assisted assemblies of *bis*-phenol:

Despite large number of literature available on *bis*-phenols, there are limited data on structural and molecular recognition by hetero-atom containing *bis*-phenols. One such example is encapsulation of reactive methyl and ethyl sulphate anion in the supramolecular assembly of protonated pyridinium *bis*-phenols.[75] The protonated

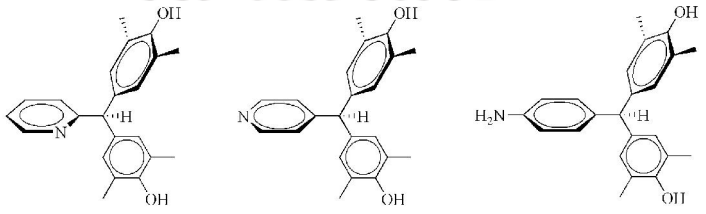

1.80 **1.81** **1.82**

Figure 1.46: Structure of *bis*-phenol **1.80**-**1.82**.

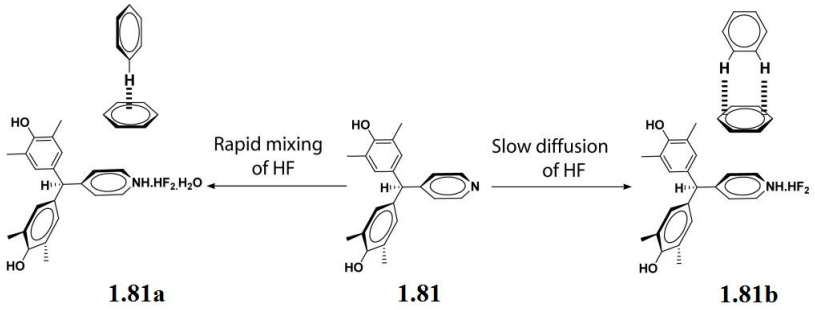

Equation 1.3: Protonation of *bis*-phenol **1.81** with hydrofluoric acid under two different conditions.

form of 2-[bis(4-hydroxy-3,5-dimethyl-phenyl)methyl]pyridine (**1.80**) stabilized methylsulphate anion where the methylsuphate anion are held in the assembly of protonated host molecule through intermolecular O-H···O hydrogen bond interactions involving the hydroxy group of the *bis*-phenols. Similarly, 4-[bis(4-hydroxy-3,5-dimethylphenyl)methyl]pyridine (**1.81**) stabilizes the ethylsulphate anion in its supramolecular assembly through two O-H···O and one N^{+}-H···O interactions.

The *bis*-phenol **1.81** stabilizes the HF_2^- anion in the form of their protonated assemblies.[76] The protonation of *bis*-phenol **1.81** with hydrofluoric acid in aqueous methanol led to two polymorphic H_2F_2 salt of the compound viz, the monohydrated H_2F_2 salt of *bis*-phenol **1.81 (1.81a)** and 1: 1 salt of *bis*-phenol **1.81** with H_2F_2 **(1.81b)** (Equation **1.3**). The structure **1.81b** contains edge-to-face approach (L-shape aromatic

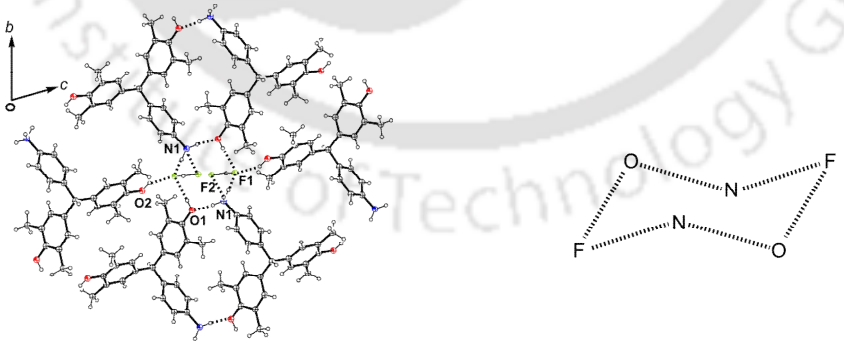

(a) **(b)**

Figure 1.47: (a) Intermolecular hydrogen bond interactions in the H_2F_2 salt of *bis*-phenol **1.82. (b)** Hexameric network in the H_2F_2 salt of *bis*-phenol **1.82.**

C-H···π interactions) of the pyridinium ring to one of the 2, 6-dimethylphenol units whereas the structure **1.81a** contains the end-to-face C-H···π interaction (point-to-face or T-shape aromatic C-H···π interaction) of the pyridinum ring with the 2,6-dimethylphenol unit. In the H_2F_2 salt of the bis(4-hydroxy-3,5-dimethylphenyl)(4-aminophenyl)-methane (**1.82**), the HF_2^- anion has extensive H-bonding with five protonated molecule of the *bis*-phenol and have characteristic short F···F interaction (2.195 Å). The structure has an interesting hexameric network structure as shown in the Figure **1.47**.

1.6 Coordination chemistry of *Bis*-phenols and their derivatives:

The metallo-supramolecular chemistry involves the combination of organic ligands and metallic reagents for the construction of both discrete and polymeric assemblies.[77] Many *bis*-phenols *e.g,* 2,2'-methylene-bis(6-tertbutyl-4-methyl-phenol) **(**$MBMPH_2$, **1.83)** and 2,2'-ethylidene-bis(4,6-di-tert-butyl-phenol) **(**MDBP-H_2, **1.84)** have been used for long time in the transition metal chemistry. These ligands are found to act as dianionic ligand under strongly basic condition that can provide stereochemically rigid framework for the metal and as a result they could affect stereo specific transformations.[78, 79]

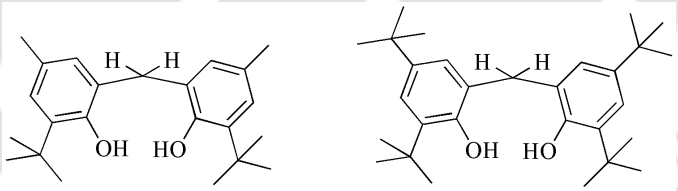

1.83 **1.84**

Figure 1.48: Structure of *bis*-phenol **1.83** and **1.84**.

Zhang et al. reported[80] the titanium complex [(MBMP)Ti($CH_2Ph)_2$] (**1.86**) of 2,2'-methylene-bis(6-tertbutyl-4-methyl-phenol) ($MBMPH_2$, **1.83**) by the reaction of [(MBMP)$TiCl_2$] (**1.85**) with $PhCH_2MgCl$ in diethylether whereas the similar reaction

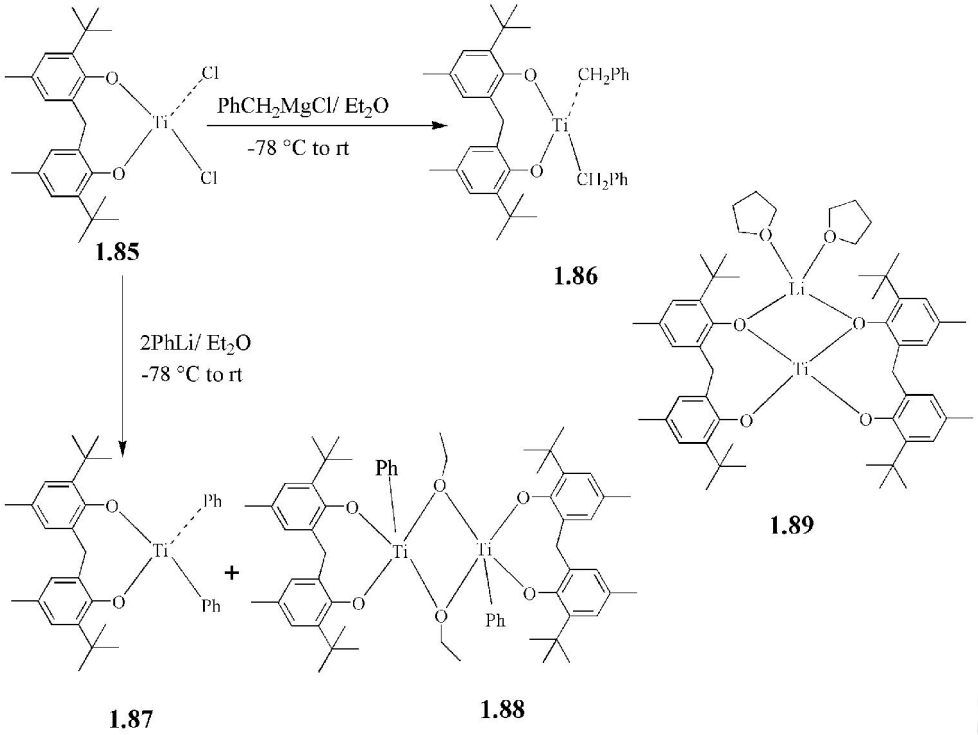

Equation 1.4: The reactivity of **1.85** with $PhCH_2MgCl$ and PhLi.

of **1.85** with PhLi gave $[(MBMP)Ti(Ph)_2]$ (**1.87)** and an unexpected ether bridged compound $\{[(MBMP)\text{-}Ti(Ph)]_2(OEt)_2\}$ (**1.88**) via carbon oxygen bond cleavage of solvent ether (Equation **1.4**). On the other hand, the reduction of **1.87** by one equivalent of $LiBEt_3H$ in THF solvent gave titanium-(III) salt $[Ti(MBMP)_2.Li(THF)_2]$ (**1.89**).

Alkali metal alkoxides have shown excellent catalytic activity toward ring opening polymerization reaction (ROP) of lactones and lactide when the complexes are supported by sterically demanding ligands.[78] Many metal complexes supported by *bis*-phenols based ligands have been developed and used as catalytic/ initiating systems for ring opening polymerization (ROP) of lactides.[78,79] Among them the sodium complexes of these types of ligands are of special interest as sodium is non-toxic and essential for human life.[81] Miller et al. reported discrete sodium complex **1.91** from 2,2′-ethylidenebis(4,6-di-tert-butylphenol) (EDBP-H_2 **1.90**)[82], which is used in controlled ring opening polymerization of lactides (Equation **1.5**).

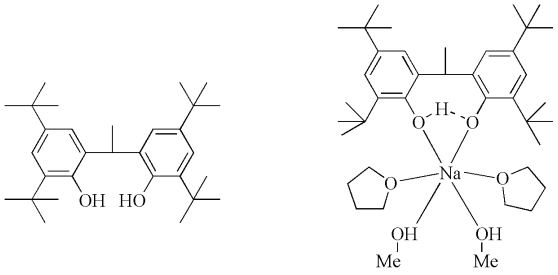

1.90 **1.91**

Figure 1.49: The structure of 2,2′-ethylidenebis(4,6-di-*tert*-butylphenol) (EDBP-H_2, **1.90**) and its sodium complex **1.91**.

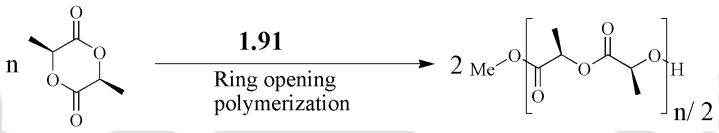

Equation 1.5: Ring opening reaction of lactide catalysed by **1.91**.

Lin et al. reported[83] a *bis*-phenol based aluminium complex [(EDBP)Al(μ-O^{i}Pr)]$_2$ (**1.93**), by the reaction of [(μ-EDBP)AlMe]$_2$ (**1.92**) with 2-propanol at ambient temperature and it showed excellent catalytic activity towards the hydrogen transfer reaction between aldehyde and 2-propanol in Meerwein-Ponndorf-Verley (MPV) reactions.

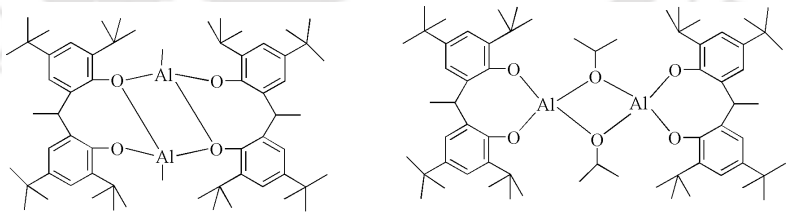

1.92 **1.93**

Figure 1.50: The structure of the aluminium complex **1.92** and **1.93** of EDBP-H_2 **(1.90)**.

Zhao et al. reported[84] the crystal structure of the two sodium complex [(μ_3-MDBP)Na_2(THF)$_2$]$_2$[(μ_3-$OCH_2CH_2OCH_3$)Na]$_2$ (**1.94**) and [(μ_1-MDBP)Na(μ_2-H_2O)

$(THF)]_2(THF)_2$ (**1.95**) of MDBP-H_2 (**1.84**) (Figure **1.51**). The first was obtained from the reaction of MDBP-H_2 with sodium metal in presence of 2-methoxyethanol in toluene followed by the removal of the solvent and crystallization from THF/ hexane

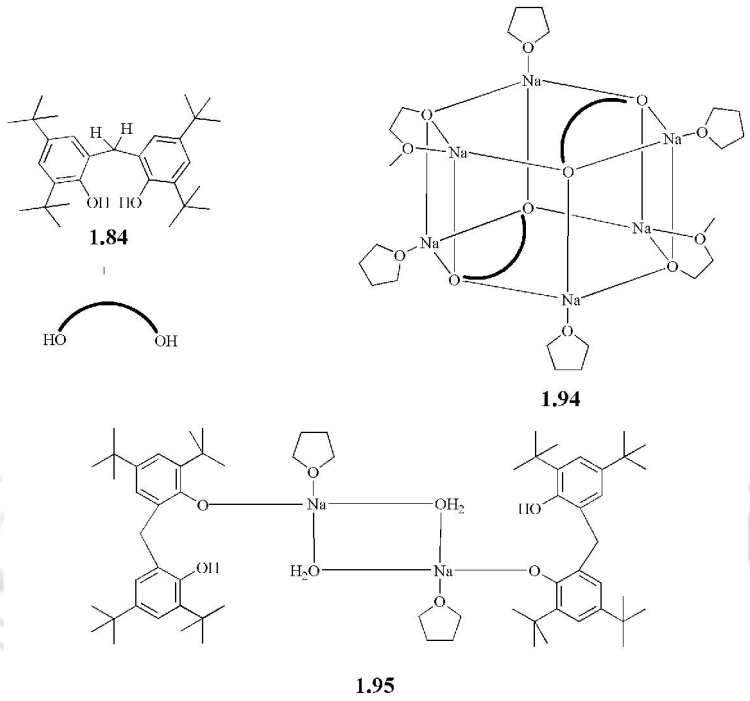

Figure 1.51: The structure of sodium complexes **1.94** and **1.95**.

whereas, the second complex was obtained from the reaction of MDBP-H_2 (**1.84**) with sodium hydroxide and crystallization from THF/hexane. The complex **1.94** efficiently initiates ring opening polymerization of L-lactide, yielding polymers with narrow polydispersity indexes.

Chen et al. reported[85] a series of titanium heterometallic complexes of *bis*-phenols (**1.96-1.98**) having lithium, sodium, magnesium and zinc as other counterpart. These complexes show activity for the controlled ring opening reactions of L-lactides.

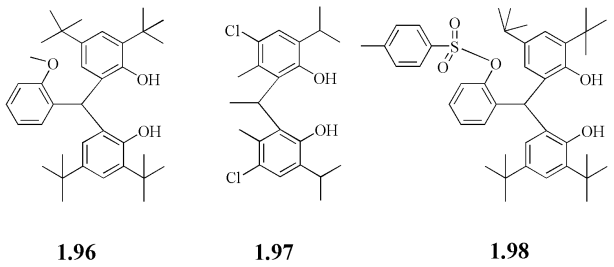

Figure 1.52: The structure of *bis*-phenol **1.96-1.98**.

Wu et al. reported[86] mixed aluminium-sodium inverse crown ether complex of *bis*-phenol **1.90** and this is the first example of bulky phenol ligand supported inverse crown ether complex (Figure **1.53**). The structure of the complex **1.99** contains discrete eight member $Na_2Al_2O_4$ ring made up of alternating oxygen and metal atoms (Figure **1.53**). The oxide ion occupies the core of the ring to make neutral complex.

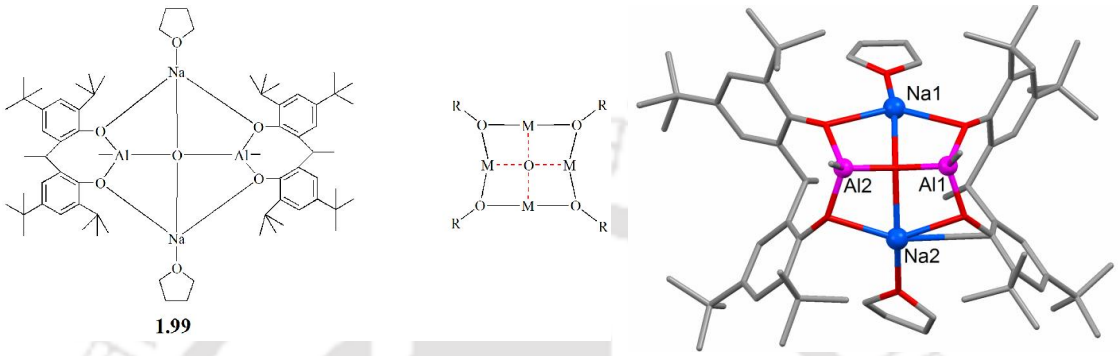

1.99

Figure 1.53: The crystal structure of *bis*-phenol supporting aluminium-sodium inverse crown ether complex **1.99**.

Generally, in oxo-inverse crowns the oxygen atoms occupy the centre of square planner geometry[87], but in this case, the central oxygen atoms are in non-planner geometry. This probably happens due to the presence of two tetrahedral aluminium centres in the complex **1.99**.[88]

Aroma et al. reported[89] a pyrazolyl based *bis*-phenol namely, 2,6-bis(5-(2-hydroxyphenyl)-pyrazol-3-yl)benzene ($BPBH_4$, **1.100**). This multi-donor ligand formed mixed valence $[Co^{III}_2Co^{II}_2]$ tetra nuclear complexes $[Co_4(BPB)_2(OH)(AcO)(py)_4]$ **(1.101)** and $[Co_4(BPB)_2(OMe)(AcO)(py)_4]$ **(1.102)**. The former is a hydroxo-bridged complex and the later is methoxy-bridged complex (Figure **1.54**). Out of the four cobalt ions in the complexes **1.101** and **1.102,** the central ions Co(II) are paramagnetic whereas the external Co(III) ions are diamagnetic.

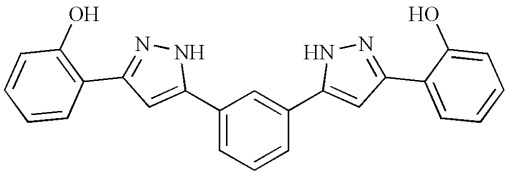

$BPBH_4$ **(1.100)**

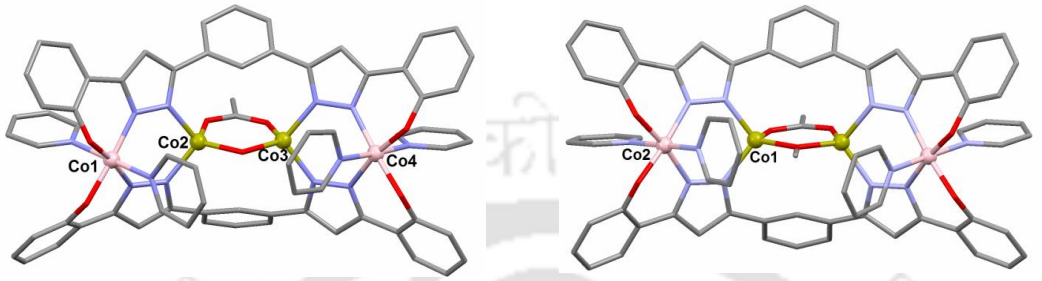

(a) **(b)**

Figure 1.54: (a) The structures of hydroxo bridged complex $[Co_4(BPB)_2(OH)(AcO)(py)_4]$ **(1.101)** and **(b)** Methoxy bridged complex $[Co_4(BPB)_2(OMe)(AcO)(py)_4]$ **(1.102)**.

Some thio-ether based *bis*-phenolato aluminium complexes (**1.103-1.106**)[90] (Figure **1.55**) were reported by Hernandez et al. These complexes showed catalytic activities towards [4+2] Diels-Alder reaction of methacrolein and cyclopentadiene (Equation **1.6**) with good regioselectivity towards the *exo*-product.

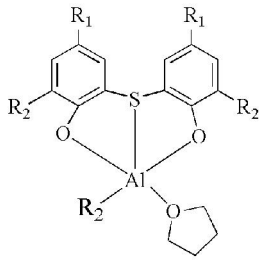

R_1= t-Bu, R_2 = Me, **1.103**
R_1= t-Bu, R_2 = t-Bu, **1.104**
R_1= Me, R_2 = Me, **1.105**

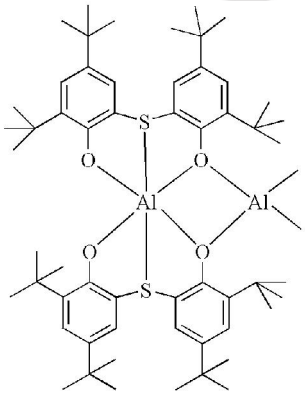

1.106

Figure 1.55: Structures of the aluminium complexes **1.03-1.106**.

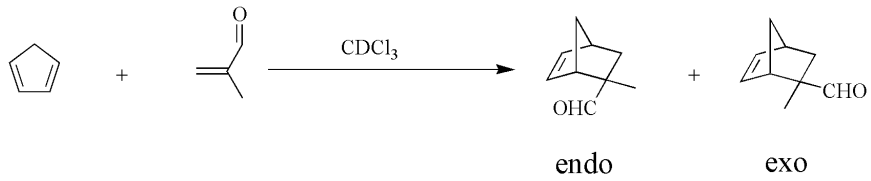

Equation 1.6: [4+2] cycloaddition between methacrolein and cyclopentadiene.

The complex **1.106** showed the best regio-selectivity (99%), but through a low conversion ratio (10%) on the other hand the complex **1.105** showed a less regio-selectivity (90%) but with a higher conversion ratio of 65%.

Flexible dicarboxylic acids with V-shaped geometry[23] are good candidate for the construction of coordination polymers as compared to *bis*-phenol. The carboxylates can bind to a metal in a chelating manner and thereby increase the stability of transition metal organic frameworks. Zheng *et. al.* reported[91] Coordination polymers of *bis*-phenol based dicarboxylic acid, 4,4'-[isopropylidenebis(*p*-phenyleneoxy)diacetic ($BPAH_2$, **1.107**) with Cd(II), Zn(II) and Pb(II). The ligand **$BPAH_2$ (1.107)** formed 1D zig-zag coordination polymer of cadmium

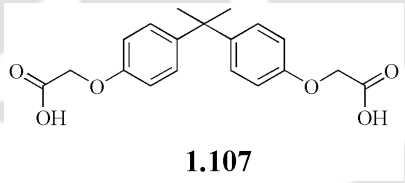

1.107

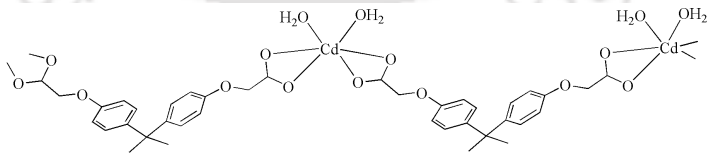

1.108

Figure 1.56: Structure of the *bis*-phenol based dicarboxylic acid **1.107** and its 1D cadmium coordination polymer **1.108.**

{[Cd(**BPA**)$(H_2O)_2]_n$} (**1.108**) (Figure **1.56**), whereas it forms a 2D coordination polymer with Zn(II) having hexagonal cavities. On the other hand, **$BPAH_2$** forms a hetero-metallic 3D coordination polymer of sodium and Pb(II) which possesses different types of isolated channels.

1.7 Scope of the present work:

From the foregoing discussion it is clear that *bis*-phenol and its analogues V-shaped compounds are suitable building blocks for crystal engineering. Various supramolecular networks such as zig-zag chain, helix, different interpenetrating ladders, and honey comb nets were generated from such molecules. The self assemblies of discrete *bis*-phenol molecules leading to supramolecular architectures serve as host and have vast possibility for guest binding.[30c] Thus, these compounds act as hosts for various aliphatic as well as aromatic guest molecules. Some of them were used for the selective separation of small organic molecules.[62] The studies on hydrogen bonded assemblies of *bis*-pheols with trigonal geometries would enable to study bottom up approach to make various assemblies for molecular recognitions. Although there is vast literature on *bis*-phenols, yet there is large scope to study the nitrogen containing *bis*-phenols as the complexity in the weak interactions can be enhanced by structural variations. Due to the limited literatures on nitrogen containing

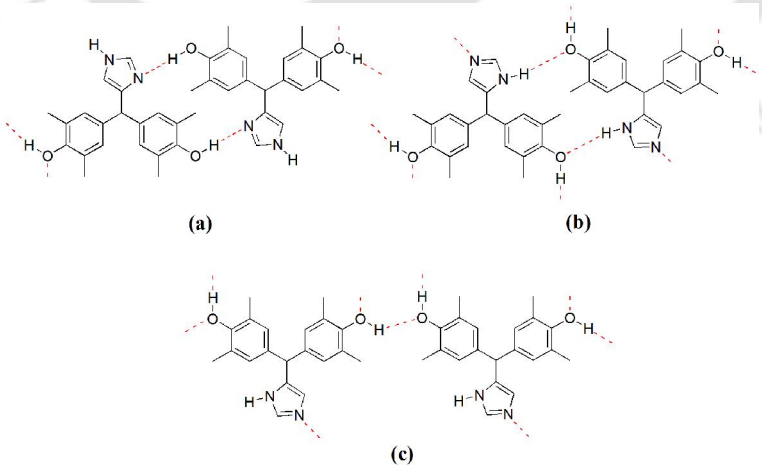

Figure 1.57: Some representative ways of weak interactions in the self-assembling of imidazole based *bis*-phenols.

bis-phenols, their host-guest chemistry is poorly understood.[75,76] Thus, the ability to form solvate and substrate binding by nitrogen containing *bis*-phenols need clear and systematic understanding.

Generally, *bis*-phenols and its related phenolic compounds possess O-H···O interactions in solid state. The introduction of one or more electronegative heteroatom such as nitrogen in one of the aromatic rings of triphenylmethyl *bis*-phenol would provide an additional interaction leading to a new dimension to the supramolecular chemistry of *bis*-phenols (Figure **1.57**). Furthermore, such protonated heteroatom would interact with different anions to give rise to new charge assisted assemblies of *bis*-phenols. Thus, we have chosen to perform a systematic study by attaching heterocyclic component such as imidazole unit to *bis*-phenols to understand their assemblies and substrate binding abilities.

Intermolecular interactions involving halogen atom, particularly the fluorine requires more attention in the field of organic crystal engineering[92] and there are also considerable crystal engineering on fluoro-phenols and other halo-phenols.[93] The advantage of using fluorine substituted organic compound is not only from the solubility and other related physical properties but it can also influence biological activity such as enzyme-substrate recognition[94] without changing its molecular size. Recrystallisation of fluorophenols under different pressure led to polymorphs which are differentiated by C-H···F-C interactions.[95] The fluorophenols with high *Z*' values are also reported[96] and the cocrystals of penta-fluorophenol with phenanzine in different proportions of host-guest ratio having C-H···F-C interactions are known.[97] Despite of low affinity to form the C-H···F-C interactions, their presence provide directional forces in fluorine containing organic compounds. Thus, fluorine containing compounds possessing other strongly hydrogen bond sites such as in fluoro *bis*-phenols may result in interesting supramolecular assemblies. There is lack of studies involving fluoro *bis*-phenols, which leaves avenues for understanding the role of C-F bond in their assemblies.

On the other hand, the two hydroxy groups of *bis*-phenols can be easily functionalized to prepare various semi-rigid or flexible V-shaped molecules. Such molecules will have versatile inorganic chemistry and would show interesting material properties. Steel et al. synthesized[98] some *bis*-phenols based polydentate ligands through coupling of various heterocycles to *bis*-phenols. These ligand can be use to construct

various metal organic frameworks. Moreover, various macrocyclic and mechanically interlocked systems such as catenane and rotaxene can be designed from *bis*-phenol

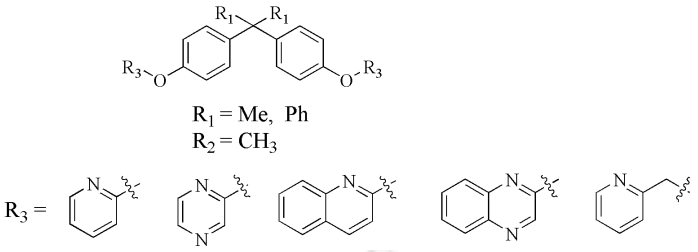

Figure 1.58: Some example of flexible *bis*-phenol based ligands.

precursors. For example, *bis*-phenol A based large-hole containing tetraphospha-macrocycle (**1.109**)[99] has four phosphorous centres separated at the corner of a 3.7 Å wide and 9.7 Å long rectangle. The macrocycle **1.109** provide a coordination space in which front to front type alignment is observed for small metal fragment such as $Ag(MeCN)_2$.

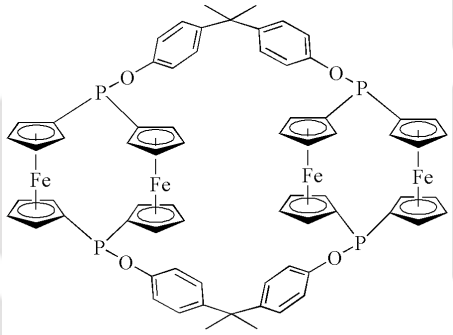

1.109

Figure 1.59: *Bis*-phenol A based large-hole tetraphosphamacrocycle (**1.109).**

Bis-phenol based [2]-Catenane **1.110,** forms divalent complexes with Cu(II), Fe(II) or Zn(II). It undergoes complete rearrangement during the coordination to the metal and brings the two coordinating fragments of each unit to close proximity. The interesting feature of **1.110** is the ability and ease to form five coordinate complexes.[100]

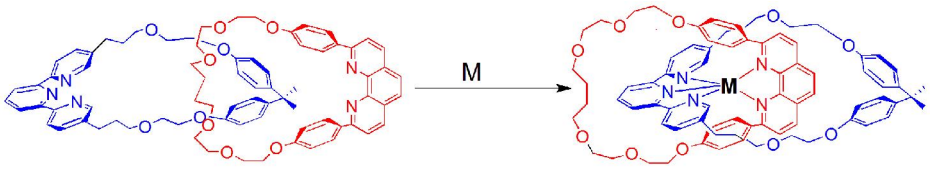

1.110 **1.111**

where, M = Fe(II), Cu (II) or Zn(II)

Equation 1.7: Reorganization of [2]-catenane (**1.110**) on interaction with metal.

The use of a flexible or less-rigid spacer for the construction of a coordination complex has an added advantage as they have many degrees of freedom and a few conformational restraints, which can give various topologies.[23] It would be of interest to functionalize some *bis*-phenols with -CH_2COOH to prepare the corresponding dicarboxylic acids. The flexibility associated with the -CH_2COOH groups and the

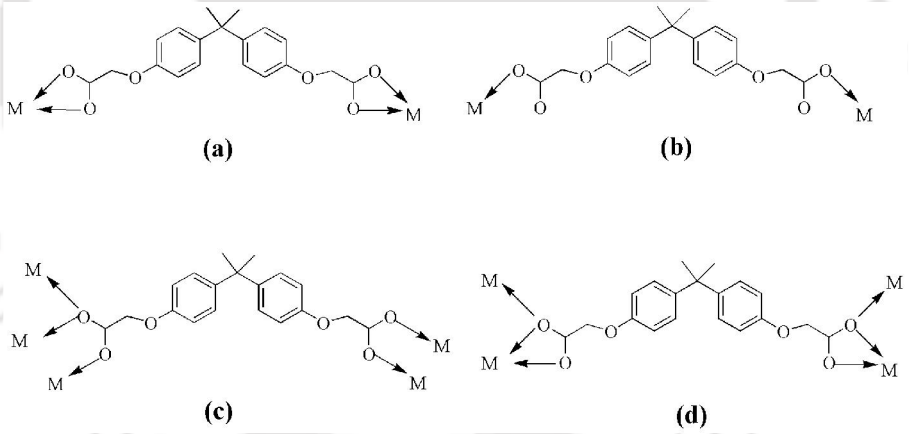

Figure 1.60: Different coordination modes of *bis*-phenol based V-shaped dicarboxylic acids.

rigidity associated with the *bis*-phenol part makes this class of ligands unique as different architectures for example, cyclic or zig-zag chains can be anticipates when these ligands attached to appropriate connections. The complicacy in predicting the architecture of the coordination complexes derived from these types of flexible ligands arises due to the different coordination modes of the carboxylate ligands. However, one may simplify this by restricting to one or two binding modes of

carboxylates leading to dinuclear complex, metallacycle or coordination polymers. Thus, looking at the potential of these functionalized *bis*-phenols to form various metal complexes we planned to prepare some functionalized *bis*-phenols, which would open new avenues for research.

The work presented in this thesis devoted to the supramolecular aspects of hetero-atom containing *bis*-phenols and the coordination chemistry of *bis*-phenol derivatives.

References:

1. (a) G. A. Jeffrey, *An Introduction to Hydrogen Bonding*, Oxford University Press, London, 1997; (b) G. R. Desiraju, *Acc. Chem. Res.*, 2002, **35**, 565-573; (c) G. R. Desiraju, *Angew. Chem., Int. Ed. Engl.* 1995, **34**, 2311-2327; (d) T. Steiner, G. R. Desiraju, *Chem. Commun.* 1998, 891-892; (e) E. Arunan, G. R. Desiraju, R. A. Klein, J. Sadlej, S. Scheiner, I. Alkorta, D. C. Clary, R. H. Crabtree, J. J. Dannenberg, P. Hobza, H. G. Kjaergaard, A. C. Legon, B, Mennucci, D. J. Nesbitt, *Pure Appl. Chem.*, 2011, **83**, 1637-1642; (f) G. R. Desiraju, *Angew. Chem. Int. Ed.*, 2011, **50**, 52-59.
2. (a) G. R. Desiraju, *Acc. Chem. Res.*, 1991, **24**, 290-296; (b) G. R. Desiraju, *Acc. Chem. Res.*, 1996, **29**, 441-449; (c) J. A. R. P. Sarma, G. R. Desiraju, *Acc. Chem. Res.*, 1986, **19**, 222-228.
3. (a) W. L. Jorgensen , J. Pranata, *J. Am. Chem. Soc.*, 1990, **112**, 2008-2010; (b) J. Pranata , S. G. Wierschke , W. L. Jorgensen, *J. Am. Chem. Soc.*, 1991, **113**, 2810-2819.
4. M. C. Etter, *Acc. Chem. Res.*, 1990, **23**, 120-126.
5. (a) G. E. Schulz, R. H. Schirmer, *Principle of Protein Structure*; Springer-Verlag: New York, 1995; (b) P. L. Wash, E. Maverick, J. Chiefari, D. A. Lightner, *J. Am. Chem. Soc.*, 1997, **119**, 3802-3806.
6. (a) J. W. Steed, J. L. Atwood, *Supramolecular Chemistry*; Wiley: Chichester, 2000; (b) G. R. Desiraju, C. V. K. Sharma, *In The Crystal as a Supramolecular Entity*; G. R. Desiraju, *Ed.;* Wiley: Chichester, 1996; (c) J. A. R. P. Sarma, Gautam R. Desiraju; *Cryst. Growth Des.*, 2002, **2**, 93-100; (d) K. M. Anderson, A. E. Goeta, J. W. Steed, *Cryst. Growth Des.*, 2008, **8**, 2517-2524. (e) D. S. Reddy, Y. E. Ovchinnikov, O. V. Shishkin, Y. T. Struchkov,

G. R. Desiraju, *J. Am. Chem. Soc.*, 1996, **118**, 4085-4089; (f) V. R. Hathwar, T. S. Thakur, R. Dubey, M. S. Pavan, T. N. Guru Row, G. R. Desiraju, *J. Phys. Chem. A*, 2011, **115**, 12852-12863.

7. (a) D. S. Reddy, D. C. Craig, G. R. Desiraju, *J. Am. Chem. Soc.*, 1996, **118**, 4090-4093; (b) A. Dey, M. T. Kirchner, V. R. Vangala, G. R. Desiraju, R. Mondal, J. A. K. Howard, *J. Am. Chem. Soc.*, 2005, **127**, 10545-10559.
8. O. Ermer, A. Eling, *J. Chem. Soc., Perkin Trans*., 1994, **2**, 925-944.
9. (a) S. G. Fleischman, S. S. Kuduva, J. A. McMahon, B. Moulton, R. D. Bailey Walsh, N. Rodríguez-Hornedo, M. J. Zaworotko, *Cryst. Growth Des.*, 2003, **5**, 909-919; (b) Q. Zeng, D. Wu, H. Ma, C. Shu, Y. Li, C. Wang, *CrystEngComm*, 2006, **8**, 189-201; (c) Y. -B. Men, J. Sun, Z. -T. Huang, Q. -Y. Zheng, *Angew. Chem., Int. Ed.*, 2009, **48**, 2873-2876; (d) Y. -B. Men, J. Sun, Z. -T. Huang, Q. -Y. Zheng, *Chem. Commun.*, 2010, 6299-6301; (e) Y. Manjare, V. R. Pedireddi, *Cryst. Growth Des.*, 2011, **11**, 5079-5086.
10. (a) J. Ceponkus, P. Uvdal, B. Nelander, J. Phys. Chem. A, 2012, **116**, 4842-4850; (b) M. Zuhayra, W. U. Kampen, E. Henze, Z. Soti, L. Zsolnai, G. Huttner, F. Oberdorfer, *J. Am. Chem. Soc.*, 2006, **128**, 424-425; (c) G. Jiang, J. Bai, H. Xing, Y. Li, X. You, *Cryst. Growth Des.*, 2006, **6**, 1264-1266; (d) L. -S. Long, Y. -R. Wu, R. -B. Huang, L. -S. Zheng, *Inorg. Chem.*, 2004, **43**, 3798-3800.
11. (a) R. Ludwig, *Angew. Chem., Int. Ed.*, 2001, **40**, 1808-1827; (b) K. Raghuraman, K. K. Katti, L. J. Barbour, N. Pillarsetty, C. L. Barnes, K. V. Katti, *J. Am. Chem. Soc.* 2003, **125**, 6955-6961; (c) J. Bernstein, *Polymorphism in Moleculer Crystal*; Oxford University Press: New York, 2002; (d) B. H. Oh, G. F. Ames, S. H. Kim, *J. Biol. Chem.*, 1994, **269**, 26323-26330; (e) A. J. Sharff, L. E. Rodseth, J. C. Spurlino, F. A. Quicocho, *Biochemistry*, 1992, **31**, 10657-10663; (f) J. A. Ernst, R. T. Clubb, H. -X. Zhou, A. M. Gronenborn, G. M. Clore, *Science*, 1995, **267**, 1813-1817.
12. M. Schmittel, G. Morbach, B. Engelen, M. Panthöfer, *CrystEngComm*, 2001, **3**, 137-140.
13. I. Y. H. Chan, V. T. Nguyen, R. Bishop, D. C. Craig, M. L. Scudder, *Cryst. Growth Des.*, 2010, **10**, 4582-4589.

14. (a) P. R. Dave, G. Doyle, T. Axenrod, H. Yazdekhasti, H. L. Ammon, *J. Org. Chem.*, 1995, **60**, 6946-6952; (b) P. R. Hemmes, L. Oppenheimer, F. Jordan, S. Nishikawa, *J. Phys. Chem.*, 1981, **85**, 98-101; (c) P. Hemmes, L. Oppenheimer, F. Jordan, *Chem. Commun.*, 1976, 929-930; (d) V. Hegde, P. Madhukar, J. D. Madura, R. P. Thummel, *J. Am. Chem. Soc.*, 1990, **112**, 4549-4550.
15. S. Hisamatsu, H. Masu, I. Azumaya, M. Takahashi, K. Kishikawa, S. Kohmoto, *Cryst. Growth Des.*, 2011, **11**, 5387-5395.
16. M, Du, Z. -H. Zhang, X. -J. Zhao, *Cryst. Growth Des.*, 2005, **5**, 1247-1254.
17. J. -H. Liao, C. -T. Chen, H. -C. Chou, C. -C. Cheng, P. -T. Chou, J. -M. Fang, Z. Slanina, T. J. Chow, *Org. Lett.*, 2002, **18**, 3107-3110.
18. (a) A. N. M. M. Rahman, R. Bishop, D. C. Craig, M. L. Scudder, *CrystEngComm*, 2002, **4**, 510-513; (b) J. Ashmore, R. Bishop, D. C. Craig, M. L. Scudder, *Cryst. Growth Des.*, 2007, **7**, 47-55; (c) S. F. Alshahateet, R. Bishop, D. C. Craig, M. L. Scudder, *Cryst. Growth Des.*, 2010, **10**, 1842-1847; (d) S. F. Alshahateet, R. Bishop, D. C. Craig, M. L. Scudder, *Cryst. Growth Des.*, 2011, **11**, 4474-4483.
19. E. M. Boyle, S. Comby, J. K. Molloy, T. Gunnlaugsson, *J. Org. Chem.*, 2013, **78**, 8312-8319.
20. S. Mukherjee, P. Thilagar, *Chem. Comm.*, 2013, **49**, 7292-7294.
21. S. C. Zimmerman, W. Wu, *J. Am. Chem. Soc.*, 1989, **111**, 8054-8055.
22. (a) E. M. Pérez, L. Sánchez, G. Fernández, N. Martín, *J. Am. Chem. Soc.*, 2006, **128**, 7172-7173; (b) K. Mulla, H. Shaik, D. W. Thompson, Y. Zhao, *Org. Lett.*, 2013, **15**, 4532-4535.
23. (a) Z. Dong, Y. Y. Wang, R. T. Liu, J. Q. Liu, L. Cui, Q. Z. Shi, *Cryst. Growth Des.*, 2010, **10**, 3311-3314; (b) H. Wang, D. Zhang, D. Sun, Y. Chen, L. F. Zhang, L. Tian, J. Jiang, Z. H. Ni, *Cryst. Growth Des*., 2009, **9**, 5273-5282; (c) L. Carlucci, G. Ciani, D. M. Proserpio, *Coord. Chem. Rev*., 2003, **246**, 247-289; (d) X. Shi, G. Zhu, X. Wang, G. Li, Q. Fang, G. Wu, G. Tain, M. Xue, X. Zhao, R. Wang, S. Qiu, *Cryst. Growth Des.*, 2005, **5**, 207-213; (e) C. D. Wu, W. Lin, *Angew. Chem., Int. Ed.*, 2007, **46**, 1075-1078; (f) R. -Q. Zou, H. Sakurai, S. Han, R. -Q. Zhong, Q. Xu, *J. Am. Chem. Soc.*, 2007, **129**, 8402-8403; (g) H. -L. Jiang, B. Liu, Q. Xu, *Cryst. Growth Des.*, 2010, **10**,

806-811; (h) J. Hu, L. Huang, X. Yao, L. Qin, Y. Li, Z. Guo, H. Zheng, Z. Xue, *Inorg. Chem.,* 2011, **50**, 2404-2414; (i) G. -X. Liu, R. -Y. Huang, L. -F. Huang, X. -J. Kong, X. -M. Ren, *CrystEngComm*, 2009, **11**, 643-656; (j) P. -C. Cheng, F. -S. Tseng, C. -T. Yeh, T. -G. Chang, C. -C. Kao, C. -H. Lin, W. -R. Liu, J. -S. Chen, V. Zima, *CrystEngComm*, 2012, **14**, 6812-6822.

24. A. M. Plonka, D. Banerjee, W. R. Woerner, Z. Zhang, J. Li, J. B. Parise, *Chem. Commun.*, 2013, **49**, 7055-7057.
25. F. Fu, D. -S. Li, Y. -P. Wu, X. -M. Gao, M. Du, L. Tang, X. -N. Zhang, C. -X. Meng, *CrystEngComm*, 2010, **12**, 1227-1237.
26. Q. Yang, X. Chen, Z. Chen, Y. Hao, Y. Li, Q. Lu, H. Zheng, *Chem. Commun*., 2012, **48**, 10016-10018.
27. H. Wang, K. Wang, D. Sun, Z. -H. Ni, J. Jiang, *CrystEngComm*, 2011, **13**, 279-286.
28. (a) C. Tu, Y. Shao, N. Gan, Q. Xu, Z. J. Guo, *Inorg. Chem.*, 2004, **43**, 4761-4766; (b) T. J. Burchell, D. J. Eisler, R. J. Puddephatt*, Cryst. Growth Des.*, 2006, **6**, 974-982; (c) V. J. Catalano, A. L. Moore, *Inorg. Chem*., 2005, **44**, 6558-6566; (d) L. Applegarth, N. Clark, A. C. Richardson, A. D. M. Parker, I. Radosavljevic-Evans, A. E. Goeta, J. A. K. Howard, J. W. Steed, *Chem. Commun*., 2005, 5423-5425; (e) V. J. Catalano, M. A. Malwitz*, Inorg. Chem*., 2003, **42**, 5483-5485.
29. Y. Liu, P. -F. Yan, Y. -H. Yu, G. -F. Hou, J. -S. Gao, J. Y. Lu, *Cryst. Growth Des.*, 2010, **10**, 1559-1568.
30. (a) N. D. Coggeshall, *J. Am. Chem. Soc.*, 1950, **72**, 2836-2844; (b) H. L. Bender, A. G. Farnham, U. S. Patent 2, 1949, **464**, 207; (c) R. J. Sarma, J. B. Baruah, *Cryst. Growth Des.,* 2007, **7**, 989-1000.
31. (a) L. Hopp, S. O. Megee, J. B. Lloyd, *J. Med. Chem.* 1998, **41**, 4421-4423; (b) A. Vessieres, S. Top, P. Pigeon, E. Hillard, L. Boubeker, D. Spera, G. Jaouen, *J. Med. Chem.* 2005, **48**, 3937-3940; (c) P. R. Kym, K. L. Hummert, A. G. Nilsson, M. Lubin, J. A. Katzenellenbogen, *J. Med. Chem.*1996, **39**, 4897-4904; (d) R. S. Muthyala, S. Sheng, K. E. Carlson, B. S. Katzenellenbogen, J. A. Katzenellenbogen, *J. Med. Chem*. 2003, **46**, 1589-1602.

32. B. D. Gehm, A. S. Levenson, H. Liu, E. J. Lee, B. M. Cushman, M. Amundsen, V. C. Jordan, J. L. Jameson, *Steroid Biochem. Mol. Biol.* 2004, **88**, 223-234.
33. M. Holmes-McNary, A. S. J. Baldwin, *Cancer Res.* 2000, **60**, 3477-3483.
34. M. M. H. Van Lipzig, A. M. ter Laak, A. Jongejan, N. P. E. Vermeulen, M. Wamelink, D. Geerke, J. H. N. Meerman, *J. Med. Chem.,* 2004, **47**, 1018-1030.
35. R. M. Giusti, K. Iwamoto, E. E. Hatch, *Ann. Intern. Med.,* 1995, **122**, 778-788.
36. (a) H. Lubczyk, R. Bachmann, R. Gust, *J. Med Chem.,* 2003, **46**, 1484-1491; (b) M. R. Schneider, E. Von Angerer, H. Schönenberger, R. T. Michel, H. P. Fortmeyer, *J. Med. Chem.,*1982, **25**, 1070-1077.
37. Y. Delaviz, H. W. Gibson, *Macromolecules,* 1992, **25**, 18-20.
38. E. Saiz, M. J. Fabre, L. Gargallo, D. Radic, I. Hernandez-Fuentes, *Macromolecules,* 1989, **22**, 3660-3662.
39. S. Abe, J. Mochizuki, T. Sone, *Anal. Chim. Acta,* 1996, **319**, 387-392.
40. A. Dondoni, C. Ghiglione, A. Marraa, M. Scoponi, *Chem. Commun.* 1997, 673-674.
41. I. Bauer, O. Rademacher, M. Gruner, W. D. Habicher, *Chem. Eur. J*., 2000, **6,** 3043- 3051.
42. I. Bauer, W. D. Habicher, *Tetrahedron Lett.,* 2002, **43**, 5245-5248.
43. (a) C. -A. Fustin, C. Bailly, G. J. Clarkson, P. D. Groote, T. H. Galow, D. A. Leigh, D. Robertson, A. M. Z. Slawin, J. K. Y. Wong, *J. Am. Chem. Soc.*, 2003, **125**, 2200-2207; (b) X. Lu, R. A. Weiss, *Macromolecules*, 1996, **29**, 1216-1221; (c) T. Yashiro, K. Matsushima, A. Kameyama, T. Nishikubo, *Macromolecules*, 2000, **33**, 7737-7742; (d) A. Alizadeh, S. Sohn, J. Quinn, H. Marand, L. C. Shank, H. D. Iler, *Macromolecules*, 2001, **34**, 4066-4078; (e) S. Carroccio, C. Puglisi, G. Montaudo, *Macromolecules*, 2002, **35**, 4297-4305.
44. D. J. Brunelle, E. P. Boden, T. G. Shannon, *J. Am. Chem. Soc*., 1990, **112**, 2399-2402.
45. (a) G. R. Desiraju, *Science*, 1997, **278**, 404-405; (b) M. Nishio, Y. Umezawa, H. Suezawa, S. Tsuboyama, In *The Importance of π-Interactions in Crystal Engineering: Frontiers in Crystal Engineering;* E. R. T. Tiekink, J. Zukerman-Schpector, Eds.; John Wiley & Sons Ltd: New York, 2012; Chapter

1; (c) M. Nishio, *Phys. Chem. Chem. Phys.*, 2011, **13**, 13873-13900; (d) O. Takahashi, Y. Kohno, M. Nishio, *Chem. Rev.*, 2010, **110**, 6049-6076; (e) M. Nishio, Y. Umezawa, *Top. Stereochem.* 2006, **25**, 255-302; (f) M. Nishio, *CrystEngComm,* 2004, **6**, 130-158.

46. C. P. Brock, L. L. Duncan, *Chem. Mater.,* 1994, **6**, 1307-1312.
47. R. J. Sarma, J. B. Baruah, *CrystEngComm*, 2005, **7**, 706-710.
48. R. J. Sarma, J. B. Baruah, *Dyes Pigm.*, 2004, **61**, 39-47.
49. R. J. Sarma, C. Tamuly, J. B. Baruah, *Dyes Pigm.*, 2007, **72***,* 75-79.
50. S. Aitipamula, G. R. Desiraju, M. Jaskólski, A. Nangia, R. Thaimattam, *CrystEngComm*, 2003, **5**, 447-450.
51. K. Yoshizawa, S. Toyota, F. Toda, M. Kato, I. Csöregh, *CrystEngComm,* 2007, **9**, 786-792.
52. M. C. Etter, *Acc. Chem. Res.*, 1990, **23**, 120-126.
53. J. Bernstein, R. Davis, L. Shimoni, N.-L. Chang, *Angew. Chem., Int. Ed. Engl.*, 1995, **34**, 1555- 1573.
54. N. Iwase, T. Kinuta, N. Tajima, T. Sato, R. Kuroda, Y. Matsubara, Y. Imai, *CrystEngComm*, 2010, **12**, 3195-3200.
55. S. Aitipamula, P. K. Thallapally, R. Thaimattam, M. Jaskolski, G. R. Desiraju, *Org. Lett.*, 2002, **4**, 921-924.
56. S. Aitipamula, A. Nangia, *Chem. Eur. J.*, 2005, **11**, 6727-6742.
57. B. Venkataramanan, W. L. G. James, J. J. Vittal, V. Suresh, *Cryst. Growth Des.* 2004, **4**, 553-561.
58. A. Jayaraman, V. Balasubramaniam, S. Valiyaveettil, *Cryst. Growth Des.*, 2006, **6**, 150-160.
59. J. N. Moorthy, P. Natarajan, *Chem. Eur. J.*, 2010, **16**, 7796-7802.
60. J. N. Moorthy, P. Natarajan, A. Bajpai, P. Venugopalan, *Cryst. Growth Des.*, 2011, **11**, 3406-3417.
61. A. Jayaraman, V. Balasubramaniam, S. Valiyaveettil, *Cryst. Growth Des.*, 2005, **5**, 1575-1583.
62. Suzuki, H. *Tetrahedron Lett*., 1992, **33**, 6319-6322; Suzuki, H.; Takagi, H. *Tetrahedron Lett*., 1993, **34**, 4805-4806; (c) Suzuki, H.; Takagi, H.; Sato, R. *Tetrahedron Lett*., 1997, **38**, 4563-4566.
63. R. Thakuria, B. Sarma, A. Nangia, *Cryst. Growth Des.,*2008, **8**, 1471-1473

64. R. Thakuria, B. Sarma, A. Nangia, *New J. Chem.*, 2010, **34**, 623-636.

65. C. Laurence, M. Berthelot, *Perspect. Drug Discovery Des.,* 2000, **18**, 39-60.

66. S. Aitipamula, A. Nangia, *Supramol. Chem.*, 2005, **17**, 17-25.

67. K. Tanaka, K. Endo, Y. Aoyama, *Chem. Lett.*, 1999, 887-888.

68. A. Bajpai, P. Natarajan, P. Venugopalan, J. N. Moorthy, *J. Org. Chem.*, 2012, **77**, 7858-7865.

69. J. N. Moorthy, R. Natarajan, P. Venugopalan, *J. Org. Chem*., 2005, **70**, 8568-8571.

70. W. C. McCrone, Polymorphism. In *Physics and Chemistry of the Organic Solid State*; D. Fox, M. M. Labes, A. Weissberger Eds.; Wiley-Interscience: New York, 1965, Vol. **2**, pp 725-767.

71. (a) *Solid-State Characterization of Pharmaceuticals*; A. Zakrzewski, M. Zakrzewski, Eds. Assa International Inc.: Danbury, CT, USA, 2006; (b) *Polymorphism in the Pharmaecutical Industry*; R. Hilfiker, Ed. Wiley-VCH: Weinheim, Germany, 2006; (c) G. R. Desiraju, *Cryst. Growth Des*., 2008, **8**, 3-5; (d) A. D. Bond, R. Boese, G. R. Desiraju, *Angew. Chem., Int. Ed.,* 2007, **46**, 615-617; (e) A. D. Bond, R. Boese, G. R. Desiraju, *Angew. Chem., Int. Ed.* 2007, **46**, 618-622; (f) A. D. Bond, R. Boese, G. R. Desiraju, *Am. Pharm. Rev.* 2007, May/June, 1–4.

72. (a) G. R. Desiraju, *CrystEngComm,* 2007, **9**, 91-92; (b) J. W. Steed, *CrystEngComm,* 2003, **5**, 169-179; (c) G. S. McGrady, M. Odlyha, P. D. Prince, J. W. Steed, *CrystEngComm*, 2002, **4**, 271-276; (d) A. Nangia, *Acc. Chem. Res*., 2008, **41**, 595-604.

73. B. Sarma, S. Roy A. Nangia, *Chem. Commun.*, 2006, 4918-4920.

74. S. Aitipamula, A. Nangia, *Chem. Commun.***,** 2005, 3159-3161.

75. R. J. Sarma, J. B. Baruah, *Sol. State Sci.*, 2008, **10**, 580-586.

76. R. J. Sarma, J. B. Baruah, *Chem. Eur. J.,* 2006, **12**, 4994-5000.

77. T. Kreickmann, C. Diedrich, T. Pape, H. V. Huynh, S. Grimme, F. Hahn, *J. Am. Chem. Soc.*, 2006, **128**, 11808-11819; (b) M. Wang, W. -J. Lan, Y. -R. Zheng, T. R. Cook, H. S. White, P. J. Stang, *J. Am. Chem. Soc.*, 2011, **133**, 10752-10755; (c) I. Sánchez-Molina, B. Grimm, R. M. K. Calderon, C. G. Claessens, D. M. Guldi, T. Torres, *J. Am. Chem. Soc.*, 2013, **135**, 10503-

10511; (d) F. D. Salvo, F. Teixidor, C. Viñas, J. G. Planas, M. E. Light, M. B. Hursthouse, N. Aliaga-Alcalde, *Cryst. Growth Des.*, 2012, **12**, 5720-5736.

78. (a) J. C. Wu, T. L. Yu, C. T. Chen, C. C. Lin, *Coord. Chem. Rev.*, 2006, **250**, 602-626; (b) H. C. Lin, L. F. Yan, F. C. Wang, Y. L. Sun, C. C. Lin, *J. Organomet. Chem.*, 1999, **587**, 151-159; (c) B. T. Ko, C. C. Wu, C. C. Lin, *Organometallics*, 2000, **19**, 1864-1869; (d) B. T. Ko, Y. C. Chao, C. C. Lin, *Inorg. Chem.*, 2000, **39**, 1463-1469; (e) W. Braune, J. Okuda, *Angew. Chem., Int. Ed.*, 2003, **42**, 64-68; (f) M. L. Hsueh, B. H. Huang, J. C. Wu, C. C. Lin, *Macromolecules*, 2005, **38**, 9482-9487; (g) B. H. Huang, B. T. Ko, T. Athar, C. C. Lin, *Inorg. Chem.*, 2006, **45**, 7348-7356.
79. (a) A. van der Linden, C. J. Schaverien, N. Meijboom, C. Granter, A. G. Orpen, *J. Am. Chem. Soc.*, 1995, **117**, 3008-3021; (b) J. Okuda, S. Fokken, H. C. Kang, W. Massa, *Chem. Ber.*, 1995,**128**, 221-227; (c) F. G. Sernetz, R. Mulhaupt, S. Fokken, J. Okuda, *Macromolecules*, 1997, **30**, 1562-1569; (d) M. H. Chisholm, J. H. Huang, J. C. Huffman, W. E. Streib, D. Tiedtke, *Polyhedron*, 1997, **16**, 2941-2949; (e) M. H. Chisholm, K. Folting, W. E. Sterib, D. D. Wu, *Inorg. Chem.*, 1998, **37**, 50-55; (f) D. Takeuchi, T. Nakamura, T. Aida, *Macromolecules*, 2000, **33**, 725-729; (g) D. R. Mulford, P. E. Fanwick, I. P. Rothwell, *Polyhedron*, 2000, **19**, 35-42; (h) M. Gonzalez-Maupoey, T. Cuenca, L. M. Frutos, O. Castanô, E. Herdtweck, *Organometallics*, 2003, **22**, 2694-2704.
80. D. Zhang, *Organometallics*, 2007, **26**, 4072-4075.
81. Percentages by mass, in: J. Emsley (Ed.), The Elements, Clarendon Press, Oxford, 1998, 194-195.
82. H.-Y. Chen, J. Zhang, C. -C. Lin, J. H. Reibenspies, S. A. Miller, *Green Chem.***,** 2007, **9**, 1038-1040.
83. (a) B. -T. Ko, C. -C. Wu, C. -C. Lin, *Organometallics*, 2000, **19**, 1864-1869 (b) B. T. Ko, Y. C. Chao, C. C. Lin, *Inorg. Chem.*, 2000**, 39***,* 1463-1469.
84. X. Xu, X. Pan, S. Tang, X. Lv, L. Li, J. Wu, X. Zhao, *Inorg. Chem. Commun*., 2013, **29**, 89-93.
85. H. -Y. Chen, M. -Y. Liu, A. K. Sutar, C. -C. Lin, *Inorg. Chem.,* 2010, **49**, 665-674.
86. J. Wu, X. Pan, N. Tang, C. -C. Lin, *Inorg. Chem.,* 2010, **49**, 5362-5364.

87. A. R. Kennedy, R. E. Mulvey, R. B. Rowlings, *J. Am. Chem. Soc.,*1998, **120**, 7816-7824.
88. N. M. Clark, P. García-Álvarez, A. R. Kennedy, C. T. O'Hara, G. M. Robertson, *Chem. Commun.,* 2009, 5835-5837.
89. G. A. Craig, J. S. Costa, D. Aguilà, L. A. Barrios, O. Roubeau, S. J. Teat, G. Aromí, *New J. Chem.*, 2011, **35**, 1202-1204.
90. N. Tiempos-Flores, A. -J. Metta-Magaña, V. Montiel-Palma, S. -A. Cortés-Llamas, M. - A. Muñoz-Hernández, *Dalton Trans.*, 2010, **39**, 4312-4320.
91. Z. -B. Zheng, R. -T. Wu, J. -K. Li, Y. -F. Sun, Y. -F. Han, *J. Mol. Struct.*, 2010, **964**, 109-118.
92. (a) M. D. Prasanna, T. N. Guru Row, *CrystEngComm,* 2000, **3**, 134-140; (b) K. Reichenbacher, H. I. Suss, J. Hulliger, *Chem. Soc. Rev*., 2005, **34**, 22-30; (c) D. Chopra, T. N. Guru Row, *CrystEngComm,* 2011, **13**, 2175-2186; (d) R. Berger, G. Resnati, P. Metrangolo, E. Weber, J. Hulliger, *Chem. Soc. Rev.*, 2011, **40**, 3496-3508; (e) A. G. Dikundwar, R. Sathishkumar, T. N. Guru Row, G. R. Desiraju, *Cryst. Growth Des.*, 2011, **11**, 3954-3963; (f) D. Chopra, *Cryst. Growth Des.*, 2012, **12**, 541-546; (g) G. Kaur, P. Panini, D. Chopra, A. R. Choudhury, *Cryst. Growth Des*., 2012, **12**, 5096-5110.
93. (a) I. J. Brass, A. T. Bullock, *J. Chem. Soc., Faraday Trans.*, 1978, **74**, 1556-1561; (b) J. L. Alderfer, A. V. Eliseev, *J. Org. Chem.*, 1997, **62**, 8225-8226; (c) M. Rappo-Abiuso, M. F. Llauro, Y. Chevaliera, P. L. Perchec, *Phys. Chem. Chem. Phys.*, 2001, **3**, 99-106; (d) C. Laurence, J. Graton, M. Berthelot, F. Besseau, J. Y. L. Questel, M. Lucon, C. Ouvrard, A. Planchat, E. Renault, *J. Org. Chem.*, 2010, **75**, 4105-4123.
94. R. B. Silverman, K. A. Bichler, A. J. Leon, *J. Am.Chem. Soc*., **1996**, **118**, 1253-1261.
95. (a) I. D. Oswald, D. R. Allan, W.D. Motherwell, S. Parsons, *Acta Crystallogr.*, B2005, **61**, 69-79; (b) I. D. Oswald, D. R. Allan, G. M. Day, W. D. Motherwell, S. Parsons, *Cryst. Growth and Des*.**,** 2005, **5**, 1055-1071.
96. (a) M. Gdaniec, *CrystEngComm,* 2007, **9**, 286-288; (b) D. Das, R. Banerjee, R. Mondal, J. A. K. Howard, R. Boese, G. R. Desiraju, *Chem Commun*., 2006, 555-557.
97. A. Czapik, M. Gdaniec, *Acta Crystallogr. C.*, 2011, **67**, o341-o345.

98. A. R. Katritzky, P. J. steel, S. N. Denisenko, *Tetrahedron*, 2001, **57**, 3309-3314.

99. T. Mizuta, Y. Inami, K. Kubo, K. Miyoshi, *Inorg. Chem.*, 2009, **48**, 7534-7536.C. Hamann, J. -M. Kern, J. -P. Sauvage, *Inorg. Chem.*, 2003, **42**, 1877-1883.

100. C. Hamann, J. -M. Kern, J. -P. Sauvage, *Inorg. Chem.*, 2003, **42**, 1877-1883.

CHAPTER 2

Quasi-isostructural solvates of an amino substituted *bis*-phenol: *bis*(4-hydroxy-3,5-dimethylphenyl)(4-N,N-dimethylaminophenyl)methane

The term isostructural relates to two crystals when they have the same structure, but compositions of such crystals are not necessarily being same. Such crystals should have a comparable variability in the atomic coordinates to that of the cell dimensions and chemical composition. So, in other words, isostructurality is a phenomenon in which two or more different systems show similar kind of structures.[1] Isostructurality is an important issue in terms of structure-property relationship as with increasing the degree of isostructurality, the properties are expected to be similar. There are many organic[2] as well as inorganic compound[3] that are isostructral. For example, calcite (calcium carbonte)[4] and nitratine (sodium nitrate)[5] are the classical example of isostructural compounds.[6] The availability of a series of isostructural solvates of a single compound offer a rare opportunity to study the effect of crystal structure on solid state properties.[7] The phenomenon of solvent inclusion by a particular host is interesting as it may lead to the formation of new polymorphic form upon desolvation.[8] Moreover, the presence of solvent molecules in the crystal lattice offer unique physical properties to the solvates.[9] For example, the solubility and the dissolution rate of the hydrates are different from those of the anhydrous form resulting in the differences of the bioavailability of drugs.[10] In some solvates the solvent molecules acts as space fillers whereas in some other solvates the solvent molecule is essential components of the lattice by interacting with the host molecules by hydrogen bonding.[11] Bingham et al. classified the former types of solvates as inclusion compounds and the other types of solvates as co-crystals.[12] A particular host is often found to exhibit solvation with several guests, and these solvates may be isostructural,[13] structurally distinct[14] or partially isostructural.[15] It was earlier shown that different series of layered or lamellar structures can be built depending upon the substituent present in *bis*-phenols, which can include benzene and toluene molecules as guest.[16] The schematic representation of the building principle is shown in Figure **2.1**. It was observed that the *bis*(4-hydroxy-3,5-dimethylphenyl)(4-N,N-dimethylaminophenyl)methane (Ambp) forms acetonitrile solvate[17] rather than

forming solvate with toluene or benzene. This could be attributed to the inability of the N-dimethylamine group to participate in strong hydrogen bonds unlike OH or NH_2 groups.

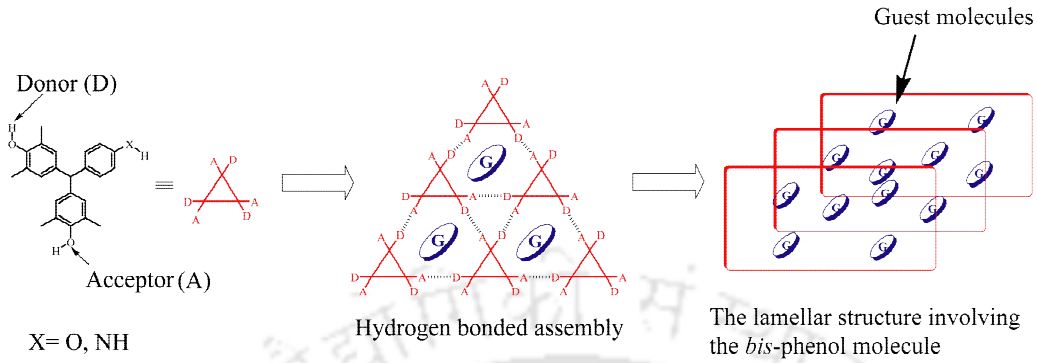

Figure 2.1: Schematic representation of the formation of lamellar structure by substituted *bis*-phenols.

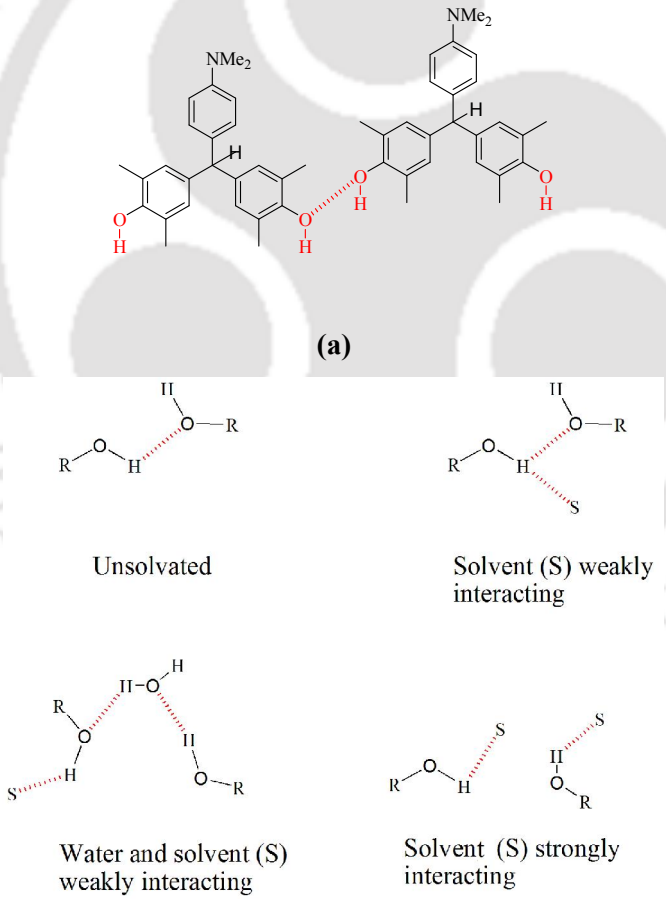

Scheme 2.1: (a) The Plausible O-H···O interactions among the *bis*-phenol Ambp (**2.1**), **(b)** Some representative ways of interactions by solvent molecules at the junctions of hydrogen bonds.

Since *bis*-phenol **2.1** is associated with strong hydrogen bonds to form a linear structural network in acetonitrile, we felt it necessary to examine possibility of retention of such hydrogen bonded motifs by the interacting solvents, during the formation of various solvates.

On the other hand, different organic hydroxy compounds form strong hydrogen bonds, among which hydrogen-bonded assemblies of *bis*-phenols and their related compounds are well-known for their ability to form selective host-guest assemblies.[18, 19] The role of guest molecules to influence the interactions among host molecules to adopt new supramolecular structures requires attention. For example, there are several ways in which solvent molecules can bind to a host molecule.[7] The formation of a particular motif would depend on the ability of the solvent to break apart the hydrogen bond/s of the host molecules, as illustrated in the Scheme **2.1 (b)**. A weak hydrogen-bond acceptor solvent will not break hydrogen bonds of self-assembled hosts, whereas a strong hydrogen-bond acceptor will break them apart. A moderate acceptor will partially break and also compete with strongly hydrogen bond former molecules from the environment to form different types of structures, as depicted in Scheme **2.1 (b)**. It would be of interest to look at the affect of the solvent polarity on stabilisation of a particular type of hydrogen bonded assembly. Besides these, the size of the guest molecules and the other functional groups of the host-guest assemblies participating in weak interactions will also determine the final packing pattern. Generally, it is a

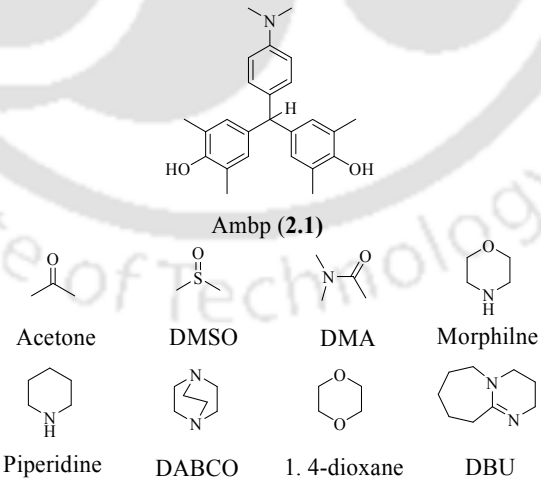

Figure 2.2: The structure of the *bis*-phenol Ambp **(2.1)** and the solvent molecules used in the study.

challenge to identify a host molecule which will form substantial numbers of solvates with various guest solvent molecules.[20] We find that bis(4-hydroxy-3,5-dimethylphenyl)(4-N,N-dimethylamino phenyl)methane (Ambp, **2.1**) is a suitable host for various small molecules, which are shown in Figure **2.2**. In this chapter we present a comprehensive study to narrate the role of weak interactions of solvent molecules in stabilizing different structural motifs around the bridging hydrogen bonds (scheme **2.1a** and **2.1b**) in the self-assembly of the host Ambp **(2.1)**. Moreover we are also emphasising on the retention or variation of the packing of the host molecules with changing the guest molecules.

2.1 Synthesis and characterization of *bis*(4-hydroxy-3,5-dimethylphenyl)(4-N, N-dimethylaminophenyl)methane (Ambp)

The *bis*-phenol *bis*(4-hydroxy-3,5-dimethylphenyl)(4-N,N-dimethylaminophenyl) methane (Ambp, **2.1**) was synthesised by condensation of N,N-4-dimethylamino-benzaldehyde and 2,6-dimethylphenol under acidic conditions using a reported procedure.[17] The compound was characterised with various spectroscopic techniques such as IR, ^{1}H-NMR, ^{13}C-NMR and mass spectrometry. The IR stretching frequencies for the hydroxy groups appear at 3603 cm^{-1} and 3499 cm^{-1}; and the IR stetching frequencies of the C-H of the different methyl groups appears at 2914 cm^{-1}, 2868 cm^{-1} and 2803 cm^{-1} (Figure **2.3a**). In the ^{1}H-NMR of **2.1,** the singlet at 2.17 ppm is for the protons of the methyl group attached to the aromatic ring, whereas the signals for the methyl protons of the tertiary amine group appear at 2.91 ppm. The characteristic methine proton of *bis*-phenol appears at 5.20 ppm (Figure **2.3b**).

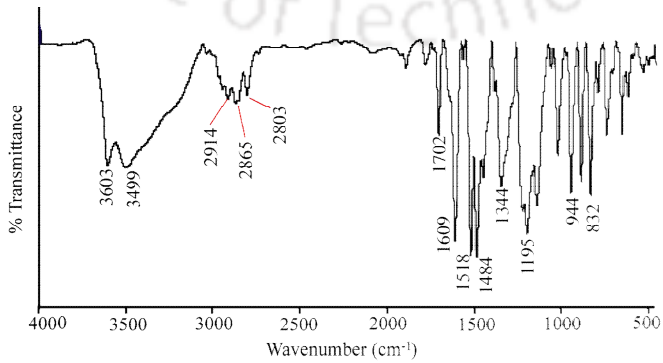

(a)

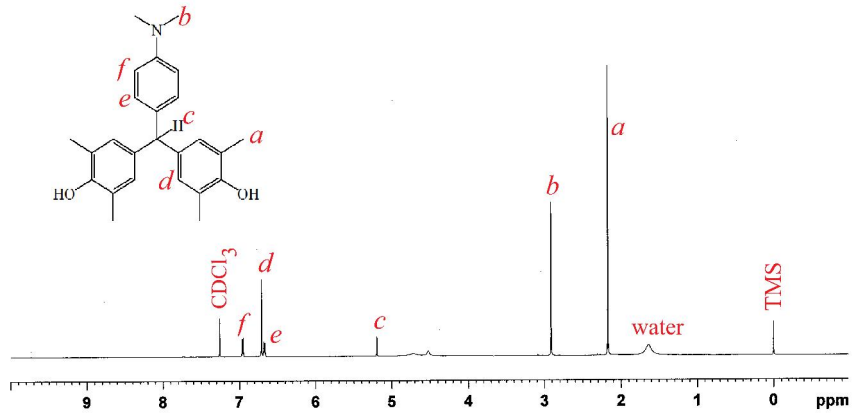

(b)

Figure 2.3: **(a)** The FT-IR (KBr, cm^{-1}) and **(b)** The ^{1}H-NMR (600MHz, $CDCl_3$) spectra of the amino *bis*-phenol **2.1**.

2.2 Solvates of *Bis*(4-hydroxy-3,5-dimethylphenyl)(4-N,N-dimethylaminophenyl) methane

Eight different solvates of Ambp **(2.1)**, namely, Ambp.acetone **(2.2)**, Ambp.DMSO **(2.3)**, Ambp.DMA **(2.4)**, Ambp.morpholine **(2.5)**, Ambp.piperidine **(2.6)**, 2Ambp. DABCO.3H_2O **(2.7)** **(DABCO**=1,4-diazabicyclo[2.2.2]octane**)**, Ambp.dioxane.H_2O **(2.8)** and Ambp.DBU **(2.9)** **(DBU**=1,8-Diazabicyclo[5.4.0]undec-7-ene**)** were prepared by crystallisation from respective solvent as described in the experimental section. They are structurally characterised **by** single crystal X-ray diffraction and other conventional techniques. The solvate **2.2-2.6** belong to space group $P2_1/c$, and the remaining three **2.7-2.9** belong to *P-1* space group. Since the *bis*-phenol molecules possesses characteristic O-H···O interaction, the solvate (**2.2-2.6**) are example of a series of structures that are suitable to analyse the interaction of the solvent molecules at the point of attachment among the host molecules. Each of the solvate **2.2-2.6** form a chain-like structure through O-H···O interaction and the O-H···O distances in these solvates are comparable except for the dimethylacetamide solvate **(2.4)**. There are three different types of H-bonding motifs between the solvent molecules and the host *bis*-phenol **2.1**; **(a)** single point contact of solvent molecules to the bridging O-H···O unit with additional weak interactions, **(b)** single point contact of the solvent molecules forming $R_2^2(6)$ types of cyclic H-bonding and **(c)** two point contact leading to $R_3^3(7)$ types of cyclic hydrogen bonded motifs. The donor acceptor distances in **2.2** and **2.3** are similar and the structures belong to the first type (Figure **2.4a** and **2.4b**)

whereas **2.5** and **2.6** have similar structures which belong to the third type (Figure **2.5a** and **2.5b**). The dimethylacetamide solvate **2.4** possesses the second type of structure. It shows very weak hydrogen bonding interactions among the host molecules, despite it has a linear chain-like structure of the host molecules. The acetonitrile solvate of **2.1** was already reported and the acetonitrile molecules attach to the O-H···O junction of the host molecules through weak O-H···N interaction and retains the chain-like structure of among the host.[17]

2.2.1 Solvates 2.2-2.6

The asymmetric unit of the acetone solvate (**2.2)** contains one host molecule and an acetone molecule. The host Ambp molecules interacts with each other through O-H···O interactions to form one dimensional chain. On the other hand, the acetone molecules are attached to the chain through O-H···O interactions at the junction of the host molecules. In the solvate **2.2** the oxygen atom of the acetone molecule involves

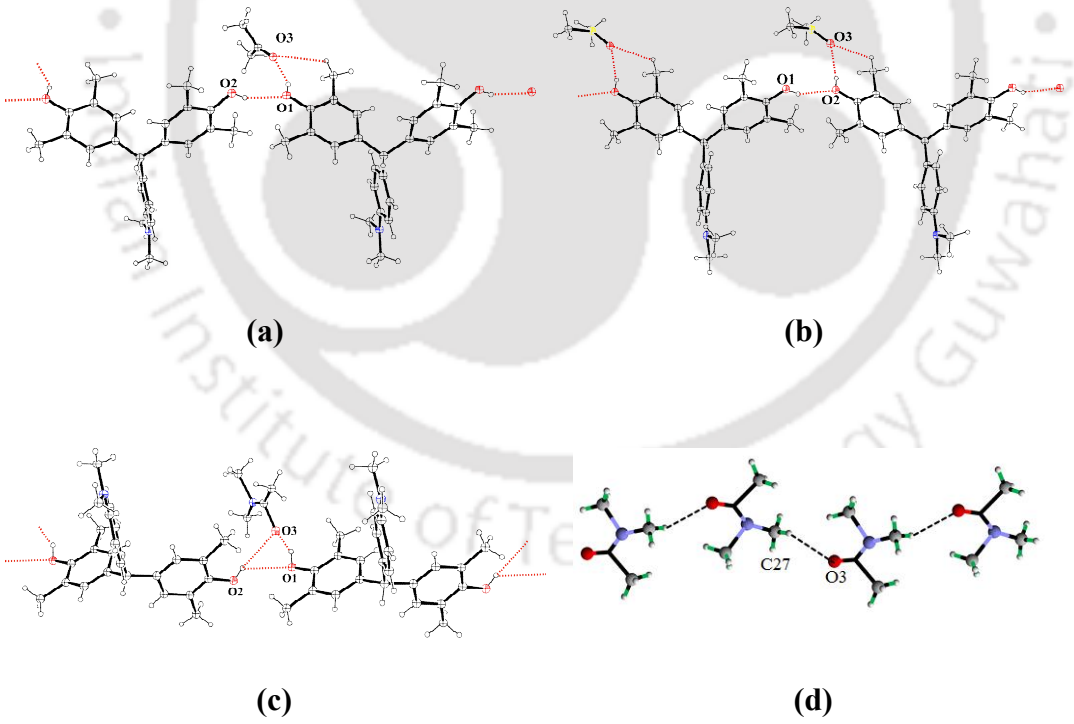

Figure 2.4: One dimensional chain in the crystal structure of **(a)** acetone solvate **2.2** **(b)** DMSO solvate **2.3** and **(c)** DMA solvate **2.4**, **(d)** Formation of chain of DMA molecules in the solvate **2.4**.

in bifurcated O(1)-H···O(3) [$d_{D\cdots A}$= 2.714 Å, ∠D-H···A=145°] and C(8)-H···O(3) [$d_{D\cdots A}$=3.335 Å, ∠D-H···A= 123.23°] interactions with one of the hydroxy group and C-H of the methyl group. The DMSO solvate (**2.3)** has the similar structure to that of the acetone solvate and in this case also the oxygen atom of the dimethylsulphoxide involves in bifurcated hydrogen bonds namely, O(3)-H···O2 [$d_{D\cdots A}$= 2.602 Å and ∠D-H···A=135.50°] and C(25)-H···O(3) [$d_{D\cdots A}$=3.181 Å and ∠D-H···A=122.65°] interactions. These result in $R_2^1(7)$ hydrogen bond motifs located at a position away from the bridge in solvates **2.2** and **2.3**. In both the cases, these one dimensional chains further connected to each other through C-H···O and C-H···π interactions resulting in the formation of three dimensional self assembled structure having channels running along the crystallographic *b*-axis. These channels are occupied by solvent molecules. The inclusion of acetone molecules by hydroxy compound is a well known phenomenon where C-H···O interactions play the important role.[21] For example, the tetra hydroxy compound 9,10-bis-(2,5-dihydroxy-1-phenyl)anthracene forms a 1D ladder like structure where the anthracene units act as rung and the acetone molecules are incorporated in the ladder through C-H···O=C interactions.[21e] On the other hand, in the case of solvate **2.4** the oxygen atom of the dimethylacetamide molecule bridges two host molecules through bifurcated O···H-O interactions namely, O(1)-H···O(3) [$d_{D\cdots A}$= 2.666 Å and ∠D-H···A=138°] and O(2)-H···O(1) [$d_{D\cdots A}$= 3.256 Å and ∠D-H···A=128.08°]. The bifurcated hydrogen bonds results in the formation of $R_2^2(6)$ types of motifs. The overall packing pattern of the solvate has a three dimensional structure containing channel along the crystallographic b-axis and DMA molecules are incorporated in the channels. The DMA molecules forms a one dimensional chains through C-H···O interaction inside the channels running along the crystallographic *b*-axis (Figure **2.4d**).

In the crystal structure of solvate **2.5** the morpholine molecule are attach to the H-bonded chain of the host molecule through O-H···N [$d_{D\cdots A}$= 2.632 Å and ∠D-H···A=163°] and C-H···O interaction (Figure **2.5a**). These chains self-assembles through N-H···π, C-H···π and C-H···O interactions which lead to the formation of channel like structure (Figure **2.7b**) running along the crystallographic *b*-axis. The N-H bond of the morpholine molecule interacts with the dimethylamino containing aromatic ring of the Ambp molecule through N-H···π interaction (Figure **2.6a**) and the oxygen atom of the morpholine molecule interacts with the Ambp molecule

through O-H···O interactions. Apart from these, the significant interactions observed between the host and the guest are C-H···O and C-H···π interactions. The N-H···π

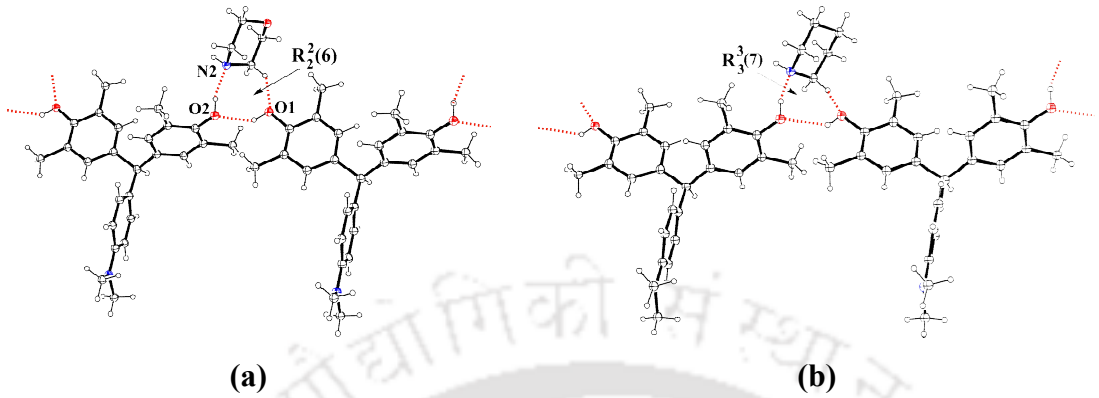

Figure 2.5: The one dimensional chains of the **Ambp** molecules in the crystal structure of the **(a)** morpholine solvate **2.5** and the **(b)** piperidine solvate **2.6**.

interaction is a relatively weak interaction having energy of 1-3 kcal/mol.[22] Although N-H···π interactions have been reported among the amino *bis*-phenols,[23] this types of N-H···π interaction was not reported in solvates of *bis*-phenols. Here we observe an interesting η^3-type of N-H···π interaction between the *bis*-phenols and the morpholine molecules which suggests that a preorganised conformation is not necessarily required for such interactions. Even though the N-H···π interactions is less in energetic terms, it is observed that they occur frequently in proteins and cumulatively these interactions provide significant energy for protein stability. The N-H···π interactions in proteins have been involved in a wide variety of functions such as secondary structure stabilization,[24] drug recognition,[25] DNA recognition[26] and enzyme action.[27] Indole-3-acetic acid (commonly known as auxin) shows N-H···π interactions while participating in biological functions such as cell division and protein synthesis.[28]

In case of the piperidine solvate **2.6**, the piperidine molecules are attached to the chain of the host molecule through O-H···N [$d_{D\cdots A}$= 2.594 Å and ∠D-H···A=163°] and C-H···O interaction. Here also the N-H bond of the piperidine participates in N-H···π interactions with the dimethylamino group containing aromatic ring of the host molecule (Figure **2.6b**). In that sense, the piperidine and morpholine molecules have

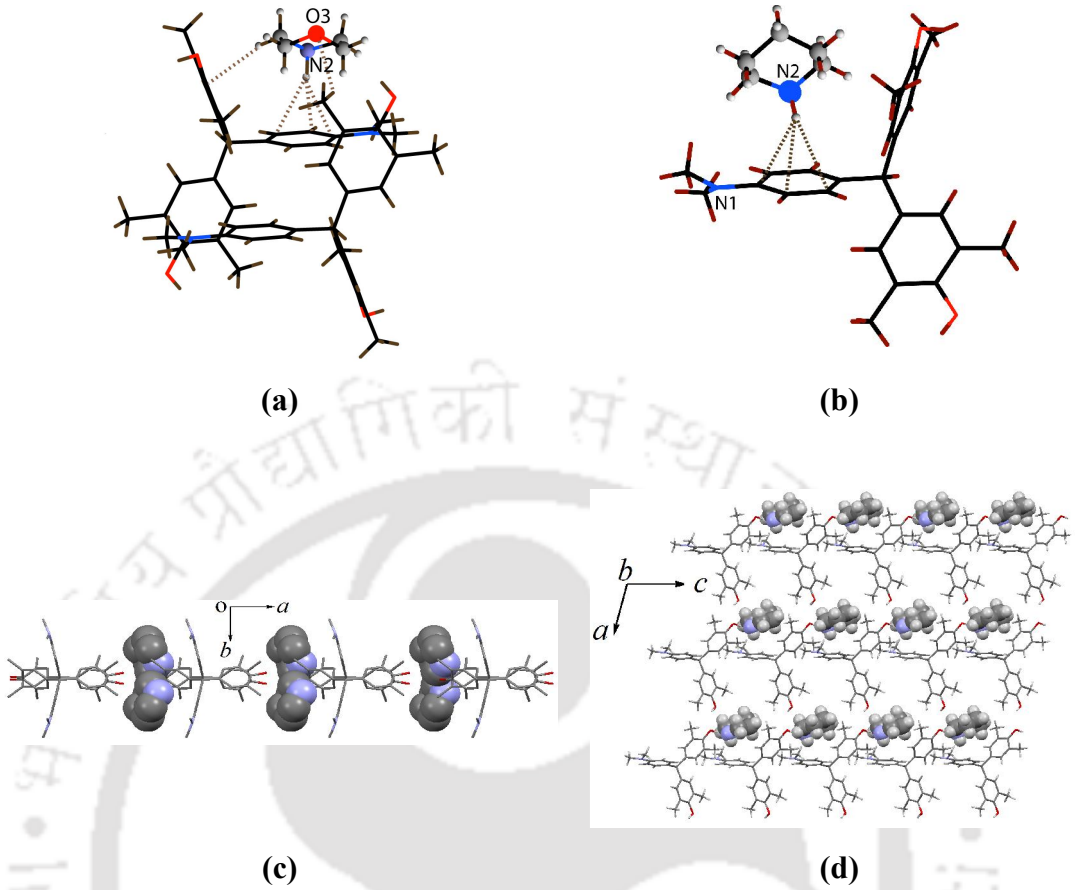

Figure 2.6: η^3-types of N-H···π interaction **(a)** in the morpholine solvate **2.5** and **(b)** piperidine solvate **2.6**, **(c)** The packing of the piperidine solvate **2.6** showing the solvents in space filled model, **(d)** 2D network of host molecules in **2.6** after removal of the solvent molecules.

similar types of interactions while binding to the host molecule in their respective lattices. The N-H···$\pi_{centroid}$ distance in the solvate **2.5** and **2.6** are almost similar and in the range of 3.480 Å and it is comparable with the N-H···π distance found N-methylformamide-benzene complex which are in the range of 3.2-3.6 Å.[29] However, the difference arise in the packing pattern of the two solvates **2.5** and **2.6** due to the presence of the oxygen atom in morpholine instead of CH_2 group present in piperidine molecule. In the piperidine solvate **2.6**, host molecules are packed in one layer across the crystallographic *ac*-plane and the guest molecules are held at the hydrogen-bond junctions of the layers, whereas in the morpholine solvate, channel-like structures

running along the *b*-crystallographic axis are formed by the *bis*-phenols, in which the guest molecules get incorporated (Figure **2.7a** and **b**).

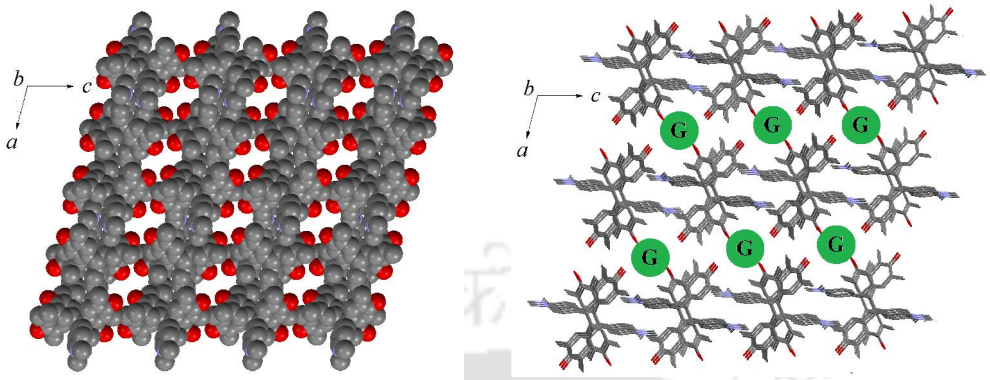

(a) **(b)**

Figure 2.7: (a) Packing diagram of the solvate **2.5** after removal of the solvent molecules, **(b)** The inclusion of the guest **(G)** molecules in the solvate **2.2-2.5**.

Table 2.1: O-H···O bond parameters of the solvate **2.2-2.6.**

Compd no	D-H···A	d_{D-H}(Å)	$d_{H\cdots A}$(Å)	$d_{D\cdots A}$(Å)	∠D-H···A (°)
2.2	O(2)-H(2)···O(1) [-1+x, y, z]	0.82	2.13	2.858(6)	148
	O(1)-H(1) ··· O(3) [1-x,-y,-z]	0.82	2.00	2.714(6)	145
2.3	O(1)-H(1)···O(2) [1 +x, y, z]	0.82	2.15	2.859(8)	144
2.4	O(2)-H(1)···O(1)	0.82	2.68	3.255	128
2.5	O(1)−H(1)···O(2) [−1+x, y, z]	0.82	2.07	2.731(2)	138
2.6	O(1)-H(1)···O(2) [−1+x, y, z]	0.76(4)	2.20(4)	2.799(3)	136(3)

The solvates **2.2-2.6** have similar unit cell parameters and crystallizes in $P2_1/c$ space group. The solvates **2.2-2.5** are isostructural with similar arrangements of the host molecules in their respective unit cells. In the solvates **2.2-2.5** the solvent molecules are located in the channels running along the [010] direction formed by the molecular framework of the host Ambp molecules (Figure **2.7b**). Although the piperidine solvate (**2.6)** have the similar unit cell parameters with the first four solvates **2.2-2.5**, the arrangements of the host molecules in its unit cell are different. In case of **2.6**, the host molecules form a 2D network through O-H···O interactions and the piperidine molecules attached to the net through O-H···N, C-H···O and N-H···π interactions (Figure **2.6d**).

2.2.2 Solvates 2.7, 2.8 and 2.9

The crystals of solvate **2.7** belong to triclinic space group and the crystallographic asymmetric unit contains two Ambp molecules, one DABCO and three water molecules of crystallization. Both the hydroxy group of the *bis*-phenol molecule are involved in hydrogen bonding with the DABCO molecules either through directly or through bridging water molecule. One of the water molecule H_2O (7) of the solvate involves in the formation of cyclic H-bonded motif which contain four Ambp molecule (two pairs having independent symmetry), two DABCO and two water molecules as shown in the Figure **2.8**.

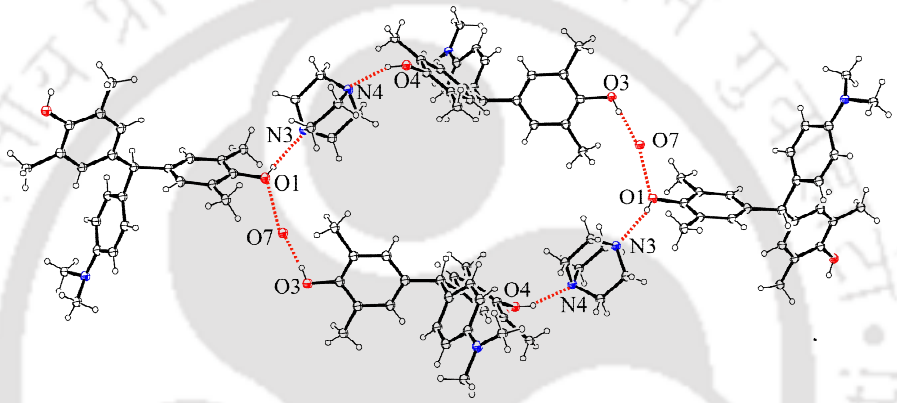

Figure 2.8: Cyclic H-bonding motifs in the solvate **2.7** involving four Ambp, two DABCO and two water molecules.

The 1,4-dioxane solvate (**2.8)** crystallizes in triclinic *P-1* space group and the crystallographic asymmetric unit contains one molecule of Ambp, half of the two symmetry non equivalent 1,4-dioxane molecule, and a water molecule of crystallization. Here, both the symmetry independent 1, 4-dioxane molecules adopts chair conformation. The two hydroxy group of the Ambp molecules form strong H-bonds, viz., O(1)-H(1)···O(3) [$d_{D\cdots A}$ = 2.894 Å and ∠D-H···A = 149°] and O(2)-H(2)···O(4) [$d_{D\cdots A}$= 2.942 Å and ∠D-H···A = 148°] with two symmetry-independent dioxane molecules of the solvate. The oxygen atoms of the dioxane molecule acts as hydrogen bond acceptor to interact with the host Ambp molecule. These interactions results in the construction of 2D layers containing channels and these 2D layers further connected to each other to give 3D host-guest networks (Figure **2.9b** and **2.9c**). Nangia and Desiraju had analyzed the formation of hydrogen bonds of dioxane molecules with O-H, N-H, and C-H groups and suggested that dioxane has a higher

tendency to form hydrogen bonds to more than one donor.[7] In the present case, out of the two dioxane molecules with different symmetry, two ends of one dioxane

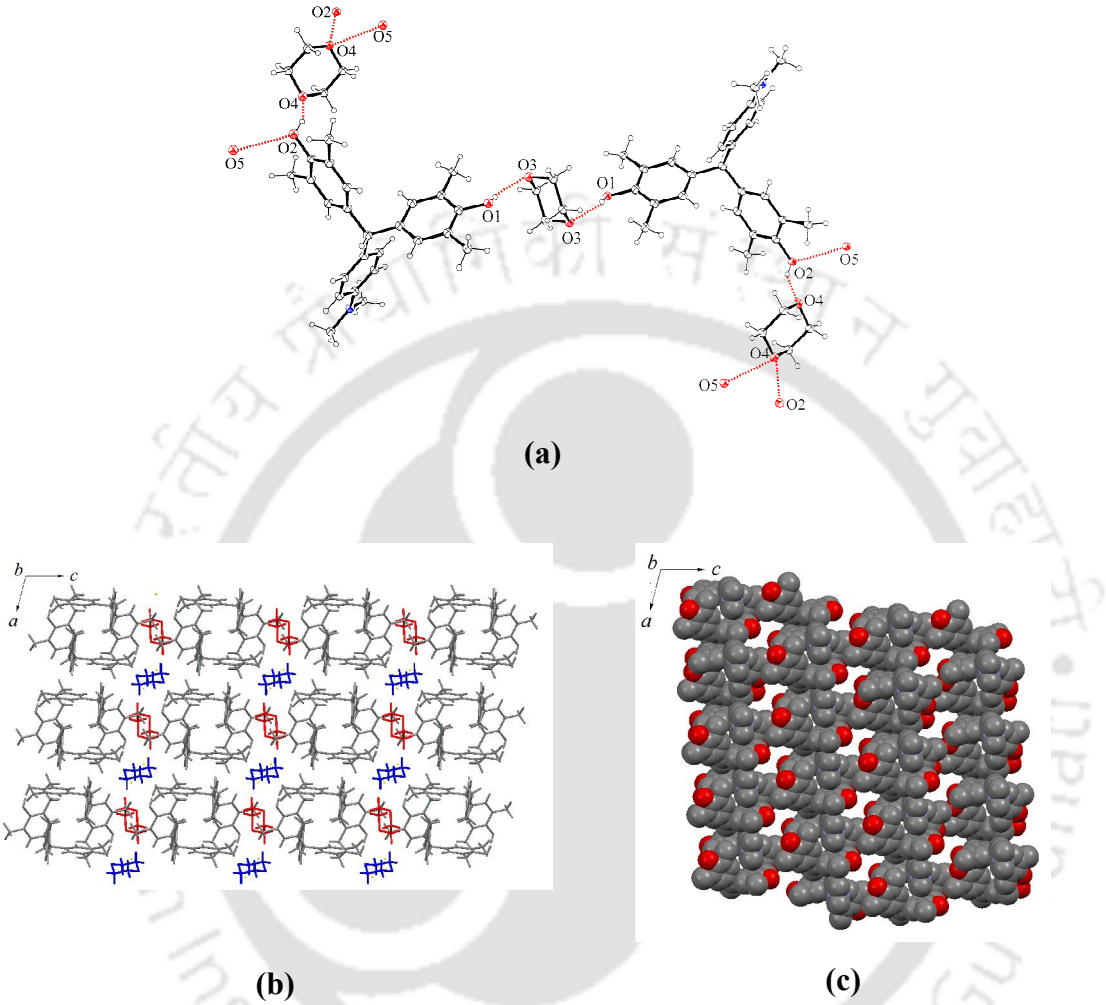

Figure 2.9: (a) Hydrogen bonding in the 1, 4-dioxane solvate **2.8**, **(b)** Packing diagram of the dioxane solvate **2.8** showing the inclusion of the solvent molecules, **(c)** Space filling model of **2.8** after removal of the solvent molecules in side the channels.

molecule are directly hydrogen-bonded to the O-H of the host Ambp, whereas the other dioxane is connected to the host molecules through intervening hydrogen-bonded water molecules. All of these interactions result in the formation of a chain-like arrangement of Ambp holding dioxane molecules. A similar type of chainlike structure was observed in the crystal structure of dioxane solvates of ethinyl estradiol, which is an analogue of estrogen.[30] The conformations of dioxane molecules in **2.8**

are similar to the conformation of the commonly observed dioxane solvates of hydroxy-compounds.[31]

In the solvate **2.9** also the hydroxy group of the Ambp molecules forms intermolecular H-bonds lead to a one dimensional chain of the host (Figure **2.10a**). There are two moderately strong hydrogen-bonds, viz., O(1)-H(1)···N(3) [$d_{D\cdots A}$= 2.657 Å and ∠D-H···A= 166°] and O(2)-H(2)···O(1) [$d_{D\cdots A}$= 2.540 Å and ∠D-H···A = 147°] in Ambp.DBU **(2.9)** solvate. The O1 atoms of the *bis*-phenol molecules interact with the DBU through O-H···N interactions, which are the prominent

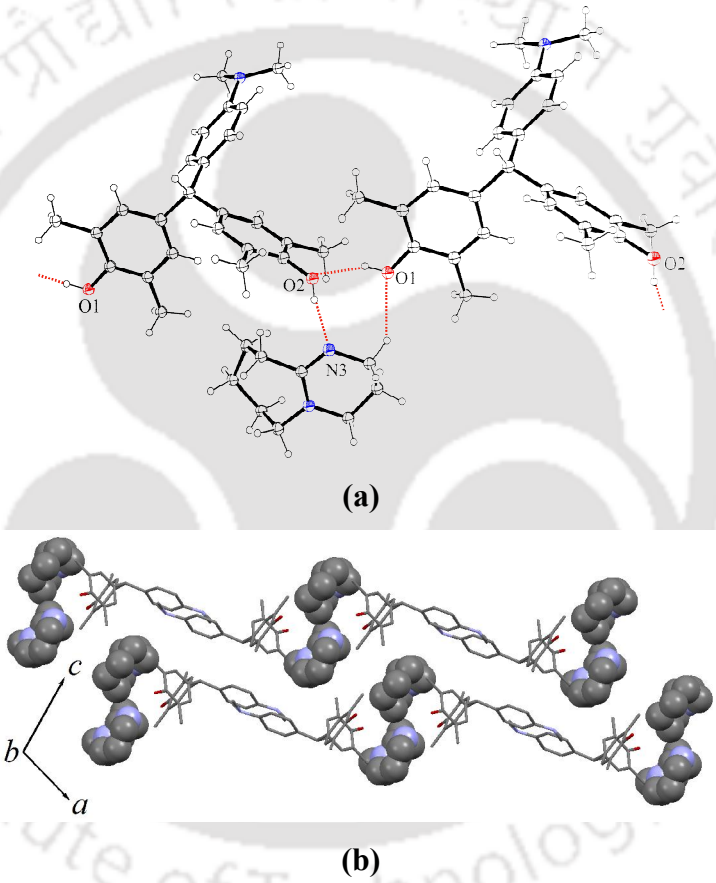

Figure 2.10: (a) One dimensional chain of Ambp molecules in the crystal structure of DBU solvate **2.9**, **(b)** Parallel sheets of Ambp and DBU in the crystal structure of **2.9**.

interaction between the host and the guest molecules in its lattice. Apart from this, there are other weak C-H···O and C-H···π interactions that help to hold the guest molecules resulting in formation of two parallel sheet-like structures (Figure **2.10b**).

Comparison of the structure of DABCO solvate **2.7** and dioxane solvate **2.8** shows that the solvent molecules compete to break apart the hydrogen bonds between the

bis-phenol molecules. During such a competitive process, the water molecule also participates so that it can act as a filler to make a tightly-packed structure. Thus, it is observed that, in the case of the dioxane solvate, two different symmetry orientations of dioxane in the lattice are observed. In the case of DABCO, the water molecules act as bridges to form cyclic arrangements in which the water molecules occupy the diagonally opposite sides. This shows that the more hydrophobic and bulky DABCO do not allow the water molecules to participate together with it but gives an advantage to form an aqua-bridged motif (Figure **2.8**) for its binding. Such aqua bridges make the extra space required to accommodate the bulky DABCO. Cao et al. had reported proton transfer from the hydroxy group of a *bis*-phenol to DABCO in crystal structure of a brominated *bis*-phenol, such proton transfer resulted in the formation of salt.[32] In the present case, the structure of the solvate **2.7** is guided by hydrogen bonds and packing pattern is devoid of electrostatic interactions. In the solvate **2.9**, DBU molecules partially break the O-H···O bonds between *bis*-phenols by participating in hydrogen-bond formation in a similar manner to that of piperidine or morpholine to form $R_3^3(7)$-type motif.

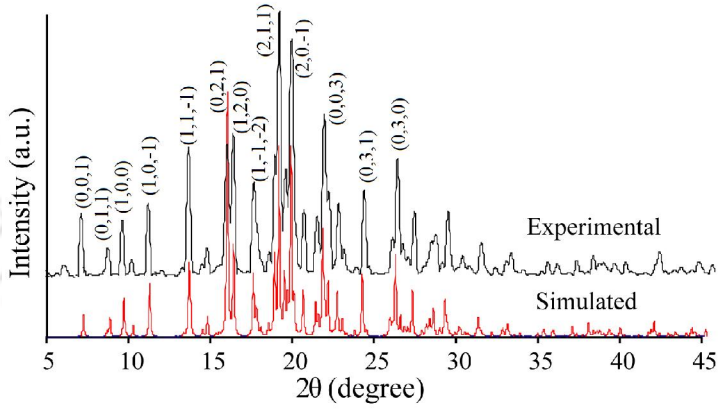

Figure 2.11: The experimental (top) and simulated (bottom) PXRD of solvate **2.8**.

The powder X-ray diffraction (PXRD) of the compounds is recorded to ascertain their phase homogeneity. We have found a good agreement of experimental and simulated PXRD data for almost all of these solvates, and it suggests the uniformity of the structural features of the bulk materials. As a representative case the powder XRD of the dioxane solvate (**2.8**) is shown in Figure **2.11**. Each diffraction peaks in the experimental powder XRD are matched with the simulated powder pattern of the structure determined by single crystal diffraction. The agreement of all the peaks

suggests the phase purity in bulk samples. The indexing is done as per the simulated diffraction pattern by using MERCURY program.

2.3 Thermo gravimetric analysis of solvate 2.2-2.9

There is extensive research on thermal properties of hydroxy compounds related to *bis*-phenols.[33] From such studies, no clear correlation is available on the thermal effect to release guest molecules from host-guest complexes, but they are qualitatively interpreted in terms of the local environment of the guest molecules. A similar qualitative explanation could be derived from thermal studies carried out on these solvates. It was seen that the solvate **2.2** lost the acetone around 65-150 °C (observed weight loss 11.0%, theoretical 13.3%). It indicates that it was tightly bounded in the channels formed by the Ambp. Similarly, for compounds **2.3** and **2.4**, the DMSO and DMA molecules lost at around 105-190 °C (observed weight loss 16.0%, theoretical

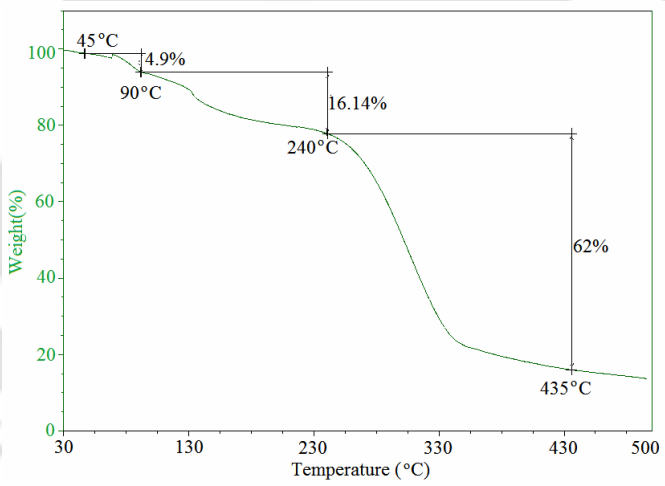

Figure 2.12: TG of the solvate **2.8** (heating rate 5°C/ minute).

17.2%) and 85-165 °C (observed weight loss 17.90%, theoretical 18.0%), respectively. Compounds **2.5** and **2.6** lost morpholine and piperidine at 80-175 °C (observed weight loss 18.43%, theoretical 18.8%) and 85-160°C (observed weight loss 15.0%, weight loss 18.4%), respectively. The solvate **2.7** lost its three waters of crystallization at around 45-70°C. In this case, the DABCO molecules were lost above 160 °C where the parent *bis*-phenol also decomposed; thus, the amount of guest solvent lost could not be ascertained. The solvate **2.9** lost the DBU molecules in the

temperature range 70-185°C (experimental weight loss 28.08%, theoretical weight loss 28.85%). The water of crystallization of the solvate **2.8** is lost at around 45-90°C (observed 4.9% weight loss, theoretical 3.7%), and the dioxane molecules are lost at around 90-240° C (observed weight loss 16.14%, theoretical 20.4%). In case of **2.8**, the water molecules act as a bridge and were lost easily on heating at relatively low temperature.

2.4 Conclusion

A series of quasi isostructural solvates of *bis*(4-hydroxy-3,5-dimethylphenyl)(4-N, N-dimethylaminophenyl)methane showed the retention of the chain-like structure of the host in a majority of these solvates. We observed that the solvate **2.2**-**2.5** are isostructural and in all the four solvates, the solvent molecules are incorporated in the channels running along the [010] direction. Apart from primary O-H···O interactions between the hosts to form a chain-like structure, the weak interactions arising from the guest molecules decide the structural motif of each solvate. According to the Abraham scale of solvation,[34] the ability to form a solvate by different solvents are morpholine > DMSO = DMA > piperidine >1, 4-dioxane. Here we have observed that the disruption of O-H···O interactions are caused by dioxane, which is much weaker than the DMSO or DMA. This is attributed to the favourable packing pattern formed by the water assisted assembly so that the dioxane molecules are accommodated in the lattice. Therefore, there is a synergic effect of the packing requirement to accommodate a solvent molecule and the solvation ability of the corresponding solvent. Bifurcated hydrogen bonds play a very important role to keep the chain-like backbone intact, and in some special cases, the chains are also stabilized by uncommon N-H···π interactions. The weakly interacting dioxane molecules require the help of water molecules as fillers to make a tightly packed structure. The steric factors of DBU and DABCO molecules control the hydrogen-bond patterns in the crystal lattices of their respective solvates, which in turn decide the stoichiometry of the host-guest complexes.

2.5 Experimental section

Synthesis of *bis*(4-hydroxy-3,5-dimethylphenyl)(4-N,N-dimethylaminophenyl) methane (2.1): 4-(Dimethylamino)aldehyde (0.745g, 5 mmol) and 2,6-dimethyl-phenol (1.22 g, 10 mmol) were dissolved in acetic acid (20 mL) and the solution was stirred for half an hour in an ice bath. A mixture of concentrated sulphuric acid and glacial acetic acid in a 1: 2 ratio (10 mL, v/v) was added drop wise to the reaction mixture. After half an hour of stirring, the mixture was kept in a deep freeze for one week. After one week, ice cold water (10 mL) was added to the reaction mixture; a pink colored precipitate appeared. The precipitate was collected by filtration and was washed with aqueous sodium bicarbonate solution (20%, 25 mL). The product was then dried in air. Yield: 78%. ^{1}H-NMR (600 MHz, $CDCl_3$, δ ppm): 6.95 (d, J=8.4 Hz, 2H), 6.71 (s, 6H), 6.66 (d, J=7.8 Hz, 2H), 5.20 (s, 1H), 2.91 (s, 6H), 2.17 (s, 12H); ^{13}C-NMR (150 MHz, DMSO-d_6, δ ppm): 150.5, 149.0, 136.9, 133.4, 130.0 129,6, 122.7, 112.8, 54.7, 41.0, 16.2; ESI Mass [M+1]: 376.2394.

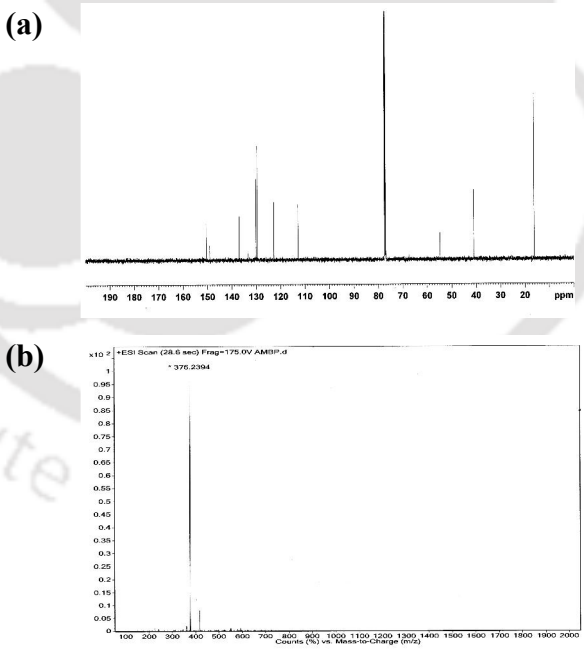

Figure 2.13: (a) The ^{13}C-NMR (150 MHz, $CDCl_3$) and **(b)** LC-MS of Ambp **(2.1)**.

Detailed synthetic methodologies of the solvate **2.2-2.9** are given below. Analytical data as well as spectroscopic data are also listed along with each of the solvates. The instrumental details and the crystallographic data are given in the Appendix.

Ambp.acetone (2.2): Ambp was dissolved in acetone and kept it undisturbed for crystallization for 4 days red coloured crystals were obtained. Yield: 80%. IR(cm^{-1}): 3465 (s), 2917 (m), 2873 (w), 2802 (w), 1611 (s), 1518 (s), 1485 (s), 1443 (m), 1346 (m), 1197 (s), 1136 (m), 1053 (w), 1021 (m), 947 (m), 882 (m), 831 (m), 784 (w), 738 (w), 654 (w), 609 (w).

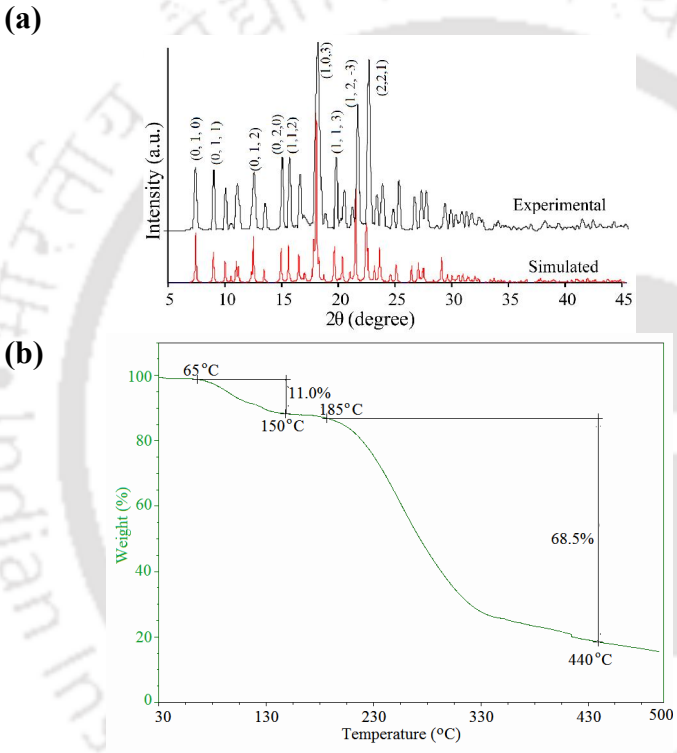

Figure 2.14: **(a)** Experimental (top) and simulated (bottom) PXRD of solvate **2.2, (b)** TG of the solvate **2.2** (heating rate 5°C/ minute).

Ambp.DMSO (2.3): After two weeks red crystals were obtained from a solution of Ambp dissolved in dimethylsulphoxide. Yield: 92%. IR(cm^{-1}): 3451 (s), 2922 (w), 2857 (w), 2791 (w), 1637 (s), 1611 (s), 1519 (s), 1484 (s), 1437 (m), 1343 (m), 1292 (m), 1220 (m), 1192 (m), 1146 (m), 1018 (s), 949 (w), 869 (w), 829 (w), 707 (w), 653 (w).

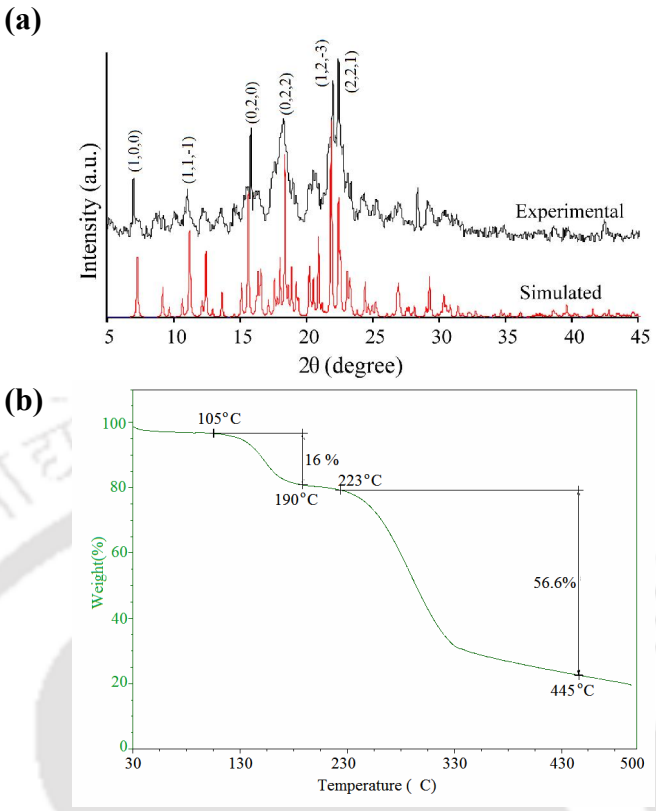

Figure 2.15: **(a)** Experimental (top) and simulated (bottom) PXRD of solvate **2.3,** (b) TG of the solvate **2.3** (heating rate 5°C/ minute).

Ambp.DMA (2.4): Ambp was dissolved in dimetylacetamide and kept it undisturbed for crystallization. After 7-8 days red coloured crystals were obtained. Yield: 85%. IR (cm^{-1}): 3444 (s), 2924 (w), 2868 (w), 1702 (m), 1633 (s), 1519 (m), 1486 (m), 1424(w), 1345(w), 1197 (m), 1163 (w), 1146 (w), 1020 (w), 942 (w), 876 (w), 826 (w), 655 (w).

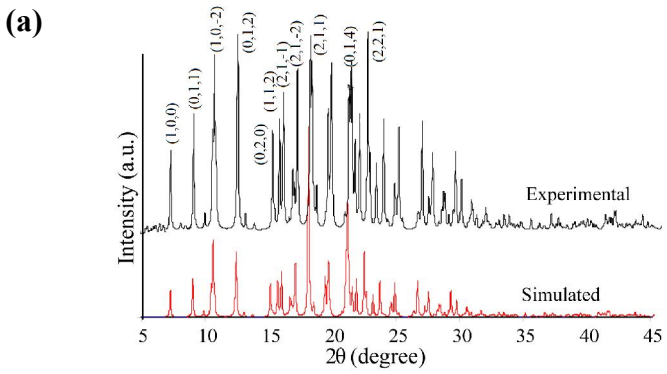

(b)

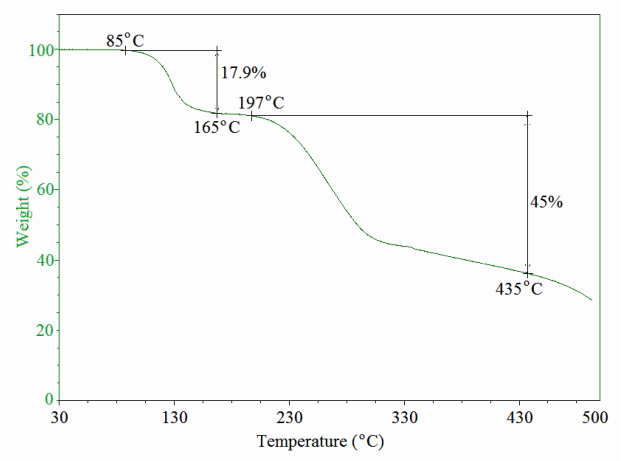

Figure 2.16: **(a)** Experimental (top) and simulated (bottom) PXRD of solvate **2.4, (b)** TGof the solvate **2.4** (heating rate 5°C/ minute).

Ambp.morpholine (2.5): Ambp was dissolved in morpholine and kept for one week for crystallisation, red crystals appeared. Yield: 95%. IR (cm^{-1}): 3431 (s), 2917 (w), 2851 (w), 1637 (s), 1518 (m), 1485 (m), 1445 (w), 1346 (m), 1195 (s), 1147 (w), 1108 (w), 940 (w), 864 (w), 827 (w), 653 (w), 614 (w).

(a)

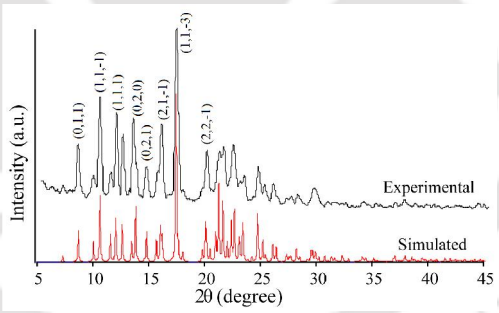

(b)

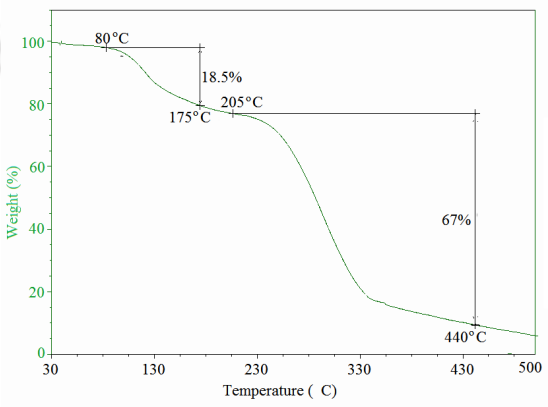

Figure 2.17: **(a)** Experimental (top) and simulated (bottom) PXRD of solvate **2.5, (b)** TG of the solvate **2.5** (heating rate 5°C/ minute).

Ambp.piperidine (2.6): A solution of Ambp in piperidine gave crystalline 7 after 7-8 days as red coloured crystal. Yield: 90%. IR (cm^{-1}): 3422 (s), 3274 (m), 2944 (s), 2851 (s), 2406 (w), 1887 (w), 1610 (s), 1518 (s), 1483 (s), 1446 (s), 1345 (s), 1294 (m), 1187 (s), 1148 (s), 1059 (m), 1016 (w), 941 (m), 856 (w), 828 (m), 805 (w), 740 (w), 655 (w), 575 (w).

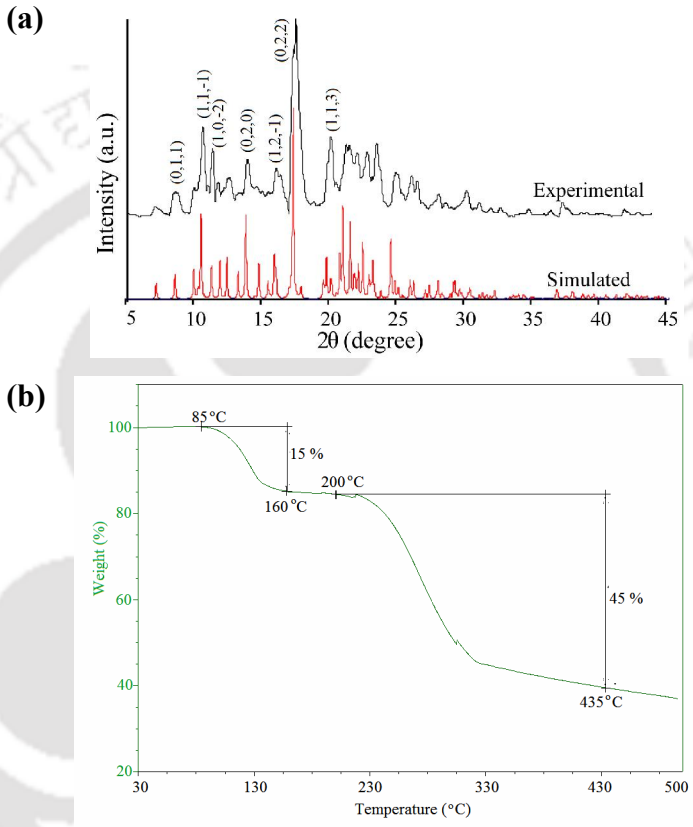

Figure 2.18: **(a)** Experimental (top) and simulated (bottom) PXRD of solvate **2.6, (b)** TG of the solvate **2.6** (heating rate 5°C/ minute).

2Ambp.DABCO.3H_2O (2.7): Ambp and DABCO was dissolved in acetonitrile in 2: 1 ratio and kept undisturbed for crystallization. After 10-12 days red coloured crystal appeared. Yield: 60%. IR (cm^{-1}): 3441 (s), 2948 (s), 1635 (m), 1519 (m), 1484 (w), 1346 (w), 1200 (w), 1056 (w), 947 (w), 884 (w), 781 (w), 617 (w).

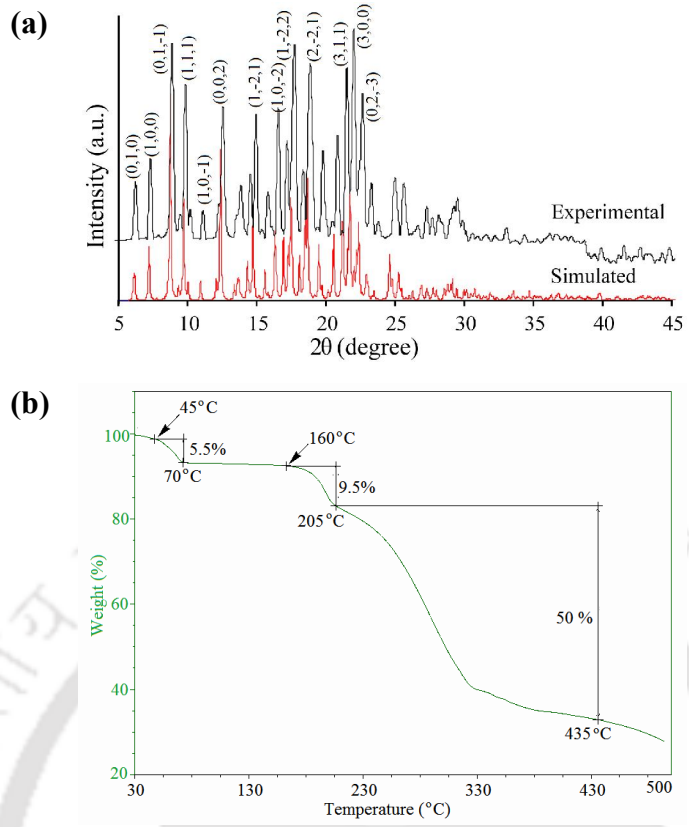

Figure 2.19: (a) Experimental (top) and simulated (bottom) PXRD of solvate **2.7, (b)** TG of the solvate **2.7** (heating rate 5°C/ minute).

Ambp.diox.H_2O (2.8): A saturated solution of Ambp in 1, 4-dioxane was kept undisturbed. After 5-6 days colorless crystals were obtained. Yield: 70%. IR(cm^{-1}): 3439 (s), 2956 (m), 2923 (m), 2862 (m), 2796 (w), 1758 (w), 1610 (s), 1519 (s), 1486 (s), 1448 (s), 1349 (s), 1297 (m), 1205 (s), 1109 (s), 1077 (m), 1020 (m), 948 (w), 880 (m), 863 (s), 828 (m), 731 (w), 655 (w), 612 (w).

Ambp.dbu (2.9): Ambp dissolved in 1, 8-diazabicyclo [5.4.0] undec-7-ene after one week led to formation of dark red coloured crystals. Yield: 75%. IR (cm^{-1}): 3428 (s), 2933 (m), 2857 (w), 1649 (s), 1610 (w), 1513 (w), 1470 (m), 1321 (m), 1297 (m), 1199 (m), 1146 (m), 1017 (w), 937 (w), 881 (w), 823 (w), 735 (w), 697 (w), 663 (w), 516 (w).

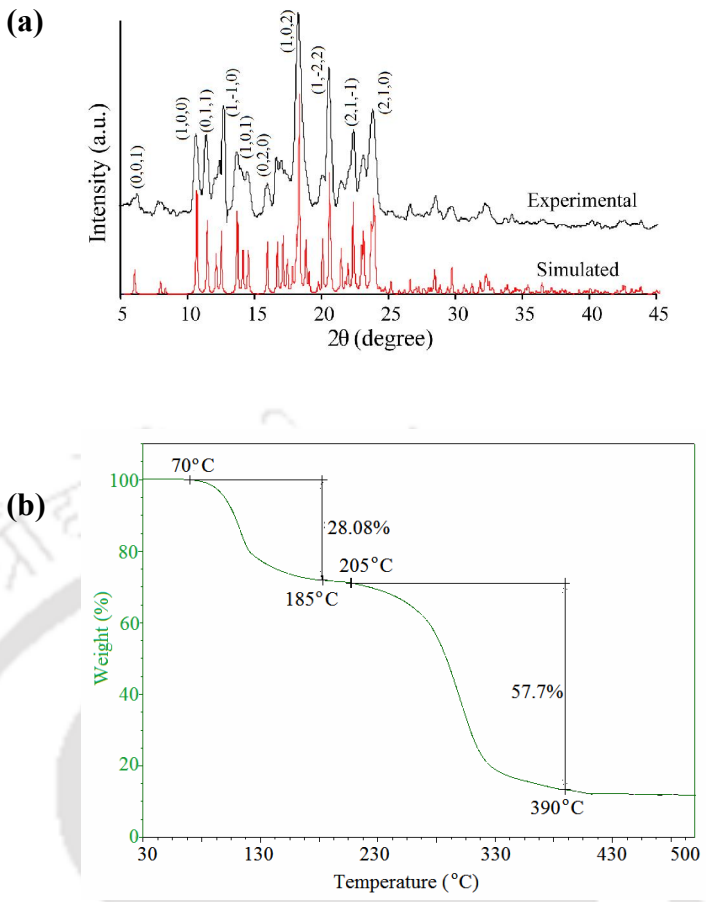

Figure 2.20: (a) experimental (top) and simulated (bottom) PXRD of solvate **2.9, (b)** TG of the solvate **2.9** (heating rate 5°C/ minute).

References:

1. (a) P. Bombicz, A. Kalman, *Cryst. Growth Des*., 2008, **8**, 2821-2823; (b) L. Rajput, K. Biradha, *CrystEngComm*, 2009, **11**, 1220-1222; (c) R. G. Gonnade, M. M. Bhadbhade, M. S. Shashidhar, *CrystEngComm*, 2010, **12**, 478-484; (d) S. Bhattacharya, B. K. Saha, *Cryst. Growth Des*., 2011, **11**, 2194-2204.
2. (a) R. Thakuria, A. Nangia, *Cryst. Growth Des.*, 2013, **13**, 3672-3680; (b) J. Galcera, E. Molins, *Cryst. Growth Des*., 2009, **9,** 327-334**;** (c) Q. Miao, T. -Q. Nguyen, T. Someya, G. B. Blanchet, C. Nuckolls , *J. Am. Chem. Soc.*, 2003, **125**, 10284-10287; (d) A. Wu, P. Mukhopadhyay, A. Chakraborty, J. C. Fettinger, L. Isaacs, *J. Am. Chem. Soc.*, 2004, **126**, 10035-10043; (e) G. Valincius, B. Nickel, *Langmuir*, 2003, **19**, 2612-2620; (f) D. J. Vanderah, T.

Parr, V. Silin, C. W. Meuse, R. S. Gates, H. La, *Langmuir*, 2004, **20**, 1311-1316.

3. (a) S. Wei, J. Lu, W. Yu, H. Zhang, Y. Qian, *Cryst. Growth Des*., 2006, **4**, 849-853; (b) H. R. Khavasi, B. M. M. Sadegh, *Cryst. Growth Des*., 2012, **12**, 4798-4804; (c) R. A. Agarwal, A. Aijaz, C. Sañudo, Q. Xu, P. K. Bharadwaj, *Cryst. Growth Des.*, 2013, **13**, 1238-1245; (d) D. Gatteschi, B. Tsukerblatt, A. L. Barra, L. C. Brunel, A. Miiller, J. Doring, *Inorg. Chem.*, 1993, **32**, 2114-2117; (e) P. L. Feng, D. N. Hendrickson, *Inorg. Chem*. 2010, **49**, 6393-6395; (f) A. Cabeza, X. Ouyang, C. V. K. Sharma, M. A. G. Aranda, S. Bruque, A. Clearfield, *Inorg. Chem*., 2002, **41**, 2325-2333; (g) S. Herold, S. J. Lippard, *Inorg. Chem.*, 1997, **36**, 50-58; (h) K. A. Morales, Y. Yang, Z. Long, P. Li, A. B. Taylor, P. J. Hart, T. I. Igumenova, *J. Am. Chem. Soc.*, 2013, **135**, 12980-12983; (i) S. A. FitzGerald, B. Burkholder, M. Friedman, J. B. Hopkins, C. J. Pierce, J. M. Schloss, B. Thompson, J. L. C. Rowsell, *J. Am. Chem. Soc.*, 2011, **133**, 20310-20318.
4. G. L. Paul, A. W. Pryor, *Acta Crystallogr., Sect. B: Struct. Crystallogr. Cryst. Chem.*, 1972, **28**, 2700-2702.
5. P. Rahe, J. Schütte, A. Kuhnle, *J. Phys: Condens. Matter*, 2012, **24**, 084006.
6. M. A. Herman, W. Richter, H. Sitter, *Epitaxy: Physical Principles and Technical Implementation*; Springer: Berlin, Germany, 2004.
7. A. Nangia, G. R. Desiraju, *Chem. Commun*., 1999, 605-606.
8. (a) W. L. Rocco, C. Morphet, S. M. Laughlin, *Int. J. Pharm*., 1995, **122**, 17-25; (b) K. F. Landgraf, A. Olbrich, S. Pauluhn, P. Emig, B. Kutscher, H. Stang, *Eur. J. Pharma. Biopharm*., 1998, **46**, 329-337; (c) O. V. Surov, M. I. Voronova, P. R. Smirnov, N. Z. Mamardashvili, G. P. Shaposhnikov, *CrystEngComm*, 2012, **14**, 533-536; (d) J. M. R. Preminger, J. Bernstein, *Cryst. Growth Des.,* 2005, **5**, 1343-1349.
9. (a) A. P. Visheswar, J. A. McMahon, J. A. Bis, M. J. Zaworotko, *J. Pharm. Sci.*, 2006, **95**, 499-514; (b) S. L. Morissette, O. Almarsson, M. L. Peterson, J. F. Remender, M. J. Read, A. V. Lemmo, S. Ellis, M. J. Cima, C. R. Gardner, *Adv. Drug Delivery Rev.*, 2004, **56**, 275-300.
10. S. R. Byrn, R. R. Pfeiffer, J. G. Stowell, *Solid-State Chemistry of Drugs*, 2nd ed.; SSCI Inc.: West Lafayette, IN, 1999.

11. (a) V. S. S. Kumar, F. C. Pigge, N. P. Rath, *Cryst. Growth Des.*, 2004, **4**, 651-653; (b) B. T. Ibragimov, K. K. Makhkamov, K. M. Beketov, *J. Inclusion Phenom. Macro. Chem.*, 1999, **35**, 583-593; (c) L. Paternostre, P. Damman, M. Dosiere, *Macromolecules*, 1999, **32**, 153-161.
12. A. L. Bingham, D. S. Hughes, M. B. Hursthouse, R. W. Lancaster, S. Travener, T. L. Threlfall, *Chem. Commum.*, 2001, 603-604.
13. (a) S. Bhattacharya, B. K. Saha, *Cryst. Growth Des.*, 2012, **12**, 169-178; (b) T. Hosokawa, S. Datta, A. R. Sheth, N. R. Brooks, V. G. Young, D. J. W. Grant, *Cryst. Growth Des.*, 2004, **4**, 1195-1201; (c) R. Banerjee, P. M. Bhatt, G. R. Desiraju, *Cryst. Growth Des.*, 2006, **6**, 1468-1478.
14. (a) S. Basavoju, S. Aitipamula, G. R. Desiraju, *CrystEngComm*, 2004, **6**, 120-125; (b) D. E. Braun, T. Gelbrich, V. Kahlenberg, R. Tessadri, J. Wieser, U. J. Griesser, *Cryst. Growth Des.*, 2009, **9**, 1054-1065.
15. S. Bhattacharya, J. Sameena, B. K. Saha, *Cryst. Growth Des.*, 2011, **11**, 905-909.
16. R. J. Sarma, J. B. Baruah, *CrystEngComm*, 2005, **7**, 706-710.
17. R. J. Sarma, C. Tamuly, J. B. Baruah, *Dyes Pigm.*, 2007, **72**, 75-79.
18. (a) R. Thakuria, B. Sarma, A. Nangia, *Cryst. Growth Des.*, 2008, **8**, 147-1473; (b) P. K. Thallapally, P. B. McGrail, S. J. Dalgarno, J. L. Atwood, *Cryst. Growth Des.*, 2008, **8**, 2090-2092; (c) K. Skobridis, G. Paraskevopoulos, V. Theodorou, W. Seichter, E. Weber, *Cryst. Growth Des.*, 2011, **11**, 5275-5288.
19. (a) H. Suzuki, *Tetrahedron Lett.*1992, **33**, 6319-6322; (b) H. Suzuki, H. Takagi, *Tetrahedron Lett.*1993, **34**, 4805-4806; (c) H. Suzuki, H. Takagi, R. Sato, *Tetrahedron Lett.* 1997, **38**, 4563-4566.
20. L. Fabian, A. Kalman, *Acta Crystallogr.* 2004, **B60**, 547-558.
21. (a) J. Chen, J. Wang, J. Ulrich, Q. Yin, L. Xue, *Cryst. Growth Des.*, 2008, **8**, 1490-1494; (b) A. Bacchi, M. Carcelli, T. Chiodo, F. Mezzadri, F. Nestola, A. Rossi, *Cryst. Growth Des.*, 2009, **9**, 3749-3758; (c) F. C. Pigge, M. K. Dighe, N. P. Rath, *Cryst. Growth Des.* 2006, **6**, 2732-2738; (d) A. Jacobs, N. L. Z. Masuku, L. R. Nassimbeni, J. H. Taljaard, *CrystEngComm*, 2008, **10**, 322-326; (e) K. Tanaka, K. Endo, Y. Aoyama, *Chem. Lett.*, 1999, 887-888.

22. F. H. Allen, J. E. Davis, J. J. Galloy, O. Johnson, O. Kennerd, C. F. Macrae, E. M. Mitchell, G. F. Mitchell, J. M. Smith, D. G. Watson, *J. Chem. Inf. Comput. Sci.*, 1991, **31**, 187-204.
23. (a) P. K. Thallapaly, A. K. Katz, H. L. Carell, G. R. Desiraju, *Chem. Commun.*, 2002, 344-345; (b) G. P. Kar, A. Karmakar, J. B. Baruah, *J. Chem. Crystallogr.*, 2010, **40**, 702-706.
24. K. M. Armstrong, R. Fairman, R. L. Baldwin, *J. Mol. Biol.* 1993, **230**, 284-291.
25. G. Kryger, I. Silman, J. L. Sussman, *Structure*, 1999, **7**, 297-307.
26. G. Parkinson, A. Gunasekera, J. Vijtechovsky, *Nat. Struct. Biol.*, 1996, **3**, 837-841.
27. S. Liu, X. Ji, G. L. Gilliland, W. J.Stevens, R. N. Armstrong, *J Am Chem Soc.*, 1993, **115**, 7910-11.
28. S. Jurado, Z. Abraham, C. Manzano, G. Lopez-Torrejo, L. F. Pacios, J. C. Del Pozoa, *Plant Cell*, 2010, **22**, 3891-3904.
29. J. Cheng, C. Kang, W. Zhu, X. Luo, C. M. Puah, K. Chen, J. Shen, H. Jiang, *J. Org. Chem.*, 2003, **68**, 7490-7495.
30. C. Guguta, I. Eeuwijk, J. M. M. Smits, R. D. Gelder, *Cryst. Growth Des.*, 2008, **8**, 823-831.
31. (a) A. Jacobs, N. Faleni, L. R. Nassimbeni, J. H. Taljaard, *Cryst. Growth Des.*, 2007, **7**, 1003-1006; (b) M. R. Caira, A. Coetzee, L. R. Nassimbeni, E. Weber, A. Wierig, *J. Chem. Soc., Perkin Trans.*, 1995, **2**, 281-284.
32. J. Lu, L. W. Han, J. X. Lin, R. Cao, *Cryst. Growth Des*., 2011, **11**, 3551-3557.
33. (a) G. Ramon, A. W. Coleman, L. R. Nassimbeni, B. Taljaard, *Cryst. Growth Des.*, 2005, **5**, 2331-2335; (b) A. Jacobs, L. R. Nassimbeni, K. L. Nohako, S. Hong, J. H. Taljaard, *Cryst. Growth Des.*, 2008, **8**, 1301-1305; (c) G. Ramon, A. Jacobs, L. R. Nassimbeni, R. Yav-Kabwit, *Cryst. Growth Des.*, 2011, **11**, 317-3182.
34. (a) M. H. Abraham, *Pure Appl. Chem.*,1993, **65**, 2503-2512; (b) A. A. Oliferenko, P. V. Oliferenko, J. G. Huddleston, R. D. Rogers, V. A. Palyulin, N. S. Zefirov, A. R. Katritzky, *J. Chem. Inf. Comput. Sci.*, 2004, **44**, 1042-1055.

CHAPTER 3

Polymorphs, solvates, polymorphs of solvate and Cs^{+}-π interactions of fluorine-substituted *bis*-phenols

The fluorine-substituted assemblies are of interest due to their enhanced solubility and superior hydrogen absorption ability.[1] The van der Waals radii of fluorine (1.47 Å) and oxygen (1.57 Å) are comparable; the difluoromethylene group is isosteric and isopolar to an ethereal oxygen atom.[2] Due to the nonpolarizable nature, the fluorine atom is a weak hydrogen bond acceptor, and a fluorine attached to a carbon is not readily involved in hydrogen bond formation.[3] Theoretical calculations show that the strengths of C-H···F-C bonds lie between 2 to 3.2 kcal/mol.[4] There are different types of interactions involving C-F bonds, such as C-H···F-C and C-F···π interactions.[5] Despite the low affinity to form the C-H···F-C interactions, their presence provides directional forces in fluorine-containing organic compounds.[6] Polymorphisms of organic fluorine compounds are also well documented.[7] Covalently linked fluorine atoms in crystal lattice are likely to be near hydrogen atoms, rather than being close to electronegative atoms such as oxygen. To adopt a stable packing pattern in such compounds, the interactions of fluorine atoms with adjacent atoms are not necessarily attractive.[8] Recrystallization of 4-fluorophenols under different pressure led to polymorphs, which are differentiated by C-H···F-C interactions (Figure **3.1**).[9] The

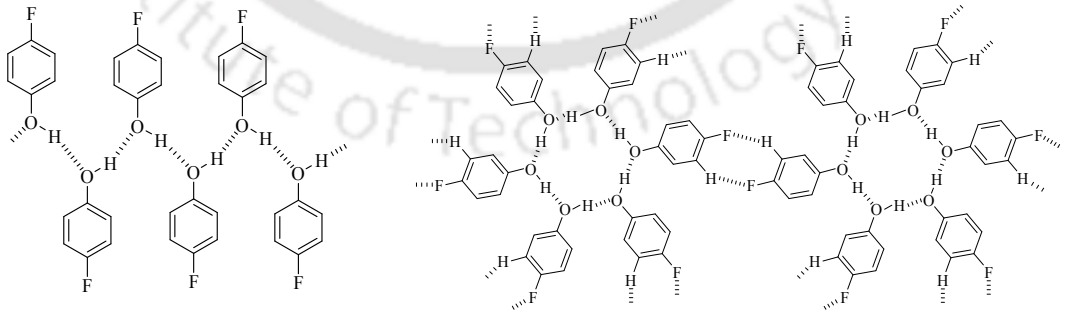

(a) **(b)**

Figure 3.1: Formation of different polymorphs of 4-fluorophenol at **(a)** high pressure, **(b)** ambient pressure.[9b]

fluorophenols with high Z′ values are also reported[10] and the co-crystals of penta-fluorophenol with phenanzine in different proportions of the host-guest ratio having C-H···F-C interactions are known.[11] Thus, the study on assemblies of fluorine containing compounds possessing other strong hydrogen bond sites such as, in fluoro *bis*-phenols may result in different polymorphic structures. We have already mentioned in the previous chapters that hydroxy groups help in assembling of organic compounds through O-H···O interactions,[12] and *bis*-phenols are no exception as hosts as they contain two hydroxy group at two ends with a rigid structure.[13] The substituents on *bis*-phenols lead to the formation of various structural motifs and there are extensive literatures on the structural studies of substituted *bis*-phenols.[14] However, there are no structural studies on fluorine substituted *bis*-phenols.

In this chapter we discuss the self-assemblies of 4-[(2-fluorophenyl)(4-hydroxy-3,5-dimethylphenyl)methyl]-2,6-dimethylphenol (*bis*-phenol **3.1**) and 2-[(2-fluorophenyl)(2-hydroxy-3,5-dimethyl phenyl)methyl]-4,6-dimethylphenol (*bis*-phenol **3.2**) (Figure **3.2**) leading to different polymorphs and polymorphs of solvate as well as cation-π interactions. To appreciate the essence of such observations, the structural properties are related through other spectroscopic and physical properties.

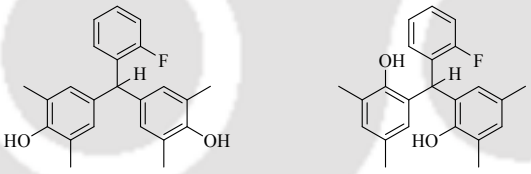

Bis-phenol **3.1** *Bis*-phenol **3.2**

Figure 3.2: The structure of the *bis*-phenols **3.1** and **3.2**.

3.1 Synthesis of *Bis*-phenol 3.1 and *Bis*-phenol 3.2

The *bis*-phenol **3.1** and **3.2** were synthesised by the condensation of 2-fluorobenzaldehyde with 2,6-dimethylphenol and 2,4-dimethylphenol respectively under acidic condition following a reported procedure.[15] These compounds were characterised by various spectroscopic techniques, such as IR spectroscopy, ^{1}H-NMR, ^{13}C-NMR and ^{19}F-NMR. From the ^{19}F-NMR it is seen that there is a multiplet at

-117.20 ppm for *bis*-phenol **3.1** and -118.22 ppm for *bis*-phenol **3.2**. In the ^{1}H-NMR, the characteristic methine protons of *bis*-phenol appears at 5.55 ppm for *bis*-phenol **3.1** (Figure **3.3a**), whereas it appears at 6.36 ppm for the *bis*-phenol **3.2** (Figure **3.3b**).

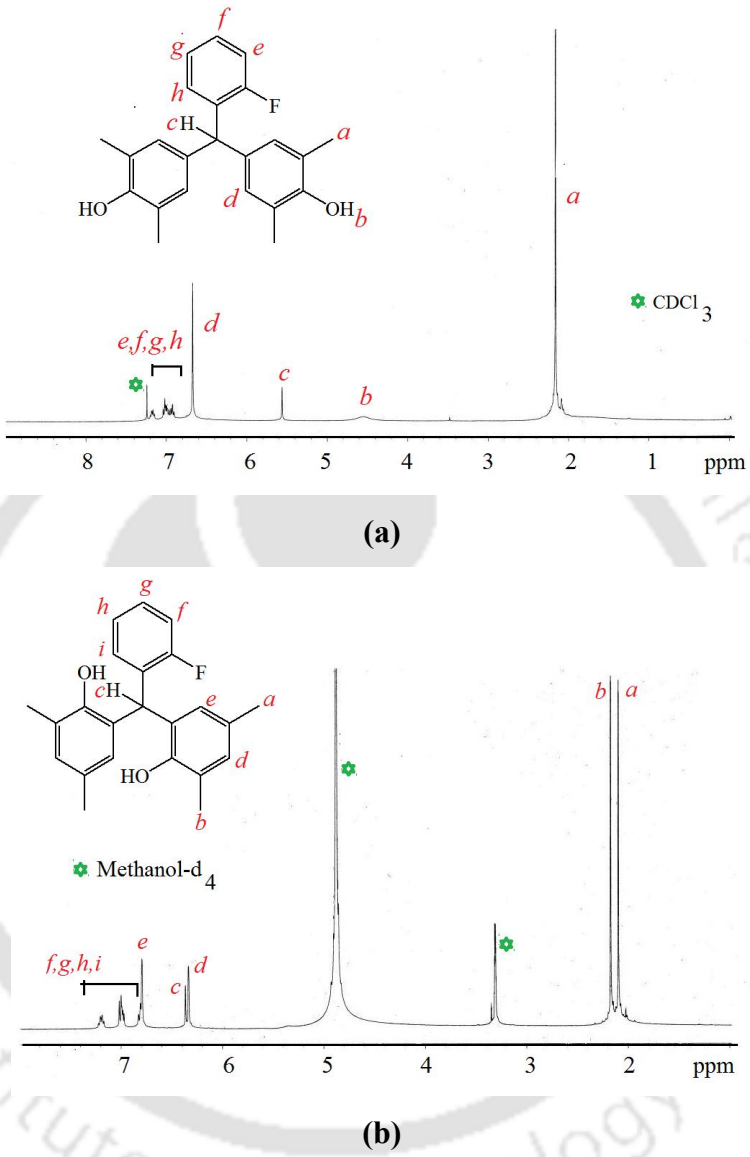

Figure 3.3: ^{1}H-NMR (400MHz) of **(a)** *Bis*-phenol **3.1** in $CDCl_3$ and **(b)** *Bis*-phenol **3.2** in methanol-d_4.

3.2 Polymorphs and solvates of *Bis*-phenol 3.1

The basic point which has helped in several new observations presented in this chapter arises from the possibilities of wide variations of packing patterns in these systems. We observed two polymorphs of *bis*-phenol **3.1**, namely, polymorph **3.1a** and polymorph **3.1b** from methanol and acetic acid respectively. Crystal

morphologies (Figure **3.4a**) of the two polymorphs are easily distinguishable. The polymorph **3.1a** crystallizes in the orthorhombic space group *Pbca* and the packing pattern has two strong O-H···O interactions, namely, O(1)-H···O(1) [$d_{D\cdots A}$= 2.923Å, ∠D−H···A=154°] and O(2)-H···O(2) [$d_{D\cdots A}$= 3.025 Å, ∠D−H···A=167°] (Table **3.1**) from the two hydroxy groups leading to the formation of a hydrogen-bonded sheet-like structure along the *ac*-crystallographic plane (Figure **3.4b**). Apart from the strong hydrogen bond interactions, weak interactions such as C-H···F-C and C-H···π interactions (based on their distance of separations) also contribute to the stability of the crystal. The C-H(3)···F(1)-C distance in this structure is found to be 2.63 Å (Figure **3.4c**). There is considerable crystal engineering on fluoro-phenols[16] and other

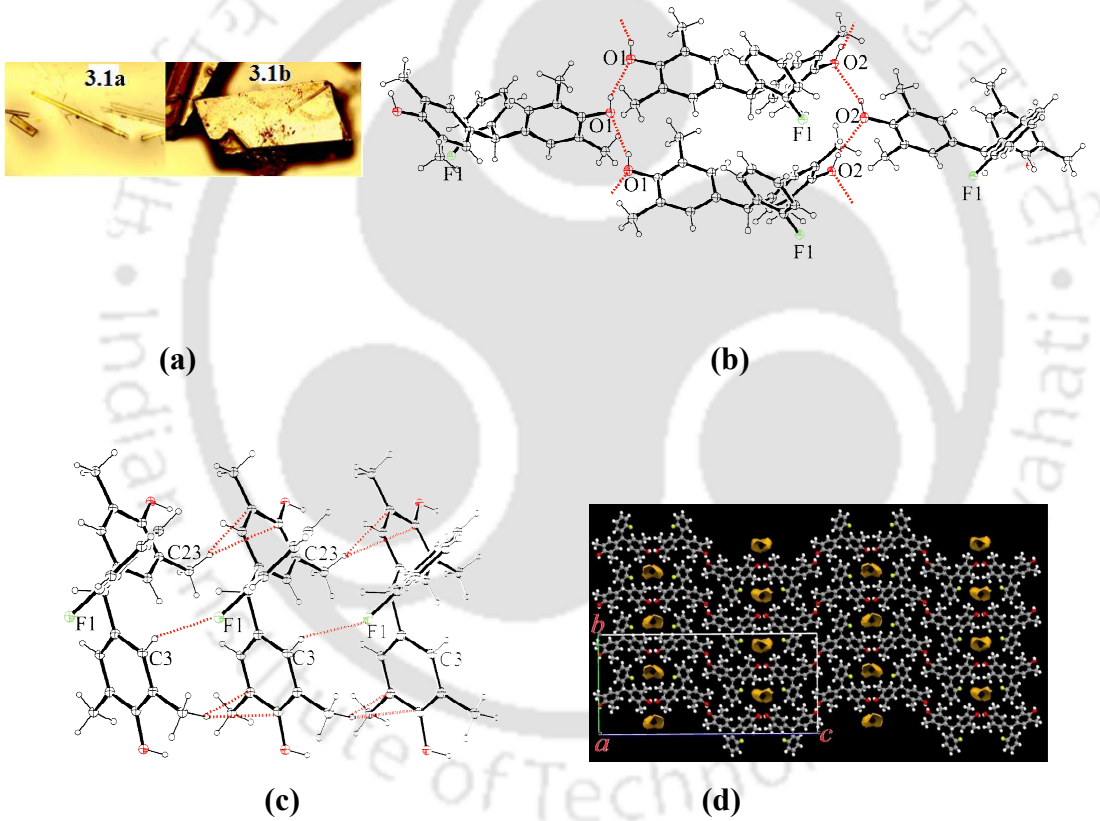

Figure 3.4: (a) Optical micrograph images of the morphologies of the two polymorphs **3.1a** and **3.1b** (10X magnification), **(b)** H-bond interactions in polymorph **3.1a**, **(c)** C-H···F-C and C-H···π interactions in polymorph **3.1a**, **(d)** Packing pattern of the polymorph **3.1a** showing the voids.

halogen substituted *bis*-phenols,[17] but there is no structural study on fluoro *bis*-phenols to make direct comparisons of such weak interactions. The polymorph **3.1a** adopts a porous structure containing voids with pore volume of 326 Å^3 and a dimension of 4.5 × 8.5 Å (Figure **3.4d**). The absence of residual amount of disordered solvent molecules in these voids has been confirmed by thermogravimetry (Figure **3.5**). The thermogram of the polymorph does not have appreciable weight loss below 200 °C. However, there is a sharp weight loss in the region of 200-300 °C, which occurs due to decomposition of the compound.

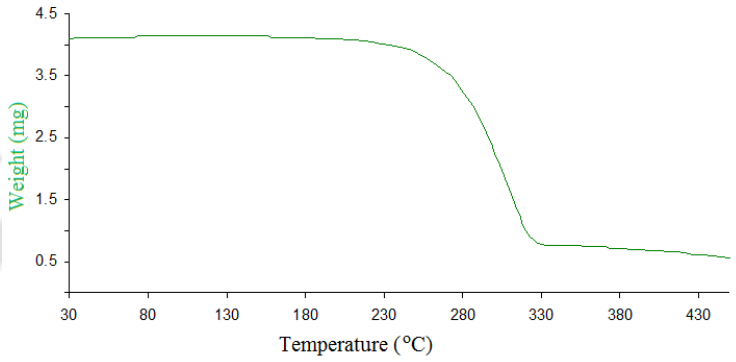

Figure 3.5: TGA of the polymorph **3.1a** (heating rate 5 °C/minute).

The polymorph **3.1b** belongs to the monoclinic space group $P2_1/c$ and it was obtained from the crystallization of **3.1** from acetic acid. In the crystal structure of **3.1b**, it is observed the two hydroxy groups do not involve in O-H···O interactions, unlike polymorph **3.1a**. However, one of the hydroxy groups is involved in the O-H···π interactions with the fluoro-substituted aromatic ring of another molecule ($d_{O1\text{-}H\cdots\pi}$ =

Table 3.1: Selected hydrogen parameters of **3.1a-3.1c**

Compd. No	D-H···A	$d_{D\text{-}H}$(Å)	$d_{H\cdots A}$ (Å)	$d_{D\cdots A}$(Å)	∠D−H···A (°)
3.1a	O(1)-H(1)···O(1) [1/2 +x, y, 1/2-z]	0.89(5)	2.10(4)	2.923(4)	154(4)
	O(2)-H(2)···O(2) [1/2 +x, 1/2 -y, -z]	0.78(4)	2.26(4)	3.025(5)	167(5)
	C(3)-H(3)···F(1)	0.93	2.63	3.477	151.57
3.1b	C(14)−H(14)···F(1)	0.931	2.632	3.488	153.16
3.1c	O(1)-H(1)···O(3) [-1/2 +x, 1/2 -y,1+z]	0.82	2.22	2.795(8)	128
	O(2)-H(2)···O(3) [1/2 +x, 1/2 -y,1+z]	0.82	2.42	2.847(8)	113
	C(24)-H(24C)···O(3)	0.96	2.43	2.760(13)	100
	C(24)-H(24C)···F(1) [1/2 +x, 1/2 -y, z]	0.96	2.48	3.003(12)	114

3.568 Å, π = centroid of the phenyl ring) to form dimer (Figure **3.6a**), and the other hydroxy group does not involve in any weak interactions. The O-H···π interactions were found to be responsible for generating polymorphs of 1,1-bis-(4-hydroxyphenyl) cyclohexane[18] where cleavage of O-H···O bonds as well as the movement of hydrogen bonded chains was shown to form the O-H···π interactions. The polymorphs **3.1a** and **3.1b** have differences in the weak C-H···F-C interactions. In the case of **3.1a**, C-H···F-C interactions are between dissimilar rings, whereas in **3.1b**, such interactions are between similar rings (Figure **3.6b**). The observed H···F distances for C-H···F-C interactions with the obtuse angle reported by other researchers are in the range of 2.2 to 2.3 Å.[19] The C-H···F-C distances in polymorph **3.1a** and polymorph **3.1b** are comparable with the distances ($d_{H\cdots F}$ = 2.61 to 2.95 Å)

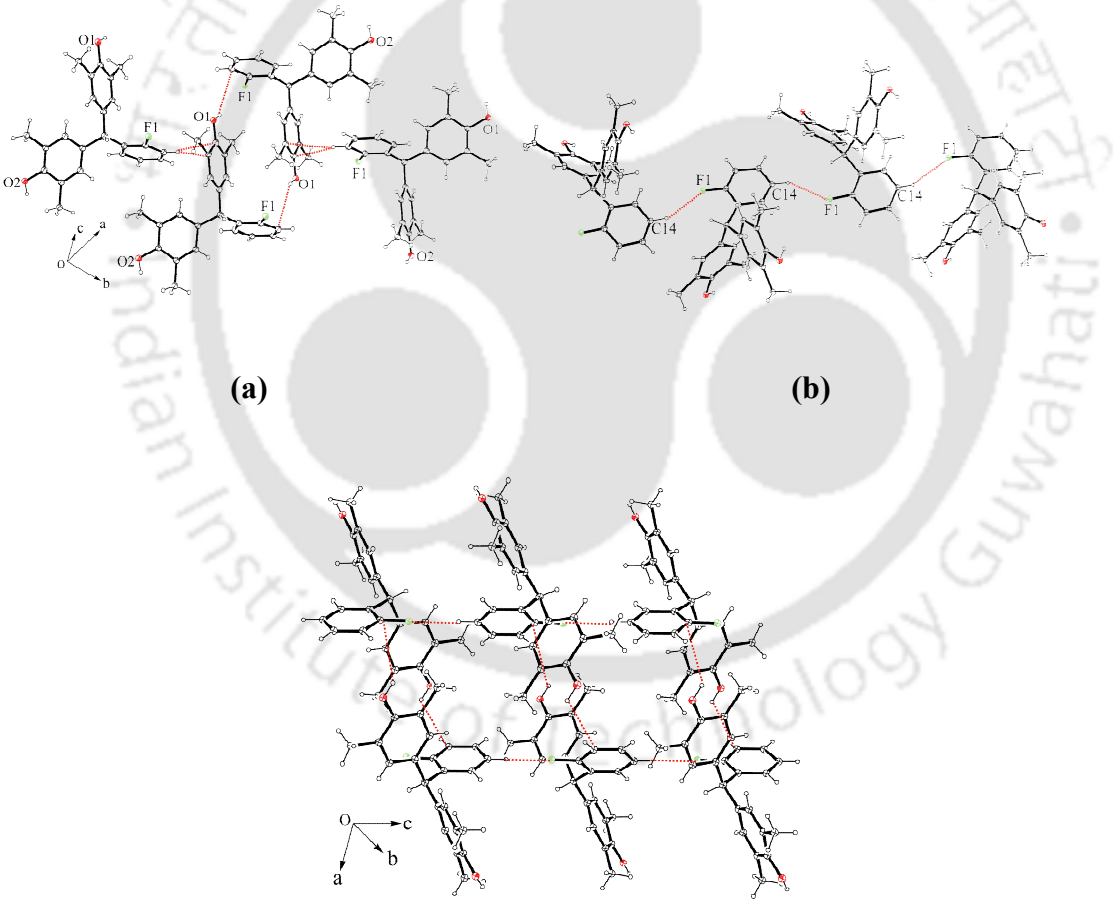

Figure 3.6: **(a)** O-H···π and C-H···π interactions in polymorph **3.1b**, **(b)** C-H···F-C interactions in polymorph **3.1b** leading to a linear chain, **(c)** Packing pattern of the polymorph **3.1b** viewed along the crystallographic ac-plane.

found in the polymorphs of 2- fluorophenyl acetylene.[5e] From the separating distances between the donors and acceptors in the structure of **3.1b**, it is clear that O-H···π and C-H···F-C interactions play a key role in the crystal packing, whereas O-H···O and C-H···F-C interactions play major roles in the packing of the polymorph **3.1a.** The conformational polymorphs in diols are well-documented.[20, 21] The variations on the numbers of molecules in unit cells were also known to cause polymorphism in *bis*-phenols.[22] There are also differences in the IR spectra of the two polymorphs, the hydroxy stretching frequency of the polymorph **3.1b** appears at 3609 cm^{-1}, whereas it appears at 3441 cm^{-1} for the polymorph **3.1a** (Figure **3.7**). The difference of 368 cm^{-1} toward the higher side in the IR-spectrum suggests its least participation in hydrogen bond in the polymorph **3.1b**.

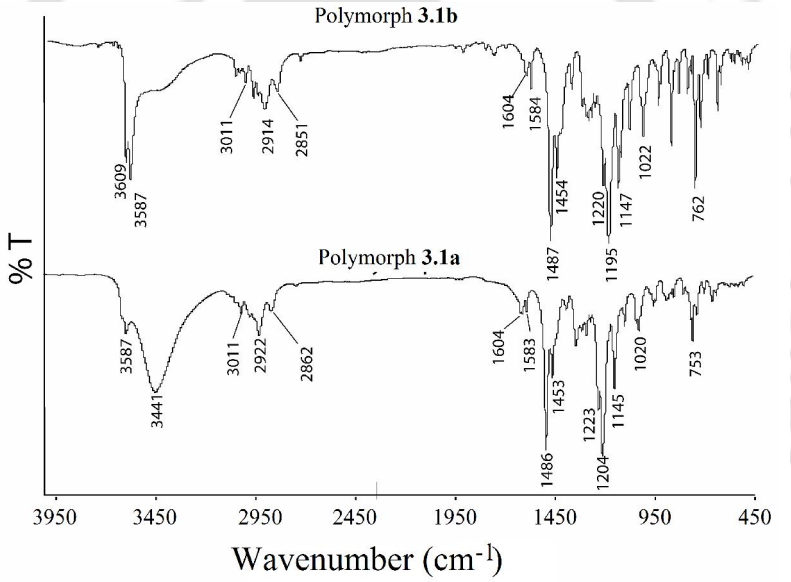

Figure 3.7: The comparison of the IR spectra (KBr, cm^{-1}) of polymorph **3.1a** and **3.1b**.

The primary difference of the two polymorphs arises from voids in the packing pattern of the polymorph **3.1a**. However, the polymorph **3.1a** melts at low temperature under vacuum and transforms to a nonporous form, which deterred us to study gas absorption. The PXRD of the two polymorphs are distinguishable which are shown in the Figure **3.8**. We observe that **3.1a** has a crystal density of 1.181 g/cm^3, and **3.1b** has a crystal density of 1.240 g/cm^3. In accordance with the Kitaigorodskii packing principle,[23a] the polymorph with larger density should have loose molecular

packing, and thus, voids in the lattices of such forms are less likely. This is an indirect outcome of the Burger-Ramberger density rule,[23b] which suggests that at absolute zero, the lower density polymorph has less stability. In the present case, to accommodate the C-H···F-C interactions in the two polymorphs, they adopt different packing patterns. In the case of **3.1a**, there is strong O-H···O interactions, which is absent in the case of **3.1b**. Such strong interactions are able to retain the voids, which is not the case in polymorph **3.1b**.

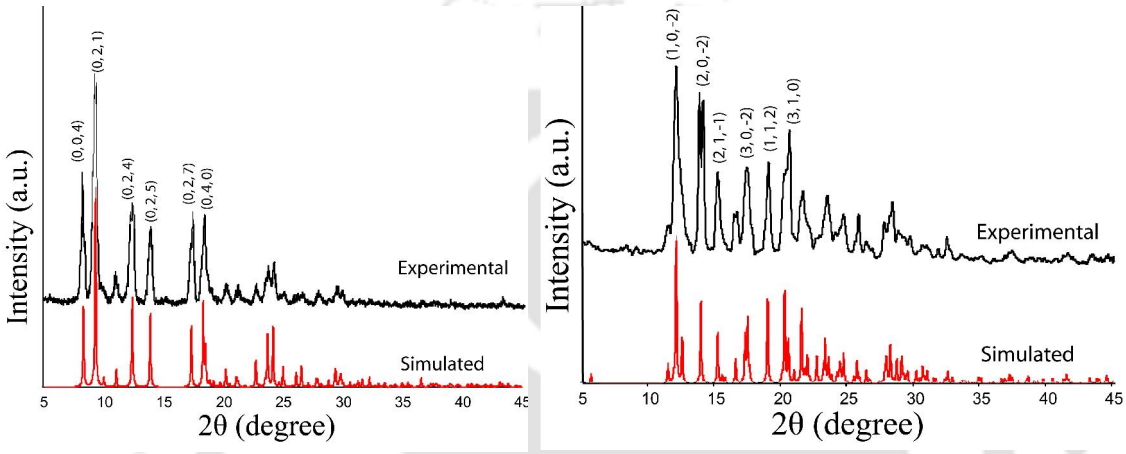

(a) **(b)**

Figure 3.8: Comparison of the simulated and experimental PXRD of **(a)** polymorph 3.1a, **(b)** polymorph **3.1b**.

From the differential scanning calorimetry (DSC) with a heating rate of 3°C per minute, it is found that the polymorph **3.1a** shows an endo-exothermic phase transition at 90°C, followed by two endothermic peaks at 162°C and 168.8°C. On the other hand, DSC of the polymorph **3.1b** shows it to melt at 172 °C (Figure **3.9**). The endo-exothermic peak at 90°C may be due to partial collapse of the porous structure to form a non porous structure **3.1b**. The second melting point of **3.1a** at 168 °C is attributed to arise from **3.1b** formed from **3.1a** through partial conversion to **3.1b** during heating. The difference in melting temperature arises due to the presence of some amount of unconverted **3.1a**, which acts as an impurity to lower the melting point of the portion of **3.1b**. The transformation of **3.1a** to **3.1b** on heating is visually noticeable, as the orange crystals of **3.1a** turns pink on heating at ~160°C. The powder XRD of the heated sample has confirmed the transformation (Figure **3.10**).

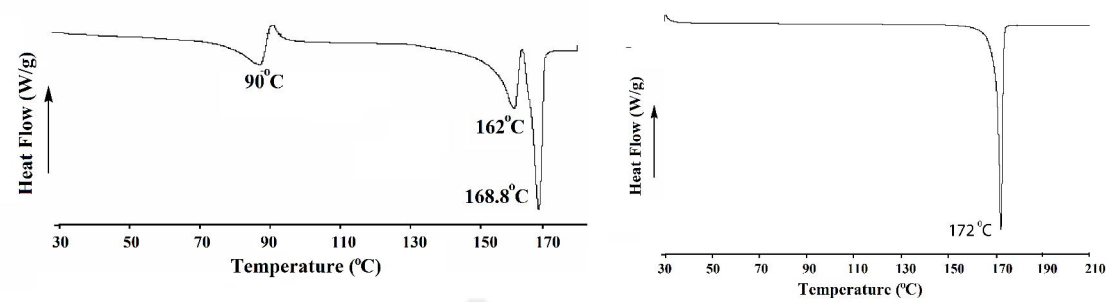

(a) **(b)**

Figure 3.9: The DSC of the **(a)** Polymorph **3.1a** and **(b)** polymorph **3.1b** (at heating rate **3**°C per minute).

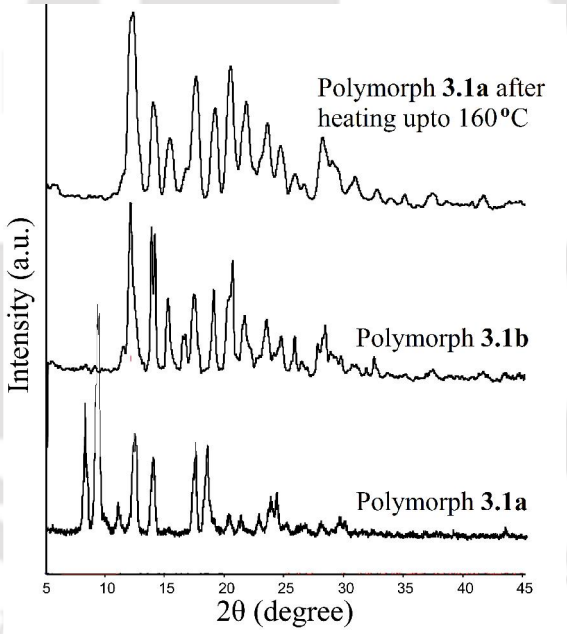

Figure 3.10: The comparison of the **PXRD** of the polymorph **3.1a,** polymorph **3.1b** and the polymorph **3.1a** after heating up to 160°C.

The dimethylformamide solvate (**3.1c)** crystallizes in the orthorhombic space group *Pna2*$_1$. The crystallographic asymmetric unit of **3.1c** contains one *bis*-phenol molecule and a DMF molecule. The DMF molecule acts as a bridge between two host molecules through two O-H···O interactions, namely, O(1)-H···O(3) [$d_{D\cdots A}$= 2.795 Å and ∠D-H···A=128°] and O(2)-H···O(3) [$d_{D\cdots A}$= 2.847 Å and ∠D-H···A=113°]

forming 1D chain (Figure **3.11**). The fluorine atoms of the host molecules interact with the DMF molecule through C-H···F-C interaction. However, there is no C-H···F-C (aromatic) interactions among the host molecules, but there exits C-H···F-C interactions [$d_{D\cdots A}$= 3.003 Å, ∠D–H···A=114°] between the C-H from the methyl group of DMF with the C-F of the aromatic ring of *bis*-phenols. The two molecules of *bis*-phenols are held together by a bifurcated hydrogen bond formed between the carbonyl oxygen atom of DMF and the hydroxy group of two *bis*-phenol molecules (Figure **3.11**). From the packing pattern, it is apparent that the solvent inclusion causes the disruption of the weak C-H···F-C interactions between the *bis*-phenols in

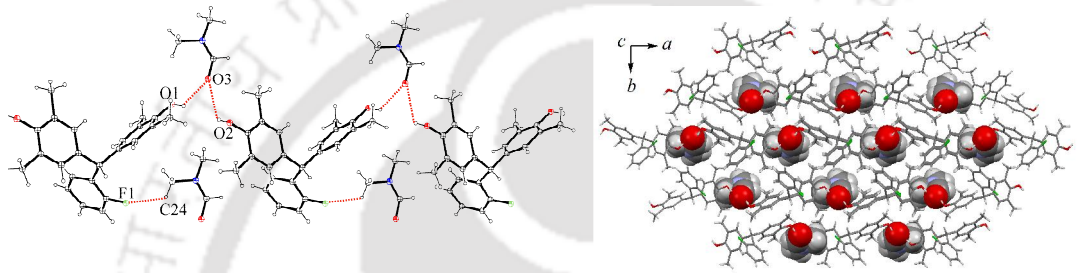

(a) **(b)**

Figure 3.11: (a) O-H···O and C-H···F-C interactions in the dimethylformamide solvate **3.1c**, **(b)** Packing diagram of solvate **1c** when viewed along the crystallographic *c*-axis.

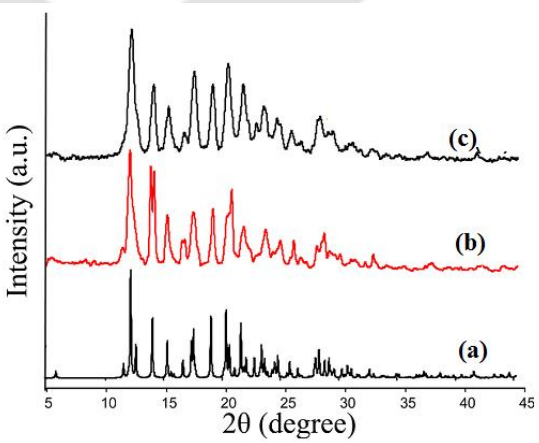

Figure 3.12: Compression of the **(a)** simulated PXRD of polymorph **3.1b**, **(b)** experimental PXRD of polymorph **3.1b** and **(c)** experimental PXRD of the DMF solvate **(3.1c)** after heating up to 140 °C.

the polymorphs **3.1a** and **3.1b**. The DMF solvate **3.1c** transforms to polymorph **3.1b** on heating at 130-140°C and is confirmed by powder-XRD (Figure **3.12**). This suggests that the elimination of guest solvent molecules lead to collapse of the voids. Thus, the thermal conversion can be a synthetic procedure for preparation of polymorph **3.1b**. The diffusion of DMF solvent to get back the solvate in this case was not successful.

3.3 Solvates and polymorphs of solvates of *Bis*-phenol 3.2

The anhydrous form **3.2a** of the *bis*-phenol **3.2** crystallizes in the monoclinic space group $P2_1/n$. Both the hydroxy groups of the molecule are involved in intermolecular hydrogen bonding (Table **3.2**) to form dimeric sub-assemblies (Figure **3.13**). The dimeric assemblies further assemble through C-H···O interactions, leading to a 1D polymeric chain. These 1D chains further connects to each other resulting in the formation of 3D structure.

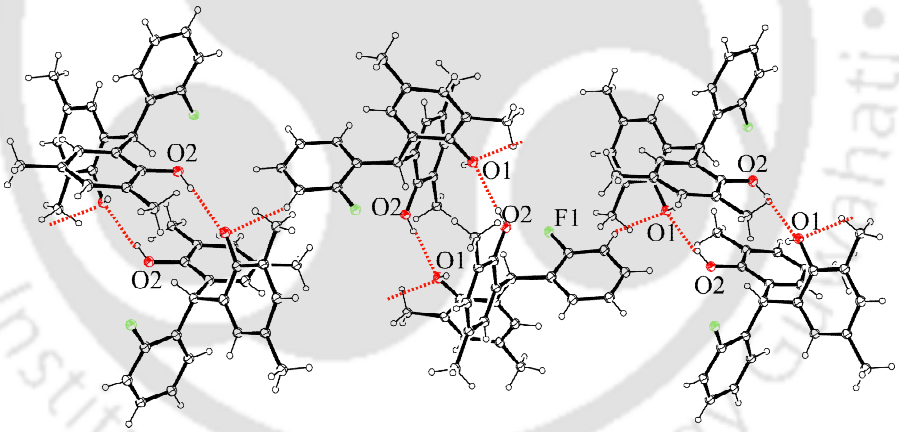

Figure 3.13: The 1D chain-like structure of the anhydrous form of **3.2a**.

Two independent DMSO solvates of *bis*-phenol **3.2** abbreviated as **3.2b** and **3.2c** with different numbers of DMSO molecules were obtained as shown in the Figure **3.14**. The crystal morphologies (Figure **3.15a**) of the two solvates are visually distinguishable; the former crystals have a block shape, and the latter have a needle shape. The solvate **3.2b** crystallizes in the orthorhombic space group *Pbcn*, and the crystallographic asymmetric unit contains one host molecule and a half DMSO

molecule. The sulfur atoms of dimethylsulfoxides are disordered, and it is modeled by sharing electron density at two equivalent positions. As in the structure of the anhydrous form **3.2a**, the solvate **3.2b** also has host components forming dimeric sub-assemblies through O-H···O bonds (Figure **3.14b**). These dimeric sub-assemblies

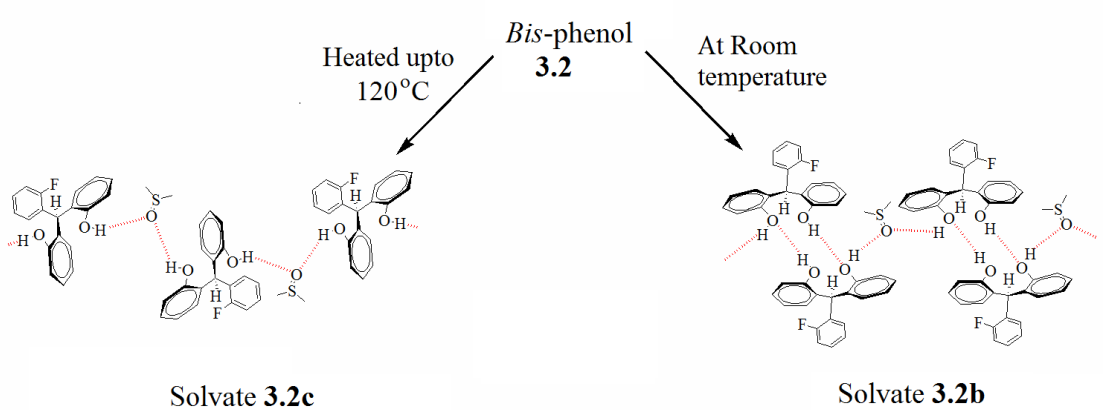

Figure 3.14: The assembling of two DMSO solvates **3.2b** and **3.2c** illustrating the more uptake of DMSO at drastic condition.

Table 3.2: Selected hydrogen bond parameters of solvate **3.2a-3.2e**

Compd .No.	D-H···A	d_{D-H}(Å)	$d_{H\cdots A}$ (Å)	$d_{D\cdots A}$(Å)	∠D−H···A (°)
3.2a	O(2)-H(2)···O(1) [1-x,1-y,1-z]	0.86(2)	2.02(2)	2.793(3)	149(3)
	C(9)−H(9)···O(2)	0.98	2.39	2.752(3)	101
3.2b	O(1)-H(1)···O(3) [-1/2 +x, -1/2 +y, 1/2 -z]	0.83(2)	1.94(2)	2.7257(18)	158(2)
	O(2)-H(2)···O(1) [-x, -y, -z]	0.80(2)	2.06(2)	2.799(2)	153(2)
3.2c	O(1)-H(1)···O(6) [x, 1/2 -y, 1/2 + z]	0.82(4)	1.87(4)	2.684(3)	170(3)
	O(2)-H(2)···O(5) [1 +x, 1/2-y, 1/2 - z]	0.80(3)	2.01(3)	2.753(3)	156(3)
	O(3)-H(3A)···O(5)	0.87(3)	1.89(3)	2.724(3)	160(3)
	C(49)-H(49A)···F(2)	0.96	2.53	3.324(4)	140
	C(47)-H(47B)···O(1) [x, 1/2 -y, -1/2 +z]	0.96	2.60	3.451(5)	148
	C(49)-H(49B)···O(3) [1 +x, y, z]	0.96	2.48	3.384(5)	157
3.2d	O(1)-H(1)···O(3) [1-x,1-y,1-z]	0.85(2)	1.91(2)	2.743(2)	168(3)
	O(2)-H(2)···O(1) [-x,1-y,1-z]	0.852(17)	2.14(2)	2.905(2)	148(2)
	C(9)-H(9)···O(2)	0.98	2.40	2.763(2)	101
3.2e	O(1)-H(1)···O(3)	0.82(2)	1.97(3)	2.717(5)	152(3)
	O(2)-H(2)···O(1) [1-x,1-y, -z]	0.82(3)	2.04(3)	2.776(4)	153(5)
	C(8)-H(8A)···F1	0.961	2.563	3.308	134.48

are bridged by the oxygen atoms of DMSO molecules through bifurcated O(1)-H···O(3) [$d_{D\cdots A}$= 2.7257 Å and ∠D-H···A=158°] bonds leading to the formation of

1D chain along the crystallographic *c*-axis (Figure **3.15b**). On the other hand, the asymmetric unit of the DMSO solvate **3.2c** contains two symmetry independent host *bis*-phenol molecules and two DMSO molecules and it crystallizes in the monoclinic space group $P2_1/c$. Unlike in the case of **3.2a** or **3.2b**; in the case of **3.2c**, the host *bis*-phenol molecules do not form dimeric units. It forms independent helical hydrogen-bonded chains, where the symmetry independent host molecules are bridged by

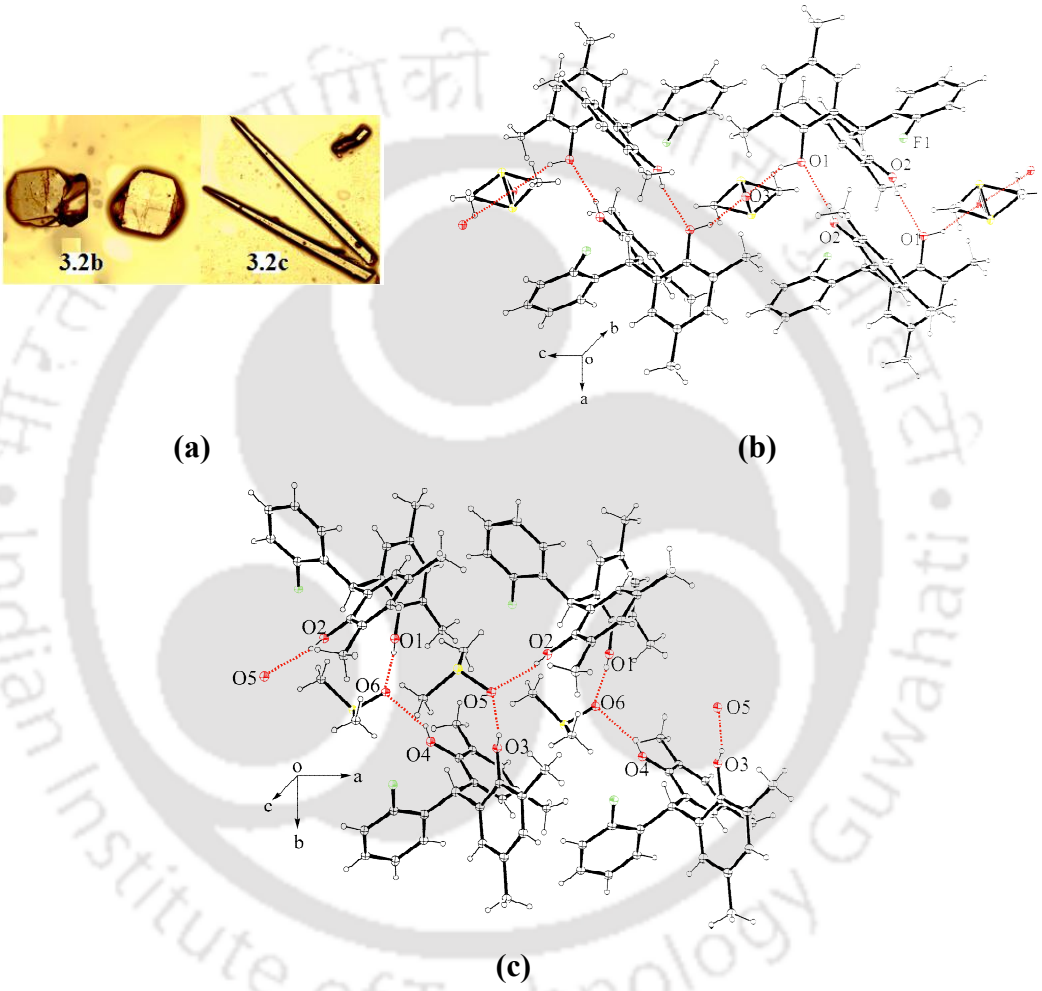

Figure 3.15: **(a)** Crystal morphologies of the DMSO solvates **3.2b** and **3.2c** (10X magnification), **(b)** The formation dimers of *bis*-phenol **3.2** through O-H···O interaction which are further bridge by DMSO molecules through O-H···O interaction, **(c)** 1D chain formed by symmetry non equivalent **3.2** and DMSO molecules through O-H···O interaction in solvate **3.2c**.

DMSO molecules in different symmetry relations (Figure **3.15c**). These independent helical chains further connected to each other through various weak interactions leading to the formation of 3D network structure. The PXRD pattern of the two DMSO solvates **3.2b** and **3.2c** are distinguishable as shown in the Figure **3.16**. The selected hydrogen-bond parameters of the solvates are given in the Table **3.2**.

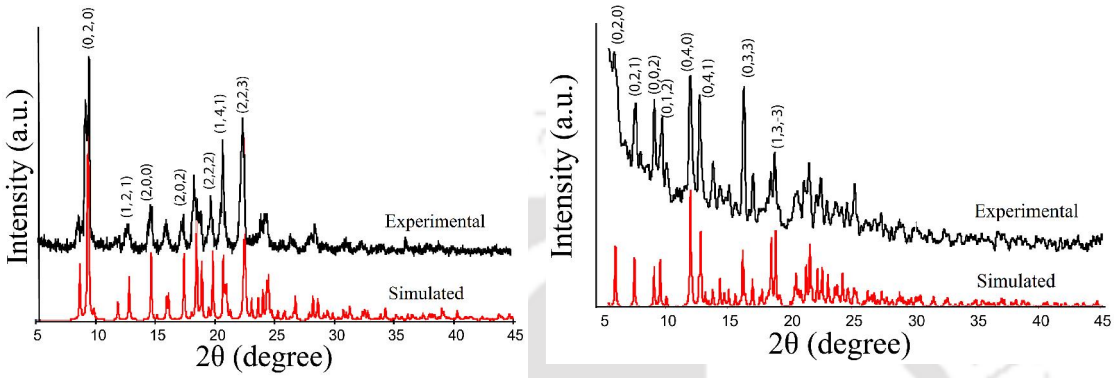

(a) **(b)**

Figure 3.16: Comparison of the simulated and experimental PXRD of the **(a)** solvate **3.2b** and **(b)** solvate **3.2c**.

The crystallization of the *bis*-phenol **3.2** from 1,4-dioxane led to the formation of two concomitant dioxane solvate of same host-guest ratios. These two polymorphs of the 1,4-dioxane solvate are abbreviated as **3.2d** and **3.2e**; their crystals are visually distinguishable (Figure **3.17a**) and they were hand-picked to separate. The solvate **3.2d** crystallizes in the triclinic *P-1* space group, and the crystallographic asymmetric unit contains one host molecule and a half dioxane molecule. The structure is mainly guided by two strong hydrogen bonding interaction, viz., O(1)-H···O(3) [$d_{D\cdots A}$= 2.743 Å and ∠D-H···A=168°] and O(2)-H···O(1) [$d_{D\cdots A}$= 2.905 Å and ∠D-H···A=148°] (Figure **3.17b**). The two hydroxy groups of the host molecules involved in the intermolecular hydrogen bonds to form dimeric units and the dioxane molecules act as bridges between such dimeric units through O(1)-H···O(3) interactions. They result in the formation of 1D chains, and these chains self-assemble to form 2D sheets parallel to the crystallographic *ab*-plane (Figure **3.17e**). On the other hand, solvate **3.2e** crystallizes in the monoclinic space group $P2_1/n$, and the crystallographic asymmetric unit contains a host molecule and a symmetric half of a 1,4-dioxane molecule. In this case also, the structure is mainly guided by similar types of O-H···O interactions

(Table **3.2**) to form dimeric units and these dimeric units are connected to each other through dioxane molecules resulting in the formation of a 1D chain. The chains self-assemble through C-H···F-C interactions to a 3D hydrogen bonded channel structure,

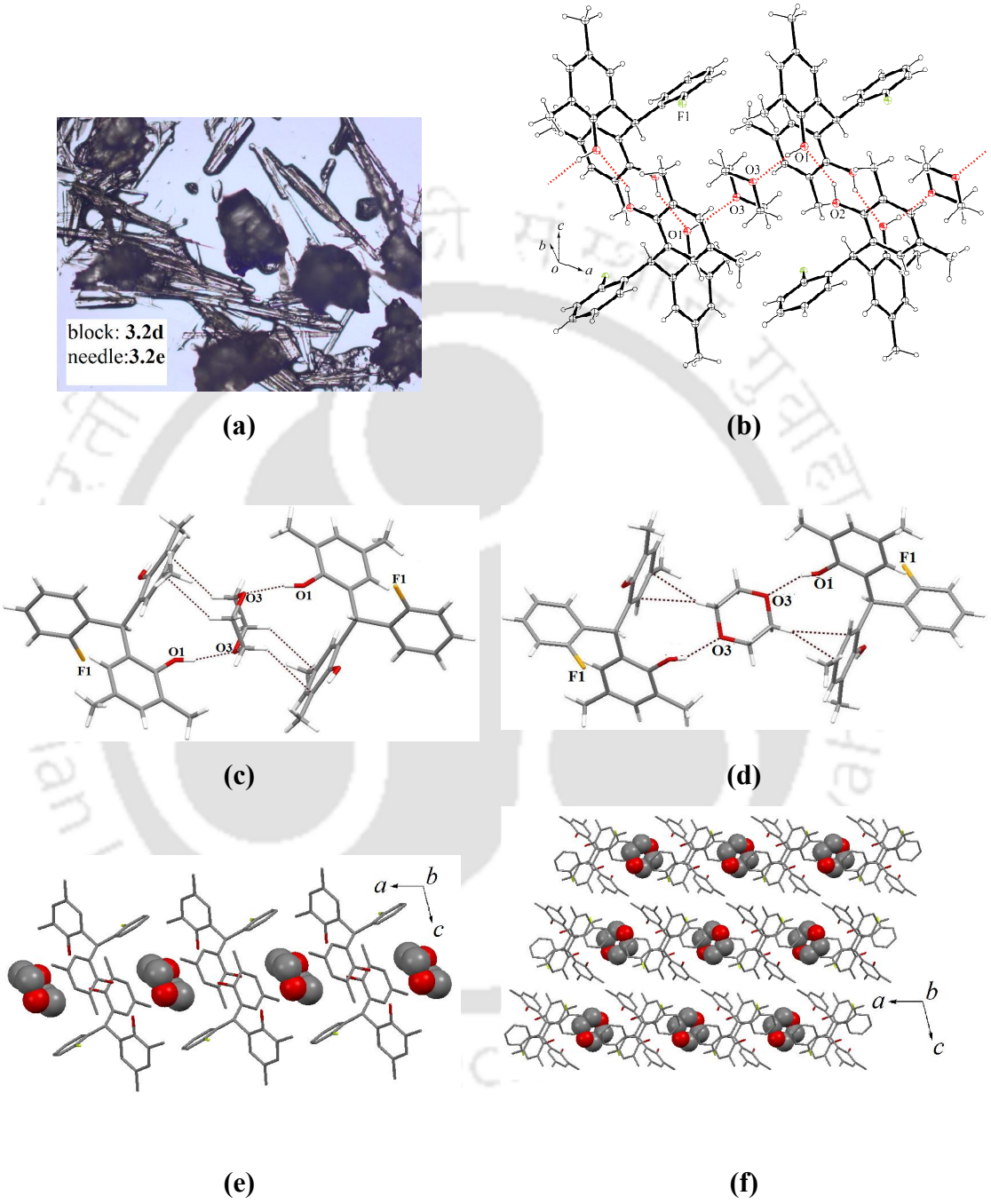

Figure 3.17: (a) Crystal morphologies of the concomitant 1,4-dioxane solvate **3.2d** and **3.2e** (10X magnification), **(b)** Hydrogen bonding interaction in dioxane solvate **3.2d** and **3.2e,** C-H···π interaction in **(c)** solvate **3.2d** and **(d)** solvate **3.2e,** Packing diagram of the **(e)** solvate **3.2d** and **(f)** solvate **3.2e**.

where the channels are occupy by dioxane molecules. The main difference between the structures **3.2d** and **3.2e** is that the latter contains C-H···F-C interactions, whereas the former does not have C-H···F-C interactions. Apart from these, the C-H···π interactions of the dioxane molecules in solvate **3.2d** and **3.2e** are distinguishable (Figure **3.17c** and **3.17d**). Dunitz and Gavezzotti had suggested that the contribution of C-H···F-C interactions in crystal packing may either stabilize or destabilize or remain silent.[8] Nonetheless, in the present case, the C-H···F-C interactions along with the C-H···π interactions distinguish the orientations and packing patterns between **3.2d** and **3.2e.** In chapter 2, we have discussed about the water assisted assemblies of the dioxane solvate of an amino *bis*-phenol. However, in that case we did not observed formation of any concomitant solvates. But in the present case, the *bis*-phenol **3.2** forms a set of concomitant solvate with same host-guest ratio which is an extremely rare phenomenon.[24a] Recently, Saha et al. has reported the concomitant solvate formation by a tripodal host 2,4,6-Triethyl-1,3,5-tris(phenoxymethyl)-benzene with tetrachloro-methane and tetrahydrofuran with different host-guest ratios.[24b] From the structural study, it is evident that similar dimeric subunits of the parent structure of **3.2** is retained in **3.2a**, **3.2b**, **3.2d**, and **3.2e**, but in the case of the **3.2c**, disruption of the dimeric assemblies was observed. The two types of assemblies observed in **3.2b** and **3.2c** are shown in Figure **3.14**. The **3.2c** was prepared at high temperature and pressure; under such conditions, it loses dimeric assemblies of the *bis*-phenol molecules. This observation shows that as the temperature and pressure is raised, the amount of DMSO intake per *bis*-phenol molecule is doubled.

3.4 Caesium complex of *Bis*-phenol 3.2

We attempted to crystallize the sodium, potassium, and caesium salts of *bis*-phenol **3.2**. We did not obtain suitable single crystals for X-ray diffraction study of sodium and potassium, but obtained crystals of the caesium complex **3.2f**. The asymmetric unit of the caesium complex **3.2f** contains one neutral, one mono deprotonated molecule of *bis*-phenol **3.2**, and a caesium cation (Figure **3.18a**). All the oxygen atoms of the two molecules bind to the caesium cation and the coordination sphere of the caesium ion is completed by four oxygen atoms of hydroxy groups and η^2 or η^4 types of the caesium-π interactions with the fluoro-substituted phenyl rings of the

ligands (Figure **3.18b**). The **3.2f** forms a 1D polymeric chain-like structure (Figure **3.18c**), where the *bis*-phenol molecules act as a linker between the caesium ions. The Cs-O distances in the complex **3.2f** are in the range of 3.05-3.12 Å; these are shorter than the reported in caesium calixarene complexes (≈4.0 Å).[25] On the basis of such observations, the Cs-O bonds in the present case are coordinate bonds.[26,27] The Cs-centroid (of aryl ring) distance between the caesium cation and the fluoro-substituted benzene rings of the *bis*-phenol **3.2** are found to be 3.417 Å (η^4-cesium-π interaction) and 3.638 Å (η^2-caesium-π interaction). Similar interactions were earlier observed in the caesium complex of the o-alkylated *p*-phosphonic acid calix-[4]-arenes, where the C_{Ar}-Cs distances in the range of 3.41 to 3.73 Å.[27]

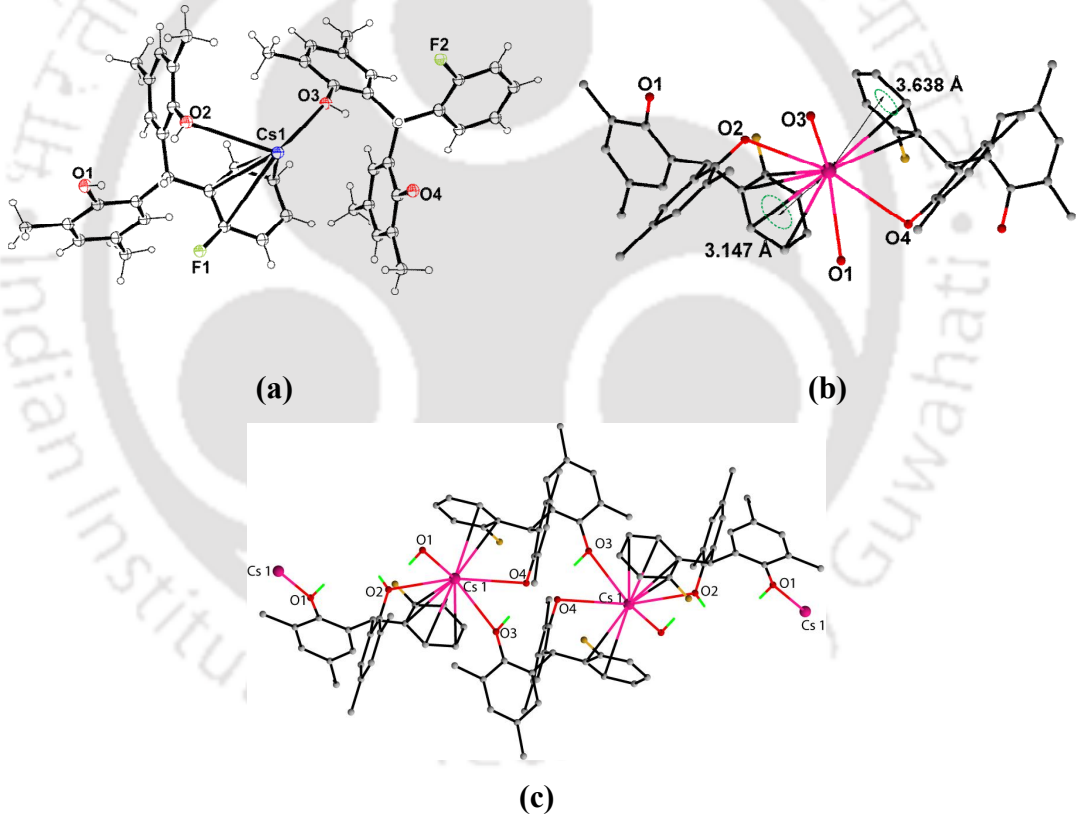

Figure 3.18: (a) Asymmetric unit of **3.2f** (30% thermal ellipsoids)**, (b)** Cation-π interaction in the **3.2f**, (hydrogen atoms are omitted for clarity), **(c)** Structure of the coordination polymer **3.2f**.

The C_{Ar}-Cs distances in the coordination polymer **3.2f** are in the range from 3.49 Å to 3.68 Å, and this separation is very close to the Cs-C distance found in methyl caesium

(3.53 Å).[28] The interaction of calixarenes with alkali metal ions, particularly caesium is widely studied as the different calixarenes provide the basis of method for the purification[29] and analysis[30] of alkali metal ions. However, the caesium complex of *bis*-phenols having caesium-π interactions is not reported to date. On the other hand, the calixarenes are a preorganized system for coordination of the metal, but the present system is very simple, which shows interesting Cs-C_π interactions. The cation-π interactions are evident in the ^{1}H-NMR spectra of the caesium complex **3.2f**. A comparison of the ^{1}H-NMR of the caesium complex with the parent *bis*-phenol shows that methine proton (H_c) in the complex **3.2f** shows a slight upfield shift, whereas the aromatic protons in the region of 6.5-7.5 ppm are significantly affected by interactions of caesium, which are a clear indication of caesium-π interactions (Figure **3.19a**). Further, the ^{19}F-NMR of the caesium complex **3.2f** has a signal at a chemical shift of -119.62, whereas it appears at -118.22 ppm for the parent *bis*-phenol **3.2**.

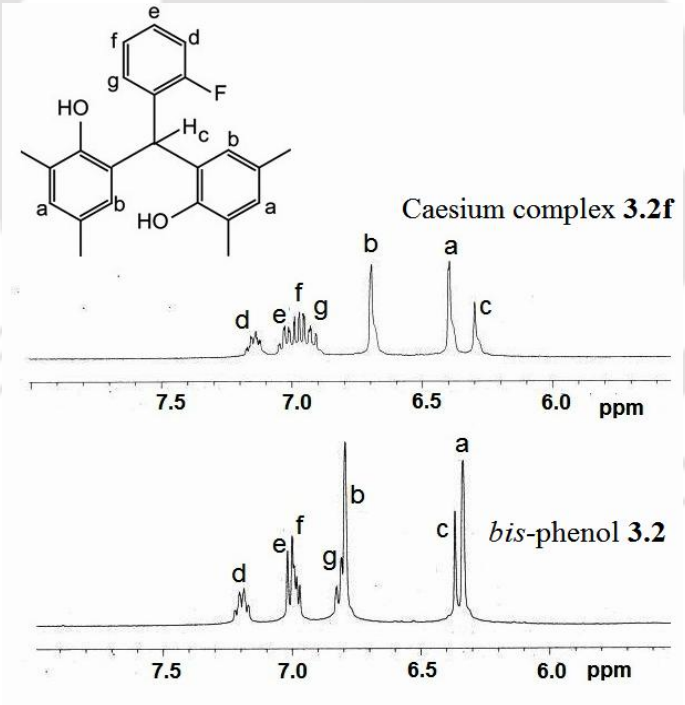

(a)

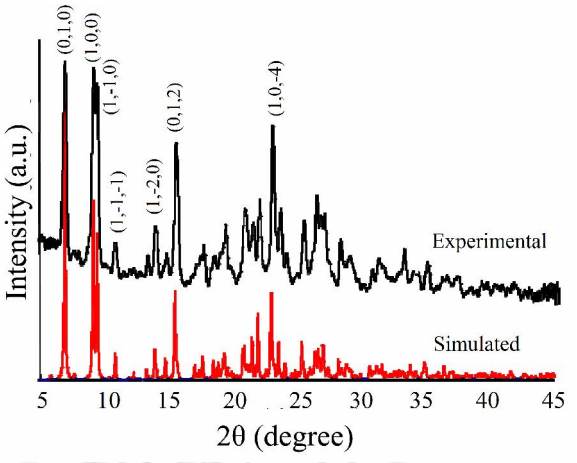

(b)

Figure 3.19: **(a)** Comparison of the ^{1}H-NMR (methanol- d_4, 400 MHz) of the *bis*-phenol **3.2** and caesium complex **3.2f**, **(b)** Comparison of the simulated and experimental PXRD of Caesium complex **3.2f**.

Table 3.3: The selected bond distances in the caesium complex **3.2f**

Cs-C	D_{Cs-C} (Å)	Cs-C	D_{Cs-C} (Å)	Cs-O	D_{Cs-O} (Å)
Cs1-C10	3.588(5)	Cs1-C15	3.565(5)	Cs-O1	3.052(4)
Cs1-C11	3.678(6)	Cs1-C33	3.688(5)	Cs-O2	3.129(4)
Cs1-C14	3.686(5)	Cs1-C38	3.499(6)	Cs-O3	3.086 (4)
				Cs-O4	3.127(3)

In most of the cases, each diffraction peak in the experimental powder XRD is matched with the simulated powder pattern of the structure determined by single crystal diffraction. The agreement of all the peaks suggests the phase purity in bulk samples. The indexing is done as per the simulated diffraction pattern by using MERCURY program.

3.5 Thermogravimetric Analysis of solvates 3.1c and 3.2b-3.2f

From the thermogravimetry study, it is seen that the solvate **3.1c** losses 17.2% (theoretical weight loss 17.28%) of its initial weight in the temperature range 90-170 °C due to the removal of dimethylformamide solvents (Figure **3.20a**). DMSO molecules of solvate **3.2b** are lost in the temperature range from 127-180 **°C**

(observed weight loss of 10.6%, theoretical weight loss of 10.0%), whereas the DMSO molecules of solvate **3.2c** are lost from 132-173 °C (observed weight loss 18.0%, theoretical weight loss 18.2%) (Figure **3.20b**). The higher thermal stability of **3.2b** is attributed to the packing patterns of the *bis*-phenols, in which dimeric assemblies hold the DMSO molecules. The dioxane solvate **3.2d** loses the solvent molecules in the temperature range from 100-150 °C (observed weight loss 10.36%, theoretical weight loss 11.2%, Figure **3.25a**), whereas the dioxane solvate **3.2e** loses the solvent molecules in the range from 80-150 °C (observed weight loss 10.4%,

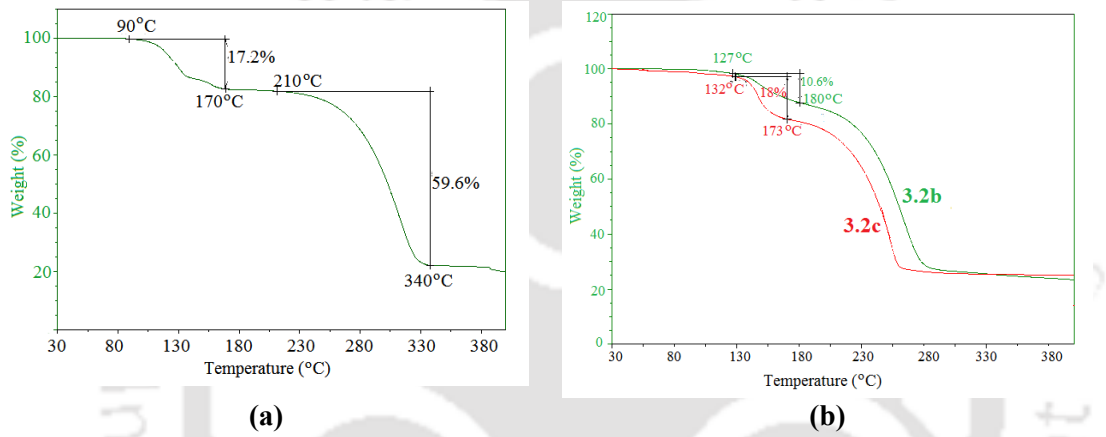

(a) **(b)**

Figure 3.20: (a) TGA of the solvate **3.1c** showing the removal of DMF solvents, Comparison of the TGA of the **(b)** DMSO solvates **3.2b** and **3.2c**.

theoretical weight loss 11.2%, Figure **3.25b**). Both the solvates have similar composition but they lost the solvent molecules at different temperatures. The **3.2d** is having a sheet-like structure that enables a sharp release of dioxane in a relatively narrow range of temperature, whereas the **3.2e** has channel-like structures which make slow release in a well-spread-out range of temperature. This indirectly points out the effect of the C-H···F-C interactions in such assemblies. The caesium complex **3.2f** is stable up to 200 °C and starts to degrade above 200 °C.

3.6 Conclusion

In conclusion, the two polymorphs of *bis*-phenol **3.1** arises from the distinguishable C-H···F-C and O-H···O interactions. These differences in weak interactions make

two different types of packing pattern in the two polymorphs. The polymorph **3.1a** has a porous structure, whereas the polymorph **3.1b** is non-porous. We have also shown the irreversible thermal conversion of the porous polymorph to the non-porous form. Moreover, dimethylfomamide solvate **3.1c** transforms to polymorph **3.1b** on heating. This phenomenon of selective formation of a particular polymorphic form on desolvation of a solvate can be helpful to find new polymorphic phases form various solvates of a compound.

Formation of DMSO solvates of the *bis*-phenol **3.2** with different compositions at different conditions is worth noting. At high temperature and pressure, disruption of the dimeric assemblies of *bis*-phenol **3.2** occurs, and it allows inclusion of higher amounts of DMSO than the corresponding DMSO solvate formed at room temperature. This example shows formation of solvate with higher amounts of guest molecules at solvothermal conditions. Moreover, we observed two concomitant polymorph of the 1,4-dioxane solvate of *bis*-phenol **3.2** with same host-guest ratio. This types of concomitant solvate formation with same host guest ratio is an extremely rare phenomenon.[24b] The two polymorphs of 1,4-dioxane solvate have distinguishable C-H···F-C and C-H···π interactions in their packing patterns, this opens the scope for discovering polymorphs in fluorinated host-guest systems.

We have also observed strong Cs^{+}-π interactions in the caesium complex **3.2f** of *bis*-phenol **3.2**. The Cs^{+}-π interactions in the caesium complex **3.2f** retains in solution also and was confirmed by ^{1}H-NMR.

3.7 Experimental Section

The detailed synthetic methodologies for synthesis of *bis*-phenols are given below. Analytical data as well as spectroscopic data are listed along with each compound. The instrumental details and the crystallographic parameters are provided in Appendix.

Synthesis of *bis*-phenol 3.1: 2-fluorobenzaldehyde (0.540 ml, 5 mmol) and 2, 6-dimethylphenol (1.22 g, 10 mmol) were dissolved in acetic acid (20 mL) and the solution was stirred for half an hour in an ice bath. A mixture of concentrated sulphuric acid and glacial acetic acid in a 1: 2 ratio (10 mL, v/v) was added drop wise to the reaction mixture. After half an hour of stirring, the mixture was kept in a deep

freeze for one week. After one week, ice cold water (10 mL) was added to the reaction mixture; a light yellow colored precipitate appeared. The precipitate was collected by filtration and was washed with aqueous sodium bicarbonate solution (20%, 25 mL). The product was then dried in air. Yield: 70%. ^{1}H-NMR (400 MHz, $CDCl_3$): 7.15 (*dd*, J = 9.6 Hz, J = 5.2 Hz, 1H), 6.94 (*m*, 2H), 6.90 (t, J = 7.6 Hz, 1H), 6.67 (s, 4H), 5.55 (s, 1H), 4.55 (s, 2H), 2.15 (s, 12H). ^{13}C-NMR (100 MHz, DMSO-d_6, δ ppm):161.2, 158.7, 151.5, 133.4, 131.9, 131.7, 130.6, 128.6, 128.0, 124.0, 115.2, 115.0, 47.4 (methine C-H), 16.7 (CH_3-). ^{19}F-NMR ($CDCl_3$, δ ppm): -117.20. ESI Mass: 350.3096 (m^+/e), 349.3061 (m^+/e-1).

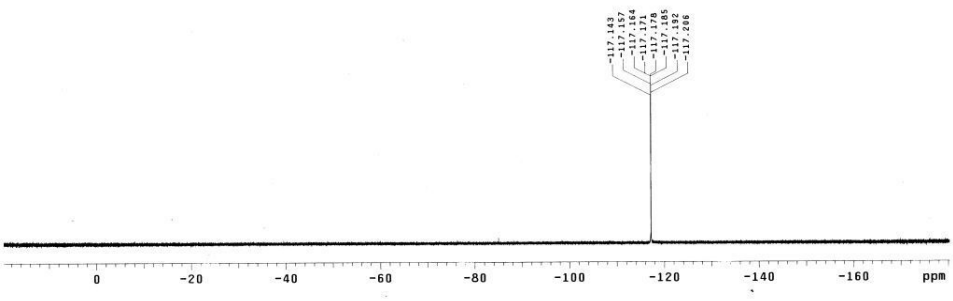

Figure 3.21: ^{19}F-NMR (400 MHz) of *bis*-phenol **3.1** in $CDCl_3$.

Polymorph 3.1a: The polymorph **3.1a** was obtained by slow evaporation of a solution of **3.1** in methanol. IR (KBr, cm^{-1}): 3587 (m), 3441 (s), 3011 (w), 2967 (w), 2922 (w), 2862 (w), 1604 (w), 1583 (w), 1486 (s), 1453 (s), 1385 (w), 1337 (m), 1223 (s), 1204 (s), 1145 (s), 1095 (m), 1020 (m), 948 (w), 883 (w), 753 (s).

Polymorph 3.1b: The polymorph **3.1b** was obtained by slow evaporation of a solution of **3.1** in acetic acid. IR (KBr, cm^{-1}): 3609 (s), 3587 (s), 3060 (w), 3011 (w), 2972 (m), 2948 (m), 2914 (m), 2851 (w), 1604 (w), 1584 (w), 1487 (s), 1454 (s), 1379 (w), 1328 (w), 1307 (w), 1296 (w), 1280 (w), 1220 (s), 1195 (s), 1147 (s), 1135 (m), 1090 (m), 1022 (m), 947 (m), 882 (m), 845 (w), 801 (w), 762 (s), 736 (m), 697 (w), 651(m).

Solvate 3.1c: The solvate **3.1c** was obtained by the slow evaporation of a solution of **3.1** in dimethylformamide. Elemental analysis Calculated for $C_{26}H_{30}FNO_3$; C, 73.73; H, 7.14; N, 3.31; Found: C, 73.69; H, 7.12; N, 3.29. IR (KBr, cm^{-1}): 3383 (s), 2924 (s), 2873 (w), 1657 (s), 1601 (m), 1487 (s), 1454 (w), 1393 (w), 1326 (w), 1281(w),

1193 (s), 1149 (m), 1104 (m), 1018 (w), 939 (w), 845(w), 798(w), 766(w), 662 (w), 526 (w).

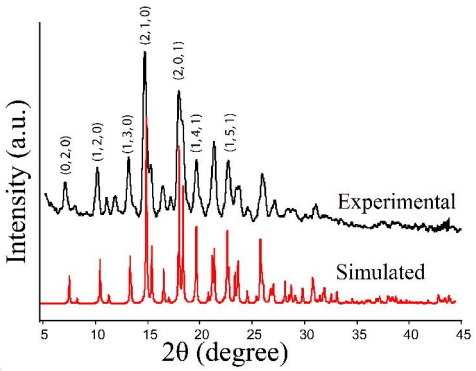

Figure 3.22: The simulated and the experimental PXRD of the solvate **3.1c**.

The *bis*-phenol **3.2** was prepared by the same procedure except 2, 4-dimethylphenol was used instead of 2, 6-dimethylphenol. Yield, 87 %.^{1}H-NMR (400 MHz, methanol-d_4, δ ppm) : 7.17 (*dd*, J = 6.8 Hz, J = 6.0 Hz, 1H), 6.97 (m, 2H), 6.80 (*d*, J = 8 Hz, 1H), 6.79 (s, 2H), 6.36 (*s*, 1H), 6.33 (*s*, 2H), 2.17 (*s*, 6H), 2.09 (*s*, 6H). ^{13}C-NMR (100 MHz, dmso-d^{6}, δ ppm), 159.3, 150.4, 131.9, 130.7, 130.3, 129.6, 127.9, 127.6, 127.2, 124.2, 123.9, 115.3, 115.0, 36.7, 20.7, 16.9. ^{19}F-NMR (methanol-d_4, δ ppm) -118.22 (m). ESI Mass: 350.3088 (m^+/e), 349.3086 (m^+/e-1).

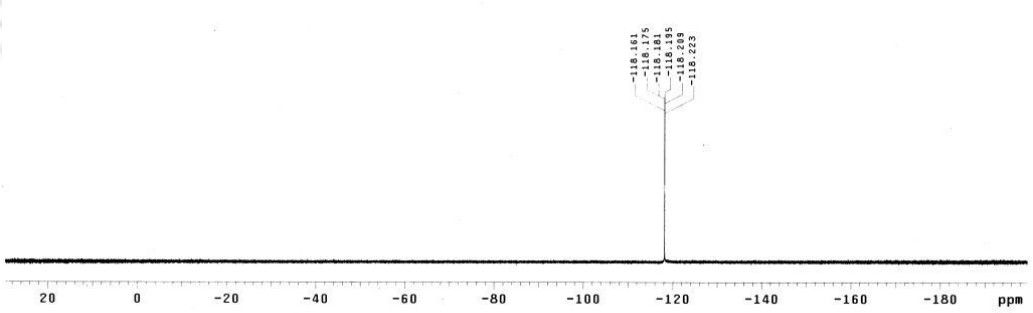

Figure 3.23: ^{19}F-NMR of *bis*-phenol **3.2** in methanol-d_4.

The unsolvated form **3.2a** is obtained by the slow evaporation of a solution of **3.2** in methanol. IR (KBr, cm^{-1}): 3486 (s), 3448 (s), 3033 (w), 2921 (s), 2860 (w), 1585 (w), 1487 (s), 1455 (s), 1380 (w), 1330 (m), 1302 (w), 1291(w), 1282 (w), 1256 (s), 1227 (s), 1194 (s), 1137 (s), 1093 (m), 1031(m), 1015 (w), 865 (m), 839 (m), 814 (w), 765 (s), 748 (s), 665 (w).

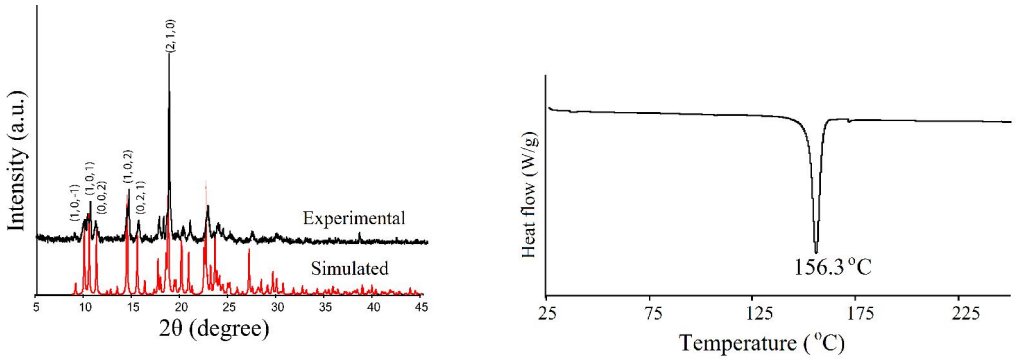

(a) **(b)**

Figure 3.24: (a) Simulated and the experimental PXRD of **3.2a**, **(b)** DSC of **3.2a**.

DMSO solvate 3.2b: When a solution of **3.2** in dimethylsulphoxide was allowed for slow evaporation it gives 1:0.5 solvate of DMSO. Elemental analysis calculated for $C_{48}H_{52}F_2O_5S$, C, 74.01; H, 6.73; Found C, 73.97; H, 6.86. IR (KBr, cm^{-1}): 3454 (s), 3190 (m), 3009 (w), 2973 (w), 2913 (m), 2862 (w), 1599 (m), 1586 (m), 1482 (s), 1455 (s), 1322 (m), 1303 (m), 1255 (m), 1227 (s), 1182 (s), 1169 (m), 1149 (w), 1095 (w), 1032 (w), 1014 (w), 994 (m), 940 (m), 933 (m), 892 (w), 868 (w), 856 (w), 839 (w), 817 (w), 786 (w), 753 (s), 667 (w).

DMSO solvate 3.2c: A solution of **3.2** in DMSO was heated in a sealed Teflon-lined steel autoclave at 120°C for 4 hours and allowed to cool slowly, it yielded needle shaped crystals. Elemental analysis calculated for $C_{25}H_{29}FO_3S$; C, 70.06; H, 6.82; Found C, 76.18, H, 6.78. IR (KBr, cm^{-1}): 3357 (s), 3000 (w), 2915 (m), 2857 (w), 1598 (w), 1583 (w), 1483 (s), 1453 (s), 1381(w), 1316 (m), 1301 (m), 1250 (m), 1224 (s), 1181 (s), 1091 (w), 1001 (s), 941 (s), 864 (m), 839 (w), 820 (w), 750 (s), 666 (w).

Dioxane solvate 3.2d and 3.2e: When a solution of **2** in 1,4-dioxane was allowed to evaporate slowly, crystals of two different morphologies **2d** and **2e** appears. Elemental analysis calculated for $C_{25}H_{27}FO_3$: C, 76.12; H, 6.90; Found C, 76.22, H, 6.94. IR (cm^{-1}) of **2d**: 3451 (s), 3009 (w), 2923 (m), 2863 (w), 1585 (m), 1483 (s), 1454 (m), 1380 (w), 1325 (w), 1298 (m), 1253 (s), 1227 (s), 1187 (s), 1146 (m), 1109 (m), 1079 (w), 1033 (w), 893 (w), 862 (s), 840 (w), 816 (w), 785 (w), 752 (s), 667 (w). For **2e:** Elemental analysis calculated for $C_{25}H_{27}FO_3$: C, 76.14; H, 6.90; Found C, 76.10, H, 6.92. IR (cm^{-1}): 3483 (s), 3209 (m), 2922 (m), 2860 (w), 1584 (w), 1482 (s),

1453 (m), 1327 (w), 1252 (m), 1223 (s), 1189 (s), 1145 (w), 1078 (w), 1035 (w), 936 (w), 861 (s), 751 (s), 623 (w).

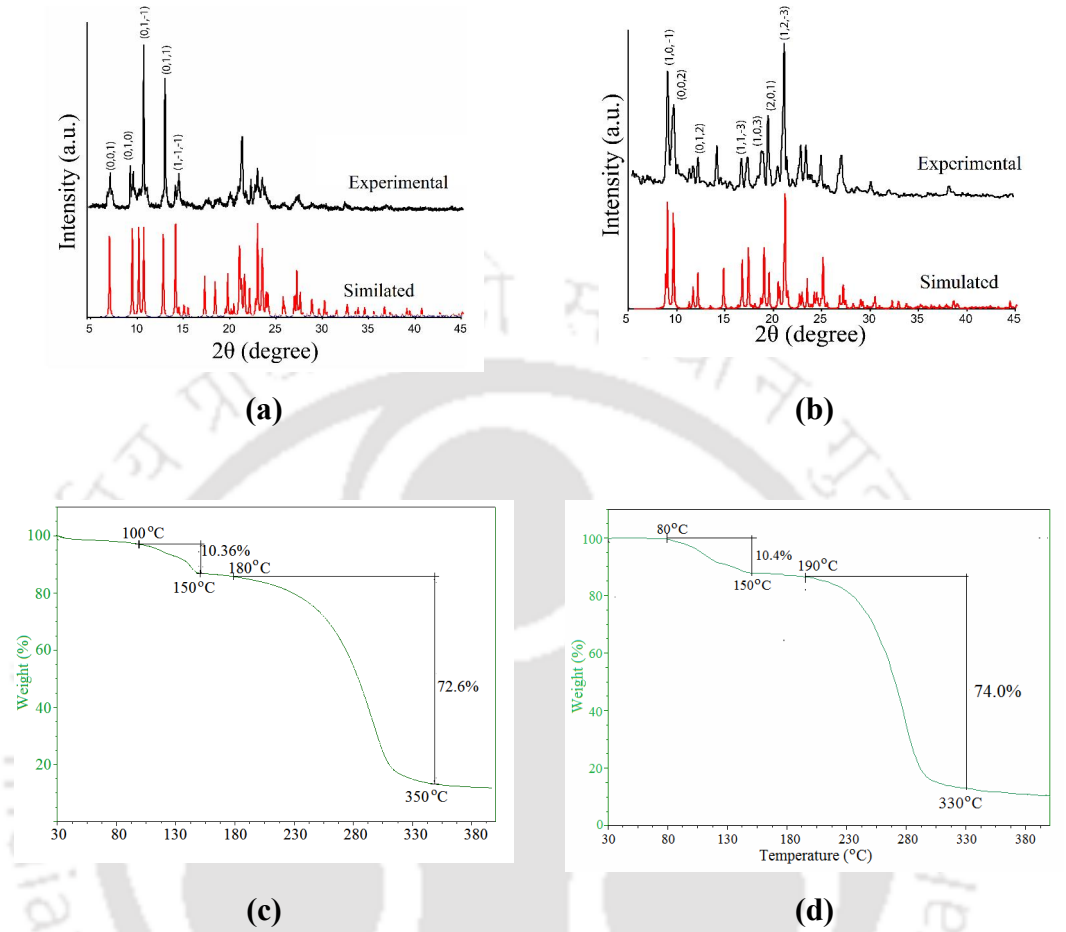

Figure 3.25: (a) and **(b)** are the comparison of simulated and experimental PXRD of 1, 4-dioxane solvate **3.2d** and **3.2e** respectively, **(c)** and **(d)** are the TGA of the solvate **3.2d** and **3.2e** respectively.

Caesium complex 3.2f: Solid Cs_2CO_3 (0.16 g, 0.5 mmol) was added to a well stirred solution **2** (0.70 g, 2 mmol) in methanol. The resulting solution was refluxed for about 4 hours. The reaction mixture was then filtered and the filtrate was kept undisturbed for crystallization. After 3-4 days colorless needle shaped crystals of **3.2f** appeared. IR (KBr, cm^{-1}): 3406 (m), 3005 (w), 2918 (m), 2851(w), 2725 (w), 1577 (w), 1482 (s), 1451(m), 1371(w), 1297 (w), 1226 (s), 1212 (s), 1146 (m), 1096 (w), 1031 (w), 1008 (w), 949 (w), 762 (s), 667 (s). ^{1}H-NMR (methanol-d_4): 7.13 (*dd*, J = 7.6 Hz, J = 5.2 Hz, 1H), 7.02 (t, J = 6.0 Hz, 1H), 6.97 (t, J = 7.2 Hz, 1H), 6.90 (d, J = 6.8 Hz,

1H), 6.69 (s, 2H), 6.39 (s, 2H), 6.29 (s, 1H), 2.12 (s, 6H), 2.05 (s, 6H), ^{19}F-NMR: -119.62 (m).

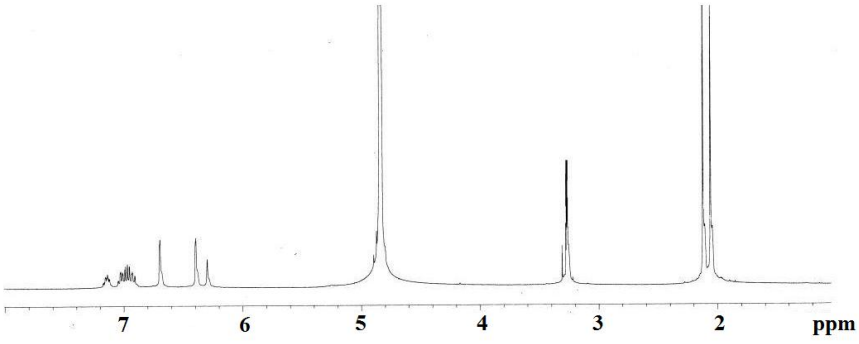

(a)

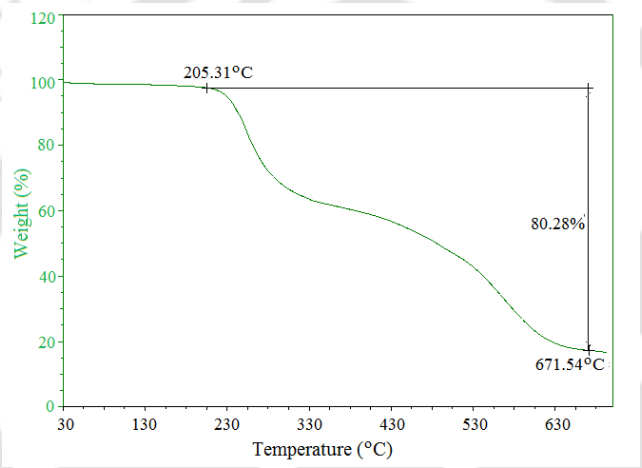

(b)

Figure 3.26: (a) The ^{1}H-NMR (methanol-d_4, 400MHz) of the Cesium complex **3.2f**, **(b)** The TGA of the caesium complex **3.2f**.

References:

1. (a) A. Orthaber, C. Seidel, F. Belaj, J. H. Albering, R. Pietschnig, U. Ruschewitz, *Inorg. Chem.*, 2010, **49**, 9350-9357; (b) Z. Hulvey, E. Ayala, J. D. Furman, P. M. Forster, A. K. Cheetham, *Cryst. Growth Des.,* 2009, **9**, 4759-4765; (c) L. Zhang, Q. Wang, Y. -C. Liu, *J. Phys. Chem.*, B2007, **111**, 4291-4295.
2. (a) A. Bondi, *J. Phys. Chem.*, 1964, **68**, 441-451; (b) G. K. Suryaprakash, J. U. Hu, T. M. Mathew, G. A. Olah, *Angew. Chem., Int. Ed.*, 2003, **42**, 5216-5219.
3. (a) L. Shimoni, J. P. Glusker, *Struct. Chem.*, 1994, **5**, 383-397; (b) J. A. K. Howard, V. J. Hoy, D. O'Hagan, G. T. Smith, *Tetrahedron*, 1996, **52**, 12613-

12622; (c) J. D. Dunitz, R. Taylor, *Chem. -Eur. J.*, 1997, **3**, 89-98; (d) G. R. Desiraju, R. Parthasarathy, *J. Am. Chem. Soc.*, 1989, **111**, 8725-8726.

4. (a) B. E. Smart, *Characteristics of C-F Systems in Organofluorine Chemistry: Principles and Commercial Applications Banks*, R. E., Ed.; Plenum Press: New York, 1994; (b) D. A. Dixon, B. E. Smart, *In Selective Fluorination in Organic and Bioorganic Chemistry*; Welch, J. T., Ed.; ACS Symposium Series 456; American Chemical Society: Washington, DC, 1991; (c) D. A. Dixon, B. E. Smart, *J. Phys. Chem.*,1991, **95**, 1609-1612.
5. (a) M. D. Prasanna, T. N. Guru Row, *CrystEngComm*, 2000, **3**, 134-140; (b) K. Reichenbacher, H. I. Suss, J. Hulliger, *Chem. Soc. Rev.*; 2005, **34**, 22-30; (c) D. Chopra, T. N. Guru Row, *CrystEngComm*, 2011, **13**, 2175-2186; (d) R. Berger, G. Resnati, P. Metrangolo, E. Weber, J. Hulliger, *Chem. Soc. Rev.*, 2011, **40**, 3496-3508; (e) A. G. Dikundwar, R. Sathishkumar, T. N. Guru Row, G. R. Desiraju, *Cryst. Growth Des.*, 2011, **11**, 3954-3963; (f) D. Chopra, *Cryst. Growth Des.*, 2012, **12**, 541-546; (g) G. Kaur, P. Panini, D. Chopra, A. R. Choudhury, *Cryst. Growth Des.*, 2012, **12**, 5096-5110.
6. (a) H. -C. Weiss, R. Boese, H. L. Smith, M. M. Haley, *Chem. Commun.*, 1997, 2403-2404; (b) V. K. Thalladi, H. -C. Weiss, D. Blaser, R. Boese, A. Nangia, G. R. Desiraju, *J. Am. Chem. Soc.*, 1998, **120**, 8702-8710; (c) T. J. Barbarich, C. D. Rithner, S. M. Miller, O. P. Anderson, S. H. Strauss, *J. Am. Chem. Soc.*, 1999, **121**, 4280-4281.
7. (a) D. Chopra, K. Nagarajan, T. N. GuruRow, *Cryst. Growth Des.*, 2005, **5**, 1035-1039; (b) D. Chopra, T. N. Guru Row, *Cryst. Growth Des.*, 2005, **5**, 1679-1681; (c) D. Chopra, T. N. Guru Row, *Cryst. Growth Des.*, 2008, **8**, 848-853.
8. (a) A. Gavezzotti, *Acta Crystallogr.*, 2010, **B66**, 396-406; (b) J. D. Dunitz, A. Gavezzotti, *Angew. Chem., Int. Ed.*, 2005, **44**, 1766-1787.
9. (a) I. D. Oswald, D. R. Allan, W. D. Motherwell, S. Parsons, *Acta Crystallogr., Sect. B*, 2005, **61**, 69-79; (b) I. D. Oswald, D. R. Allan, G. M. Day, W. D. Motherwell, S. Parsons, *Cryst. Growth Des.*, 2005, **5**, 1055-1071.
10. (a) M. Gdaniec, *CrystEngComm*, 2007, **9**, 286-288; (b) D. Das, R. Banerjee, R. Mondal, J. A. K. Howard, R. Boese, G. R. Desiraju, *Chem Commun.*, 2006, 555-557.

11. A. Czapik, M. Gdaniec, *Acta Crystallogr., Sect. C*, 2011, **67**, o341-o345.
12. (a) J. W. Steed, J. L. Atwood, *Supramolecular Chemistry*; Wiley: Chichester, 2000; (b) G. R. Desiraju, J. J. Vittal, A. Ramanan, *Crystal Engineering: A Textbook*; World Scientific: Singapore, 2012; (c) G. A. Jeffrey, *An Introduction to Hydrogen Bonding*; Oxford University Press: Oxford, 1997.
13. (d) M. R. Caira, L. R. Nassimbeni, F. Toda, D. Vujovic, *J. Am. Chem. Soc.*, 2000, **122**, 9367-9372; (e) N. B. Bathori, L. R. Nassimbeni, *Cryst. Growth Des.*, 2012, **12**, 2501-2507; (f) M. R. Caira, T. Roex, L. R. Nassimbeni, E. Weber, *Cryst. Growth Des.*, 2006, **6**, 127-131; (g) R. Mondal, J. A. K. Howard, *Cryst. Growth Des.*, 2008, **8**, 4359-4366.
14. (a) R. Thakuria, B. Sarma, A. Nangia, *Cryst. Growth Des.*, 2008, **8**, 1471-1473; (b) P. K. Thallapally, P. B. McGrail, S. J. Dalgarno, J. L. Atwood, *Cryst. Growth Des.*, 2008, **8**, 2090-2092; (c) K. Skobridis, G. Paraskevopoulos, V. Theodorou, W. Seichter, E. Weber, *Cryst. Growth Des.*, 2011, **11**, 5275-5288.
15. R. J. Sarma, J. B. Baruah, *Dyes Pigm.*, 2004, **61**, 39-47.
16. (a) I. J. Brass, A. T. Bullock, *J. Chem. Soc.*, *Faraday Trans*., 1978, **74**, 1556-1561; (b) J. L. Alderfer, A. V. Eliseev, *J. Org. Chem.*, 1997, **62**, 8225-8226; (c) M. Rappoabiuso, M. F. Llauro, Y. Chevaliera, P. L. Perchec, *Phys. Chem. Chem. Phys.*, 2001, **3**, 99-106; (d) I. D. H. Oswald, D. R. Allan, G. M. Day, W. D. S. Motherwell, S. Parsons, *Cryst. Growth Des.*, 2005, **5**, 1055-1071; (e) S. Aitipamula, A. Nangia, *Chem.-Eur. J.*, 2005, **11**, 6727-6742; (f) C. Laurence, J. Graton, M. Berthelot, F. Besseau, J. Y. L. Questel, M. Lucon, C. Ouvrard, A. Planchat, E. Renault, *J. Org. Chem.*, 2010, **75**, 4105-4123.
17. (a) M. Tominaga, H. Masu, I. Azumaya, *CrystEngComm*, 2011, **13**, 5299-5302; (b) M. Tominaga, H. Masu, I. Azumaya, *Cryst. Growth Des.*, 2011, **11**, 542-546; (c) J. Lü, L. W. Han, J. X. Lin, R. Cao, *Cryst.Growth Des.*, 2011, **11**, 3551-3557.
18. B. Sarma, S. Roy, A. Nangia, *Chem. Commun.*, 2006, **49**, 18-4920.
19. (a) J. D. Dunitz, *ChemBioChem*, 2004, **5**, 614-621; (b) A. J. Mountford, S. J. Lancaster, S. J. Coles, P. N. Horton, D. L. Hughes, M. B. Hursthouse, M. E. Light, *Inorg. Chem.*, 2005, **44**, 5921-5933.
20. S. Aitipamula, A. Nangia, *Chem. Commun*., 2005, 3159-3161.

21. K. Kobayashi, N. Kobayashi, M. Ikuta, B. Therrien, S. Sakamoto, K. Yamaguchi, *J. Org. Chem.*, 2005, **70**, 749-752.
22. (a) G. R. Desiraju, *CrystEngComm*, 2007, **9**, 91-92; (b) J. W. Steed, *CrystEngComm*, 2003, **5**, 169-179; (c) G. S. McGrady, M. Odlyha, P. D. Prince, J. W. Steed, *CrystEngComm*, 2002, **4**, 271-276.
23. (a) A. I. Kitaigordoskii, *Molecular Crystals*; Nauka: Moscow, 1971; (b) A. Burger, R. Ramberger, *Microchim. Acta*, 1979, **II**, 259-271.
24. (a) A. Bacchi, M. Carcelli, T. Chiodo, F. Mezzadri, F. Nestola, A. Rossi, *J. Am. Chem. Soc*., 2012, **134**, 673-684; (b) S. Bhattacharya, B. K. Saha, *Cryst. Growth Des.*, 2013, **13**, 606-613.
25. J. M. Harrowfield, M. I. Ogden, W. R. Richmond, A. H. White, *J. Chem. Soc., Chem. Commun.*,1991, 1159-1161.
26. D. E. Fenton, *In Comprehensive Coordination Chemistry*; J. A. McCleverty, R. D. Gillard, G. Wilkinson, Eds.; Pergamon Press: Oxford, 1987, **Vol.3**, p1.
27. T. E. Clark, M. Makha, A. N. Sobolev, D. Su, H. Rohrs, M. L. Gross, C. L. Raston, *Cryst. Growth Des.*, 2009, **9**, 3575-3580.
28. E. Weiss, H. Koster, *Chem. Ber.*, 1977, **110**, 717-720.
29. *Calixarenes a Versatile Class of Macrocyclic Compounds*; J. Vicens, V. Bohmer, Eds.; Kluwer Academic Publishers: Dordrecht, The Netherlands, 1991.
30. (a) D. N. Reinhoudt, E. J. R. Sudholter, *Adv. Mater.*, 1990, **2**, 23-32; (b) K. Kimura, T. Miura, M. Matsuo, T. Shono, *Anal. Chem.*, 1990, **62**, 1510-1513.

CHAPTER 4

Polymorphs, solvates and anion assisted assemblies of imidazole based *bis*-phenols

Although there are many literatures available on the self-assembly and host-guest chemistry of *bis*-phenols,[1] there are only a few references found on heteroatom containing *bis*-phenols.[2] Generally, *bis*-phenols and their related phenolic compounds possess O-H···O, C-H···O and O-H···π (aromatic) interactions in the solid state.[3] The introduction of N-containing heterocyclic ring such as imidazole in *bis*-phenols can introduce additional interactions leading to new supramolecular architectures. Various types of packing patterns can be generated in assemblies of such *bis*-phenol molecules by changing the donor-acceptor interactions. Some representative arrangements are illustrated in Figure **4.1.** Moreover, different imidazolium cations that can readily form on acid treatment of imidazole derivatives generally self-assemble through N-H···N interactions.[4]

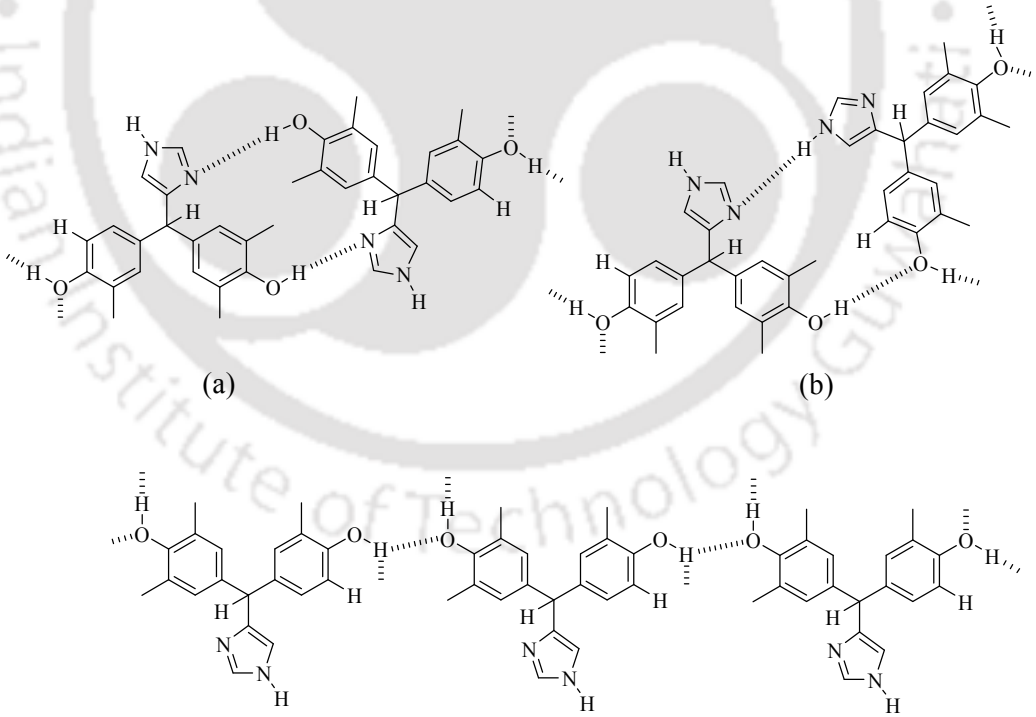

(a) (b)

(c)

Figure 4.1: Some representative ways to form hydrogen bonded assemblies through **(a)** O-H···N, **(b)** N-H···O and O-H···O and **(c)** O-H···O interactions among neighbouring molecules of an imidazole containing *bis*-phenol.

The nitrogen atoms in imidazole based *bis*-phenol may also interact with various anions to give new charge assisted assemblies of *bis*-phenols. Imidazole derivatives are attractive due to their ability to form supramolecular isomers and solvatopolymorphs.[5] Thus, it would be interesting to attach an imidazole unit on *bis*-phenol to study self-assembled structures. With these anticipations we synthesised two new imidazole based *bis*-phenols, 4-[(4-hydroxy-3,5-dimethylphenyl)(5-methyl-1H-imidazol-4-yl)methyl]-2,6-dimethylphenol (**4.1**) and 2-((2-hydroxy-3,5-dimethyl-phenyl)(imidazol-4-yl)methyl)-4,6-dimethylphenol (**4.2**) and studied the structural aspects of their polymorphs and solvates.

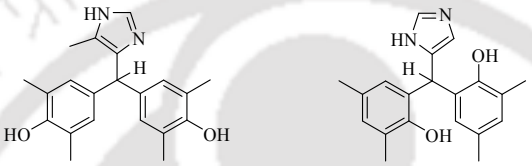

4.1 **4.2**

Figure 4.2: The structures of the *bis*-phenols **4.1** and **4.2**.

Beside these, charge assisted assemblies of *bis*-phenol **4.1** and *bis*-phenol **4.2** on interaction with various organic and inorganic anions are studied**.** These studies were performed with the anticipation that such new imidazole containing *bis*-phenol would interact to different anions depending on the availability of interacting sites. Earlier, pyridine containing *bis*-phenols were used to stabilize methyl and ethyl sulfate salts of pyridinium *bis*-phenols.[2]

4.1 Synthesis and characterization of *Bis*-phenol 4.1 and *Bis*-phenol 4.2:

Bis-phenol **4.1** was synthesised by condensation of 4-methyl-5-imidazolecarboxaldehyde with 2,6-dimethylphenol under acidic condition following a reported procedure.[6] The *bis*-phenol **4.2** was synthesised by the condensation of 4(5)-imidazolecarboxaldehyde with 2,4-dimethylphenol following a similar procedure. The *bis*-phenol **4.1** and *bis*-phenol **4.2** were characterised by various spectroscopic techniques such as FT-IR, ^{1}H-NMR, ^{13}C-NMR, mass spectrometry. The ^{1}H-NMR showed the characteristic signals for methine proton at 5.09 ppm and 5.74 for *bis*-phenol **4.1** and **4.2** respectively (Figure **4.3a** and **4.3b**).

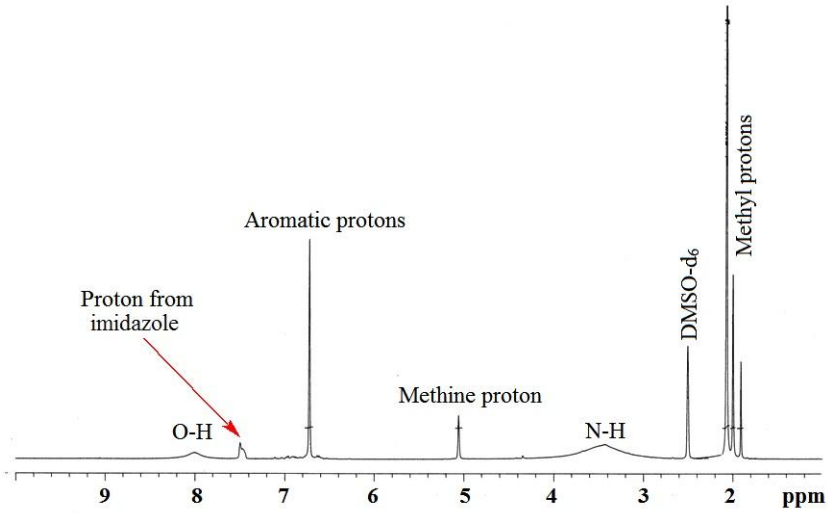

(a)

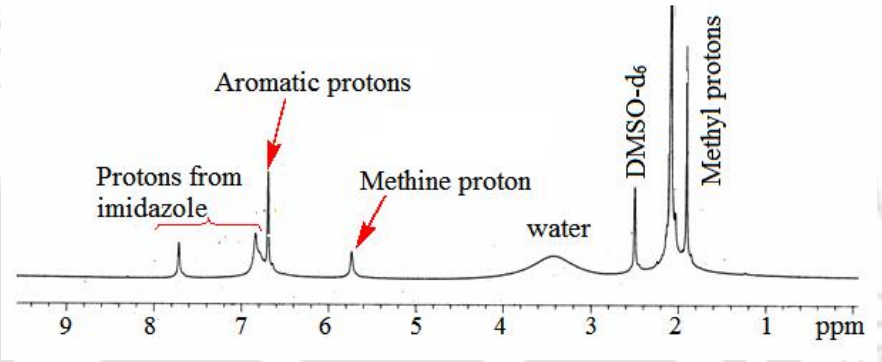

(b)

Figure 4.3: ^{1}H-NMR (400 MHz, DMSO-d_6) of the **(a)** *bis*-phenol **4.1** and **(b)** *bis*-phenol **4.2**.

4.2 Supramolecular assemblies of *bis*-phenol 4.1

4.2.1 Polymorph and solvates of *bis*-phenol 4.1

The crystallization of *bis*-phenol **4.1** from a methanolic solution led to the formation of crystals with two different morphologies. These crystals are concomitant polymorphs of *bis*-phenol **4.1**, whose components are abbreviated as polymorph **4.1a** and polymorph **4.1b**. The crystals of each polymorph are visually distinguishable in color and shape and they can be handpicked and separated. The crystals of polymorph **4.1a** are colorless needles whereas the crystals of polymorph **4.1b** are yellow colored blocks**.** The crystal morphologies of the polymorph **4.1a** and

polymorph **4.1b** are shown in the Figure **4.4**. *Bis*-phenol **4.1** forms a 1:0.5 solvate with acetone (**4.1c**) and 1:1 monohydrated solvate (**4.1d**) with dimethylsulphoxide (Scheme **4.1**).

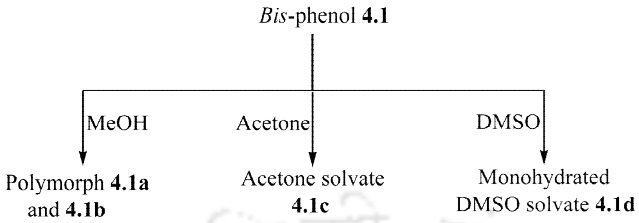

Scheme 4.1: The polymorphs and solvates of *bis*-phenol **4.1.**

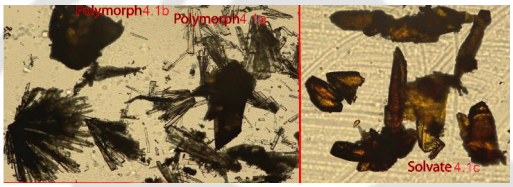

Figure 4.4: The crystal morphologies of the polymorph **4.1a**, **4.1b** and solvate **4.1c** (10X magnification).

The crystals of polymorph **4.1a** belong to the monoclinic space group $P2_1/c$. The parent molecules in polymorph **4.1a** self-assemble through various weak interactions. The prominent weak interactions present in the self-assembly are O(2)-H···N(2) [$d_{D\cdots A}$= 2.669 Å, ∠D-H···A = 154˚] and O(1)-H···O(2) [$d_{D\cdots A}$ = 2.705 Å, ∠D-H···A = 152˚] interactions. The nitrogen atom (N2) of the imidazole ring of *bis*-phenol **4.1** involves in intermolecular hydrogen bond with O(2)-H of a neighbouring molecule (Figure **4.5a**). This results in the formation of a hydrogen bonded dimeric motifs of *bis*-phenol **4.1**. These dimeric motifs are further connected to each other through O-H···O interactions to form hydrogen bonded sheets along the *bc*-plane (Figure **4.6a**). Apart from the strong hydrogen bond interactions, weak interactions such as N-H···π interactions also contribute to the stability of the lattice. The N-H bond of the imidazole involves in η^3-type N-H···π interactions ($d_{N\text{-}H\cdots\pi}$ = 3.361 Å) with one of the rings of the phenolic part of the *bis*-phenol **4.1** (Figure. **4.5b**). The N-H···π interactions were previously observed in phenolic compounds possessing amino

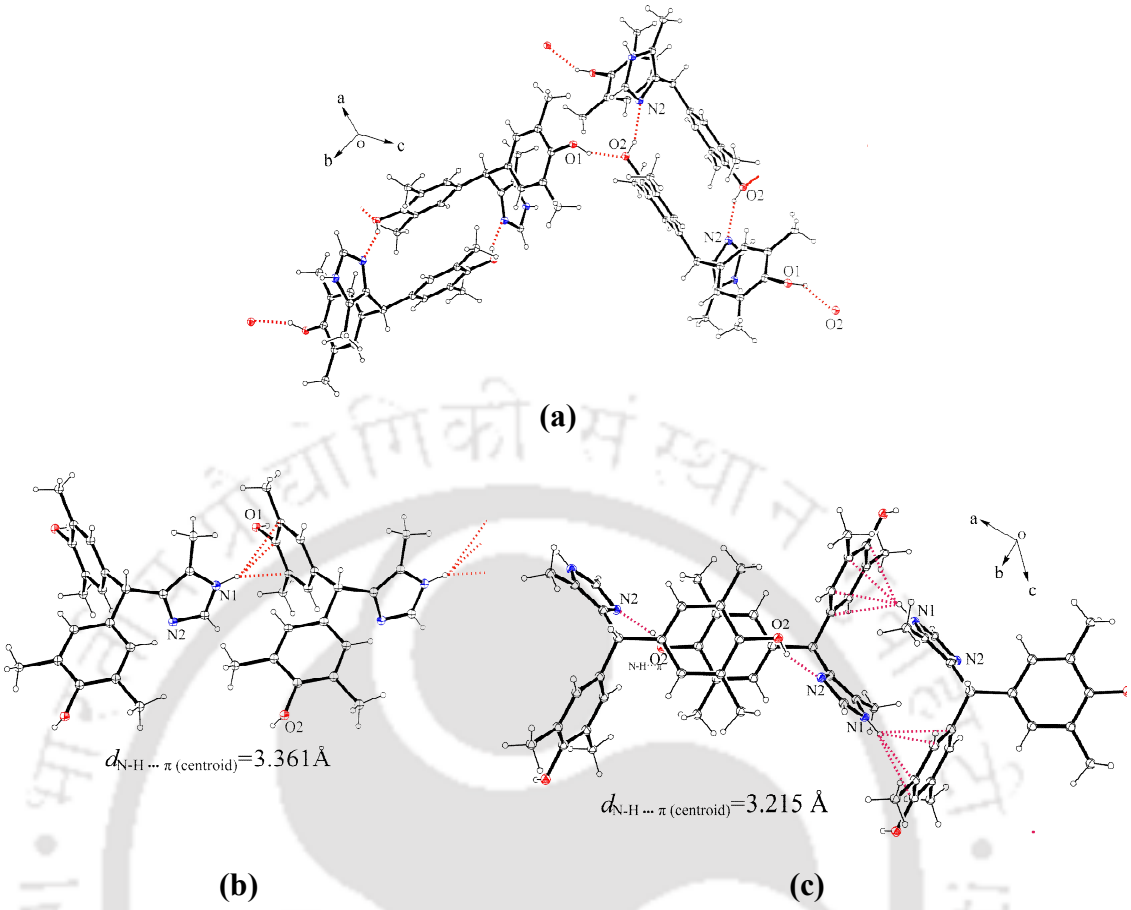

(a)

(b) **(c)**

Figure 4.5: (a) O-H···O and O-H···N interactions in the polymorph **4.1a** and **4.1b**, **(b)** η^3- type N-H···π interactions in polymorph **4.1a**, **(c)** η^4- types of N-H···π interactions in polymorph **4.1b.**

groups.[7] However, the observed N-H···π distances in that cases are around 2.68 Å-2.82 Å which is much less than the present case. The strength of the N-H···π interactions are much weaker in comparison to the related hydrogen bond interactions.[8a] In general, they are in the range of ~4 kcal mol^{-1}.[8b] Thus these interactions may be considered as secondary interactions contributing to the stability of the assemblies.

Polymorph **4.1b** crystallizes in monoclinic space group C2/c. Similar to polymorph **4.1a**, the molecules in polymorph **4.1b** also form hydrogen bonded dimers through O(2)-H···N(2) interactions [$d_{D\cdots A}$= 2.617Å, ∠D-H···A= 157˚] (Figure **4.5a**). In the case of **4.1b** also, these dimers are connected to each other through O(1)-H···O(2) interactions [$d_{D\cdots A}$= 2.680Å, ∠D-H···A= 161˚]. The differences between the

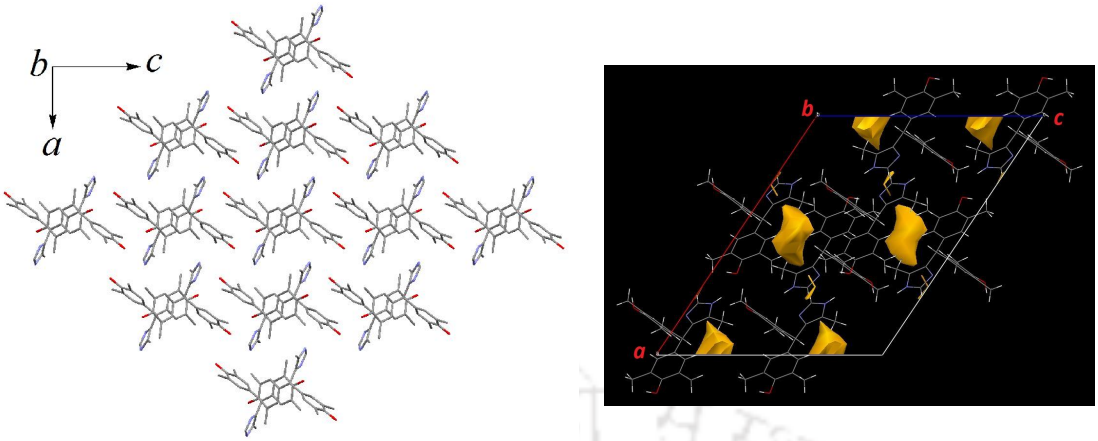

(a) **(b)**

Figure 4.6: Packing pattern of the **(a)** polymorph **4.1a** and **(b)** polymorph **4.1b**.

structures of the two polymorphs are the slight reorganization of the molecules in polymorph **4.1b** to have η^4-type N-H···π interactions between the imidazole N-H bond and the π-cloud of one of the benzene rings ($d_{N\text{-}H\cdots\pi}$= 3.215 Å) of *bis*-phenol **4.1**. These interactions are such that a new set of dimeric motifs are formed (Figure **4.5c**). Finally, this polymorph adopts a structural pattern that contains voids with a radius of 1.2 Å running along the crystallographic [010] plane (Figure **4.6b**). The volumes of these voids are found to be around 556 $Å^3$ and they occupy 13.4% of the unit cell volume. Thus, N-H···π interactions distinguish the packing patterns of polymorphs **4.1a** and **4.1b**.

The porosity of **4.1b** is also established from its surface study. The nitrogen adsorption-desorption isotherm of polymorph **4.1b** is shown in Figure **4.7b**. The total BET surface area of polymorph **4.1b** is found to be 81.672 m^2g^{-1}. The nature of the nitrogen adsorption-desorption isotherm is of type II according to the IUPAC classification[9] and the total pore volume is 0.1374 mLg^{-1}. Further, the absence of any kind of disordered solvent molecules in these voids is supported by thermogravimetry (TG) since it does not show any appreciable amount of weight loss for solvent molecules (Figure **4.7a**).

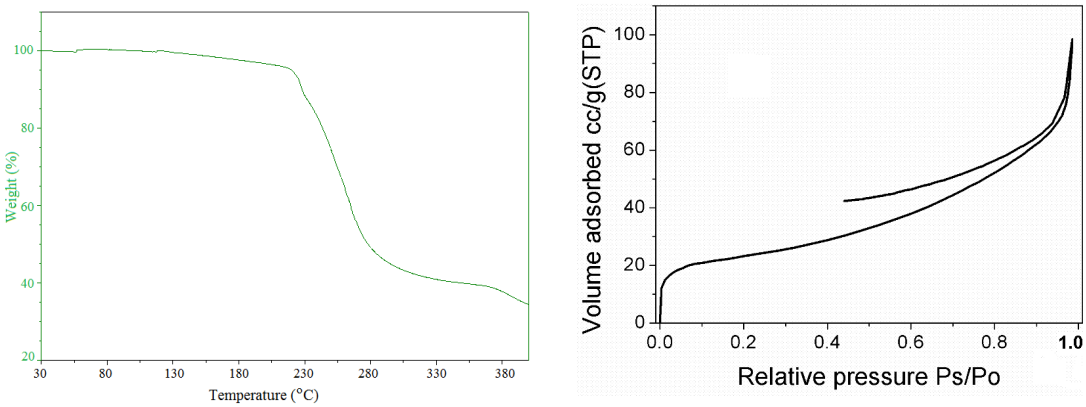

(a) **(b)**

Figure 4.7: **(a)** The TG of the polymorph **4.1b** at 3 °C per minute, **(b)** Nitrogen adsorption-desorption isotherm of polymorph **4.2b**.

The crystallographic asymmetric unit of acetone solvate **4.1c** contains one host molecule and half of an acetone molecule. As in the structures of the two polymorphs, here also the molecules of **4.1** form self assembled dimers through O(1)-H···N(2) [$d_{D\cdots A}$= 2.6241 Å, ∠D-H···A= 155˚] interactions and the dimers are connected to each other through O(2)-H···O(1) [$d_{D\cdots A}$= 2.6750 Å, ∠D-H···A= 153˚] interactions. In this case, the N-H of the imidazoles are involves in η^5-type of N-H···π interactions (Figure **4.8a**) with the phenolic ring ($d_{N\text{-}H\cdots\pi}$= 3.233 Å) where the H···$\pi_{centroid}$ distance of 2.267 Å. There is a great similarity in the packing of solvate **4.1c** with polymorph

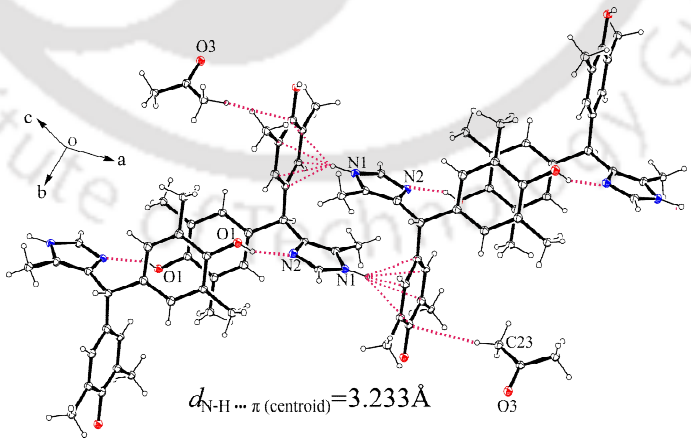

(a)

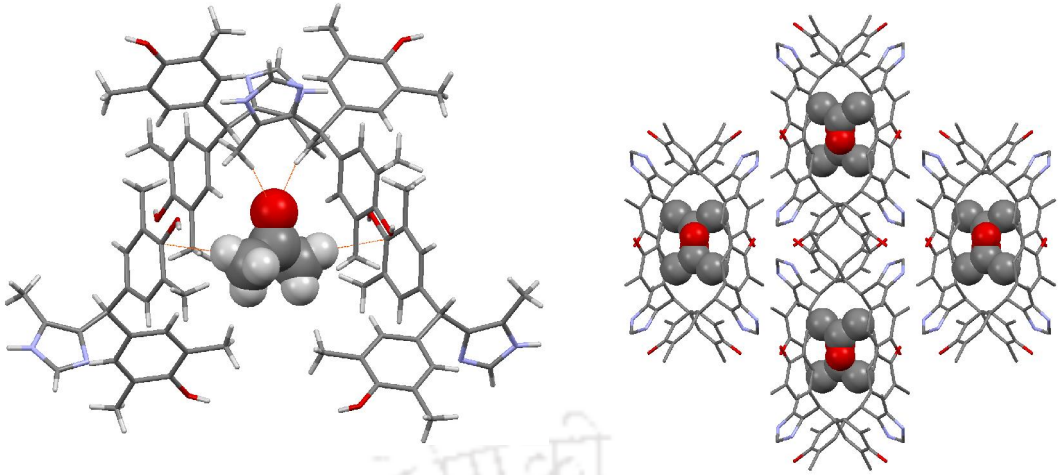

(b) **(c)**

Figure 4.8: (a) The η^5-type N-H···π interactions, **(b)** the C-H···O and C-H···π interactions and **(c)** Packing diagram of the solvate **4.1c.**

4.1b. In solvate **4.1c**, the guest acetone molecules are embedded through C-H···O and C-H···π interactions (Figure **4.8b**) in the cavities formed by the assembly of the host molecules (Figure **4.8c**). The PXRD patterns of polymorph **4.1a** and **4.1b** are distinguishable (Figure **4.9a** and **4.9b**). The simulated PXRD pattern of polymorph **4.1b** and the simulated PXRD pattern of solvate **4.1c** are compared (Figure **4.9c**) and it is seen that they are non-overlapping but similar sets of peaks are observed in the two cases. In general, acetone solvates exhibit weak interactions through the C-H bond of the methyl groups and the carbonyl oxygen. Thus, polymorph **4.1b** can be considered as a porous host for acetone molecules, whereas **4.1c** is a pseudopolymorph of *bis*-phenol **4.1**.[10] Due to the presence of weak interactions, polymorph **4.1b** can easily exchange acetone molecules. It is a difficult task in crystal engineering to predict the formation of a particular polymorph.[11] However, the solvents used in the crystallization processes may have a significant role in their formation.[12] There are many examples in which the structural frameworks of porous materials are changed while heating or due to the loss of solvent molecules.[13] A study on such factors helps to decide reversible guest inclusion. For example, the conversion of hydrated *p*-phenylenediamine crystals to the anhydrous form requires[14] translational motion of the diamine molecules along with in-plane rotation of every fourth *p*-phenylenediamine molecule by about 60° angles. Moreover, the thermal desolvation can pass through phase transitions.[15] We observed that when solvate **4.1c**

was heated to about 60°C, the acetone molecules were lost from the solvate and the single crystals after heating showed a weak diffraction pattern (we could not solve the structure of the heated sample due to its poor diffraction). However, the PXRD

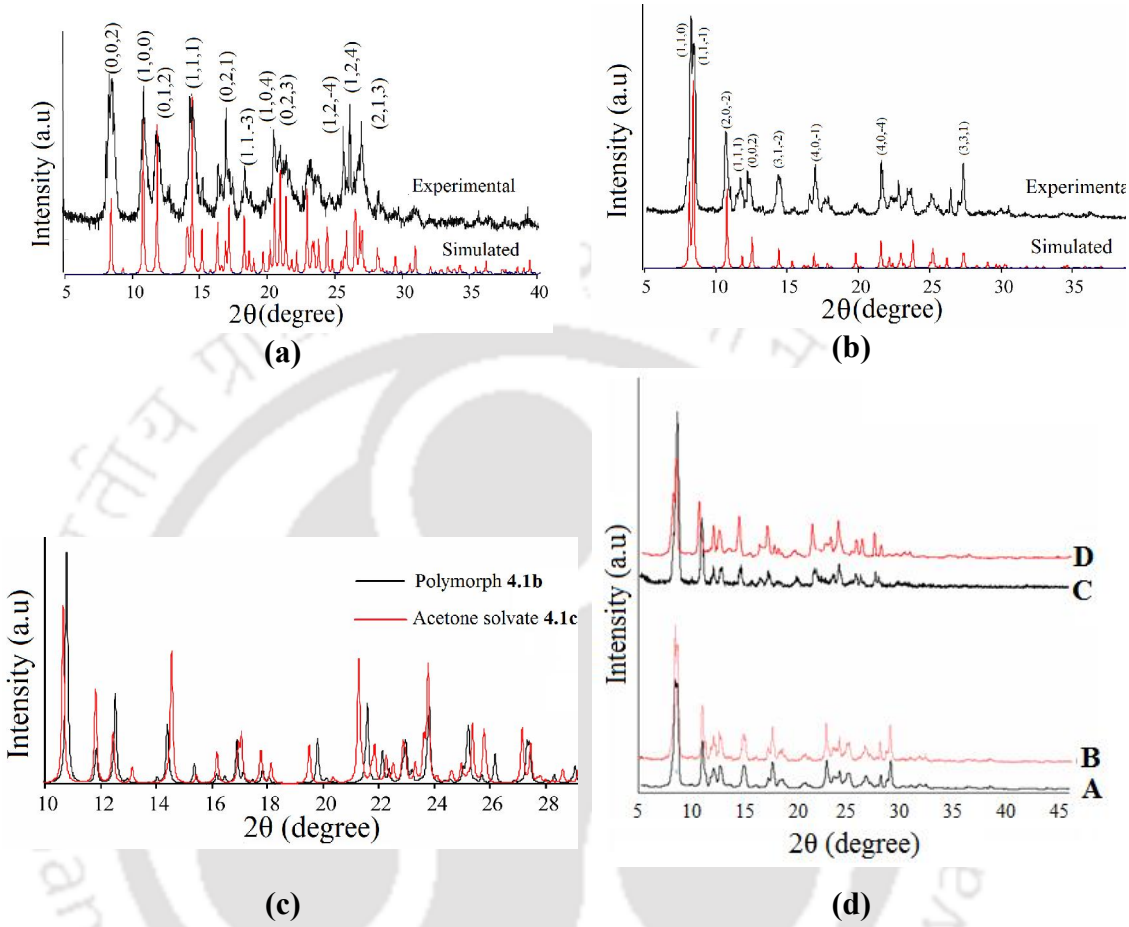

Figure 4.9: PXRD of the polymorph of **(a) 4.1a** and **(b) 4.1b**, **(c)** Comparison of the simulated PXRD of polymorph **4.1a** and with the simulated PXRD of acetone solvate **4.1c, (d)** Comparison of the powder pattern of the **(A)** polymorph **4.1b**, **(B)** acetone solvate **4.1c** after removal of acetone on heating, **(C)** polymorph **4.1b** after exposing to acetone vapour and **(D)** acetone solvate **4.1c.**

pattern of the heated single crystals of **4.1c** resembles to the PXRD pattern of polymorph **4.1b** (Figure **4.9d**). Again, we found that the porous polymorph **4.1b** absorbs diffused acetone when it is exposed to acetone vapour at ambient conditions for about a day in a closed vessel to form solvate **4.1c.** The reversibility of the acetone binding by polymorph **4.1b** has been established by comparing the PXRD patterns (Figure. **4.9d**) of solvate **4.1c** with acetone absorbed sample of **4.1b** prepared by the

diffusing acetone vapour. The PXRD of the acetone diffused sample of polymorph **4.1b** is identical with acetone solvate **4.1c**. Furthermore, the PXRD of the acetone absorbed sample upon heating resembles the PXRD of **4.1b**.

The DMSO solvate of **4.1** was obtained as monohydrate. The crystallographic asymmetric unit of the DMSO solvate **4.1d** contains one molecule of **4.1**, DMSO and a water molecule. This structure is not an exception to the structure of the acetone solvate in terms of the dimers formed through O(1)-H···N(2) [$d_{D\cdots A}$= 2.721 Å and ∠D-H···A = 169°] interactions. But in this case, the dimeric assemblies are connected to each other through bridging water molecules (Figure **4.10a**). The N-H bonds of the imidazole rings are involved in η^3-type N-H···π interactions with the π-bonds of the phenol rings, so polymorph **4.1a** and solvate **4.1d** have similar N-H···π interactions.

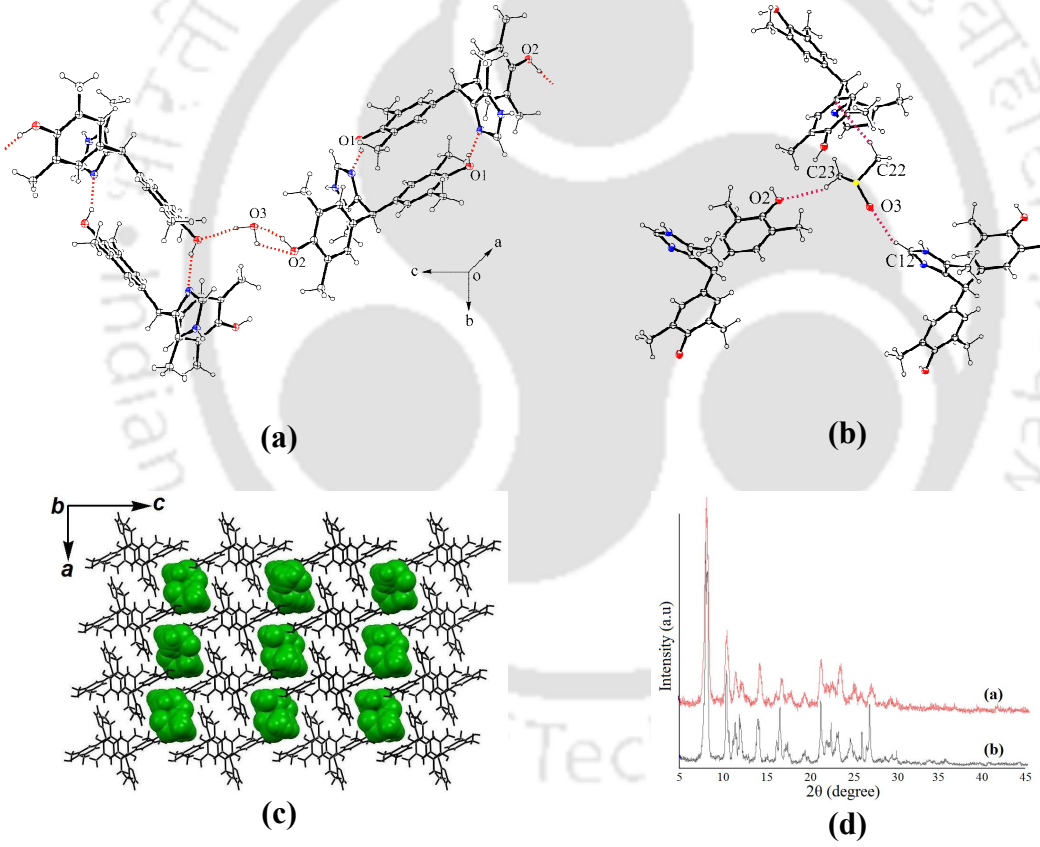

Figure 4.10: (a) Water assisted assembly of dimeric unit of **4.1** in DMSO solvate **(4.1d)** showing the O-H···O and N-H···O interactions, **(b)** the C-H···O and C-H···π interactions in **4.1d**, **(c)** Packing diagram of the DMSO solvate **4.1d** and **(d)** Comparison of the PXRD of DMSO solvate **4.1d** after heating up to 200°C and the polymorph **4.1b**.

The formation of water assisted assemblies in **4.1d** leads to a modified host system having a channel-like structure along the crystallographic b-axis (Figure **4.10c**). The solvent molecules are embedded in the channels through C-H···O and C-H···π interactions (Figure **4.10b**). Generally, dimethylsulphoxide molecules involve in various weak interactions when it forms host-guest assemblies with various hosts.[11] Furthermore, the DMSO molecules can be disordered depending on the environments.[16a,f] However, in the present case, each DMSO molecule is flanked by three molecules of **4.1** and has different interactions from three different directions and hence no disorder is observed. When **4.1d** was heated to 200 °C to expel the DMSO molecules, it transforms to the porous polymorph **4.1b** and it is confirmed through PXRD (Figure **4.10d**).

Table 4.1: Some selected hydrogen parameters of **4.1a**-**4.1d**:

Compd no.	D-H···A	$d_{D\text{-}H(Å)}$	$d_{H\cdots A(Å)}$	$d_{D\cdots A(Å)}$	∠D-H···A(°)
4.1a	O(1)-H···O (2) [x, 3/2-y,1/2+z]	0.82	1.95	2.705 (2)	152
	O(2)-H···N(2) [1-x, 2-y, -z]	0.82	1.91	2.669(3)	154
4.1b	O(1)-H···O (2) [1/2+x, 1/2-y,1/2+z]	0.82	1.89	2.680(8)	161
	O(2)-H···N(2) [-x, 1-y, 1-z]	0.82	1.84	2.617(7)	157
4.1c	O(1)-H···N(2) [1-x,-y,-z]	0.82	1.86	2.6241	155
	O(2)-H···O(1) [-1/2+x,1/2-y,-1/2+z]	0.82	1.92	2.6750	153
4.1d	O(1)-H···N(2) [1-x,1-y,-z]	0.86(6)	1.87(6)	2.721(5)	169(5)
	O(2)-H···O(4)	0.87(6)	1.91(4)	2.702(6)	151(5)
	O(4)-H···O(2)	0.84(5)	2.24(13)	2.702(6)	114(10)
	O(4)-H···O(1) [x,1/2-y,1/2+z]	0.87(3)	2.04(4)	2.889(6)	164(4)
	C(15)-H···O(1) [1-x,1-y,-z]	0.93	2.57	3.490(5)	172
4.1e	O(1) -H(1)···O(6) [2-x,1-y,1-z]	0.82	2.11	2.899(4)	162
	N(1) -H(1M)···O(3) [-1+x,1+y,z]	0.91(5)	2.32(5)	3.146(5)	151(4)
	N(1) -H(1M)···O(6) [-1+x,1+y,z]	0.91(5)	2.37(4)	3.102(4)	137(4)
	O(2) -H(2)···O(3) [1-x,-y,-z]	0.82	2.54	3.219(5)	141
	N(2) -H(2M)···O(1) [1-x,1-y,1-z]	1.00(4)	2.02(4)	2.914(3)	149(3)
4.1f	O(1) -H(1)···F(3) [-x,-y,1-z]	0.82	2.21	2.931(2)	147
	N(1) -H(1M)···F(1) [1/2-x,1/2-y,1-z]	0.88(3)	2.43(3)	2.946(3)	118(2)
	N(1) -H(1M)···F(2) [1/2-x,1/2-y,1-z]	0.88(3)	1.94(3)	2.827(3)	177(2)
	N(1) -H(1M)···F(3) [1/2+x,1/2-y,-1/2+z]	0.88(3)	2.49(3)	2.997(3)	117(2)
	O(2) -H(2)···F(1) [x,1-y,-1/2+z]	0.82	2.09	2.791(2)	144
	N(2) -H(2M) ···F(2) [1/2-x,1/2+y,3/2-z]	0.87(3)	2.42(3)	3.083(3)	134(2)
	N(2) -H(2M) ···F(3) [1/2-x,1/2+y,3/2-z]	0.87(3)	2.29(3)	2.857(3)	123(3)
	N(2) -H(2M) ···O(1) [1/2-x,1/2-y,1-z]	0.87(3)	2.26(3)	2.961(3)	138(2)

The acetone solution of polymorph **4.1b** is yellow in color and it shows absorption at 425 nm with a feeble absorption at 605 nm. A solution of **4.1b** in DMSO is intense blue (Figure **4.11a**) and absorbs at 605 nm. Based on this, we carried out a visible spectroscopic titration by adding DMSO to a solution of **4.1b** in acetone. It was found

that as the amount of DMSO was increased, there was an increase in the absorption at 605 nm at the cost of the absorption at 425 nm (Figure **4.11b**). The absorption changes passed through an isosbestic point at 570 nm. This suggested 1:1 inter-conversion between the two states. Although acetone and DMSO have structural similarity, they have different polarity indices. Acetone has a polarity index[17a] of 5.1, whereas DMSO has a polarity index of 7.2. Hence, **4.1b** strongly binds to DMSO and this causes the difference in the electronic properties in solution. We have taken the visible spectra of **4.1b** in DMSO by adding acetone to it. In this experiment, no

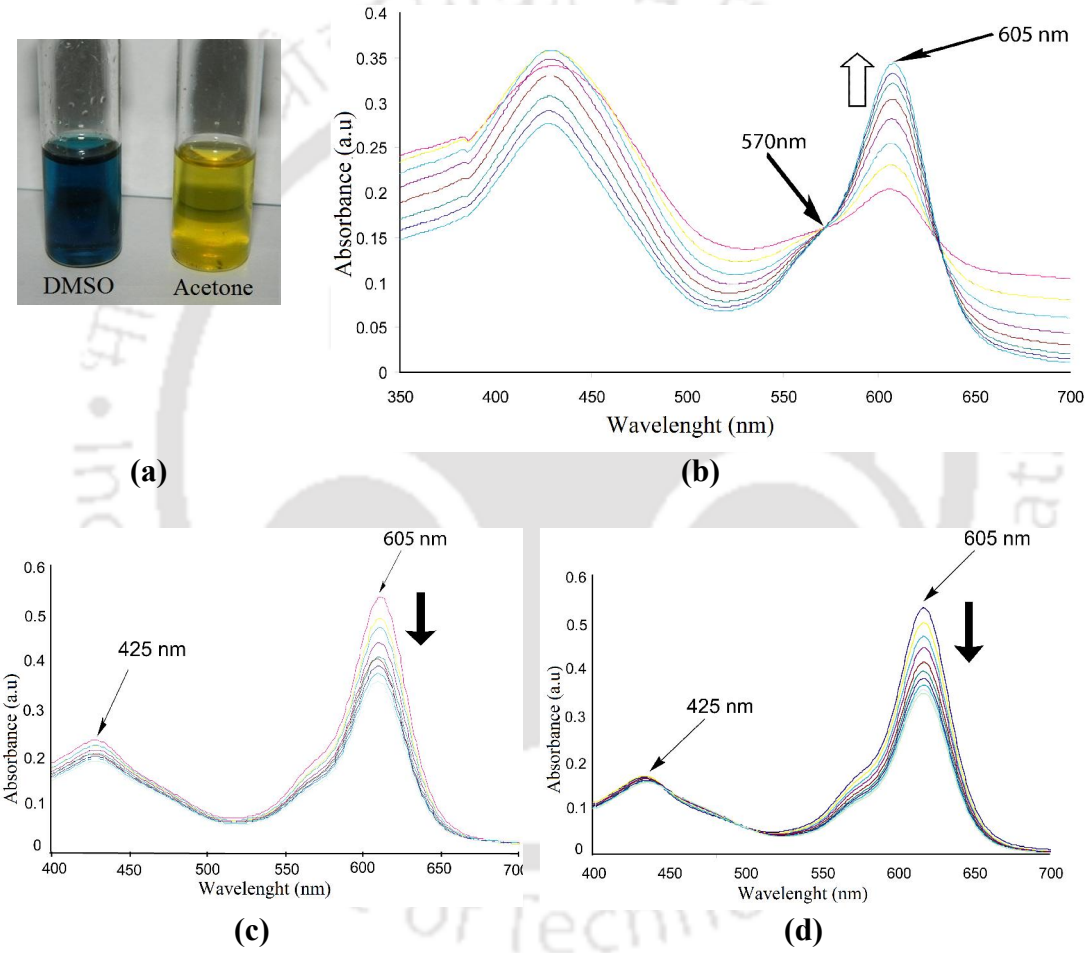

Figure 4.11: **(a)** Solution of **4.1b** in DMSO and acetone, **(b)** Visible spectra of polymorph **4.1b** in acetone (1.2×10^{-2} M, 2 mL) on addition of different aliquots of DMSO (50 µL in each aliquot), **(c)** UV-visible spectra of DMSO solvate (2×10^{-2}) with 50 µL incremental addition of acetone and **(d)** The UV spectra of the compound in DMSO (2×10^{-2}) with 50 µL incremental addition of DMSO.

changes other than a decrease in the intensity of the absorption at 605 nm and 425 nm were observed (Figure **4.11c**) due to the dilution effect. The dilution effect is confirmed by recording the UV-visible spectra of **4.1b** in a DMSO solution followed by the addition of DMSO in different aliquots (Figure **4.11d**). Such addition resulted in identical spectra, as observed in the titration of a solution of **4.1b** in DMSO with acetone. The ability of DMSO to change color is due to its ability to bind strongly with labile hydrogen and has been reported in the literature.[17b] There is also difference in the ^{1}H-NMR of **4.1** in DMSO-d_6 and Acetone-d_6. The hydroxy protons of *bis*-phenol **4.1** appear at 8.0 ppm in DMSO-d_6 whereas it appears at 4.5 ppm in acetone-d_6 (Figure **4.12**). There are many examples of molecular recognition by phenolic compounds. [18] *Bis*-phenol A and its derivatives form charge transfer complexes with *p*-benzoquinone and it was used as visible indicator for various *bis*-phenol derivatives as different *bis*-phenols give different color with *p*-benzoquinone in solid state.[19] Moreover, phenolic compounds are also used towards the recognition of anions. Boron based *bis*-phenolates were used for the colorimetric detection of fluoride and chloride ions.[20] Quinoline based and amino containing phenolic compounds were used for the selective detection of biologically important zinc ions.[21] Apart from these various phenolic compounds are used for the selective detection of biologically important anions such as phosphate, acetate, fluoride and chloride etc.

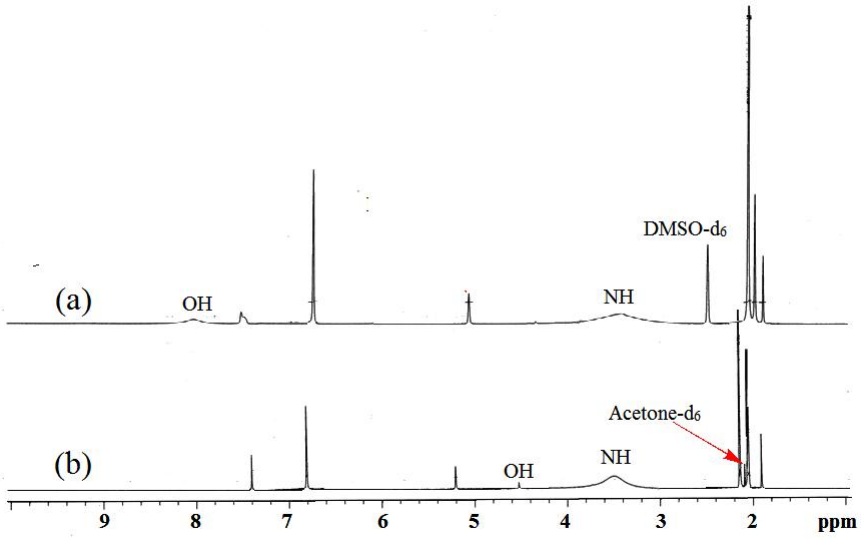

Figure 4.12: Overlay of ^{1}H-NMR of *bis*-phenol **4.1** in **(a)** DMSO-d_6 and **(b)** acetone-d_6 (400 MHz).

4.2.2 Anion assisted assemblies of *Bis*-phenol 4.1:

The perchlorate (**4.1e**) and the hexafluorosilicate **(4.1f)** salts of **4.1** crystallises in 1:1 ratio. In both the salt **4.1e** and **4.1f** the host cations form dimmeric units through two N-H···O [N(2)-H···O(1) with $d_{D\cdots A}$= 2.914 Å, ∠D-H···A= 149° and $d_{D\cdots A}$= 2.961 Å, ∠D-H···A= 138° respectively for **4.1e** and **4.1f**] (Figure **4.13a,b**) interactions instead of O-H···N interactions as observed in case of the polymorphs and the solvates of **4.1**. These dimmeric units further assemble with the ClO_4 and SiF_6 anions through various weak interactions to give 3D network structures. In case of the **4.1f**, the 3D assembly have channel like structure running along the crystallographic c-axis where the channels are occupied by the SiF_6 anions (Figure **4.13d**).

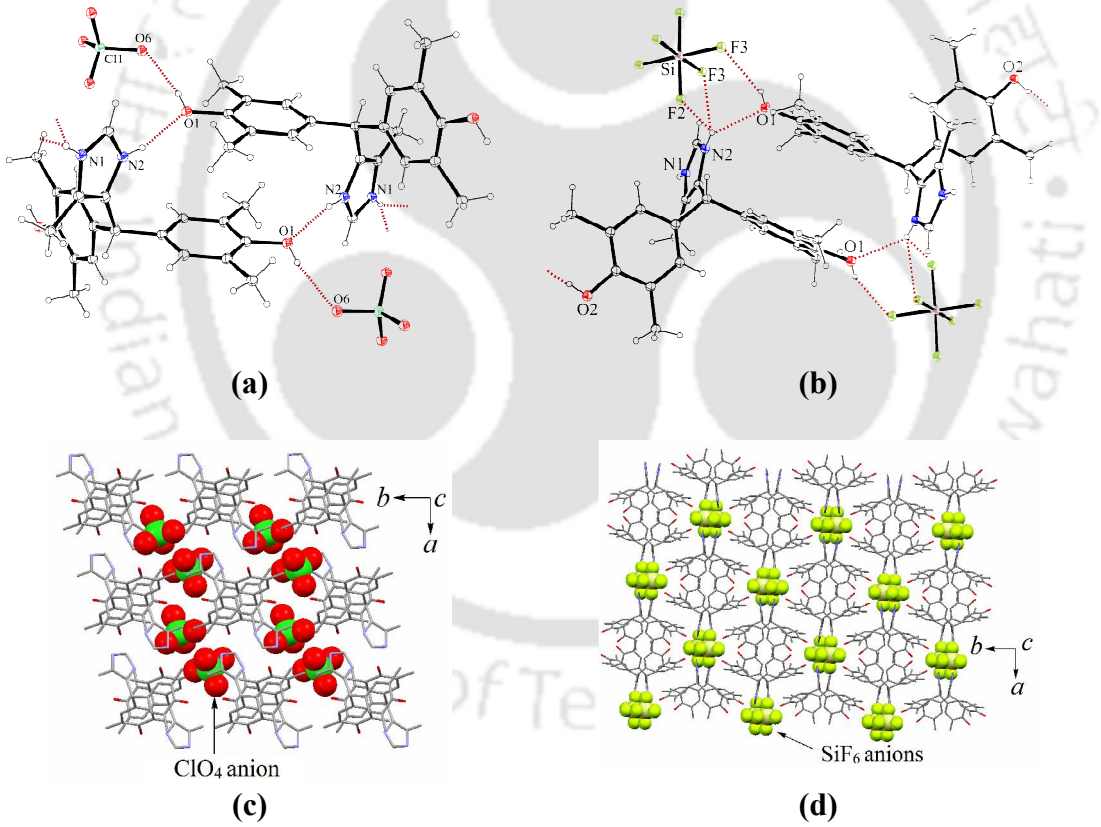

Figure 4.13: The formation of dimmeric unit in **(a)** Perchlorate salt **4.1e** and **(b)** hexafluorosilicate salt **4.1f**, Packing diagram of the **(c)** nitrate salt **4.1e** and **(d)** hexafluorosilicate salt **4.1f.**

However, we did not observe suitable single crystal of the salts of **4.1** with other anions such as sulphate, nitrate and tetrafluoroborate which deterred us from further studies.

4.3 Supramolecular assemblies of *Bis*-phenol 4.2:

On the other hand, in case of the imidazole *bis*-phenol **4.2** we did not observed any polymorphism**.** But, we were able to crystallize the solvent free form of **4.2 (4.2a)** from dimethylsulfoxide and as 1:1 methanol solvate **(4.2b)** from methanol**.** Moreover, we have prepared a series of imidazolium *bis*-phenol salts of *bis*-phenol **4.2** with dicarboxylic acid such as maleic and fumeric acid; and with acids such as perchloric acid, sulphuric acid, nitric acid and $NaBF_4$. The whole results are summarized in the Scheme **4.2**.

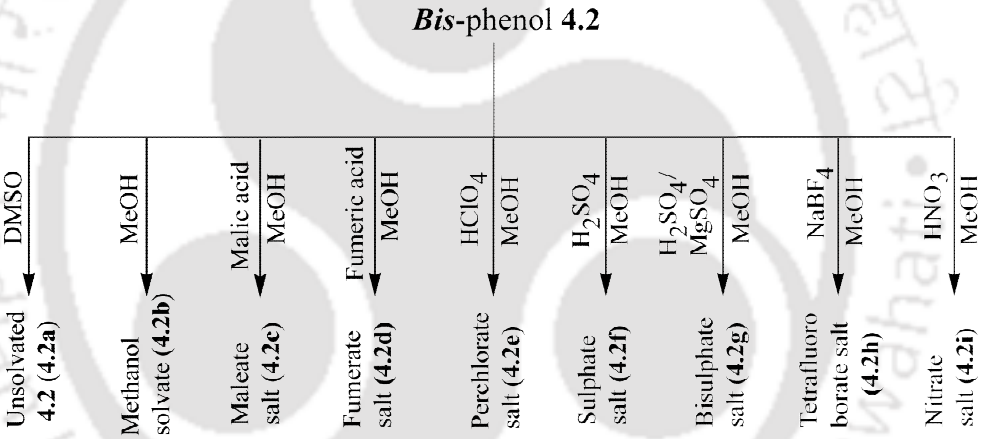

Scheme 4.2: The solvates and salts of *bis*-phenol **4.2**.

4.3.1 Solvates of *bis*-phenol 4.2

The anhydrous form **4.2a** crystallizes in monoclinic space group $P2_1/n$ and has moderately strong hydrogen bonded structure in the form of self-assembly. There are two moderate H-bonds, viz., N(1)-H···N(2) [∠D-H···A=164° and $d_{D\cdots A}$=2.991(3) Å] and O(2)-H···N(2) [∠D-H···A=145° and $d_{D\cdots A}$=2.816(3) Å]. The two hydroxy groups of each *bis*-phenol molecule form strong intramolecular H-bonds with ∠D-H···A= 174° and $d_{D\cdots A}$=2.720(3) Å. The combination of these H-bonds leads to the formation of two different types of cyclic H-bonding motifs as shown in Figure **4.14a** and **4.14b**.

Apart from these H-bonds, there are other interactions such as C-H···O and C-H···π interactions which also contribute to the stability of the system.

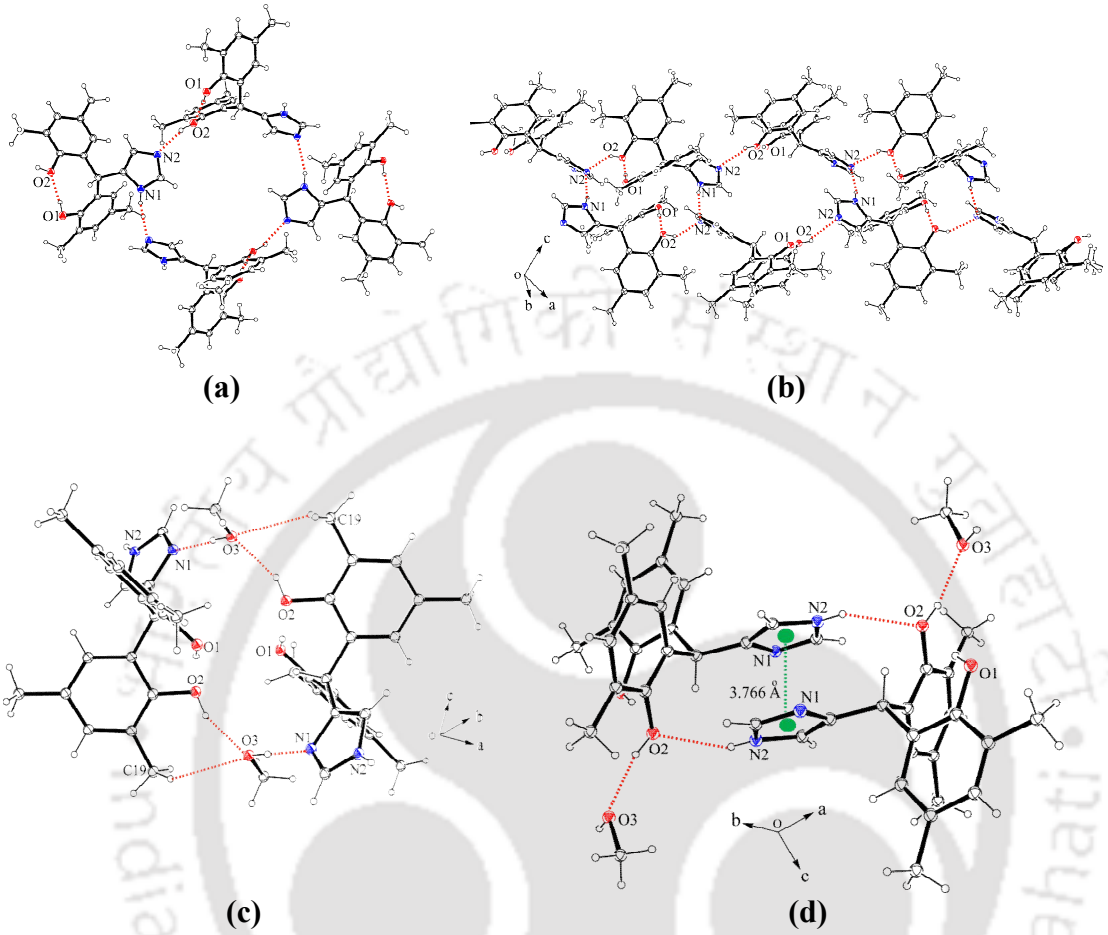

Figure 4.14: (a) Tetrameric assembly of **4.2a** through O-H···N and N-H···N interactions, **(b)** Different types of cyclic H-bonding motifs in **4.2a**, **(c)** and **(d)** Different types of hydrogen bonding and π···π interactions in the methanol solvate **4.2b**.

The methanol solvate **4.2b** crystallizes in triclinic space group *P-1* and its asymmetric unit contains a methanol molecule along with a molecule of *bis*-phenol **4.2**. The N-H group of the imidazole ring involves in N-H···**O** interaction [N(2)-H···O(2), $d_{D\cdots A}$, 3.071 Å and ∠D-H···A, 144°] with one of the hydroxy group of the host molecule forming dimeric units of the *bis*-phenol **4.2**. These dimeric units are further stabilize by the π···π interactions among the imidazole ring where the centroid-centroid separation is found to be 3.766 Å (Figure **4.14d**). Methanol molecules acts as a bridge between such dimeric units of *bis*-phenol through O-H···O interaction [O(2)-

H···O(3), $d_{D\cdots A}$=2.664 Å and ∠D-H···A=155°] and O-H···N [O(3)-H···N(1), $d_{D\cdots A}$, 2.748 Å and ∠D-H···A=177°] interactions leading to infinite 2D sheet-like structure parallel to the crystallographic *ab*-plane.

Table **4.2**: Some selected hydrogen parameters of **4.2a-4.2d:**

Compd. no.	D-H···A	$d_{D\text{-}H(Å)}$	$d_{H\cdots A(Å)}$	$d_{D\cdots A(Å)}$	∠D-H···A(°)
4.2a	O(1)-H(1)···O(2)	0.82	1.90	2.720(3)	174
	N(1)-H(1A)···N(2) [-1/2−x, 1/2 +y, 1/2 -z]	0.85(3)	2.17(3)	2.991(3)	164(3)
	O(2)-H(2)···N(2) [1/2 +x, 1/2-y, 1/2 + z]	0.82	2.11	2.816(3)	145
	C(9)-H(9)···O(1)	0.98	2.48	2.905(3)	106
4.2b	O(1)-H(1)···O(2)	0.82	2.32	3.1352(18)	174
	O(2)-H(2)···O(3) [1-x,1-y, -z]	0. 82	1.90	2.664(2)	155
	N(2)-H(2A)···O(1) [-1+x, y, z]	0.86	2.53	3.123(2)	126
	N(2)-H(2A)···O(2) [-x,1-y,-z]	0.86	2.33	3.071(2)	144
	O(3)-H(3A)···N(1)	0.82	1.93	2.748(2)	177
4.2c	O(1)-H(1)···O(7) [x, 3/2 -y, -1/2 +z]	0.89(3)	1.78(3)	2.669(2)	172(3)
	N(1)-H(1A)···O(3) [-x,1-y,-z]	0.86	1.91	2.750(2)	166
	O(2)-H(2)···O(1)	0.82	1.98	2.789(2)	167
	N(2)-H(2A)···O(4) [x, 3/2 -y, 1/2 + z]	0.86	1.95	2.772(2)	158
	O(5)-H(5A)···O(3)	0.82	1.61	2.425(2)	170
	O(7)-H(7E)···O(5) [-x, 1/2 + y, 1/2 -z]	0.86(3)	2.07(3)	2.893(2)	160(3)
	O(7)-H(7F)···O(6)	0.89(3)	1.93(3)	2.812(2)	170(3)
4.2d	O(1)-H(1)···O(3) [1-x,1-y,1-z]	0.82	1.95	2.6950(17)	150
	N(1)-H(1A)···O(4) [-x,1-y,1-z]	0.96(3)	1.75(3)	2.6712(18)	159(2)
	O(2)−H(2)···O(1)	0.82	1.98	2.7953(18)	173
	N(2)-H(2A)···O(3) [-x, -y,1-z]	0.90(3)	1.78(3)	2.6721(17)	169(2)

4.3.2 Anion assisted assemblies of *Bis*-phenol 4.2:

When the *bis*-phenol **4.2** was treated with maleic acid (H_2mal) it formed mono hydrated salt, namely, **4.2H·Hmal·H_2O (4.2c)**. The salt **4.2c** crystallizes in a monoclinic space group $P2_1/c$. The crystallographic asymmetric unit consists of the **4.2**H cation, a maleate anion and a water molecule of crystallization. Strong intramolecular H-bonding (O-H···O) is observed within the maleate ion. The maleate anion generally forms an intramolecular hydrogen bonded structure.[23] Such anions participate in hydrogen bond formation with host. The water of interest in the structure acts as a bridge between the host cation and maleate anion on one side whereas the other side of the maleate anion directly forms hydrogen bond to the host cation (Figure **4.15a**). Moreover, the two hydroxy groups of the host cation **(4.2H)** also are involved in intramolecular O(2)-H···O(1) [$d_{D\cdots A}$=2.789 Å and ∠D-H···A=167°] hydrogen bonding. The water molecule is coordinated to one hydroxy

group of the host molecule and two Hmal anions through O-H···O interactions where the Hmal anion forms water bridged zigzag polymeric chain (Figure **4.15b**).

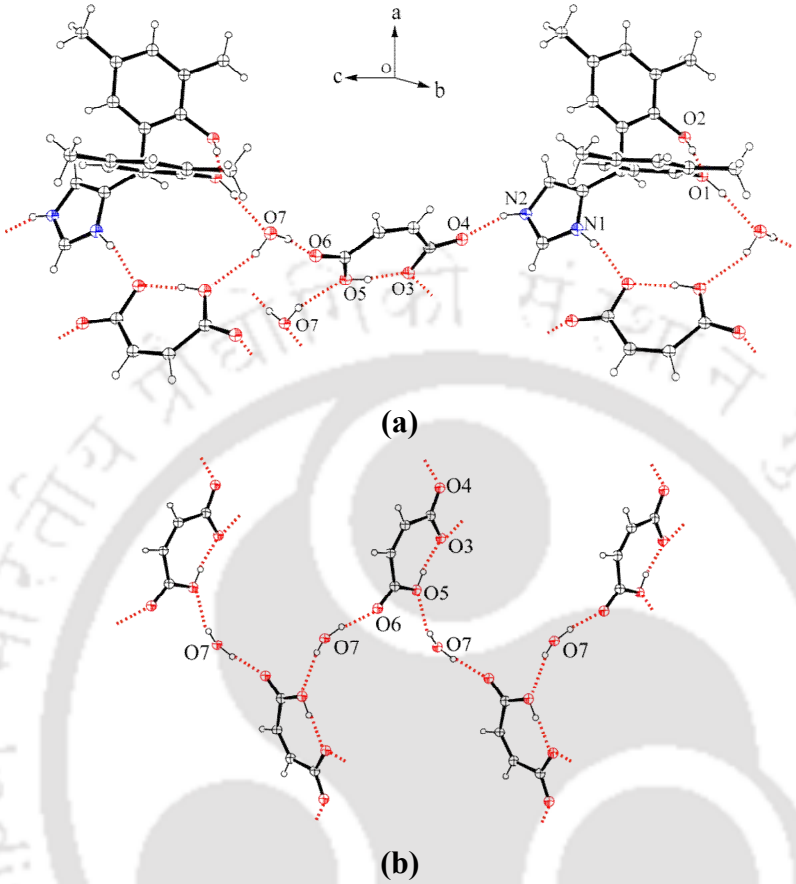

Figure 4.15: **(a)** N-H···O and O-H···O interactions in the salt **4.2c**, **(b)** Formation of zig-zag 1D chain of maleate mono anion and water through H-bonding in **4.2c**.

It is shown that the maleic acid on reaction with **4.2** forms mono-deprotonated salt, whereas its *trans* counterpart, fumeric acid forms a di-deprotonated salt with the cation of the *bis*-phenol **4.2**. For charge balance, two molecules of imidazolinium *bis*-phenol cation accept one fumerate anion to give **4.2H·0.5 fum (4.2d)**. The pK_{a2} of maleic acid is 6.62 whereas it is 4.44 for fumeric acid and these differences are due to geometry of the two acids. The former acid adopts a strong intramolecular hydrogen bonded structure upon first deprotonation. The salt **4.2d** crystallizes in triclinic space group *P-1* and the crystallographic asymmetric unit contains one host cation **4.2H**, and the half of the fumerate anion. The host molecules form dimers with two fumerate ions through N-H(imidazole)···O^- and O-H···O interactions (Figure **4.16a**). The intramolecular O2-H···O1 interaction in the host molecule is also observed as in the

earlier cases. Each fumerate ion interacts with six host molecules through N-H(imidazole)···O^- and O-H···O interactions, resulting in the encapsulation of the

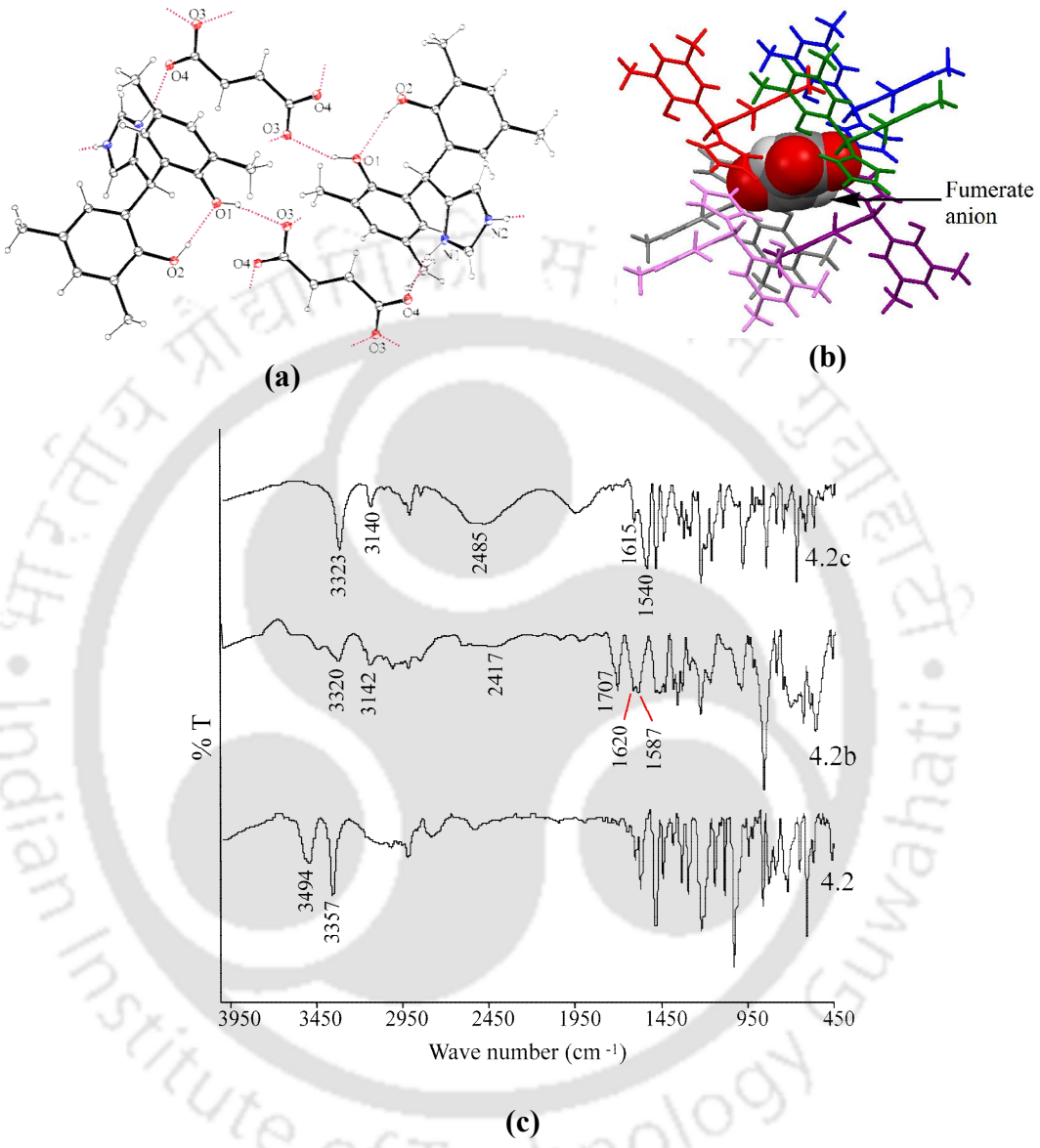

Figure 4.16: **(a)** O-H···O and N-H···O interactions in fumerate salt **4.2d, (b)** Encapsulation of fumerate ions in the hexameric assembly of the host cations in **4.2d, (c)** Comparison of the FT-IR of **4.2, 4.2c** and **4.2d.**

anion in the hexameric cavity formed by the host cation (Figure **4.16b**). From the FT-IR of the **4.2c** it is seen that the C=O stretching frequency for the carboxylic acid group of maleic acid appears at 1707 cm^{-1}. However, this peak disappears in case of

the fumarate salt which indicates the di-deprotonation of the fumeric acid in **4.2d**. In the FT-IR spectra of **4.2c** and **4.2d,** the peaks at 2417 cm^{-1} and 2485 cm^{-1} appears due to the stretching of the N^{+}-H bond (Figure **4.16c**).

The perchlorate salt of **4.2H·ClO$_4$ (4.2e)** crystallizes in a monoclinic space group $P2_1/c$, and its asymmetric unit contains one protonated host molecule and a perchlorate anion. Both the N-H and the N^{+}-H of the imidazole ring act as H-bond donor and engage in hydrogen bonding with the perchlorate ion forming a ladder like

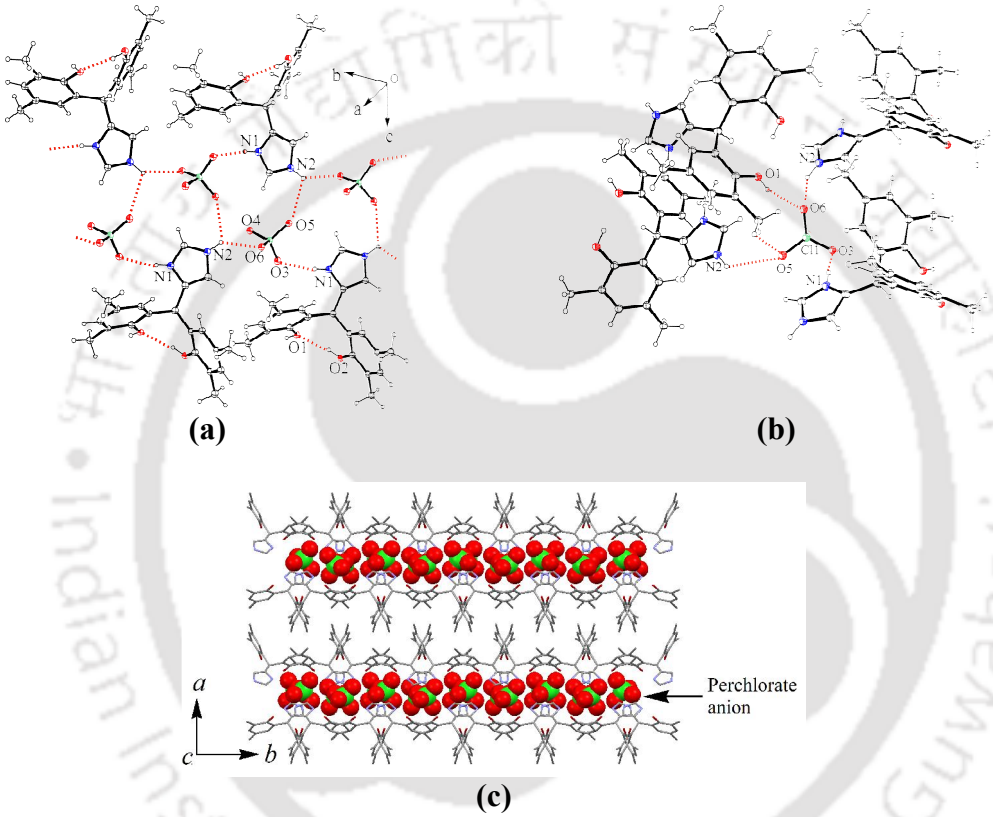

Figure 4.17: **(a)** N-H···O and O-H···O interactions in perchlorate salt **4.2e, (b)** Interaction of each perchlorate anions with four host cation through N-H···O and O-H···O interactions. **(c)** Packing pattern of the perchlorate salt **4.2e.**

H-bonded network when viewed along the a-axis (Figure **4.17a**). These types of supramolecular features were found in the crystal structure of theophylline-perchlorate salt.[24] As in the earlier cases, the hydroxy groups of the host cation involve in intramolecular H-bonds. Over and above these, one of the hydroxy groups participating in the intramolecular hydrogen bond has a hydrogen atom free, which acts as H-bond donor to the oxygen atom of the perchlorate anion. Each perchlorate

ion interacts with four host cations through N-H···O, O-H···O and C-H···O interactions (Figure **4.17b**) and finally the salt forms two discrete sheets each of which intercalate the perchlorate anions (Figure **4.17c**).

The sulfate salt **4.2H·0.5SO$_4$ (4.2f)** forms in 1: 0.5 cation-anion ratio and crystallize in R3$_2$ space group and the crystallographic asymmetric unit contains one host cation and half of a sulphate anion. One of the hydroxy groups of the host cation involves in intermolecular H-bond (both as donor and acceptor) with the same hydroxy group of two neighbouring molecules resulting in the formation of a trimeric assembly through $R_3^3(6)$-types of cyclic H-bonding as shown in the Figure **4.18a**. These types of two trimeric assemblies connected to each other via O3 of three sulphate anion through O-H···O and N-H···O interactions leading to the formation of circular assemblies when viewed along the crystallographic c-axis (Figure **4.18b**). These circular assemblies further connected to each other by O4 of sulfate through N2-H···O4 interactions to form 2D sheet.

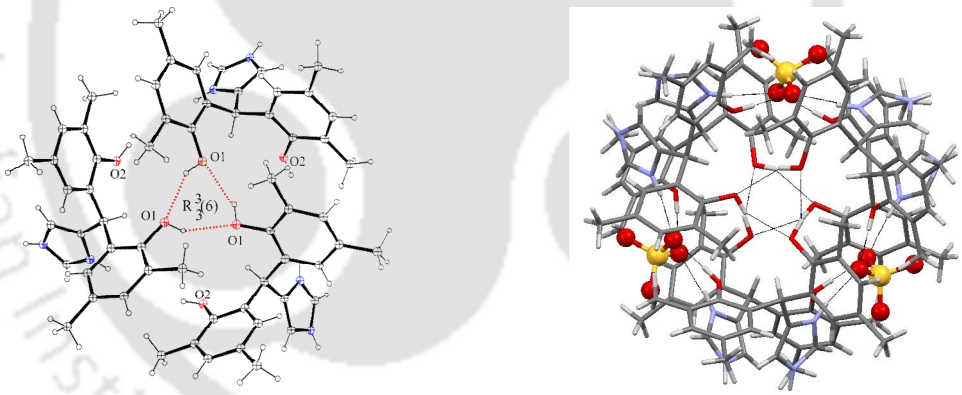

(a) **(b)**

Figure 4.18: **(a)** Trimeric assembly of the host cation through $R_3^3(6)$ types of O-H···O interactions in the sulphate salt **4.2f**, **(b)** Interaction of two trimeric assemblies through sulfate anion leading to a circular assembly.

A bisulphate salt of *bis*-phenol **4.2** was formed serendipitously. When magnesium sulfate hexahydrate was treated with *bis*-phenol **4.2** in aqueous methanol, it led to formation of **4.2H·HSO$_4^-$ (4.2g)**. The formation of the bisulphate salt is attributed to hydrolytic disproportionation of magnesium sulfate in methanol as shown in Equation 1.

$$SO_4^{2-} + H_2SO_4 \longrightarrow 2HSO_4^- \quad \text{Equation 1}$$

The 1:1 bisulphate salt **4.2g** crystallizes in the *P-1* space group and the crystallographic asymmetric unit contains one **4.2H** cation and bisulphate anion. The HSO_4^- anions form a dimeric structure through $R_2^2(8)$ types of cyclic H-bonds, and these dimers are held in the assembly of the protonated host molecules of **4.2** through O-H···O and N-H···O interactions involving the hydroxy and the N-H groups of the host molecule (Figure **4.19a**). There are no strong intermolecular interactions among the host cations, but the two hydroxy groups of the host cation are involved in intramolecular H-bond interactions. Hydrogen sulfate salts have found applications in various devices such as H_2 and H_2O sensors, fuel and stream cells, and high-energy-density batteries.[25] Braga et al. had reported the crystal structure of the stabilized hydrogen sulfate adducts of crown ethers.[26] Hydrogen sulfate salts are of interest in supramolecular aspects and crystal engineering because of its analogy to biologically relevant biphosphate anion and the presence of H-bonding between the ions for self-association.[27] Apart from these, the stabilization of the bisulphate anion along with the sulfate anion by 3,5-diphenylpyrazole has been reported.[28]

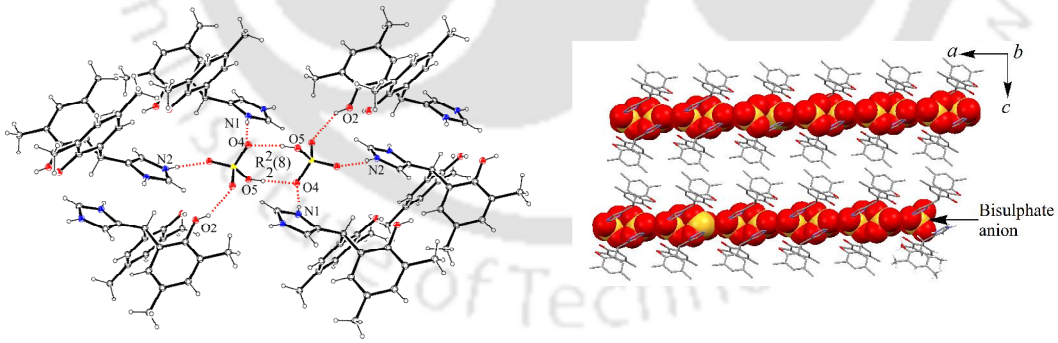

(a) **(b)**

Figure 4.19: **(a)** Formation of $R_2^2(6)$ types of cyclic H-bonding by the bisulphate anion in the bisulphate salt **4.2g**, **(b)** Packing pattern of the bisulphate salt **4.2g.**

The reaction of sodium tetrafluoroborate in wet methanol forms 1:1 salt of **4.2**, **4.2H·BF_4·H_2O (4.2h)** which crystallizes in a triclinic space group *P-1*. The

crystallographic asymmetric unit contains the host cation **4.2H**, tetrafluoroborate anion, and water molecule of crystallization. Formation of such salts from sodium tetrafluoroborate may be considered as unique, as it forms through a hydrolytic reaction between sodium tetrafluoroborate with water leading to tetrafluoroboric acid. In such process the counter base has to be sodium hydroxide. The stabilization of

Table 4.3: Some selected hydrogen parameters of **4.2e-4.2i**

Compd. no.	D-H···A	$d_{D-H(Å)}$	$d_{H\cdots A(Å)}$	$d_{D\cdots A(Å)}$	∠D-H···A(°)
4.2e	O(1)-H(1)···O(6)	0.74(6)	2.07(6)	2.719(7)	146(5)
	N(1)-H(1A)···O(3) [x, 3/2 -y, -1/2 +z]	0.79(6)	2.14(6)	2.895(6)	161(5)
	O(2)-H(2)···O(1)	0.82	2.01	2.817(5)	170
	N(2)-H(2A)···O(6) [x, ½-y, -1/2 +z]	0.93(7)	2.23(7)	2.988(6)	138(6)
4.2f	O(1)-H(1)···O(1) [-y, x-y, z]	0.82	2.15	2.864(8)	146
	N(1)-H(1A)···O(3) [-y, x-y, z]	0.86	1.91	2.759(8)	171
	O(2)-H(2)···O(3)	0.82	2.15	2.826(7)	140
	N(2)-H(2A)···O(4) [1-x,1-x+y, -z]	0.86	1.86	2.719(8)	176
4.2g	O(1)-H(1)···O(2)	0.82	1.99	2.800(2)	169
	N(1)-H(1A)···O(4) [x, -1+y,1+z]	0.83(2)	2.07(2)	2.869(2)	162.1(18)
	O(2)-H(2)···O(6) [-x,1-y,1-z]	0.82	2.07	2.818(2)	151
	N(2)-H(2A)···O(3) [1 +x, -1+y,1+z]	0.86(3)	2.05(2)	2.888(2)	165.6(18)
	O(5)-H(5A)···O(4) [1-x,1-y, -z]	0.82	1.93	2.738(2)	169
4.2h	O(1)-H(1)···F(2) [1 +x,1+y, z]	0.82	2.11	2.832(3)	146
	N(1)-H(1A)···O(3) [1-x,1-y,1-z]	0.86(4)	1.89(4)	2.729(5)	166(3)
	O(2)-H(2)···O(1)	0.82	2.05	2.853(3)	166
	N(2)-H(2A)···F(4)	0.91(3)	2.21(3)	2.886(5)	131(3)
	N(2)-H(2A)···O(2) [1-x,1-y,1-z]	0.91(3)	2.18(4)	2.939(3)	140(3)
	O(3)-H(3N)···F(1) [1-x, -y,1-z]	0.82(9)	2.32(10)	2.997(5)	140(8)
4.2i	O(1)-H(1)···O(3)	0.85(13)	1.93(12)	2.762(7)	167(12)
	O(1)-H(1)···O(5)	0.85(13)	2.36(14)	2.999(8)	133(9)
	N(1)-H(1A)···O(5) [−1+x, y, z]	0.86	1.98	2.765(6)	152
	O(2)-H(2)··· O(1)	0.82	1.98	2.791(6)	170
	N(2)-H(2A)···O(3) [x, y,1+z]	1.00(7)	1.84(8)	2.803(6)	162(7)
	N(2)-H(2A)···O(4) [x, y,1+z]	1.00(7)	2.46(8)	3.249(8)	135(8)

tetrafluoroborate anion by quinoline based receptor is already reported by our group, which was obtained by similar hydrolytic reaction of sodium tetrafluoroborate with the receptor in wet DMF.[29] In the salt **4.2h**, the water molecule of crystallization acts as a donor toward the tetrafluoroborate anion and acceptor toward N-H of the imidazole ring. The protonated N^+-H of the imidazole ring is involved in bifurcated H-bonding with one hydroxy group of the host cation and to the tetrafluoroborate anion. The host cation forms a dimer through N(2)-H···O(2) hydrogen bonding interactions (Figure **4.20**). These dimers are connected to each other via tetrafluoroborate anions through N-H···O, O-H···F, and N-H···F interactions (Table **4.3**). Such interactions lead to the formation of sheet-like structures. These sheet-like

structures intercalate tetrafluoroborate anions and they are held together by C-H···π interaction.

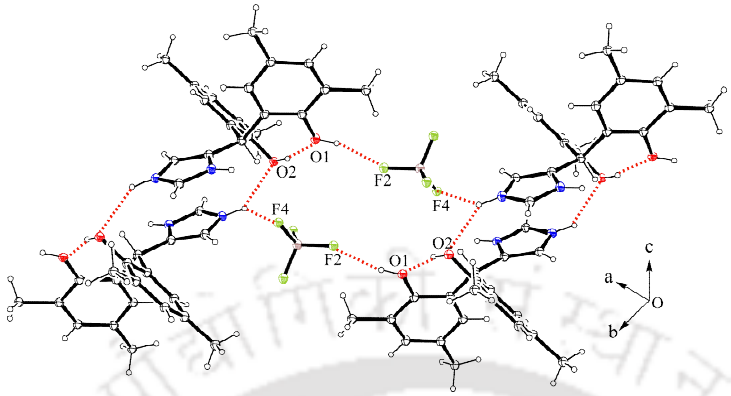

Figure 4.20: N-H···O, O-H···O and O-H···F interactions in the tetrafluoroborate salt **4.2h**.

The nitrate salt **4.2H·NO_3 (4.2i)** is a 1:1 electrolyte and crystallizes in a monoclinic space group $P2_1/c$. The crystallographic asymmetric unit of **4.2i** contains one host cation and a nitrate anion. Both the N^+-H and N-H bonds of the imidazole act as H-bond donor toward the nitrate anion (Figure **4.21a**). In this case also, two hydroxy groups of the host cation involves in intramolecular H-bonding. One of the hydroxy group acts as H-bond donor to the nitrate anion. This assembly forms a sheet parallel to the ac-plane which incorporates the nitrate anions as shown in the Figure **4.21b**.

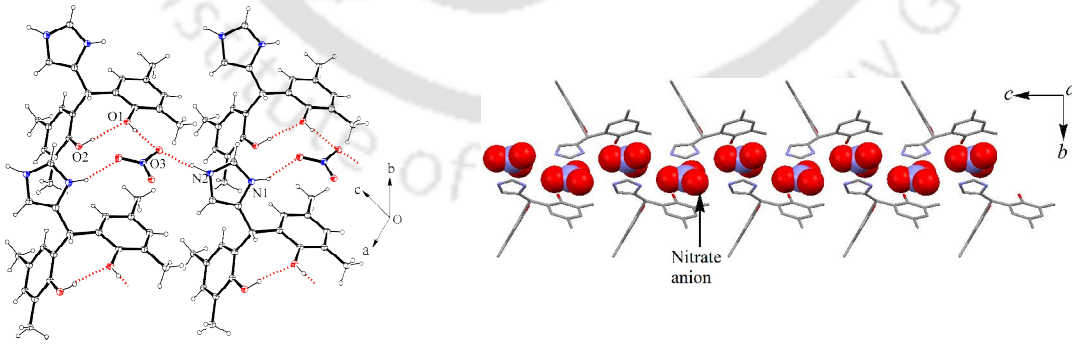

(a) **(b)**

Figure 4.21: **(a)** N^+-H···O, N-H···O, and O-H···O interactions in nitrate salt **4.2i**, **(b)** Packing pattern of the nitrate salt **4.2i**.

We have studied the preferential crystallization process of the salts **4.2e-4.2i** by adding the salts to another acid solution. We observed that weak perchlorate anion or nitrate anion can be successfully replaced by sulfate anion from their respective salt. However, the reverse process, namely, the sulfate salt does not lead to formation of perchlorate or nitrate salt on treatment with perchloric acid and nitric acid, respectively. Because of the lack of distinguishable and characteristic absorption maxima in the UV region, we have not carried out the competitive binding of anion. The formation of salts in case of **4.2c-4.2i** is also confirmed by ^{1}H-NMR spectra (Figure **4.22**), as the protons on the imidazole ring shifted to a higher δ-value on interaction with anions. For example, the methine proton of *bis*-phenol shows down field shift in salts **4.2e**, **4.2f**, **4.2g** and **4.2i** compared to the parent *bis*-phenol molecule. Moreover, the protons of the two phenol rings and the imidazole ring are also significantly affected on interaction with the anions.

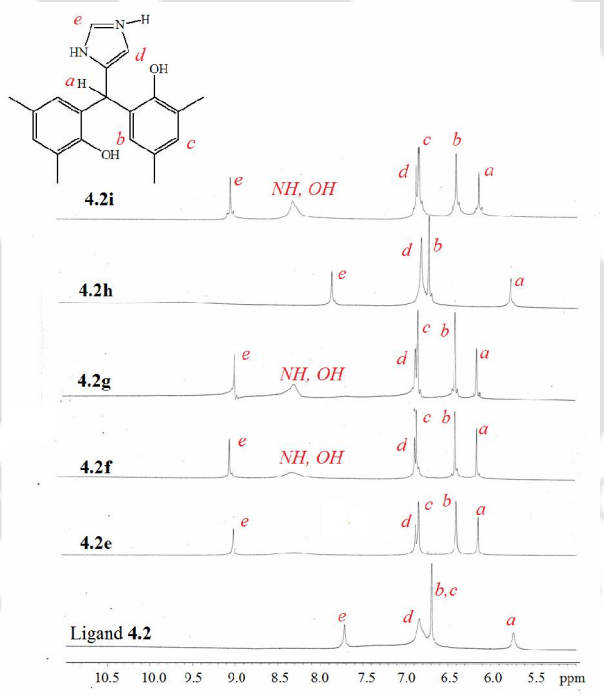

Figure 4.22: The overlaid ^{1}H-NMR (DMSO-d_4, 400 MHz) of **4.2** and its salts **4.2e-4.2i**

4.4 Thermogravimetric Analysis:

The differential scanning calorimetry (DSC) of crystalline solids is generally useful to understand different thermal properties,[30] such as phase transitions and reversibility in the release of guest molecules. The DSC plots of all the polymorphs and solvates show a flat baseline with sharp peaks, which is consistent of the high purity of the

bulk materials. From the DSC, it is seen that for the polymorph **4.1a** endothermic peaks appear at 234.4°C and 238.4 °C, whereas for the polymorph **4.1b** these appear at 230.0°C and 243.7°C (Figure **4.23**). From the TG analysis it was seen that **4.1c** loses the acetone molecules in the temperature range of 50-95 °C (theoretical weight loss 7.8%, experimental weight loss 7.74%, Figure **4.25a**). The solvate **4.1d** loses

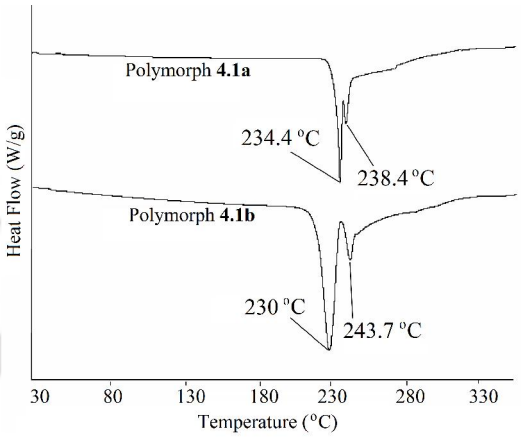

Figure 4.23: DSC of the polymorph **4.1a** and **4.1b** (heating rate 3 °C/ minute)

water and DMSO molecules when it is heated up to 190°C (theoretical weight loss 22.0%, experimental weight loss 21.4%, Figure **4.26a**). The loss of DMSO molecules at a relatively high temperature is supportive of its firm binding in the lattice. From the DSC it is seen that the compound **4.2** melts at 240°C. The methanol solvate **4.2b** losses the methanol molecules at around 80-100 °C (theoretical weight loss 9.0%, experimental weight loss 8.4%, Figure **4.28a**). From the TG analysis of **4.2c**, it is seen that the water of crystallization is lost at around 134°C (theoretical weight loss 3.90%, experimental weight loss 4.0%, Figure **4.29a**), which indicates that the water molecule is strongly bound in the assembly. Whereas in the case **4.2h**, the water of crystallization is lost at around 85-95°C (experimental weight loss 7.7%, theoretical weight loss 4.2%, Figure **4.34**). In this case water molecules are attached to two dimeric assemblies of the cations and are relatively weakly bound compared to water molecules in **4.2c**.

4.5 Conclusion:

In conclusion, we have reported two polymorphs **4.1a** and **4.1b** of imidazole based *bis*-phenol **4.1** formed by the combination of O_{phenol}-H···N type and O_{phenol}-H···O type motifs. The O-H···N and O-H···O interactions in the polymorph **4.1a** and **4.1b** are similar. However, the difference in packing of the two polymorphs arises due to the difference in the NH···π interactions. the polymorph **4.1b** has a porous structure and we have established its porosity by nitrogen adsorption-desorption experiment. The actone solvate **4.1c** is isostructural with the porous polymorph **4.1b**. The acetone solvate **4.1c** and the DMSO solvate **4.1d** transform to the porous polymorph **4.1b** on heating. Conversly, the porous polymorph **4.1b** transforms to the acetone solvate **4.1c** on exposure to acetone vapour. It may be mentioned that the porous structures generated by desolvation are generally unstable. But in case of *bis*-phenol **4.1**, we have crystallographically determined the structure of a porous form which considered as a difficult task.

On the other hand, in case of the *bis*-phenol **4.2** we have not observed any polymorphism. However, a large structural variations by directional hydrogen bonds in anion assisted assemblies of *bis*-phenol **4.2** are shown. Among the two isomeric *cis* and *trans* dicarboxylic acids, maleic acid leds to the monodeprotonated salt, whereas fumeric acid (*trans*) led to the dideprotonated salt. In the former case a water-assisted sheetlike layered structure observed, whereas in the latter case anion encapsulated assembly is formed through assembling of cations.

Among the tetrahedral anions sulphate led to trimeric sub-assemblies of the cationic *bis*-phenols part which is held together by sulphate ions forming assemblies with circular shapes. The circular assemblies and structures are very common in biological systems.[31] In case of the sulphate salt **4.2f**, the outer diameter of the circular assembly is 15.19 Å. This types of circular structures are important in the sense that large circular structures may be benificial for the discovery of new porous material.[32] On the other hand bisulphate anion is trapped from the acidolysis of magnesium sulfate and sulphuric acid in methanol. Stabilization of bisulphate anion by *bis*-phenol guest from this reaction is unprecedented to best of our knowledge.

The intramolecular hydrogen bonds between the phenolic hydroxy groups of the *bis*-phenol **4.2** molecules are observed in all the cases except in the case of the sulphate salt (**4.2f**). It is attributed to large electrostatic interactions offered by the sulfate

dianion. The formation of the tetrafluoroborate salt of **4.2** from sodium tetrafluoroborate in methanol is a very rare phenomenon.

4.6 Experimental Section

Synthesis of 4-[(4-hydroxy-3,5-dimethylphenyl)(5-methyl-1H-imidazol-4-yl)methyl]-2,6-dimethylphenol (**4.1**): 4-methyl-5-imidazolecarboxaldehyde (0.550 g, 5 mmol) and 2,6-dimethylphenol (1.22 g, 10 mmol) were dissolved in acetic acid (20 mL) and the solution was stirred for half an hour in an ice bath. A mixture of concentrated sulphuric acid and glacial acetic acid in a 1: 2 ratio (10 mL, v/v) was added dropwise to the reaction mixture. After half an hour of stirring, the mixture was kept in a deep freeze for one week. After one week, ice cold water (10 mL) was added to the reaction mixture and a pale yellow precipitate appeared. The reaction mixture was filtered and the precipitate was washed with an aqueous sodium bicarbonate solution (20%, 25 mL). The product was then dried in air and recrystallised from methanol. Yield: 78%. ^{1}H-NMR (400 MHz, DMSO-d_6): 7.31 (s, 1H), 6.61 (s, 4H), 5.09 (s, 1H), 2.07 (s, 12H), 1.95 (s, 3H), ^{13}C-NMR (100 MHz, DMSO-d_6): 151.3, 134.8, 133.1, 128.5, 126.7, 125.9, 123.8, 46.0, 16.9, 10.9; ESI mass: [M+1]: 337.2061.

(a)

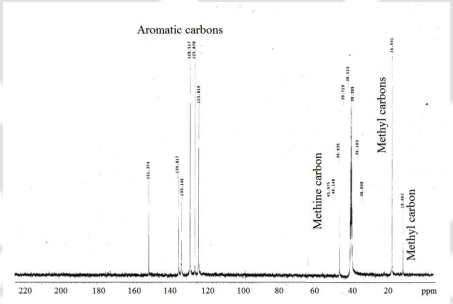

(b)

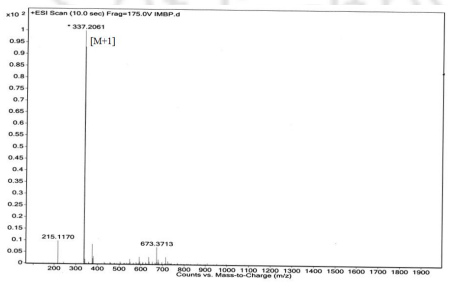

Figure 4.24: (a) ^{13}C-NMR (100 MHz, DMSO-d_6) and **(b)** LC-MS of the *bis*-phenol **4.1**.

When **4.1** was dissolved in methanol and kept undisturbed for crystallization, crystals of two different morphologies, namely, colorless needles of polymorph **4.1a** and yellow blocks of polymorph **4.1b** appeared together. The crystals of each polymorph were hand-picked using a magnifying glass.

Polymorph 4.1a: Yield: 55%. IR (KBr, cm^{-1}): 3351 (s), 2916 (m), 1598 (m), 1486 (s), 1440 (m), 1353 (m), 1299 (m), 1204 (s), 1143 (s), 1077 (m), 1024 (w), 966 (w), 879 (w), 803 (w), 736 (w), 668 (w), 633 (w), 597 (w).

Polymorph 4.1b: Yield: 40%. IR (KBr, cm^{-1}): 3359 (s), 2944 (m), 2917 (m), 1639 (w), 1594 (m), 1489 (s), 1456 (w), 1342 (m), 1306 (m), 1235 (s), 1208 (s), 1156 (s), 1081(s), 1029 (s), 971 (m), 887 (w), 792 (m), 741 (w), 685 (w), 660 (m), 634 (m), 603 (s), 489 (w).

Acetone solvate 4.1c: Solvate **4.1c** was obtained as red crystals from acetone. Yield: 65%. IR (KBr, cm^{-1}): 3444 (s), 2972 (w), 2946 (w), 2918 (w), 1743 (m), 1638 (s), 1489 (s), 1459 (w), 1358 (w), 1342 (w), 1307 (m), 1236 (s), 1209 (s), 1156 (s), 1082 (s), 1029 (m), 971 (w), 940 (w), 881 (w), 793 (m), 739 (m), 727 (w), 698 (m), 660 (m), 635 (m), 603 (m).

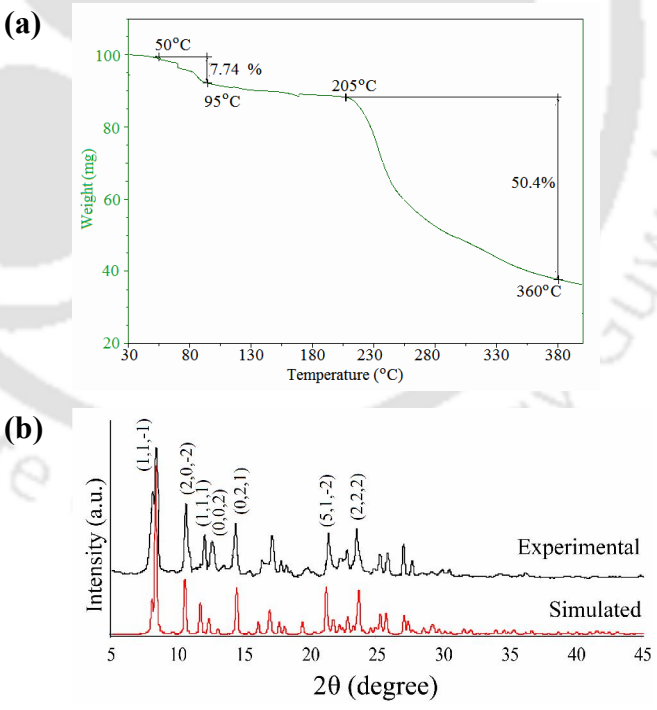

Figure 4.25: (a) TG of the acetone solvate **4.1c** showing the loss of the acetone molecules, **(b)** Comparison of simulated and experimental PXRD of the DMSO solvate **4.1c.**

DMSO Solvate 4.1d: Solvate **4.1d** was obtained as yellow block crystals from its solution in dimethyl sulphoxide. Yield: 80%. IR (KBr, cm^{-1}): 3449 (m), 3349 (s), 3258 (w), 3115 (w), 2919 (m), 2851 (w), 1596 (m), 1489 (s), 1434 (m), 1325 (m), 1304 (m), 1221 (s), 1156 (m), 1081 (m), 1027 (s), 965 (w), 949 (w), 842 (w), 790 (w), 696 (w), 636 (w), 600 (w).

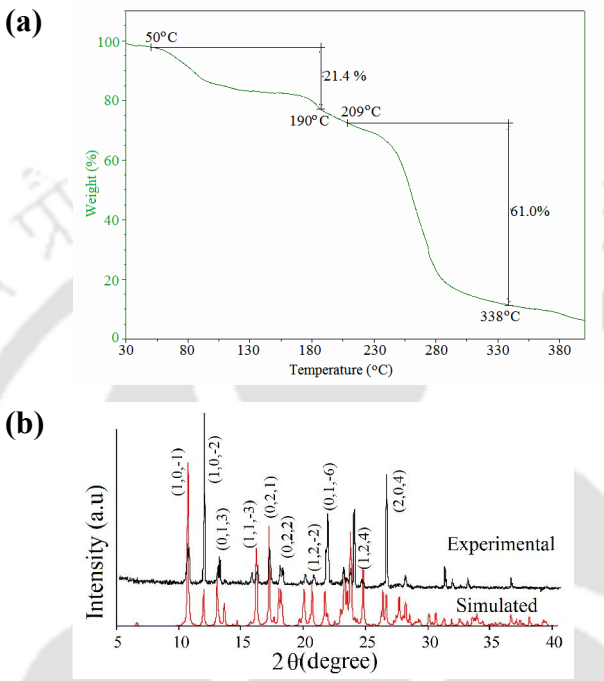

Figure 4.26: (a) TG of the DMSO solvate **4.1d** showing the loss of the DMSO solvents, **(b)** Comparison of simulated and experimental PXRD of the DMSO solvate **4.1d**.

Perchlorate salt of 4.1 (4.1e): Equimolar amounts of **4.1** (0.161 g, 0.5 mmol) and $HClO_4$ were dissolved in methanol (10 mL) and solution was left for crystallization. Yellow colored block crystals were formed after one week. Yield: 70%. IR (cm^{-1}): 3555 (m), 3236 (m), 3130 (w), 2918 (m), 1641 (m), 1608 (w), 1492 (s), 1335 (m), 1302 (w), 1286 (w), 1214 (s), 1151 (m), 1024 (m), 921 (w), 777 (w), 732 (m), 621 (s).

Hexafluoro silicate salt of 4.1 (41f): **4.1** was dissolved in methanol and excess amount of HF was added to it. The reaction mixture was kept for crystallization in a glass vessel. Yellow color block crystals were formed after one week. Yield: 55%. IR (cm^{-1}): 3509 (m), 3297 (w), 3185 (w), 3093 (w), 2917 (m), 1640 (s), 1491 (s), 1453

(w), 1321 (w), 1301 (w), 1204 (s), 1149 (m), 1023 (m), 946 (w), 883 (s), 722 (s), 484 (m).

Synthesis of 2-((2-hydroxy-3,5-dimethylphenyl)(imidazol-4-yl)methyl)-4,6-dimethylphenol (**4.2**): It is synthesised by the same procedure as *bis*-phenol **4.1** but 4(5)-imidazolecarboxaldehyde and 2,4-dimethylphenol was used instead of 4-methyl-5-imidazolecarboxaldehyde and 2,6-dimethylphenol respectively. Yield: 86 %. ^{1}H-NMR (400 MHz, DMSO-d_6): 7.73 (s, 1H), 6.85 (s, 2H), 6.71 (s, 2H), 5.74 (s, 1H), 2.11 (s, 6H), 2.09 (s, 6H); ^{13}C-NMR (100 MHz, DMSO-d_6): 150.6, 140.2, 134.7, 130.3, 129.5, 128.3, 127.2, 125.0, 116.7, 40.1, 20.7, 17.0; ESI mass: [M+1]: 323.0767.

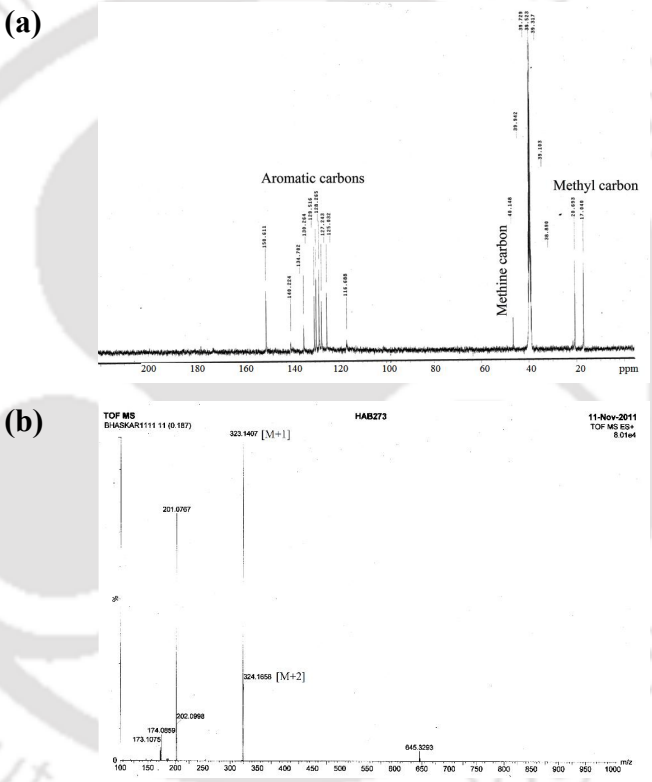

Figure 4.27: (a) ^{13}C-NMR (100 MHz, DMSO-d_6) and **(b)** LC-MS of the *bis*-phenol **4.2.**

The solvent free form **4.2a** is obtained by the crystallization of **4.2** from dimethylsulphoxide. IR (cm^{-1}): 3840 (w), 3439 (s), 3148 (m), 2912(w), 1615 (s), 1550 (s), 1486 (s), 1440 (m), 1325 (m), 1226 (s), 1185 (m), 1094 (w), 1012 (w), 935 (w), 856 (w), 751 (w), 658 (w). On the other hand the methanol solvate **4.2b** is obtained from the methanolic solution of **4.2**. IR (cm^{-1}): 3494 (m), 3357 (s), 2921 (w), 2783 (w), 1602 (w), 1570 (m), 1486 (s), 1441 (m), 1382 (w), 1334 (m), 1292 (m), 1218 (s),

1142 (m), 1082 (m), 1029 (s), 861 (s), 828 (m), 787 (m), 718 (m), 648 (m), 607 (s), 568 (w).

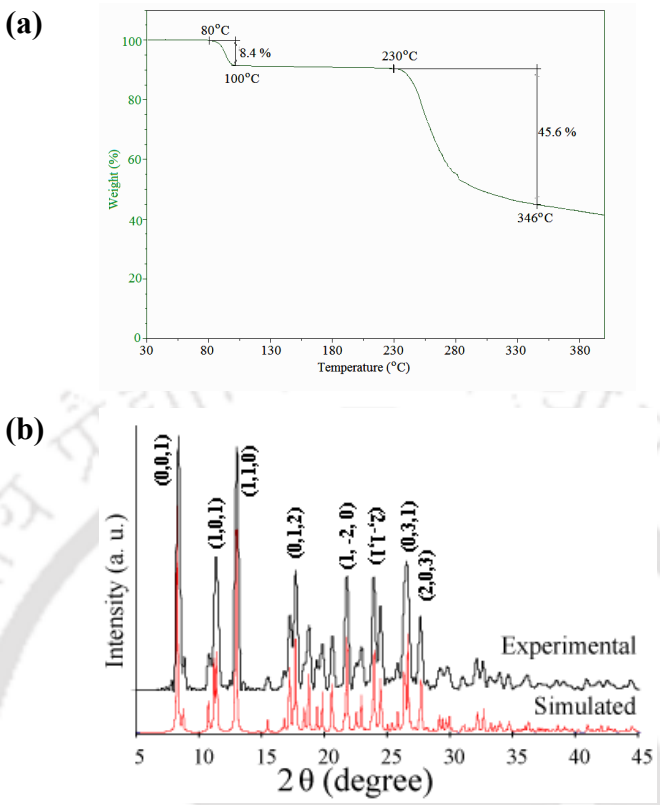

Figure 4.28: (a) TG of the methanol solvate **4.2b** showing the loss of methanol molecules, **(b)** Comparison of the simulated and experimental PXRD of salt **4.2b**.

4.2H·Hmal·H_2O (4.2c): Equimolar amounts (0.5 mmol) of **4.2** (0.161 g) and maleic acid (0.058 g) were dissolved in methanol (10 mL) and kept for crystallization. After one week, colorless crystals appeared. Yield: 96%. IR (cm^{-1}): 3461 (s), 3135 (m), 2920 (m), 1620(s), 1578 (s), 1489 (s), 1443 (m), 1387 (m), 1363 (s), 1298 (w), 1212 (s), 1149 (w), 1089 (w), 993 (w), 863 (s), 788 (w), 751 (s), 661 (w), 625 (w), 568 (w). ^{1}H-NMR (400MHz, DMSO-d_6): 8.98 (s, 1H), 6.86 (s, 1H), 6.81 (s, 2H), 6.38 (s, 2H), 6.14 (s, 2H), 6.12 (s, 1H), 2.13 (s, 6H), 2.09 (s, 6H).

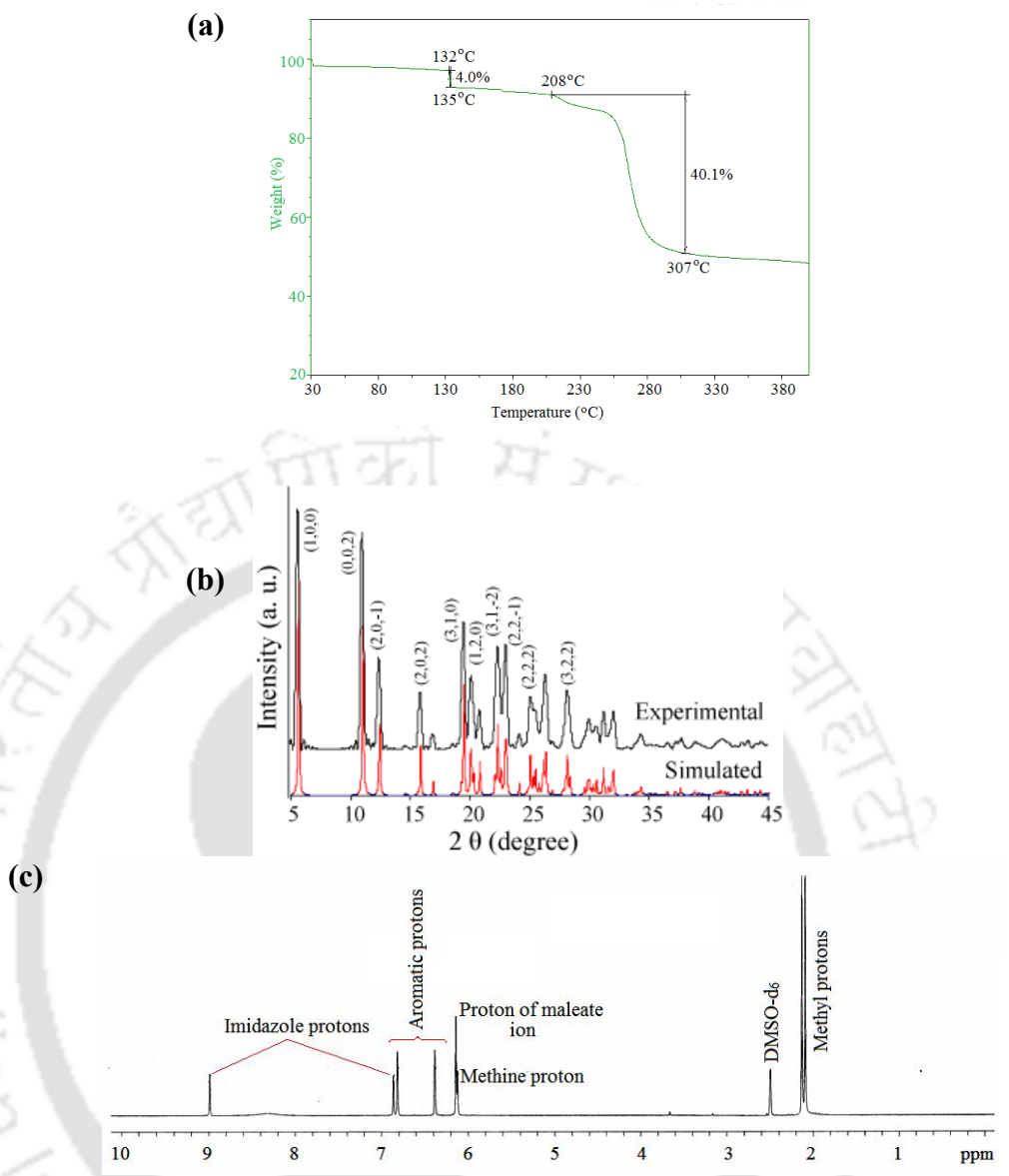

Figure 4.29: (a) TG of the salt **4.2c, (b)** Comparison of the simulated and experimental PXRD of salt **4.2c**, **(c)** ^{1}H-NMR of the salt **4.2c** (DMSO-d_6, 400 MHz).

4.2H·0.5fum (4.2d): 4.2 (0.322 g, 1 mmol) and fumeric acid (0.058 g, 0.5 mmol) were dissolved in methanol (15 mL) and kept for crystallization. After one week colorless crystals appeared. Yield: ~94%. IR (cm-1): 3324 (s), 3140 (m), 2916 (s), 2569 (m), 1538 (s), 1489 (s), 1443 (s), 1352 (m), 1325 (m), 1304 (m), 1289 (m), 1228 (s), 1166 (s), 1101 (m), 988 (s), 920 (w), 874 (w), 846 (m), 790 (m), 750 (m), 674 (s), 641 (w), 620 (w), 574 (w). ^{1}H-NMR (400MHz, DMSO-d_6): 2.08 (s, 12H), 5.78 (s, 1H), 6.60 (s, 1H), 6.71 (s, 2H), 6.78 (s, 3H), 7.84 (s, 1H).

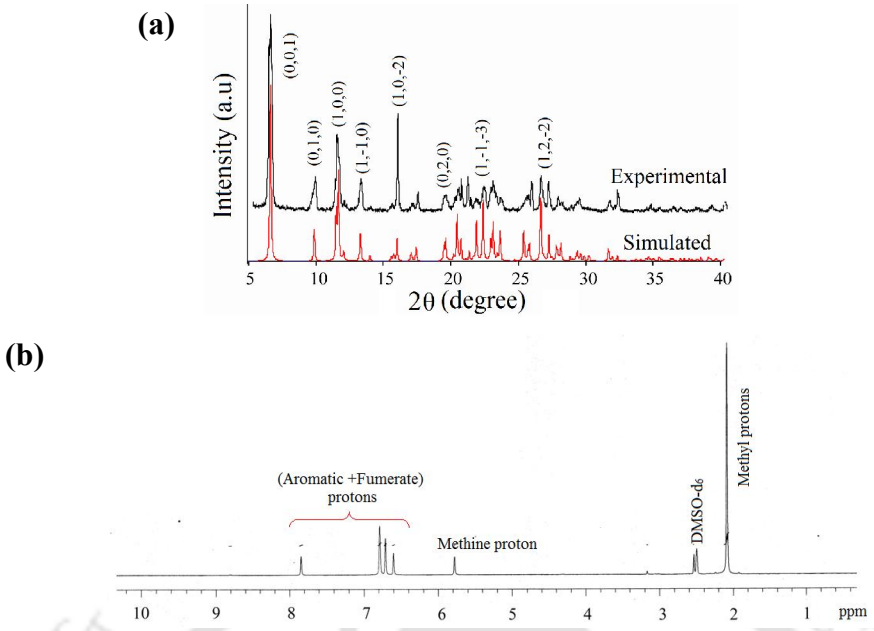

Figure 4.30: (a) Comparison of the simulated and experimental PXRD of salt **4.2c**, **(b)** ^{1}H- NMR of the salt **4.2d** (DMSO-d_6, 400 MHz).

4.2H·ClO_4 (4.2e): Equimolar amounts of **4.2** (0.161 g, 0.5 mmol) and $HClO_4$ were dissolved in methanol (10 mL) and solution was left for crystallization. Colorless crystals were formed after one week. Yield: 93%. IR (cm^{-1}): 3391 (s), 3159 (s), 3010 (m), 2917 (m), 1613 (s), 1487 (s), 1378 (w), 1337 (w), 1298(m), 1229(m), 1182 (m), 1142 (s), 1120 (s), 1087 (s), 1031(m), 984 (w), 929 (w), 866 (w), 806 (w), 789 (w), 624 (s). ^{1}H-NMR (400MHz, DMSO-d_6): 2.09 (s, 6H), 2.13 (s, 6H), 6.12 (S, 1H), 6.38 (s, 2H), 6.82 (s, 2H), 6.86 (s, 1H), 8.98 (s, 1H).

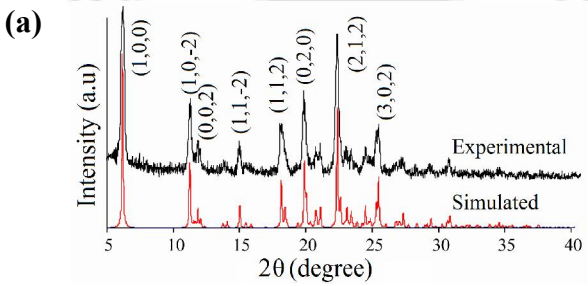

(b)

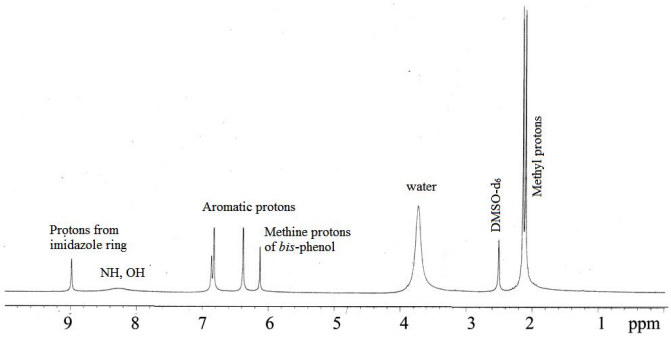

Figure 4.31: **(a)** Comparison of the simulated and experimental PXRD of salt **4.2e**, **(b)** ^{1}H- NMR of the salt **4.2e** (DMSO-d_6, 400 MHz).

4.2H·0.5SO$_4$ (4.2f): **4.2** (0.322 g, 1 mmol) and H_2SO_4 in a 2:1 molar ratio were dissolved in methanol (15 mL) and kept for crystallization. Colorless crystals were formed after one week. Yield: 96%. IR (cm^{-1}): 3391 (s), 3136 (s), 2856 (s), 1617 (s), 1490 (s), 1377 (w), 1340 (w), 1191 (s), 1154 (s), 1093 (m), 1060 (s), 931 (w), 864 (s), 817 (m), 787 (w), 750 (w), 590 (s). ^{1}H-NMR (400MHz, DMSO-d_6): 2.09 (s, 6H), 2.13 (s, 6H), 6.12 (s, 1H), 6.37 (s, 2H), 6.81 (s, 2H), 6.84 (s, 1H), 8.98 (s, 1H).

(a)

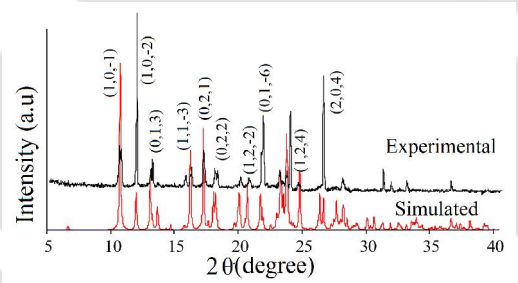

(b)

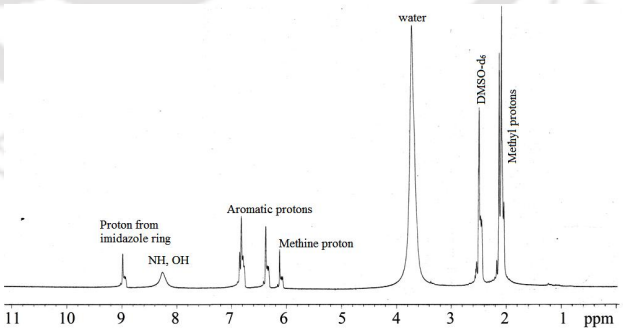

Figure 4.32: (a) Comparison of the simulated and experimental PXRD of salt **4.2f**, **(b)** ^{1}H- NMR of the salt **4.2f** (DMSO-d_6, 400 MHz).

4.2H·HSO$_4$ (4.2g): 4.2 (0.322 g, 1 mmol) and magnesium sulfate heptahydrate (0.124 g, 0.5 mmol) were dissolved in methanol and then a few drops of sulphuric acid was added to it and the clear solution thus obtained was kept undisturbed. After 3 days pink color crystals appeared. Yield: 91%. IR (cm^{-1}): 3397 (s), 3131 (w), 3025 (w), 2918 (w), 1617 (s), 1483 (s), 1376 (w), 1340 (w), 1192 (w), 1154 (w), 1093 (m), 1060 (m), 931 (w), 864 (s), 589 (s), 493 (w). ^{1}H-NMR (400MHz, DMSO-d$_6$): 2.09 (s, 6H), 2.13 (s, 6H), 6.12 (s, 1H), 6.37 (s, 2H), 6.82 (s, 2H), 6.85 (s, 2H), 8.35 (s, 1H), 8.99 (s, 1H).

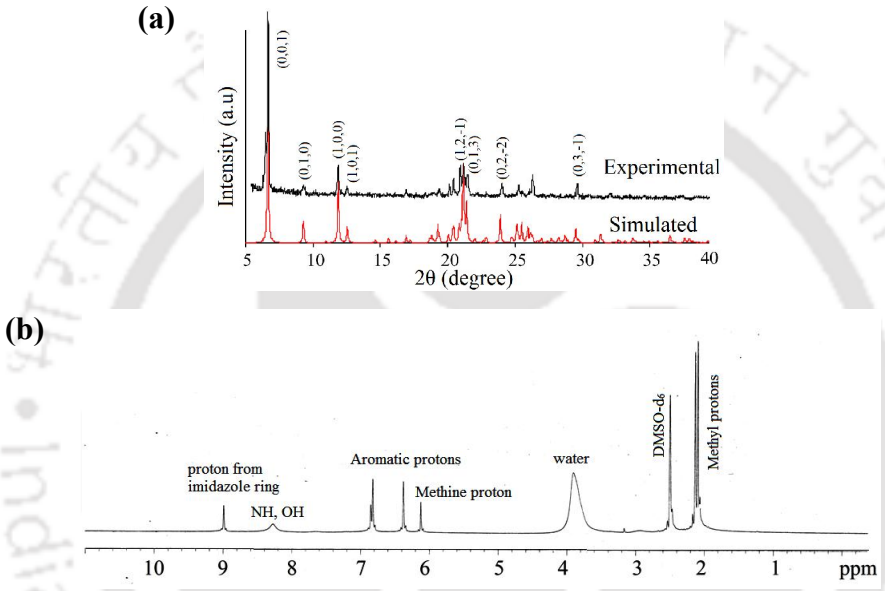

Figure 4.33: (a) Comparison of the simulated and experimental PXRD of salt **4.2g**, **(b)** ^{1}H- NMR of the salt **4.2g** (DMSO-d$_6$, 400 MHz).

4.2H·BF$_4$·H$_2$O (4.2h): Equimolar amounts (0.5 mmol) of **4.2** (0.161 g) and NaBF$_4$ (0.055 g) were dissolved in methanol (15 mL) and kept for crystallization. After one week, colorless crystals formed were filtered. Yield: 94%. IR (cm^{-1}): 3344 (s), 3151 (m), 3016 (s), 2915 (m), 2851 (w), 1614 (m), 1551 (s), 1489 (s), 1439 (m), 1329 (w), 1303 (w), 1229 (s), 1185 (m), 1084 (w), 856 (w), 788 (w), 751 (w), 660 (w), 631 (w). ^{1}H-NMR (400MHz, DMSO-d$_6$): 2.08 (s, 12H), 5.76 (s, 1H), 6.70 (s, 2H), 6.79 (s, 3H), 7.82 (s, 1H).

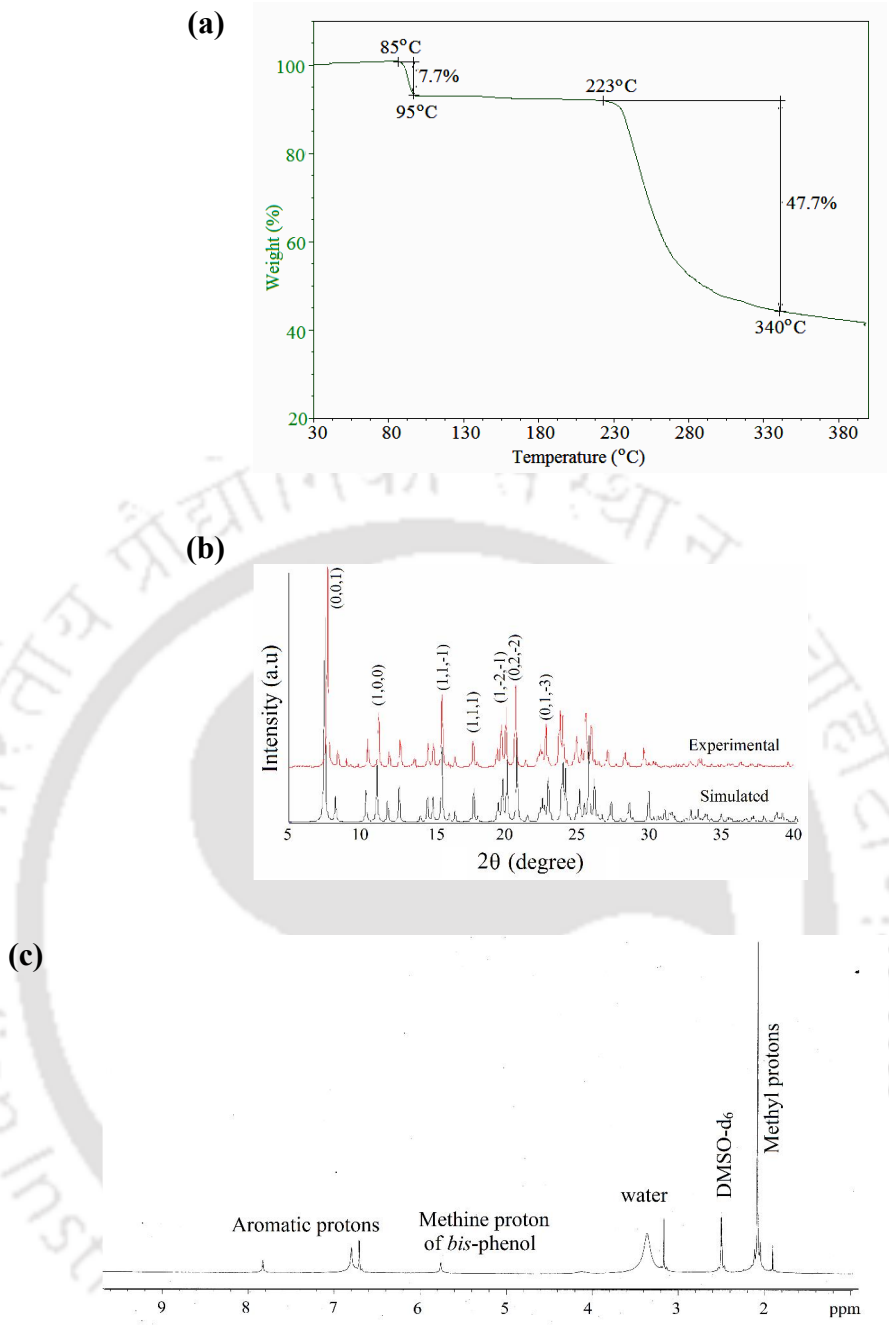

Figure 4.34: **(a)** TG of the salt **4.2h**, **(b)** Comparison of the simulated and experimental PXRD of salt **4.2h**, **(c)** ^{1}H-NMR of the salt **4.2h** (DMSO-d_6, 400 MHz).

4.2H·NO_3 (4.2i): A solution prepared from an equimolar amount (0.5 mmol) of **4.2** (0.161 g) and HNO_3 was allowed to crystallize. After one week, colorless crystals were obtained. Yield: 95%. IR (cm^{-1}): 3352 (s), 3125 (s), 3024 (s), 2914 (s), 1744 (w), 1615 (s), 1491 (s), 1439 (m), 1419 (m), 1384 (s), 1330 (s), 1300 (s), 1260 (s), 1226 (s), 1188 (s), 1096 (m), 1041 (m), 987 (w), 934 (w), 834 (m), 626 (w), 565 (w). ^{1}H-

NMR (400MHz, DMSO-d_6): 2.10 (s, 6H), 2.14 (s, 6H), 6.13 (s, 1H), 6.38 (s, 2H), 6.82 (s, 2H), 6.85 (s, 1H), 8.27 (s, 2H), 9.00 (s, 1H).

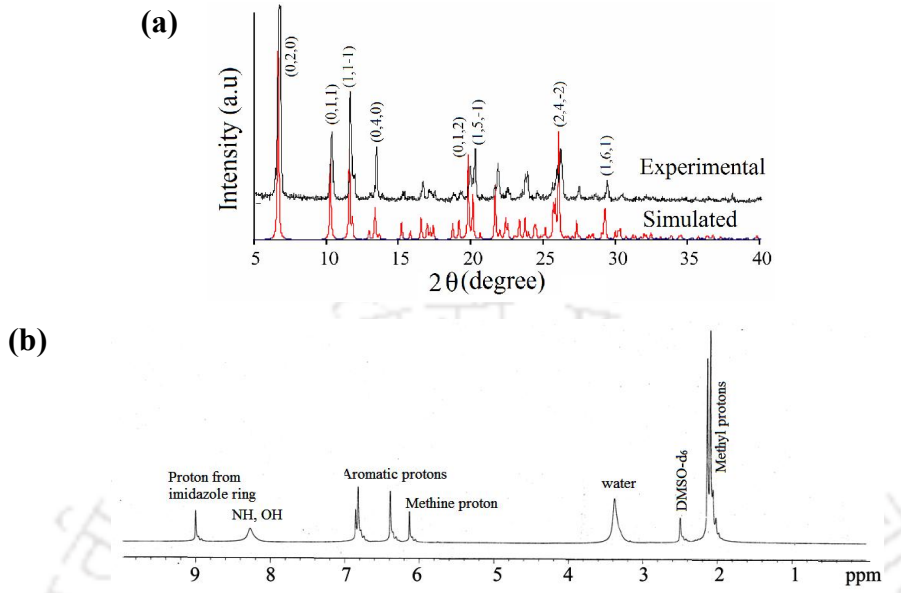

Figure 4.35: **(a)** Comparison of the simulated and experimental PXRD of salt **4.2i**, **(b)** ^{1}H- NMR of the salt **4.2i** (DMSO-d_6, 400 MHz).

References:

1. (a) R. Thakuria, B. Sarma, A. Nangia, *Cryst. Growth Des.*, 2008, **8**, 147-1473; (b) P. K. Thallapally, P. B. McGrail, S. J. Dalgarno, J. L. Atwood, *Cryst. Growth Des.*, 2008, **8**, 2090-2092; (c) K. Skobridis, G. Paraskevopoulos, V. Theodorou, W. Seichter, E. Weber, *Cryst. Growth Des.*, 2011, **11**, 5275-5288; (d) R. J. Sarma, J. B. Baruah, *Cryst. Growth Des.*, 2007, **7**, 989-1000; (e) J. Lü, L. -W. Han, J. -X. Lin, R. Cao, *Cryst. Growth Des.*, 2011, **11**, 3551-3557; (f) M. Tominaga, H. Masu, I. Azumaya, *Cryst. Growth Des.*, 2011, **11**, 542-546; (g) H. Masu, M. Tominaga, I. Azumaya, *Cryst. Growth Des.*, 2013, **13**, 752-758; (h) N. Iwase, Y. Shigeno, T. Wakabayashi, T. Sato, N. Tajima, R. Kuroda, Y. Imai, *CrystEngComm*, 2014, **16**, 159-163.
2. (a) R. J. Sarma, J. B. Baruah, *Sol. State Sci.*, 2008, **10**, 580-586; (b) R. J. Sarma, J. B. Baruah, *Chem. Eur. J.,* 2006, **12**, 4994-5000; (c) C. Tamuly, R. J. Sarma, A. S. Batsanov, A. E. Goeta, J. B. Baruah, *Acta Crystallogr. Sect. C*: Cryst. *Struct. Commun.*, 2005, **C61**, o324-o327.

3. a) G. R. Desiraju, *Acc. Chem. Res.*, 1996, **29**, 441-449; (b) T. Steiner, G. R. Desiraju, *Chem. Commun.*1998, 891-892. (c) G. R. Desiraju, *Science*, 1997, **278**, 404-405; (d) M. Nishio, Y. Umezawa, H. Suezawa, S. Tsuboyama, In *The Importance of π-Interactions in Crystal Engineering: Frontiers in Crystal Engineering;* E. R. T. Tiekink, J. Zukerman-Schpector, Eds.; John Wiley & Sons Ltd: New York, 2012; Chapter 1; (e) C. P. Brock, L. L. Duncan, *Chem. Mater.,* 1994, **6**, 1307-1312; (f) R. J. Sarma, J. B. Baruah, *CrystEngComm*, 2005, **7**, 706-710.
4. (a) R. D. Gandour, N. A. R. Nabulsi, F. R. Fronczek, *J. Am. Chem. Soc.*, 1990, **112**, 7816- 7817; (b) J. C. MacDonald, P. C. Dorrestein, M. M. Pilley, *Cryst. Growth Des.*, 2001, **1**, 29-38.
5. (a) C. E. Willans, S. French, K. M. Anderson, L. J. Barbour, J.-A. Gertenbach, G. O. Lloyd, R. J. Dyer, P. C. Junk, J. W. Steed, *Dalton Trans.*, 2011, **40**, 573-582; (b) M. du Plessis, L. J. Barbour, *Dalton Trans*., 2012, **41**, 3895-3898.
6. R. J. Sarma, J. B. Baruah, *Dyes Pigm.*, 2004, **61**, 39-47.
7. (a) G. P. Kar, A. Karmakar, J. B. Baruah, *J. Chem. Crystallogr.*, 2010, **40**, 702-706; (b) P. L. Coupar, G. Furguson C. Glidewell, *Acta Crystallogr., Sect. C: Cryst. Struct. Commun.*, 1996, **C52**, 3055-3057.
8. (a) G. R. Desiraju, T. Steiner, *The Weak Hydrogen Bond: In Structural Chemistry and Biology*, Oxford University Press, 2001; (b) J. Cheng, C. Kang, W. Zhu, X. Luo, C. M. Puah, K. Chen, J. Shen, H. Jiang, *J. Org. Chem.*, 2003, **68**, 7490-7495.
9. K. S. W. Sing, D. H. Everett, R. A. W. Haul, L. Moscou, R. A. Pierotti, J. Rouquerrol, T. Siemieniewska, *Pure Appl. Chem.*, 1985, **57**, 603-619.
10. A. Nangia, G. R. Desiraju, *Chem. Commun.*, 1999, 605-606.
11. (a) G. R. Desiraju, I. C. Paul, D. Y. Curtin, *J. Am. Chem. Soc.*, 1977, **99**, 1594-1601; (b) J. Bernstein, R. J. Davey, J. O. Henck, *Angew. Chem., Int. Ed.*, 1999, **38**, 3440-3461; (c) M. L. Greer, B. J. McGee, R. D. Rogers, S. C. Blackstock, *Angew. Chem., Int. Ed. Engl.*, 1997, **36**, 1864-1866; (d) S. R. Byrn, *Solid State Chemistry of Drugs*, Academic Press, New York, 1982; (e) W. H. DeCamp, in *Crystal Growth of Organic Materials*, ed. A. S. Myerson, D. A. Green, P. Meenan, ACS Proceedings Series: American Chemical Society, Washington, DC, 1996; (f) J. D. Dunitz, J. Bernstein, *Acc. Chem. Res.*, 1995, **28**, 193-200;

(g) G. R. Desiraju, *Nat. Mater.*, 2002, **1**, 77-79; (h) A. Nangia, G. R. Desiraju, *Chem. Commun.*, 1999, 605-606; (i) T. Laird, *Org. Process Res. Dev.*, 2000, **4**, 371-379; (j) R. D. Rogers, *Cryst. Growth Des.*, 2003, **3**, 867-867.

12. (a) S. Long, S. Parkin, M. A. Siegler, A. Cammers, T. Li, *Cryst. Growth Des.*, 2008, **8**, 4006-4013; (b) A. Nangia, *Acc. Chem. Res.*, 2008, **41**, 595-604; (c) G. R. Desiraju, *Acc. Chem. Res.*, 1996, **29**, 441-449; (d) G. R. Desiraju, *Acc. Chem. Res.*, 2002, **35**, 565-573.
13. (a) C. N. R. Rao, A. K. Cheetham, A. Thirumurugan, *J. Phys.: Condens. Matter*, 2008, **20**, 083202/1-083202/21; (b) S. J. Blundell, F. L. Pratt, *J. Phys.: Condens. Matter*, 2004, **16**, R771-R828; (c) Y. Yoshida, K. Inoue, M. Kurmoo, *Inorg. Chem.*, 2009, **48**, 10726-10736.
14. A. Czapik, H. Konowalska, M. Gdniec, *Acta Crystallogr., Sect. C: Cryst. Struct. Commun.*, 2011, **66C**, o128-o132.
15. S. Bhattacharya, B. K. Saha, *Cryst. Growth Des.*, 2013, **13**, 606-613.
16. (a) A. J. Cruz-Cabeza, G. M. Day, W. Jones, *Phys. Chem. Chem. Phys.*, 2011, **13**, 12808-12816; (b) J. B. Baruah, A. Karmakar, N. Barooah, *CrystEngComm*., 2008, **10**, 151-154.
17. (a) A. R. Katritzky, D. C. Fara, H. Yang, K. Tamm, T. Tamm, M. Karelson, *Chem. Rev.*, 2004, **104**, 175-198; (b) H. D. P. Ali, P. E. Kruger and T. Gunnlaugsson, *New J. Chem.*, 2008, **32**, 1153-1161.
18. (a) Suzuki, H. *Tetrahedron Lett*., 1992, **33**, 6319-6322; (b) Suzuki, H.; Takagi, H. *Tetrahedron Lett*., 1993, **34**, 4805-4806; (c) Suzuki, H.; Takagi, H.; Sato, R. *Tetrahedron Lett*., 1997, **38**, 4563-4566; (d) K. Tanaka, K. Endo, Y. Aoyama, *Chem. Lett.*, 1999, 887-888; (e) C. Zhang, C.-F. Chen, *CrystEngComm*, 2010, **12**, 3255-3261; (f) V. R. Vangala, R. Mondal, C. K. Broder, J. A. K. Howard, G. R. Desiraju. *Cryst. Growth and Des*.**,** 2005, **5**, 99-104; (g) A. Roth, D. Koth, M. Gottschaldt, W. Plass, *Cryst. Growth and Des*.**,** 2006, **6**, 2655-2657; (h) J. Lu, L.-W, Han, J.-X. Lin, R. Cao, *Cryst. Growth and Des*.**,** 2011, **11**, 3551-3557; (i) H. Degenbeck, A.-S. Felten, J. Etxebarria, E. C. Escudero-Adan, J. Benet-Buchholz, A. Vidal-Ferran, *Cryst. Growth and Des*.**,** 2012, **12**, 2719-2723; (j) Y. Imai, K. Kamon, T. Kinuta, N. Tajima, T. Sato, R. Kuroda, Y. Matsubara, *Cryst. Growth and Des*.**,** 2009**, 9,** 4096-4101**.**

19. N. Iwase, T. Kinuta, N. Tajima, T. Sato, R. Kuroda, Y. Matsubara, Y. Imai, *CrystEngComm*, 2010, **12**, 3195-3200.
20. E. Galbraith, T. M. Fyles, F. Marken, M. G. Davidson, T. D. James, *Inorg. Chem.*, 2008, **47**, 6236-6244.
21. (a) X. Zhou, B. Yu, Y. Guo, X. Tang, H. Zhang, .W. Liu, *Inorg. Chem.*, 2010, **49**, 4002-4007; (b) G. Ambrosi, M. Formica, V. Fusi, L. Giorgi, A. Guerri, E. Macedi, M. Micheloni, P. Paoli, R. Pontellini, P. Rossi, *Inorg. Chem.*, 2009, **48**, 5901-5912.
22. (a) L. Y. Zhao, G. K. Wanga, J. H. Chen, L. M. Zhang, B. Liu, J. F. Zhang, Q. H. Zhao, Y. Zhou, *J. Fluorine chem*., 2014, **158**, 53-59; (b) A. Okudan, S. Erdemir, O. Kocyigit, *J. Mol. Struct.*, 2013, **1048**, 392-398; (c) S. Dalapati, M. A. Alam, S. Jana, S. Karmakar, N. Guchhait, *Spectrochim. Acta, Part A*, 2013, **102**, 314-318.
23. (a) L. Orola, M. V. Veidis, I. Mutikainen, I. Sarcevica, *Cryst. Growth Des.*, 2011, **11**, 4009-1016; (b) S. Basavoju, D. Boström, S. P. Velaga, *Cryst. Growth Des.*, 2006, **6**, 2699-2708; (c) V. Sethuraman, N. Stanley, P. T. Muthiah, W. S. Sheldrick, M. Winter, P. Luger, M. Weber, *Cryst. Growth Des.*, 2003, **3**, 823-828; (d) K. A. Wichmann, P. D. W. Boyd, T. Söhnel, G. R. Allen, A. R. J. Phillips, G. J. S. Cooper, *Cryst. Growth Des.*, 2007, **7**, 1844-1850.
24. K. Biradha, S. Samai, A. C. Maity, S. Goswami, *Cryst. Growth Des.*, 2010, **10**, 937-942.
25. (a) S. M. Haile, D. A. Boyens, C. R. I. Chisholm, R. B. Merie, *Nature*, 2001, **400**, 910-913; (b) C. R. I. Chisholm, S. M. Haile, *Solid State Ionics*, 2000, **136**, 229-241; (c) J. Lipkowski, B. Baranowski, A. Lunden, *Pol. J. Chem.*, 1993, **67**, 1867-1876; (d) S. M. Haile, *Mater. Res. Soc. Symp. Proc.*, 1999, **547**, 315-326; (e) P. G. Bruce, *Dalton Trans.*, 2006, 1365-1369.
26. D. Braga, M. Gandolfi, M. Lusi, M. Polito, K. Rubini, F. Grepioni, *Cryst. Growth Des.*, 2007, **7**, 919-924.
27. (a) D. Braga, L. Maini, M. Polito, F. Grepioni, *Struct. Bonding(Berlin),* 2004, **111**, 1-32; (b) D. Braga, E. D'Oria, F. Grepioni, F. Mota, J. J. Novoa, C. Rovira, *Chem. -Eur. J.*, 2002, **8**, 1173-1180.

28. U. P. Singh, S. Kashyap, H. J. Singh, R. J. Butcher, *CrystEngComm.*, 2011, **13**, 4110-4120.
29. D. Kalita, J. B. Baruah, *CrystEngComm*, 2010, **12**, 1562-1567.
30. (a) B. Rodriguez-Spong, C. P. Price, A. Jayasankar, A. J. Matzer N. Rodriguez-Hornedo, *Adv. Drug Delivery Rev.*, 2004, **56**, 241-274; (b) A. Burger, R. Ramberger, *Microchim. Acta*, 1979, **2**, 259-279; (c) K. Kawakami, *J. Pharm. Sci.*, 2007, **96**, 982-989.
31. (a) S. M. Mali, T. F. Schneider, A. Bandyopadhyay, S. V. Jadhav, D. B. Werz, H. N. Gopi, *Cryst. Growth Des.*, 2012, **12**, 5643-5648; (b) A. Bertram, G. Pattenden, *Nat. Prod. Rep.*, 2007, **24**, 18-30; (c) M. C. Bagley, J. W. Dale, E. A. Merritt, X. Xiong, *Chem. Rev.*, 2005, **105**, 685-714.
32. J. R. Gardinier, H. M. Tatlock, J. S. Hewage, S. V. Lindeman, *Cryst. Growth Des.*, 2013, **13**, 3864-3877; (b) B. Hasenknopf, J. -M. Lehn, N. Boumediene, A. Dupont Gervais, A. V. Dorsselaer, B. Kneisel, D. Fenske, *J. Am. Chem. Soc.*, 1997, **119**, 10956-10962; (c) S. Leininger, B. Olenyuk, P. J. Stang, *Chem. Rev.*, 2000,**100**, 853-908.

CHAPTER 5

Alkali metal complexes of *bis*-phenol based flexible dicarboxylic acids

The coordination of s-block metals with carboxylate oxygen atoms is mainly ionic in nature which complicates the prediction of coordination geometry.[1] It is a challenge in carrying out systematic studies of coordination networks based on s-block metal ions due to the lack of predictive coordination behaviour. Despite of these difficulties, alkali metal ions have been employed in hybrid frameworks, as their oxophilicity and H_2 affinity can offer binding sites for H_2, CO_2, and other guest molecules.[2] The alkali metals (Na, K) are among the 10 most abundant elements in nature; they are cheap, non-toxic, and essential in many biological processes.[3] Metal organic frameworks of alkali metals provide interesting structural features.[4] Various flexible[5] and semi-rigid[6] di- and polycarboxylate ligands were employed to construct MOF of alkali metals. The diaqua-bridged sodium carboxylate complexes have interest as model for biological mimic of sodium complex of glyphosate.[7] The assemblies of mixed anionic carboxylate complexes show versatilities in optical properties.[8]

The rigid V-shaped geometry of *bis*-phenol can be modified to flexible or semi-rigid structure by functionalizing the hydroxy groups at two ends.[9] A *bis*-phenol generally adopts propeller type of structure (Figure **5.1 A**).[10] However, the two phenolic ends

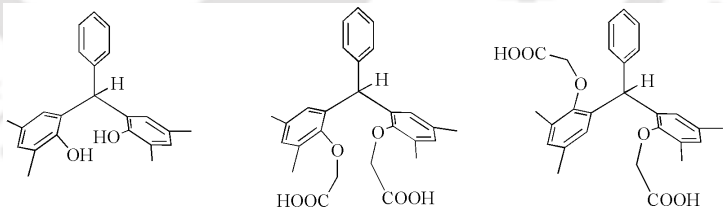

(A) Pincer like structure (B) (C)

Figure 5.1: **(A)** Propeller geometry of *bis*-phenol, **(B)** and **(C)** pincer like compound derived form *bis*-phenol having two flexible arms connected to rigid propeller geometry.

can be expanded through ether bond with functional groups such as -CH_2COOH which results in the formation of pincer type of ligands. Pincer type ligands[11] can

coordinate to metal ions to give coordination complexes of various dimensions. Since, the functional groups are connected to a sp^3 carbon centre through the ether link, there are different possibilities of orientation of such ligands as illustrated in Figure **5.1** (**B** and **C**). The stabilization of such conformation through metal complexation would be of interest to generate mononuclear, cyclic or polymeric structures.

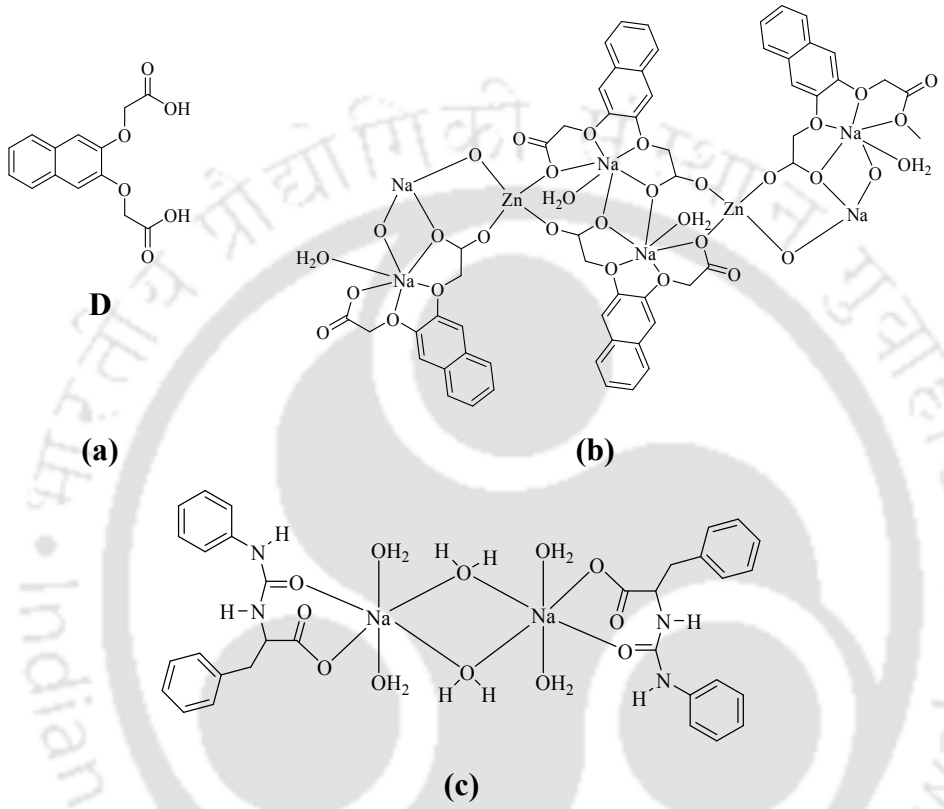

Figure 5.2: **(a)** Structure of the ether based flexible dicarboxylic acid ligand D, **(b)** Heterometallic Zn-Na coordination polymer of D, **(c)** Dinuclear aqua bridged sodium complex of L-3-phenyl-2-(3-phenyl-ureido)-propionic acid.

It may also be noted that ligands having similar scaffold such as **D** was studied earlier to make various metal complexes.[12] In such cases a wide variation of structures was observed through coordination to different metal ion in presence of wide range of ancillary ligands. Sodium cations were shown to be embedded in crown-like geometries created by complexation to metal ions.[12] On the other hand, rigid pincer shaped 2, 6-dipicolinic acid forms coordination complexes of different dimension with alkali metals.[13] Urea based flexible carboxylate ligand, L-3-phenyl-2-(3-phenyl-

ureido)-propionic acid forms sodium complex which has aqua bridge dinuclear structure.[14] Based on these, we have taken up synthesis and characterization of a series of dicarboxylic acid ligands having structural skeleton of **D** as shown in the Figure **5.1**. In this chapter we demonstrate structural variations of sodium, potassium and caesium complexes of V-shaped pincer type of dicarboxylic acid ligands derived from unsubstituted and substituted *bis*-phenols.

5.1 Synthesis of the *bis*-phenol based dicarboxylic acids H_2L^1 (5.1), H_2L^2 (5.2), H_2L^3 (5.3) and H_2L^4 (5.4)

The dicarboxylic acid ligands H_2L^1 **(5.1)**, H_2L^2 **(5.2)**, H_2L^3 **(5.3)** and H_2L^4 **(5.4)** were synthesized by multi-step synthetic procedures starting from *bis*-phenols **(5.1a-5.4a)**. The *bis*-phenols **(5.1a-5.4a)** were reacted with methyl bromoacetate to obtain the corresponding ester **(5.1b-5.4b)**. The esters **(5.1b-5.4b)** were further hydrolyzed to form the dicarboxylic acids. The reaction steps are illustrated in Scheme **5.1**. These new ligands are characterised by various convensional spectroscopic techniques such as, FT-IR, ^{1}H-NMR, ^{13}C-NMR and ESI mass spectrometry. For example, in ^{13}C-NMR spectra of **5.1**, the signals at 15.9 and 20.7 ppm are due to carbon of methyl groups attached to aromatic rings. The signals at 43.1 ppm and 69.3 ppm are due to methylene carbon and methine carbon. Whereas signal for carbon of carbonyl group appears at 170.3 ppm. In the IR spectra of **5.1**, the OH of carbonyl appears at 3446 cm^{-1} and the streching frequeny for the C=O group appears at 1741 cm^{-1}.

We have also determined the structure of **5.1** and **5.3** using single crystal X-ray diffractometer. But we did not obtain siutable single crystal of **5.2** and **5.4** which deterred us to determine their strcutures.

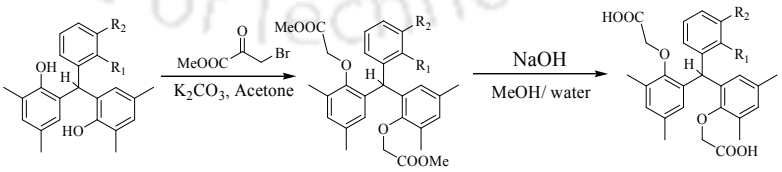

Where R_1= H, R_2= H **(5.1a)**
R_1= F, R_2= H **(5.2a)**
R_1= NO_2, R_2= H **(5.3a)**
R_1= H, R_2= NO_2 **(5.4a)**

Where R_1= H, R_2= H **(5.1b)**
R_1= F, R_2= H **(5.2b)**
R_1= NO_2, R_2= H **(5.3b)**
R_1= H, R_2= NO_2 **(5.4b)**

Where R_1= H, R_2= H **(5.1)**
R_1= F, R_2= H **(5.2)**
R_1= NO_2, R_2= H **(5.3)**
R_1= H, R_2= NO_2 **(5.4)**

Scheme 5.1: Syntheses of the ligands **5.1-5.4.**

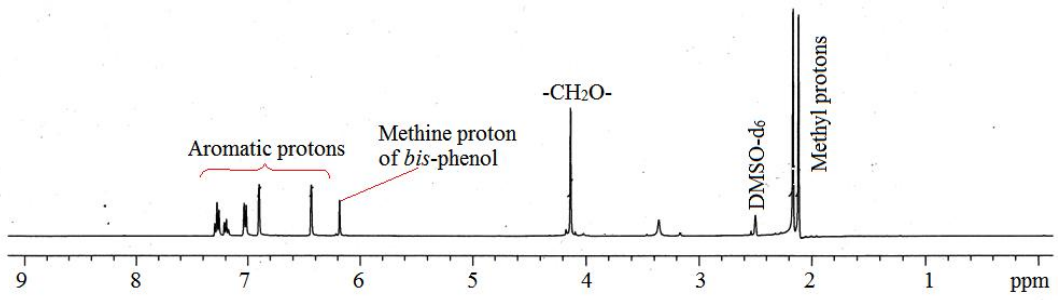

Figure 5.3: ^{1}H-NMR of ligand H_2L^1**(5.1)** (400MHz, DMSO-d_6)

5.2 Structures of the ligands H_2L^1 (5.1) and H_2L^3 (5.3)

From the single crystal analysis it is seen that both **H_2L^1 (5.1)** and **H_2L^3 (5.3)** have pincer-like geometries. The pincer-like geometries originate from the projection of the two aromatic rings bearing a central methine carbon (C11). The arms bearing flexible carboxylic acid groups are attached to the two aromatic rings through oxygen atoms. Thus, the flexible arms are suitably oriented to adopt a favourable conformation for coordination to metal ions. The ligand **5.1** forms H-bonded assemblies with a

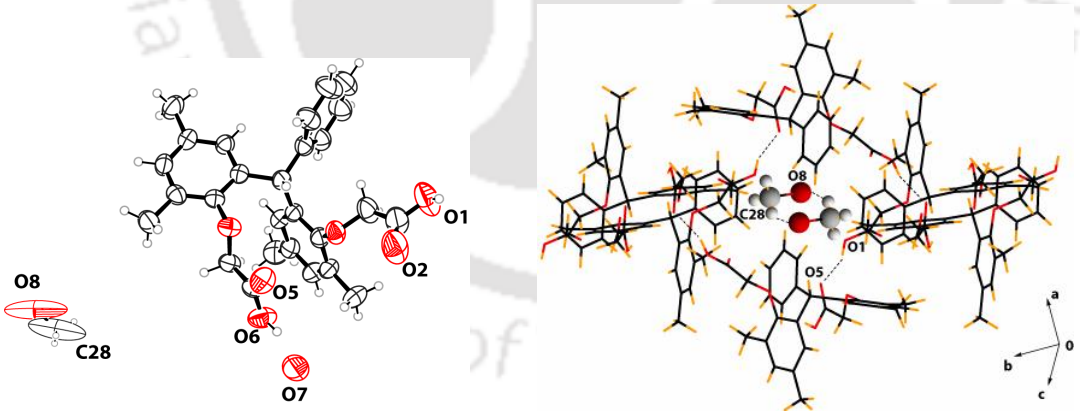

(a) **(b)**

Figure 5.4: (a) Asymmetric unit of the ligand H_2L^1 **(5.1)** (drawn with 30% thermal ellipsoids; hydrogen atoms of methanol and water are omitted), **(b)** Encapsulation of methanol molecules in the cavity formed by self assembly of **4.1**.

methanol and one water molecule**.** The methanol molecules are encapsulated in the cavities formed by the host molecules through various weak interactions as shown in the Figure **5.4b**. From the TG analysis it is seen that the water and methanol molecules losses at around 90°C.

On the other hand, **5.3** was crystallized from methanol in solvent free form. In the crystal structure, the molecules of **5.3** self assembles through two different types of $R_2^2(8)$-types of cyclic hydrogen bonds to give 1D polymeric chian (Figure **5.5b**). The nitro group at the ortho position of the third aromatic ring also involves in the formation of 1D hydrogen bonded chain. These types of 1D chain further self-assembles to each other through various weak interactions to 2D sheet-like structure (Figure **5.5b**). The selected hydrogen bond parameters of **5.1** and **5.3** are given in the Table **5.1**.

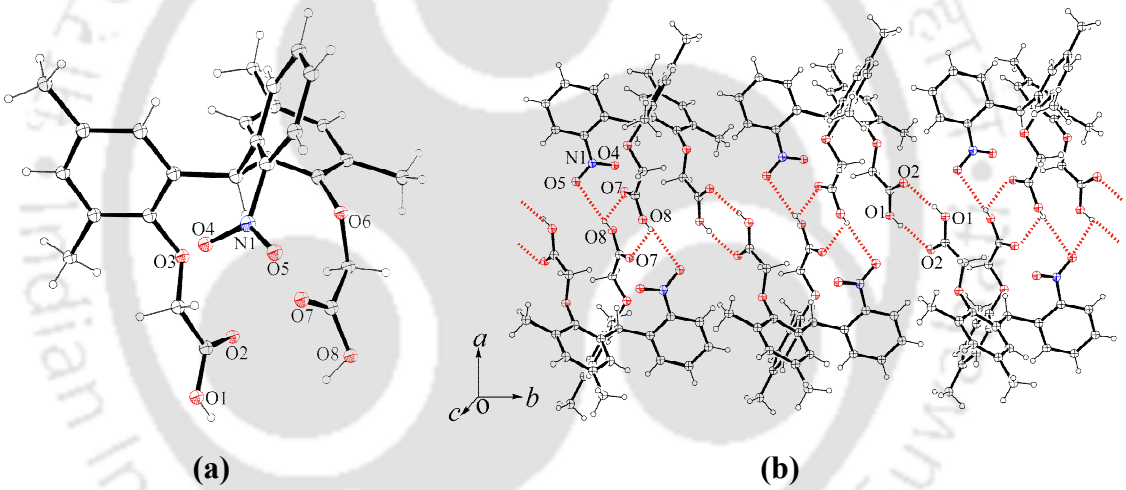

Figure 5.5: **(a)** Asymmetric unit of the ligand **5.3** (drawn with 30% thermal ellipsoids), **(b)** self assembling of ligand **5.3** through R_2^2 (8) type of cyclic hydrogen bonds.

5.3 Alkali metal complexes of H_2L^1 (5.1), H_2L^2 (5.2) and H_2L^3 (5.3)

5.3.1 Sodium, potassium and caesium coordination polymer of H_2L^1 (5.1):

The reaction of H_2L^1 with sodium acetate (or sodium hydroxide) and potassium acetate (or potassium hydroxide) at ambient condition results in the formation of

disodium salt $\{[Na_2L^1(\mu\text{-}H_2O)(H_2O)_3].H_2O\}_n$ **(5.1c)** and $[K_4(L^1)_2(\mu\text{-}H_2O)_2(H_2O)_2](H_2O)_n$ **(5.1d)** respectively**,** whereas a similar reaction with caesium acetate (or caesium carbonate) lead to mono deprotonated salt $[Cs(HL^1)(\mu\text{-}H_2O)(H_2O)]_n$ **(5.1e)**. We were able to crystallize the complexes **5.1c**, **5.1d** and **5.1e** and determined their crystal structures.

Table 5.1: Selected hydrogen bond parameters of **5.1** and **5.3**.

Compd No.	D-H···A	$d_{D\text{-}H(Å)}$	$d_{H\cdots A(Å)}$	$d_{D\cdots A(Å)}$	∠D-H···A(°)
5.1	O(1)-H(1)···O(5) [1-x,-1/2+y,3/2-z]	0.82	1.95	2.710(4)	155
	O(6)-H(6A)···O(7) [1-x,1/2+y,3/2-z]	0.85(4)	1.71(3)	2.537(5)	164(4)
	C(28)-H(28B)···O(8) [1-x,1-y,1-z]	0.96	1.38	2.050(15)	122
5.3	O(1)-H(1)···O(2) [-x,1-y,-z]	0.82	1.97	2.778(4)	168
	O(8)-H(8)···O(5) [-x,-y,-z]	0.82	2.36	2.977(6)	133
	O(8)-H(8) ···O(7) [-x,-y,-z]	0.82	2.44	3.026(6)	130

The crystallographic asymmetric unit of **5.1c** has two diaquated sodium ions attached to one dicarboxylate ligand (Figure **5.6a**). Each sodium ion is engaged in formation of chelate by coordination of one carboxylate group in mono-dentate binding mode and that of ethereal oxygen atom of the $-OCH_2-$ part on the ligand. One of the carboxylate group of the ligand acts as μ-O type of bridge between two sodium ions. These types of bridging mode of carboxylate O-atom was earlier observed in 2D sodium coordination polymer of 4-carboxy-TEMPO.[15] The coordination polymer **5.1c** has two types of sodium environment, namely one has five coordinate distorted square pyramidal and other has six coordinate anti-prism geometry as illustrated in Figure **5.6c**. It has a 2D-polymeric structure and the overall structure of the polymer has two aqua bridged sodium units forming $[Na_2(H_2O)_2]$-core. Such units are held together by another set of sodium ions which have five coordinated geometry. In addition to these, each dinuclear unit has one water molecule of crystallization which participates in hydrogen bonding between the chains of polymers resulting in self-assembled structure. The sodium ions are arranged as repeated hexanuclear units, each of which is in the form of chair like arrangement (Figure **5.6b**). The Na···Na distance in the dinuclear core $[Na_2(H_2O)_2]$ of the coordination polymer **5.1c** is 3.343 Å. These types of dinuclear $[Na_2(H_2O)_2]$ core was earlier observed in the coordination polymer of L-3-phenyl-2-(3-phenyl-ureido)-propanoic acid where the Na-Na distance is 3.470Å.[14] The sodium ions in disodium salt of terephthalic acid adopt prismatic structures.[16] In

the present case we observe combination of dinuclear and mononuclear units in the polymer; which may be attributed to originate from the flexibility of the ligand (L^1). Form the FT-IR of **5.1c**, it is seen that the carbonyl stretching frequency for the carboxylate C=O group appears at 1595 cm^{-1} and it indicates the binding of sodium by the carboxylate groups. In the ^{1}H-NMR of **5.1c** in DMSO-d_6, the methine proton

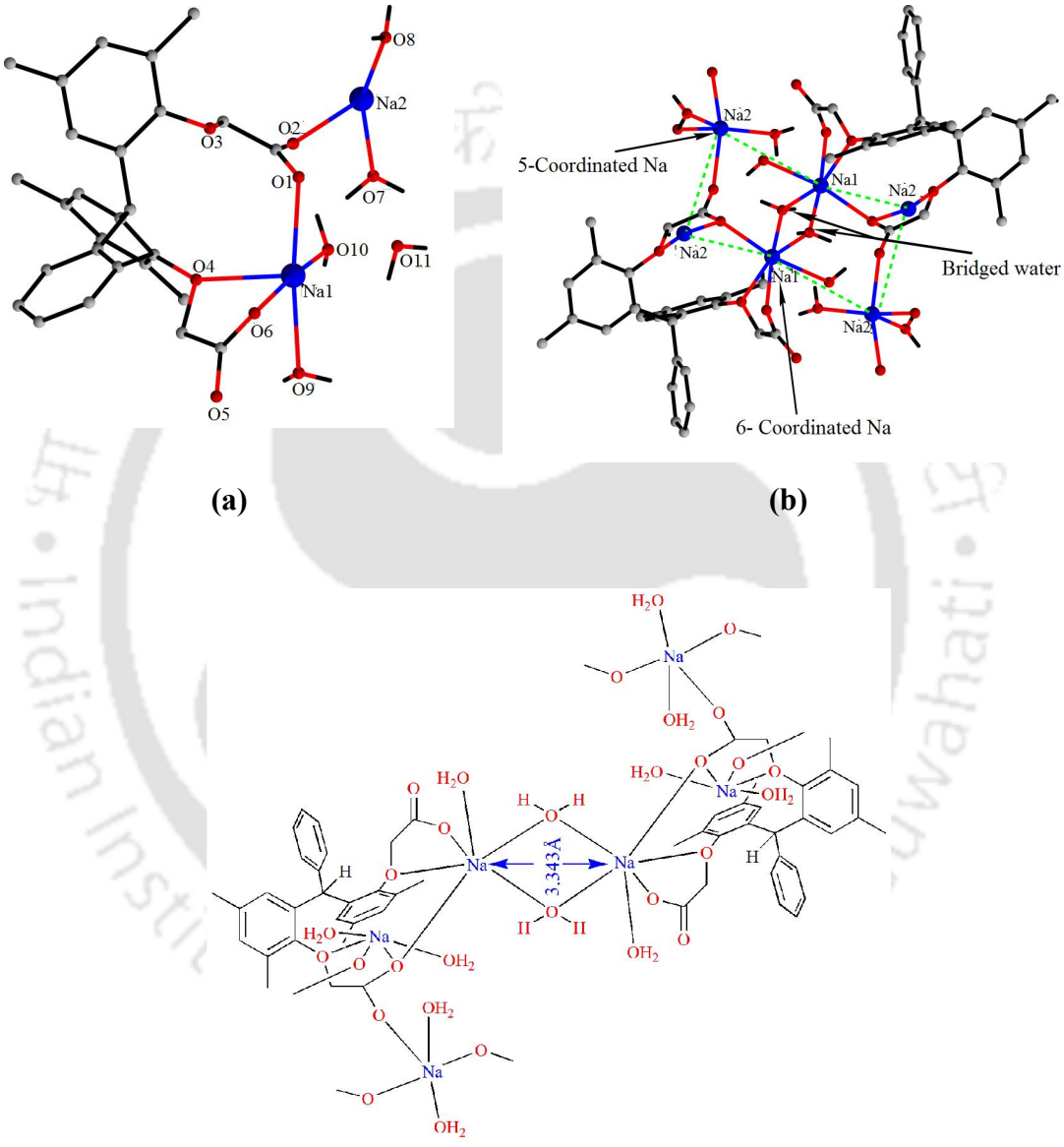

Figure 5.6: (a) Asymmetric unit of the sodium coordination polymer **5.1c**, **(b)** Connections between two hexacoordinate sodium ions in **5.1c**, **(c)** Coordination environment of the sodium atoms in the coordination polymer **5.1c**.

of *bis*-phenol appears at 6.38 ppm and it shows a slight down field shift compared to that of the parent ligand (Figure **5.15b**). From the TG analysis of the coordination polymer it is seen that the coordination polymer **5.1c** losses five water molecules in the temperature range of 45°C-105°C (theoretical weight loss 15.44% , experimental weight loss 13.27%, Figure **5.15a**).

The potassium salt of H_2L^1 **(5.1d)** crystallizes in monoclinic space group $P2_1/c$ and the crystallographic asymmetric is shown in the Figure **5.7a**. The salt **5.1d** is a 2D coordination polymer but has a completely different structure from that of sodium salt **5.1c**. However, the coordination modes of the two carboxylate arms of the ligand **5.1** are similar in the salts **5.1c** and **5.1d**. In the coordination polymer, we observed two different coordination environments for potassium ions; namely, one has six coordinated octahedral geometry and another has seven coordinated pentagonal bipyramidal geometry (Figure **5.7b**, **5.7c**). The two hexacoordinated potassium ions are bridged by two water molecules to form $[K_2(H_2O)_2]$ core. The K2···K2 distance in the dinuclear core is 3.352 Å. On the other hand, the hexacoordinated K2 and the hepta- coordinated K1 are connected by another bridging water molecule. The main difference between the two structures is different types of bridging water molecules. In case of the coordination polymer **5.1c** there is only one type of bridging water molecule, whereas coordination polymer **5.1d** has two different types of bridging water molecules. There are many examples of sodium and potassium complexes that are bridged by water molecules.[17] For example, *p-tert*-butylcalix[8] arene forms 1D coordination polymer with potassium where two different types of bridging water molecule were observed.[18] Moreover, there are some examples of sodium complexes, where two sodium ions were bridged by hydroxide,[19a] sulphide[19b] or perchlorate anions.[19c] The FT-IR spectra of the coordination polymer **5.1d** shows stretching frequency for the C=O group at 1591 cm^{-1} whereas it appears at 1741 cm^{-1} for the parent ligand indicating the coordination of the carboxylate group to metal. The ^{1}H-NMR of the potassium complex **5.1d** is slightly different from that of the ligand. For example, the signals at 7.03 ppm (d, J= 7.2 Hz, 2H) and 6.90 ppm (s, 2H) of H_2L^1 shifted to 7.12 ppm (d, J= 7.2 Hz, 2H) and 6.82 ppm (s, 2H) respectively on coordination to potassium ion. On the other hand, the methine proton of the potassium complex **5.1d** appears at 6.28 ppm whereas it appears at 6.18 ppm for the free ligand (Figure 5.**16b**). The coordination polymer **5.1d** shows 12.70 % (theoretical weight

loss 14.80 %, Figure **5.16a**) weight loss in the temperature range 40°C- 105°C due to the loss of five water molecules.

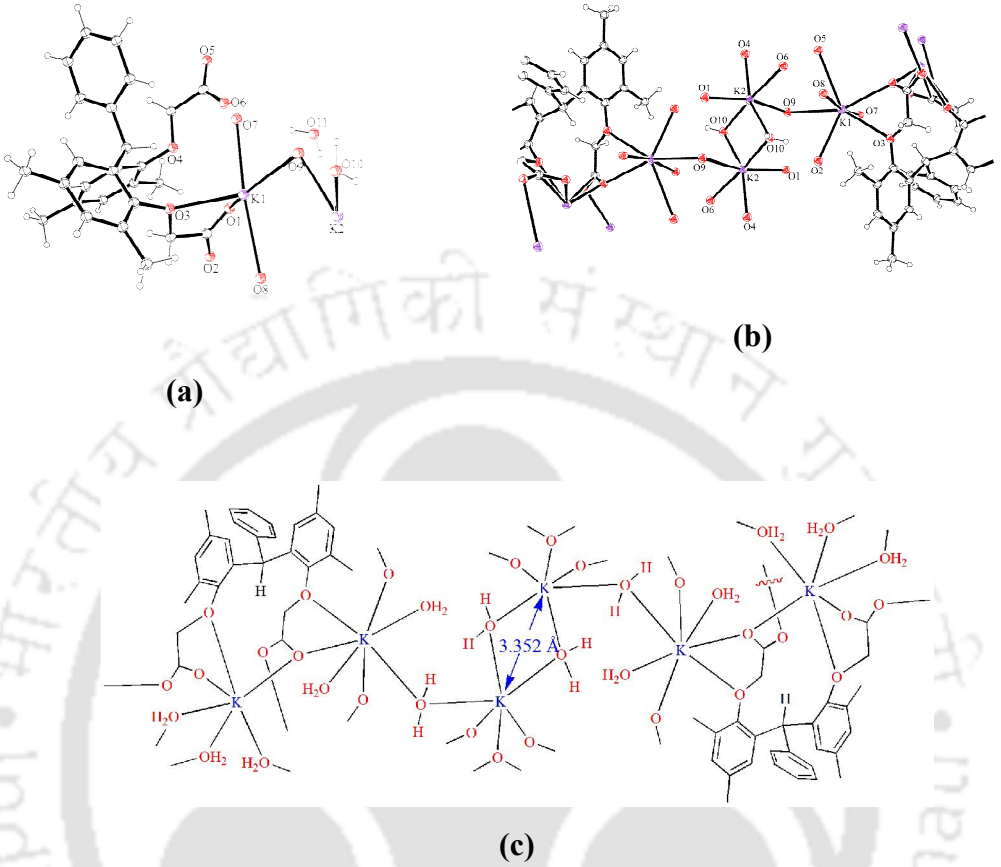

Figure 5.7: **(a)** Asymmetric unit of the coordination polymer **5.1d**, **(b)** Coordination environment of the potassium atom in the coordination polymer **5.1d, (c)** Structure of the coordination polymer **5.1d** showing two different types of bridging water molecules.

The caesium coordination polymer of H_2L^1 is comprised of mono deprotonated ligand and has composition $[Cs\ (HL)\ (\mu\text{-}H_2O)\ (H_2O)]_n$ **(5.1e)**. The coordination polymer **5.1e** has octa-coordinate caesium ions. The repeated unit of the coordination polymer **5.1e** is comprised of $[(HL)Cs(H_2O)_2]$, in which one carboxylic acid group binds in a monodentate fashion to corresponding caesium ion. On the other hand, each oxygen atoms of the other carboxylate group coordinate to two caesium ions (Figure **5.8c**). Thus, one of the carboxylate groups simultaneously holds four caesium ions. There is extensive bifurcated type of metal-oxygen bonds in each of the binuclear repeat units. The O5 and O6 of one of the carboxylate group simultaneously coordinates to two

caesium ion to form a dinuclear unit where the Cs···Cs distance is of 4.034Å. Moreover, each caesium ion of repeat unit is associated with one aqua bridge (Figure **5.8a**). The free carboxylic acid groups of different chains interact with each other through strong O2-H···O2 hydrogen bond interactions [$d_{D\cdots A}$=2.473 Å], providing additional supramolecular features. The caesium 1,2,4,5-benzenetetracarboxylate was earlier shown to possess very strong hydrogen bond interactions with close O···O separations.[20] The stretching frequency of the C=O group of the carboxylic acid appears at 1728 cm^{-1} and 1657 cm^{-1} which indicates the existence of both the

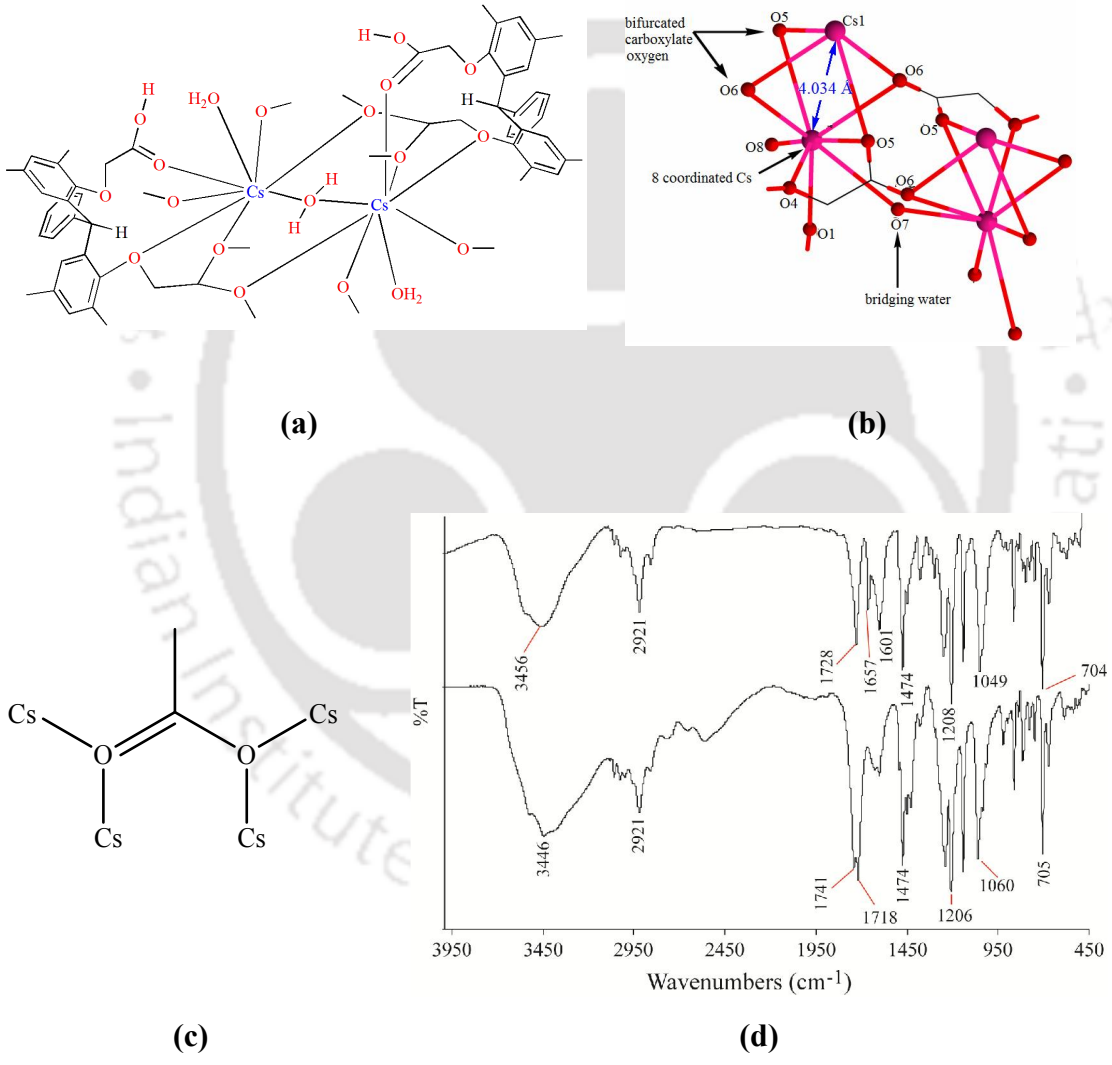

Figure 5.8: (a) Structure of the coordination polymer **5.1e**, **(b)** Coordination environments of the Caesium atom, **(c)** Bifurcated modes of coordination by carboxylate oxygen to caesium in **5.1e**, **(d)** Overlaid FT-IR spectra of ligand H_2L^1 **(5.1)** and Caesium complex **5.1e**.

carboxylate and free carboxylic acid group in the coordination polymer **5.1e** (Figure **5.8d**). From the ^{1}H-NMR of the caesium coordination polymer **5.1e** it is seen that the methine proton shows a downfield shift (from 6.18 ppm to 6.29 ppm) whereas the -CH_2O- protons show up-field shift (from 4.17 ppm to 3.89 ppm) compared to the

Table 5.2: Selected bond length and bond angles of the coordination polymer **5.1c**-**5.1e**.

Compnd. No.	M-L bond	Distance (Å)	< L-M-L	Angle (°)	< L-M-L	Angle (°)
5.1c	Na1- O4	2.404(2)	O10- Na1- O10	89.46(10)	O2 -Na2- O8	95.58(11)
	Na1- O1	2.448(2)	O10- Na1- O6	92.87(9)	O8- Na2 -O1	94.18(10)
	Na1 -O6	2.385(3)	O10- Na1- O4	108.68(9)	O2- Na2 -O3	88.79(9)
	Na1- O9	2.541(3)	O6 -Na1- O4	67.73(8)	O8- Na2- O3	103.05(10)
	Na1 -O10	2.344(3)	O10- Na1 -O1	80.59(9)	O1- Na2 -O3	65.34(8)
	Na2- O2	2.337(3)	O10 -Na1- O1	97.91(9)	O2 -Na2 -O7	94.64(10)
	Na2 -O8	2.364(3)	O6 -Na1- O1	106.65(9)	O8- Na2-O7	158.29(12)
	Na2- O1	2.410(2)	O4- Na1- O1	95.63(8)	O1- Na2 -O7	84.86(10)
	Na2- O7	2.595(3)	O10 -Na1- O9	85.76(11)	O3- Na2- O7	96.26(9)
	Na2- O3	2.425(2)	O6 -Na1- O9	87.02(10)	O4 -Na1- O9	89.46(9)
5.1d	K1- O2	2.693(4)	O2- K1- O7	98.85(14)	O1- K1- O5	85.13(11)
	K1 -O7	2.705(5)	O7 -K1- O1	85.13(14)	O8 -K1 -O5	73.04(13)
	K1- O1	2.732(4)	O2 -K1 -O3	82.09(11)	O9 -K1- O5	72.01(11)
	K1 -O3	2.801(4)	O7 -K1- O3	89.95(14)	O10- K2 -O10	89.61(15)
	K1- O8	2.864(5)	O1 -K1- O3	56.48(10)	O10- K2- O6	91.45(15)
	K1- O9	3.057(4)	O2- K1- O8	89.87(14)	O4 -K2 -O6	66.92(13)
	K1- O5	3.061(4)	O1- K1- O8	89.51(13)	O10- K2- O1	96.66(15)
	K2- O10	2.377(4)	O3- K1- O8	93.02(12)	O4 -K2- O1	93.93(13)
	K2- O4	2.399(4)	O2- K1 -O9	70.47(11)	O6 -K2- O1	109.86(15)
	K2 -O6	2.413(4)	O7- K1- O9	78.99(13)	O10- K2- O9	83.58(15)
	K2- O1	2.417(4)	O8- K1- O9	102.49(12)	O4- K2 -O9	92.71(14)
	K2- O9	2.571(5)	O7 -K1- O5	99.37(14)	O6- K2- O9	86.69(15)
5.1e	Cs1- O1	3.056(7)	O1- Cs1 -O6	122.4(2)	O7- Cs1 -O5	146.07(12)
	Cs1- O6	3.119(5)	O6- Cs1 -O7	72.89(16)	O5- Cs1- O5	105.26(11)
	Cs1- O7	3.197(4)	O6- Cs1- O5	76.68(13)	O4- Cs1 -O5	117.11(12)
	Cs1- O5	3.266(5)	O7 -Cs1- O5	65.64(18)	O6- Cs1- O8	117.4(3)
	Cs1- O4	3.325(4)	O1- Cs1- O4	95.09(16)	O7 -Cs1- O8	104.7(4)
	Cs1 -O8	3.452(15)	O7 -Cs1- O4	81.64(11)	O4- Cs1- O8	137.6(3)
			O6- Cs1- O5	74.92(12)		

free ligand (Figure **5.17b**). The caesium coordination polymer **5.1e** losses two water molecules in the temperature range of 40°C-113°C (theoretical weight loss 5.90 %, experimental weight loss 4.80 %, Figure **5.17a**). The selected bond length and bond angles of the complex **5.1c-5.1e** are given in the table **5.2**.

5.3.2 Sodium and caesium coordination polymer of H_2L^2 (5.2):

In case of the ligand **5.2,** we obtained single crystal of sodium complex (**5.2c**) and caesium complex (**5.2d**). But we did not obtained any single crystal of the potassium salt of the ligand H_2L^2 (**5.2**). The disodium salt (**5.2c**) of H_2L^2, has a composition $[\{Na_2L^2\ (\mu\text{-}H_2O)\ (H_2O)_3\}.H_2O]_n$. It is a two dimensional coordination polymer and the repeat units are comprised of two sodium ions. One sodium ion is pentacoordinate with square pyramidal geometry and the other is hexacoordinate with distorted octahedral geometry (Figure **5.9**). Both the ethereal oxygen atoms of the ligand form coordinate bonds with the metal ions. Ethereal oxygen atoms play key roles to provide the dimensionality to coordination polymers of alkali metal carboxylates.[21] In this case also the coordination of ethereal oxygen provides a definite direction to the ligand. The coordination polymer **5.2c** has bridging as well as monodentate water molecules in the coordination spheres. The fluorine atoms in this case do not interact with sodium ions. The selected bond lengths and bond angles of the complex are given in the Table **5.3**. There is similarity of the coordination polymer **5.1c** with **5.2c**, both possess diaqua bridged sodium dimers. From the TG of coordination polymer

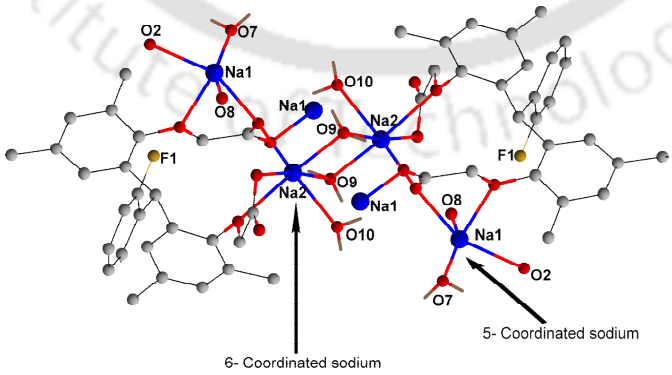

Figure 5.9: The structure of the coordination polymer **5.2c** showing the coordination environments of the sodium atoms.

5.2c, we observed that it losses the five water molecules at around 50°C-100°C (theoretical weight loss 15.0%, experimental eight loss 13.0%, Figure **5.19a**). From the ^{1}H-NMR of the complex **5.2c** it is seen that the peak for methyl protons appears at 2.10 ppm and 2.14 ppm whereas the signal for the methine proton appears at 6.29 ppm (Figure **5.19b**).

The caesium salt of H_2L^2 is also a coordination polymer, it has composition $[\{(H_2O)Cs(\mu\text{-}H_2O)_2(\mu\text{-}L^2)Cs(H_2O)_2\}]_n$ (**5.2d**). The crystal structure of this coordination polymer shows two types of environment for caesium ions which are either hexacoordinate or nonacoordinate (Figure **5.10b** and **5.10c**). The hexacoordinated caesium atoms involves in the formation of dinuclear $[Cs_2(H_2O)_2]$ core where the Cs···Cs distance is 4.428 Å. Generally, the Cs···Cs distance in any other reported systems are in the range of 3.84-4.66 Å.[22] The hexacoordinate caesium ion adopts antiprism type geometry. Another interesting feature of the coordination polymer is the presence of Cs···F-C coordination bond. The coordination polymer **5.2d** losses the water molecules at around 32°C-182°C (theoretical weight loss 6.9%, experimental eight loss 4.5%, Figure **5.20a**). The ^{1}H-NMR of the caesium coordination polymer **5.2d** has signal for the methine proton of the ligand at 6.39 ppm; whereas the signals for the aromatic protons of the methyl containing aromatic rings appear at 6.37 and 6.85 ppm. Two singlets for the methyl groups appear at 2.10 and 2.14 ppm; whereas another singlet due to the -CH_2O- appears at 3.48 ppm (Figure **5.20b**). The caesium complex **5.2d** shows ^{19}F-NMR resonance at -117.31 ppm (Figure **5.20c**) whereas the ligand has signal at -118.18 ppm, this indicates coordination of the fluorine atom of C-F bond and thus it undoubtedly acts as a donor toward the caesium cation.

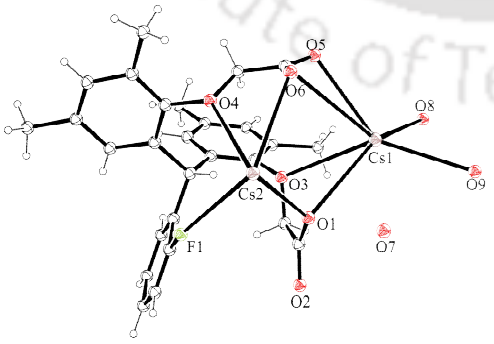

(a)

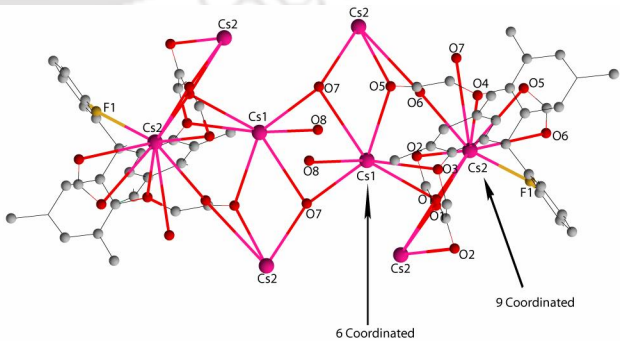

(b)

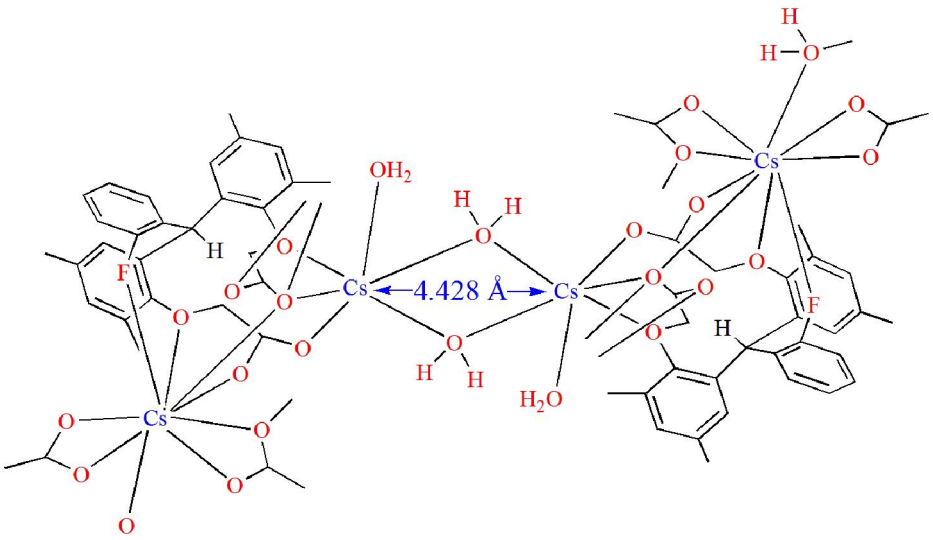

(c)

Figure 5.10: **(a)** the asymmetric unit of the caesium coordination polymer **5.2d**, **(b)** Coordination environments of the two caesium atom in the coordination polymer **5.2d**, **(c)** The structure of the coordination polymer **5.2d**.

5.3.3 Potassium coordination polymer of H_2L^3 (5.3):

In case of the ligand **5.3**, we did not obtain suitable single crystal of the sodium and caesium complex. However, we obtained single crystals of the potassium salt (**5.3c**) of the ligand **5.3** having compositions $[K_2L^3(H_2O)]_n$ and it is a two dimensional coordination polymer. The coordination polymer has two different coordination environments for potassium; these are seven (K2) and eight (K1) coordination

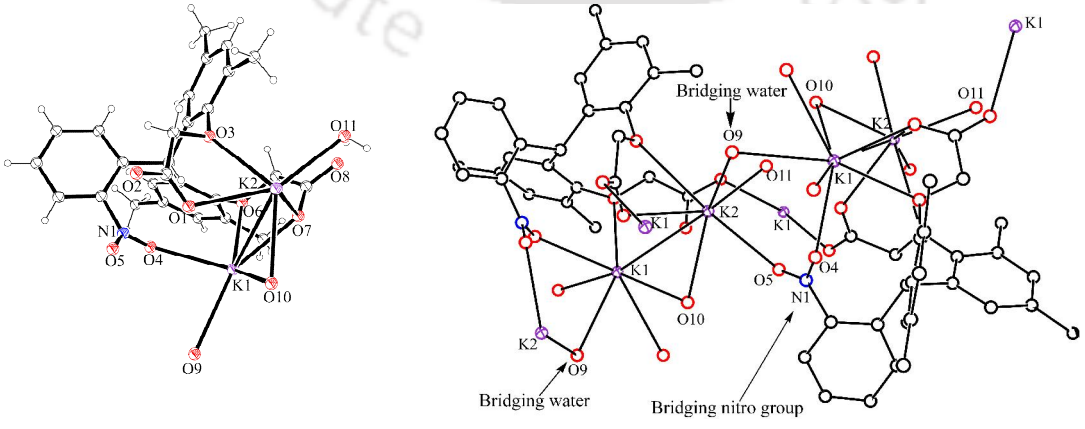

(a) **(b)**

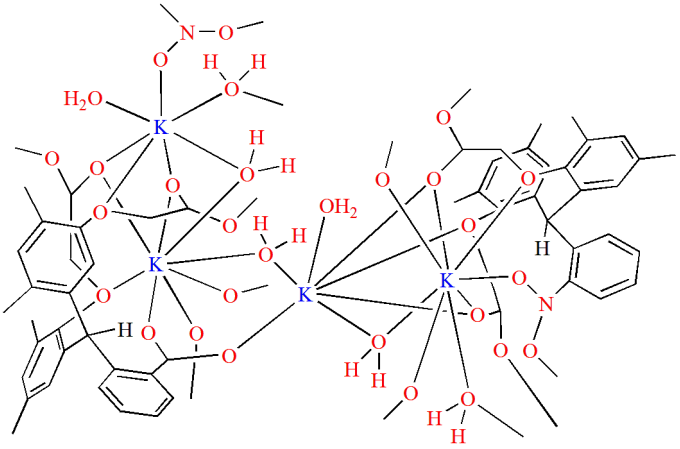

(c)

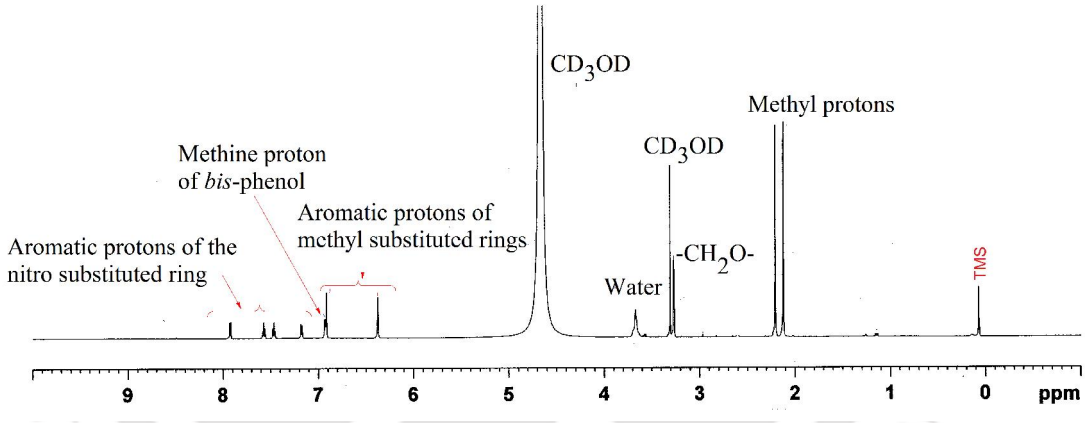

(d)

Figure 5.11: **(a)** Asymmetric unit of the coordination polymer **5.3c**, **(b)** Bridging nitro group and the water molecules in the coordination polymer **5.3c**, **(c)** The structure of the coordination polymer **5.3c**, **(d)** The ^{1}H-NMR of the potassium complex **5.3c** (methanol-d_4, 600 MHz).

geometry (Figure **5.11b**). The interesting feature of the coordination polymer **5.3c** is the coordination of the nitro group present at the ortho-position of the aromatic ring. The nitro group along with a water molecule act as a bridge between two potassium ions K1 and K2. Two different types of bridging water molecule were observed between K1 and K2. The two ethereal oxygen atoms of the ligand H_2L^3 coordinated to two different metal centres. The coordination polymer **5.3c** losses 8.17 % (theoretical

weight loss 8.71%) of its weight at around 55°C-135°C due to the removal of three water molecules (Figure **5.22**). From the FT-IR of the coordination polymer **5.3c** it is

Table 5.3: Selected bond angles and bond lengths of **5.2c**, **5.2d** and **5.3c**.

Compd. No.	M-L	d_{M-L} (Å)	<L-M-L	Angle (°)	<L-M-L	Angle (°)
5.2c	Na1-O2	2.352(5)	O1- Na1- O8	93.46(17)	O9- Na2- O9	89.86(18)
	Na1- O8	2.372(5)	O2- Na1 -O3	86.93(17)	O5- Na2- O4	67.89(15)
	Na1 -O1	2.401(5)	O3- Na1- O8	105.11(17)	O9- Na2 -O1	98.79(17)
	Na1- O7	2.526(6)	O1 -Na1- O3	65.14(16)	O5- Na2- O1	106.07(17)
	Na1- O3	2.433(5)	O2 -Na1 -O7	95.8(2)	O4 -Na2- O1	95.17(16)
	Na2 -O9	2.342(5)	O1 -Na1 -O7	85.44(19)	O9- Na2-O10	86.17(19)
	Na2- O5	2.377(5)	O3- Na1- O7	96.15(17)		
	Na2- O4	2.406(4)	O5- Na2- O10	86.97(18)		
	Na2- O1	2.438(4)	O4 -Na2- O10	89.24(16)		
	Na2- O10	2.529(5)	O9-Na2-O10	80.62(18)		
5.2d	Cs2- O1	3.065(9)	O9 -Cs1- O8	71.0(3)	O6- Cs2- O2	84.99(18)
	Cs2 -O1	3.146(7)	O9- Cs1- O1	109.3(3)	F1 -Cs2- O2	151.67(17)
	Cs2 -O6	3.223(9)	O8- Cs1- O1	137.1(2)	O5- Cs2- O2	106.8(2)
	Cs2 -O4	3.231(5)	O9- Cs1- O3	138.7(2)	O6 -Cs2- O6	122.47(8)
	Cs2 -F1	3.275(6)	O5- Cs1 -O3	78.38(19)	O4- Cs2- O6	97.80(17)
	Cs2 -O5	3.329(10)	O8 -Cs1- O3	102.2(2)	O2- Cs2- O6	99.75(19)
	Cs2 -O2	3.332(8)	O1- Cs1- O9	151.8(3)		
	Cs2 -O6	3.516(9)	O1- Cs1- O8	118.2(2)		
	Cs2 -O9	3.637(13)	O3 -Cs1-O8	154.57(17)		
	Cs2- O7	3.782(12)	O1 -Cs2- O6	88.4(2)		
	Cs1- O9	3.075(10)	O1- Cs2 -O6	114.8(2)		
	Cs1 -O5	3.101(10)	O1 -Cs2- F1	72.8(2)		
	Cs1 -O8	3.146(9)	O1 -Cs2-F1	112.8(2)		
	Cs1- O1	3.211(9)	O6- Cs2- F1	121.22(17)		
	Cs1- O3	3.274(6)	O4- Cs2- F1	75.66(14)		
	Cs1-O9	3.447(11)	F1- Cs2- O5	86.92(19)		
	Cs1- O8	3.705(10)	O1- Cs2- O2	99.7(2)		
5.3c	K1-O7	2.684(2)	O7- K1- O8	121.00(8)	O9 -K2- O10	130.94(9)
	K1-O8	2.730(2)	O8 –K1 -O6	78.42(6)	O11- K2 -O3	94.31(7)
	K 1-O6	2.8037(19)	O4- K1 -O9	83.78(8)	O10- K2 -O3	121.69(9)
	K1-O4	2.867(4)	O6 -K1- O10	128.43(8)		
	K1- O9	2.991(3)	O7 -K1- O2	93.44(8)		
	K1-O10	2.993(4)	O8 -K1 -O2	97.13(8)		
	K1-O2	3.005(3)	O6 -K1- O2	138.10(8)		
	K1-O1	3.367(3)	O6 -K1 -O1	91.55(6)		
	K2-O1	2.716(3)	O9 -K1 -O1 O1	100.74(7)		
	K2-O11	2.736(3)	-K2- O5	129.86(13)		
	K2-O5	2.802(4)	O11- K2- O5	82.68(13)		
	K2-O7	2.819(2)	O1- K2- O7	95.98(9)		
	K2-O9	2.839(2)	O5- K2 -O7 O1	100.41(12)		
	K2-O10	2.849(3)	-K2- O9	89.00(9)		
	K2-O3	3.0779(19)	O5- K2- O9	96.14(11)		

seen that the carbonyl stretching frequency appears at 1624 cm^{-1}. In the ^{1}H-NMR (Figure **5.11d**) of the coordination polymer **5.3c** the methine proton appears at 6.93 ppm and whereas it appears at 6.53 ppm for the free ligand. However, we did not obtain single crystal of any of the alkali metal complexes with the ligand H_2L^4 **(5.4)**.

5.4 Discussion:

From the above studies it was seen that the unsubstituted ligand H_2L^1 forms 2D coordination polymers with sodium and potassium whereas it forms mono deprotonted 1D polymeric salt with caesium ion. The use of ligand to metal 1:2 or 1:1 stoichiometry at room temperature gave the same result. This showed that the complete deprotonation of the ligand was easily achieved by sodium or potassium ions, which is not the case with caesium ions. This types of mono-deprotonted 1D coordination polymer was observed in caesium coordination polymer of 2,6-dipicolinic acid.[13] In case of the caesium dipicolinic acid complex the coordination number of caesium was nine, whereas in the present case it is found to be eight coordinated. On the other hand, sodium and potassium form discrete mononuclear and dinuclear complex with 2, 6-dipicolinic acid, but ligand **5.1** forms 2D coordination polymer in both the cases (Figure **5.12**).

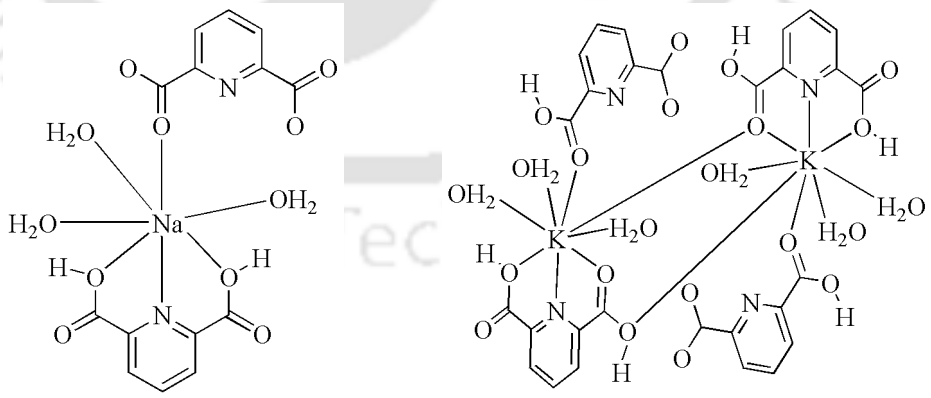

(a) **(b)**

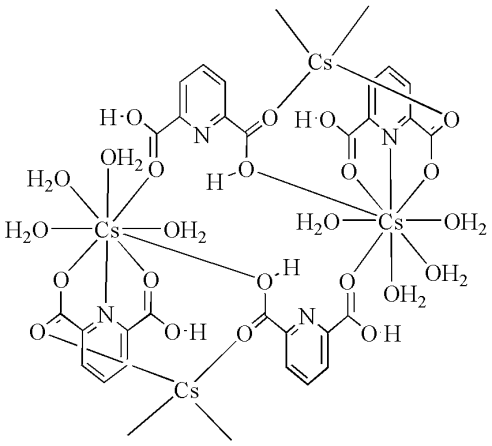

(c)

Figure 5.12: The structure of the mono-deprotonated **(a)** Sodium, **(b)** Potassium and **(c)** caesium complex of 2, 6-dipicolinic acid.

Both the sodium and caesium complexes of H_2L^2 are two 2D coordination polymers. The structures of the sodium polymer **5.1c** and **5.2c** have similar structures. There was no sodium-fluorine interaction observed in case of the sodium coordination polymer **5.2c**. However, in case of the caesium complex **5.2d** of the fluoro-substituted ligand we have observed interesting types of Cs···F-C interactions where the Cs···F distance is 3.275 Å. It may be noted that the M···F-C coordination bond in metal complexes were used to encapsulate alkali metal cations.[23] The C-F···M type coordination mode is rarely encountered, they are generally observed in solid state to meet steric demand of ligands to have closed packed structures.[23b-e, 24] However, there are examples of some exceptional cases on the observation of C-F···M interactions in solution state.[25]

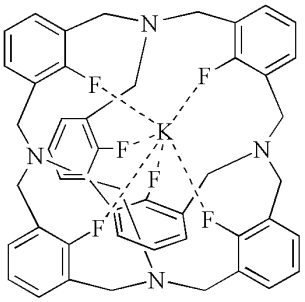

Figure 5.13: K···F-C interaction in a macrocyclic cage compound.

Takemura et. al. had reported the C-F···K interactions in the fluorinated macrocyclic cage compound (Figure **5.13**) where the K···F distance was found to be in the range of 2.704- 2.920 Å.[25d]

On the other hand, in the coordination polymer **5.3c** the nitro group bridges two potassium ions (Figure **5.14a**). Barium complex of 2-nitrobenzoate shows the coordination of the nitro group to the metal.[26] In the caesium complex of 3,5-dihydroxy-2,4,6-trinitrophenolate the nitro groups coordinate to the caesium ions (Figure **5.12b**).[27] In this compound, each caesium ions are coordinated to 12 oxygen atoms from eight different 3,5-dihydroxy-2,4,6-trinitrophenolate (DHTNP) anions, and each DHTNP-anion coordinates with eight caesium cations. The oxygen atoms of the phenolic hydroxyl group and from all of the nitro groups of the DHTNP-anion simultaneously bind to neighbouring caesium ions.

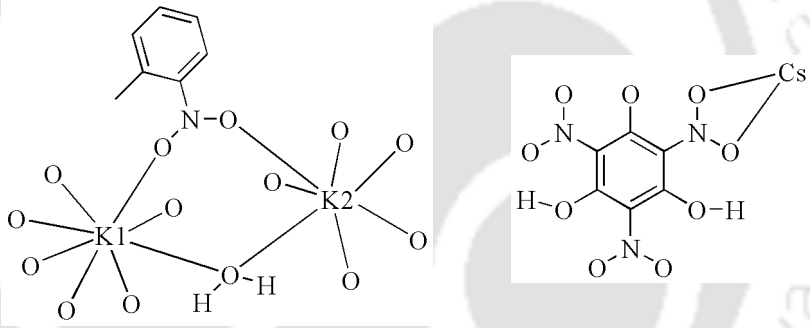

Figure 5.14: (a) The bridging coordination modes of the nitro group in the ligand H_2L^3 **(5.3)** with potassium ion, **(b)** coordination of the nitro group in different 3, 5-dihydroxy-2, 4, 6-trinitrophenolate (DHTNP) anions to caesium ion.

5.5 Conclusion:

From the structural studies of the ligands H_2L^1 **(5.1)** and H_2L^3 **(5.3)** it is seen that they have pincer type of arrangements in solid state. The coordination abilities of H_2L^1, H_2L^2 and H_2L^3 towards sodium, potassium and caesium ions were investigated. It was found that changing the substituents on the ligands or changing the respective alkali metal cation causes large difference among the structures of the alkali metal

coordination polymers. For example, the unsubstituted ligand H_2L^2 forms 2D coordination polymer with sodium and potassium, whereas it forms mono-deprotonatd 1D polymeric chain with caesium ion irrespective of the metal ligand ratio used in the reactions. On the other hand, fluoro-substituted ligand H_2L^2 **(5.2)** forms 2D coordination polymer of caesium, whereas the similar reaction of the unsubstituted ligand gives a 1D mono-deprotonated coordination polymer of caesium**.** We have shown the coordination of fluorine atom of a covalently linked C-F bond to caesium ion is a rare finding, which were generally observed in solid state to meet the steric demands. The coordination of the nitro group to potassium in a bridging fashion is an important observation. This type of the coordination of nitro group to potassium was also observed in the nitro substituted urea based tripodal receptor where the nitro groups coordinated to potassium ions bounded by crown ether to form 1D polymeric salt. These observations suggest there is a need to strengthen structural studies on alkali metal carboxylates.

5.6 Experimental Section:

Synthesis of H_2L^1 (5.1): The 2-[(2-hydroxy-3, 5-dimethylphenyl)(phenyl)methyl]-4, 6-dimethylphenol **(5.1a)** (1.62 g, 5 mmol) was dissolved in dry acetone (30 mL). To the reaction mixture, K_2CO_3 (1.38 g, 10 mmol) was added and stirred for 20 min. Then methylbromoacetate (0.95 mL, 10 mmol) was added and refluxed at 60°C for 22 h (progress of the reaction was monitored at regular intervals using TLC). After completion of the reaction, the reaction mixture was filtered; the solvent from the filtrate was removed under reduced pressure to obtain the crude product which was further purified by column chromatography (silica gel; hexane/ethyl acetate) to obtain pure **5.1b**. Isolated yield: 78%. Compound **5.1b** (2.38 g, 5 mmol) and sodium hydroxides (0.48 g, 12 mmol) were dissolved in mixed methanol: water (4: 1, 20 mL) and refluxed for 1 h at 60 °C. After completion of the reaction, the solvent was removed under reduced pressure, then 10 mL of water was added and the solution was acidified with dilute hydrochloric acid (20 mL, 10%) solution. A white solid H_2L^1 was obtained on acidification. The solid was filtered and washed with water until it was free from the acid. The product was isolated as a white solid and was further purified by recrystallizing from methanol. Isolated yield: 59% based on diester. IR

(KBr, cm^{-1}): 3440 (bs), 2926 (s), 2857 (w), 1741 (s), 1718 (s), 1602(s), 1493 (m), 1473 (m), 1404 (w), 1300 (w), 1207 (s), 1138 (s), 1094 (s), 1063 (s), 872 (w), 824 (s), 803 (w), 702 (w), 685 (w), 605 (w); ^{1}H-NMR (DMSO-d_6, 400 MHz): 7.27 (t, J= 7.2 Hz, 2H); 7.19 (*t*, J= 7.6 Hz, 1H); 7.03 (d, J= 7.2 Hz, 2H); 6.90 (*s*, 2H); 6.43 (s, 2H); 6.18 (s, 1H); 4.13 (s, 4H); 2.16 (s, 3H); 2.11 (s, 3H); ^{13}C-NMR (DMSO-d_6, 100 MHz): 170.3, 152.5, 143.6 136.4, 132.4, 130.4, 130.3, 129.2, 128.2, 126.2, 69.3, 43.1, 20.7, 15.9. LCMS (m/e) [M-1]: 447.09.

Synthesis of $\{[Na_2L^1(\mu\text{-}H_2O)(H_2O)_3)].H_2O\}_n$ (5.1c): To a well stirred solution of H_2L^1 (0.224 g, 0.5 mmol) in methanol (10 mL), 0.4 g of sodium acetate (1 mmol) was added. The reaction mixture was stirred for 30 min and a colorless transparent liquid obtained. This was kept undisturbed for crystallization. After 5 days colorless crystals **5.1a** appeared. Isolated yield: 60 %. IR (KBr, cm^{-1}): 3444 (s), 2924 (m), 1595 (s), 1470 (m), 1413 (s), 1325 (m), 1294 (w), 1240 (w), 1202 (m), 1140 (m), 1030 (s), 932 (w), 860 (w), 823 (w), 776 (w), 749 (w), 706 (m). Elemental analysis Calculated for $[Na_2L^1(H_2O)_5]_n$, Calculated: C, 55.48; H, 6.55; Found: C, 55.39, H, 6.62. ^{1}H-NMR (400 MHz, DMSO-d_6): 7.25 (t, J= 7.2 Hz, 2H). 7.18 (t, J= 7.2 Hz, 1H), 7.13 (d, J= 7.2 Hz, 2H), 6.50 (s, 2H), 6.81 (s, 2H), 3.47 (s, 2H), 6.38 (s, 1H), 3.43 (s, 2H), 2.11 (s, 12H).

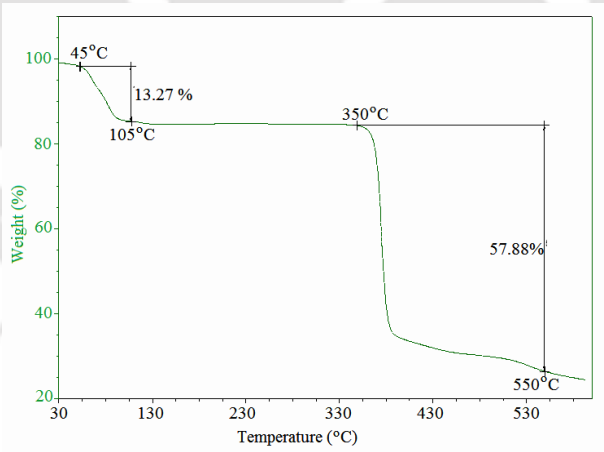

(a)

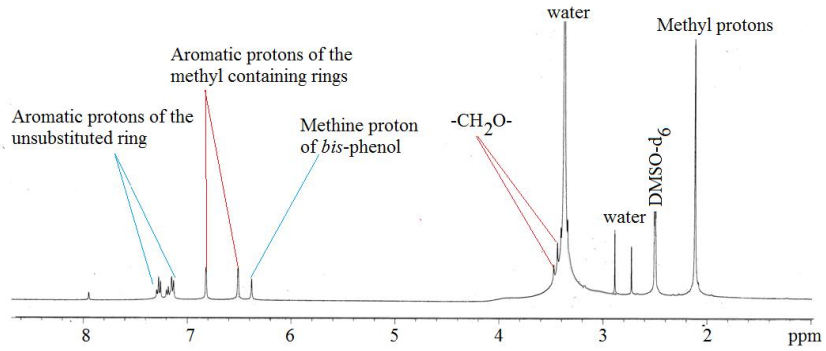

(b)

Figure 5.15: (a) TG of the sodium coordination polymer **5.1c, (b)** ^{1}H-NMR of the coordination polymer **5.1c** (DMSO-d_6, 400 MHz).

Synthesis of $[K_4(L^1)_2(\mu\text{-}H_2O)_2(H_2O)_2](H_2O)_n$ (5.1d): To a well stirred solution of ligand H_2L^1(0.9 g, 2 mmol) in dimethylformamide, potassium hydroxide (4 mmol) was added. The reaction mixture was stirred for another half an hour to dissolve it and then filtered to remove any solid impurity. The transparent liquid was kept for crystallization. After one week colorless block crystals of **5.1b** were obtained. Isolated yield 65%. IR (KBr, cm^{-1}): 3400 (s), 2921 (m), 1591 (s), 1467 (m), 1448 (m), 1416 (s), 1327 (m), 1297 (w), 1239 (w), 1212 (m), 1140 (m), 1033 (s), 933 (w), 861 (w), 779 (w), 946 (w), 706 (m). Elemental analysis Calculated for $[K_2L^1(H_2O)_5]_n$, Calculated: C, 52.58; H, 6.21; Found: C, 52.62, H, 6.16. ^{1}H-NMR (DMSO-d_6, 400 MHz): 7.27 (t, J= 8.0 Hz, 2H), 7.17 (d, J= 7.2 Hz, 1H), 7.12 (d, J= 7.2 Hz, 2H), 6.82 (s, 2H), 6.46 (s, 2H), 6.28 (s, 1H), 3.22 (s, 2H), 3.28 (s, 2H), 2.11 (s, 12H).

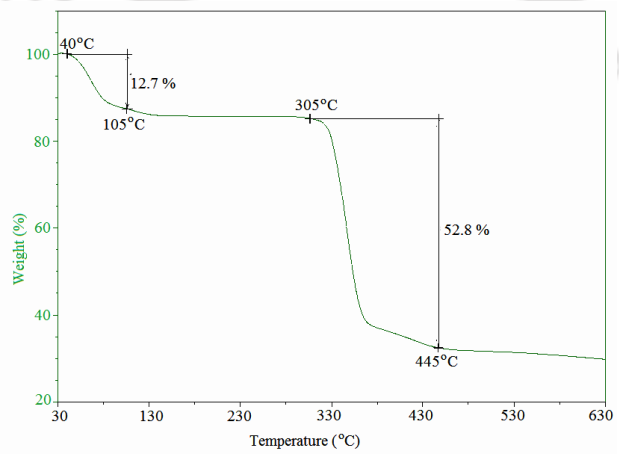

(a)

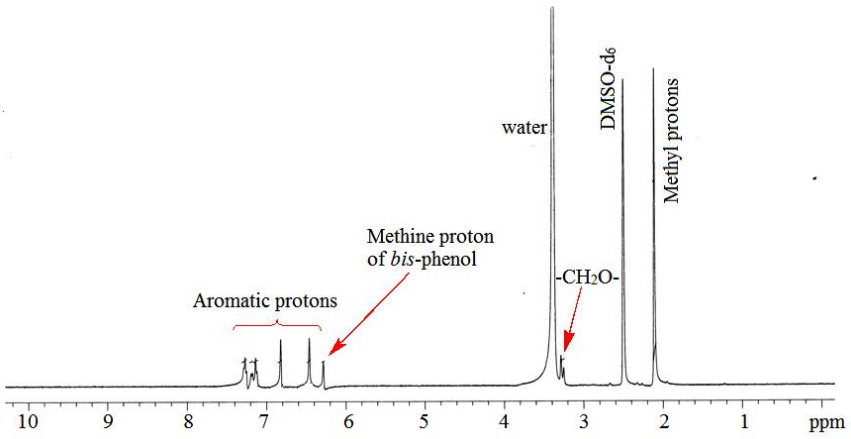

(b)

Figure 5.16: (a) TG of the potassium coordination polymer **5.1d, (b)** ^{1}H-NMR of the coordination polymer **5.1d** (DMSO-d_6, 400 MHz).

Synthesis of $[Cs(HL^1)(\mu\text{-}H_2O)(H_2O)]_n$ (5.1e): To a well stirred solution of H_2L^1 (0.224 g, 0.5 mmol) in methanol (10 mL), 0.2 g of caesium acetate (1 mmol) was added. The reaction mixture was stirred for 30 min and a colorless transparent liquid obtained. This was kept undisturbed for crystallization. After one week colorless crystals of **5.1b** appeared. Isolated yield: 55 %. IR (KBr, cm^{-1}): 3456 (s), 2921 (s), 1728 (s), 1657 (s), 1601 (s), 1474 (m), 1378(w), 1298 (w), 1206 (s), 1140 (s), 1049 (s), 862 (m), 704 (s); Elemental analysis Calculated for $[CsHL^1(H_2O)_2]_n$, Calculated: C, 52.52; H, 5.22; Found: C, 52.58, H, 5.12. ^{1}H-NMR (400 MHz, DMSO-d_6): 7.24 (t, J= 7.6 Hz, 2H), 7.16 (t, J= 7.2 Hz, 1H), 7.02 (d, J= 7.6 Hz, 2H), 6.85 (s, 2H), 6.44 (s, 2H), 6.29 (s, 1H), 3.89 (s, 4H), 2.14 (s, 6H), 2.10 (s, 6H).

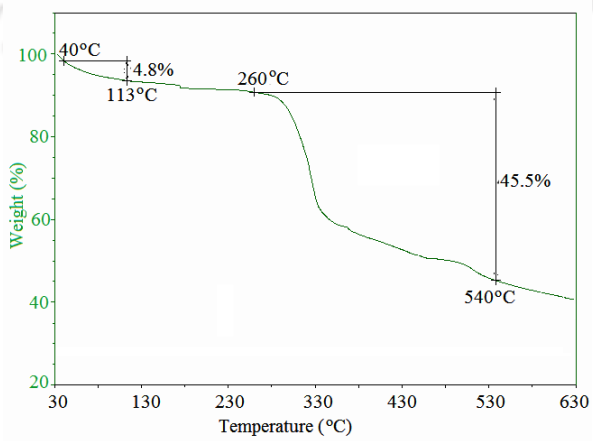

(a)

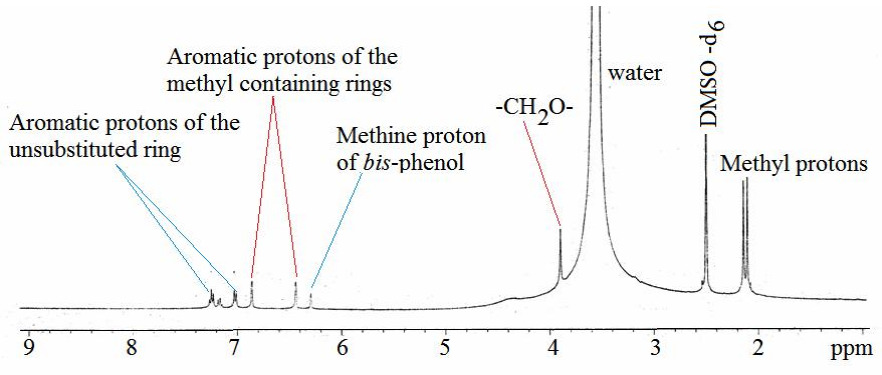

(b)

Figure 5.17: (a) TG of the caesium coordination polymer **5.1e. (b)** ^{1}H-NMR of the coordination polymer **5.1e** (DMSO-d_6, 400 MHz).

Synthesis of H_2L^2 (5.2): Ligand **5.2** was synthesized by a similar procedure adopted for ligand H_2L^1 **(5.1)** and it was prepared starting from bis-phenol **5.2a**.Isolated yield: 72%. IR (KBr, cm^{-1}): 3435 (s), 2922 (s), 2549 (w), 1739 (s), 1610 (w), 1584 (w), 1476 (s), 1454 (s), 1377 (w), 1226 (s), 1208 (s), 1143 (s), 1094 (w), 1062 (s), 861 (m), 841 (w), 822 (w), 757 (s), 671 (s), 582 (s). LCMS (m/e) [M+ Na^+]: 488.16. ^{1}H-NMR (DMSO-d_6, 400 MHz): 7.26 (dd, J= 7.2 Hz, 5.2 Hz, 1H), 7.11 (d, J= 7.2 Hz, 1H), 7.10 (d, J= 7.2 Hz, 1H), 6.92 (s, 2H), 6.77 (t, J=8 Hz, 1H), 6.39 (s, 2H), 6.34 (s, 1H), 4.02 (s, 4H), 2.16 (s, 6H), 2.12 (s, 6H). ^{13}C-NMR (DMSO-d_6, 100 MHz): 169.8, 152.3, 134.8, 132.8, 130.8, 130.5, 130.3, 128.5, 127.9, 124.0, 115.4, 115.2, 68.9, 39.1, 20.6, 15.9; ^{19}F-NMR (DMSO-d_6): -118.18 (using C_6F_6 as internal reference)

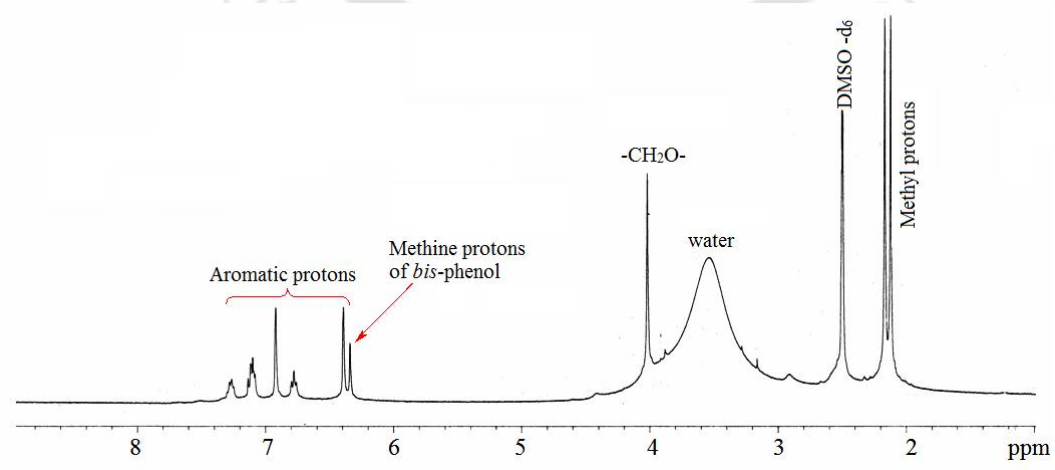

(a)

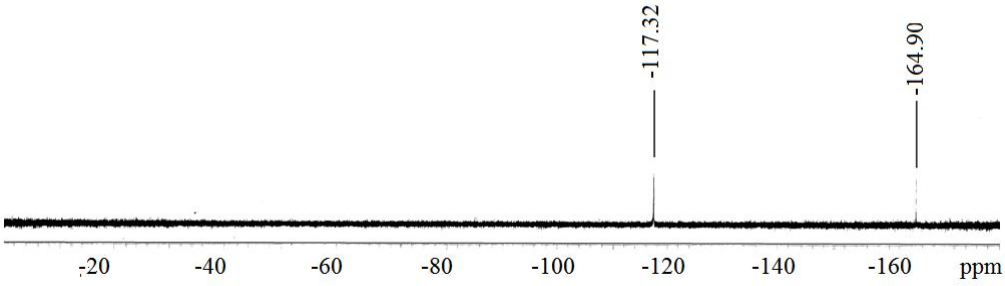

(b)

Figure 5.18: (a) ^{1}H-NMR of the ligand **5.2** (DMSO-d_6, 400 MHz). **(b)** ^{19}F-NMR of the ligand **5.2**.

Synthesis of [{$Na_2L^2(\mu\text{-}H_2O)(H_2O)_3$}.$H_2O$]$_n$ (5.2c): To a well stirred solution of H_2L^2 (0.233 g, 0.5 mmol) in methanol (10 mL), 0.4 g of sodium acetate (1 mmol) was added. The reaction mixture was stirred for 30 minutes and a colorless transparent liquid obtained and was kept undisturbed for crystallization. After 5 days colorless crystals were appeared. Isolated yield: 60 %. IR (KBr, cm^{-1}): 3442 (s), 2922 (w), 1594 (s), 1446 (s), 1413 (s), 1325 (w), 1240 (w), 1208 (m), 1141 (m), 1029 (s), 894 (m), 863 (s), 705 (m), 687 (m), 577 (m). Elemental analysis Calculated for [$C_{27}H_{35}FNa_2O_{11}$]$_n$, Calculated: C, 54.0; H, 5.87, Found: C, 54.21; H, 5.84; ^{1}H-NMR (DMSO-d_6): 7.23 (t, J= 7.6 Hz, 2H), 7.14 (t, J= 7.2 Hz, 1H), 7.02 (d, J= 7.6 Hz, 2H), 6.85 (s, 2H), 6.44 (s, 2H), 6.29 (s, 1H), 3.89 (s, 4H), 2.14 (s, 6H), 2.10 (s, 6H).

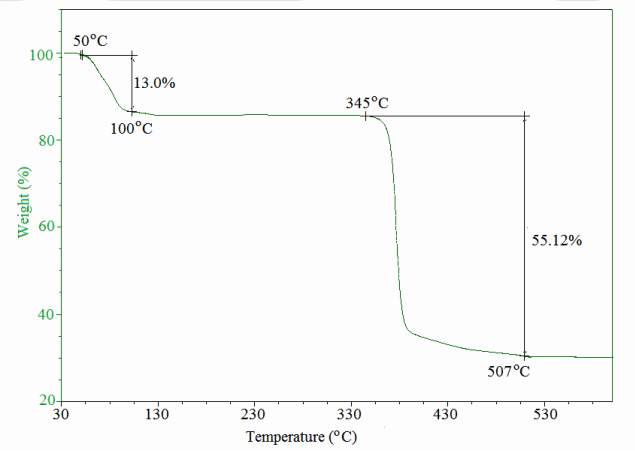

(a)

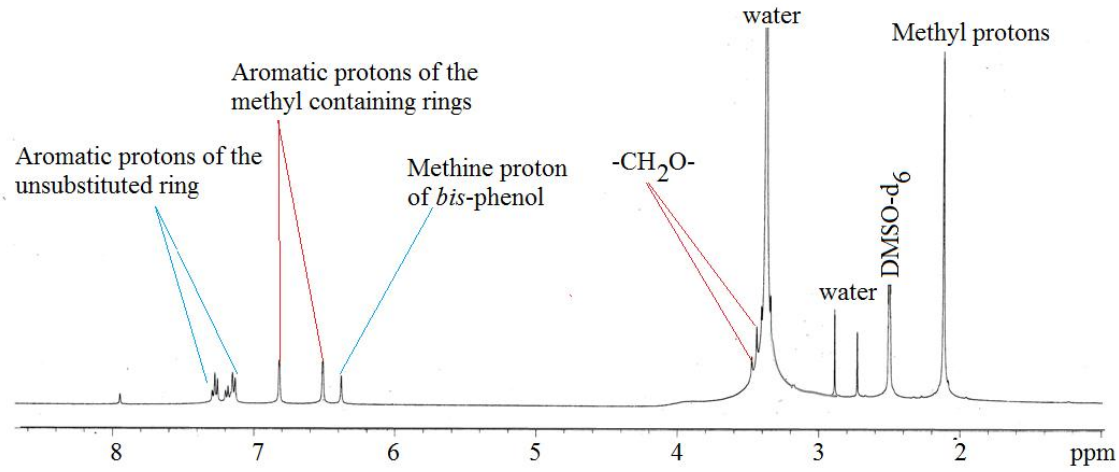

(b)

Figure 5.19: (a) TG of the sodium coordination polymer **5.2c, (b)** ^{1}H-NMR of the coordination polymer **5.2c** (DMSO-d_6, 400 MHz).

Synthesis of $[\{(H_2O)Cs(\mu\text{-}H_2O)_2(\mu\text{-}L^2)Cs(H_2O)_2\}]_n$ (5.2d): To a well stirred solution of H_2L^2 (0.233 g, 0.5 mmol) in methanol (10 mL) caesium acetate (1 mmol) was added. The reaction mixture was stirred for about half an hour and the resulting mixture was filtered to obtain a colorless transparent liquid. The transparent liquid was kept undisturbed for crystallization. After 5 days, colorless crystals were observed. Isolated yield: 70 %. IR (KBr, cm^{-1}): 3385 (s), 1596 (s), 1473 (w), 1410 (s), 1321 (w), 1299 (w), 1241 (w), 1212 (m), 1141 (m), 1094 (w), 1031 (s), 929 (m), 863 (m), 824 (w), 757 (s), 667 (w). Elemental analysis calculated for $[C_{27}H_{31}FCs_2O_9]_n$, Calculated: C, 41.35; H, 3.98. Found: C, 41.42; H, 4.01. ^{1}H-NMR (DSMO-d_6): 7.22 (dd, J= 6 Hz, J= 7.2 Hz, 1H), 7.70 (t, J= 8 Hz, 2H), 6.85 (s, 2H), 6.80 (d, J= 7.6 Hz, 1H), 6.39 (s, 1H), 6.37 (s, 2H), 2.14 (s, 6H), 1.98 (s, 6H). ^{19}F-NMR (DMSO-d_6): -117.31 (C_6F_6 as internal reference).

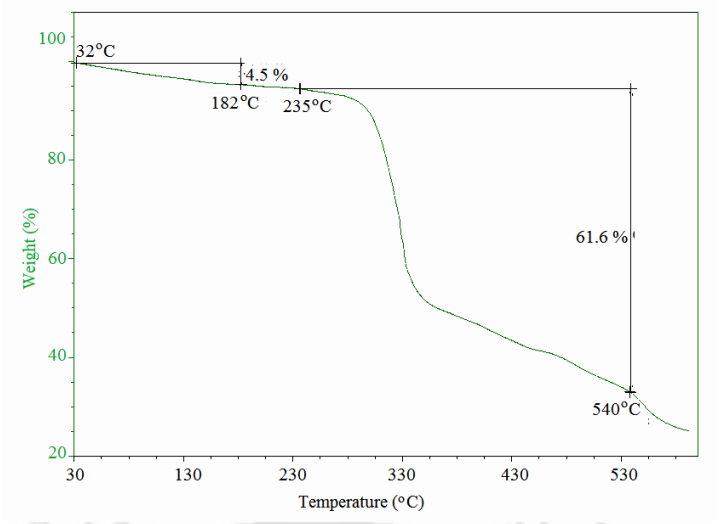

(a)

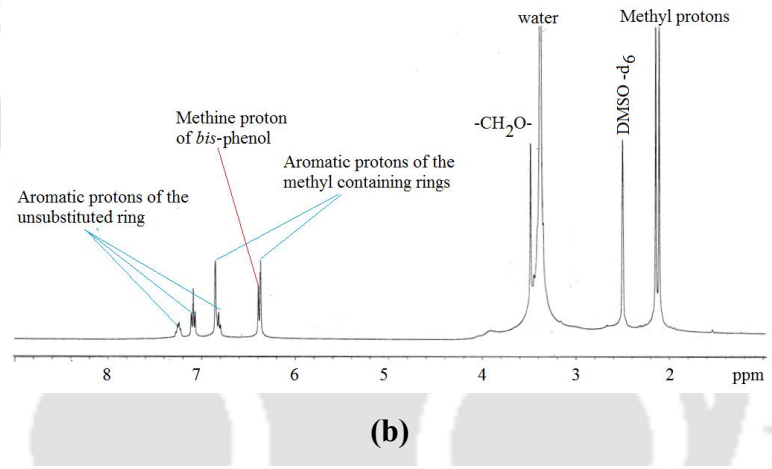

(b)

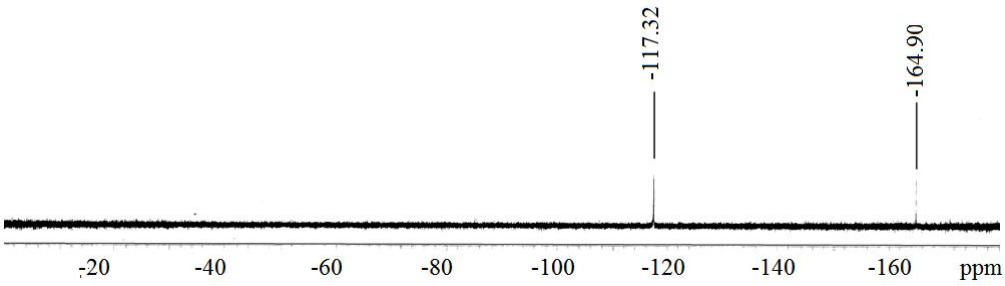

(c)

Figure 5.20: **(a)** TG of the sodium coordination polymer **5.2d, (b)** ^{1}H-NMR of the coordination polymer **5.2d** (DMSO-d_6, 400 MHz), **(c)** ^{19}F-NMR of the coordination polymer **5.2d**.

Synthesis of H_2L^3 (5.3): Ligand **5.3** was synthesized by a similar procedure adopted for ligand H_2L^1 **(5.1)** and H_2L^2 **(5.2)** and it was prepared starting from *bis*-phenol **5.3a**

Isolated yield: 65%. IR (KBr, cm^{-1}): 3468 (bs), 2067 (w), 1748 (s), 1638 (s), 1526 (s), 1474 (m), 1441 (m), 1354 (m), 1300 (w), 1254 (w), 1235 (w), 1209 (m), 1143 (s), 1067 (m), 968 (w), 869 (w), 714 (m); ^{1}H-NMR (DMSO-d_6, 400 MHz): 7.99 (d, J= 8 Hz, 1H), 7.63 (t, J= 8 Hz, 1H), 7.51 (t, J= 8 Hz, 1H), 6.98 (d, J= 8 Hz, 1H), 6.94 (s, 2H), 6.53 (s, 1H), 6.28 (s, 2H), 4.18 (s, 4H), 4.08 (s, 1H), 2.17 (s, 6H), 2.11 (s, 6H). ^{13}C-NMR (DMSO-d_6, 100 MHz): 169.8, 152.4, 148.8, 137.3, 135.0, 133.0, 132.8, 131.6, 131.1, 130.5, 128.0, 127.6, 124.9, 68.7, 38.9, 20.6, 15.9; LCMS (m/e) [M + Na^{+}]: 516.681.

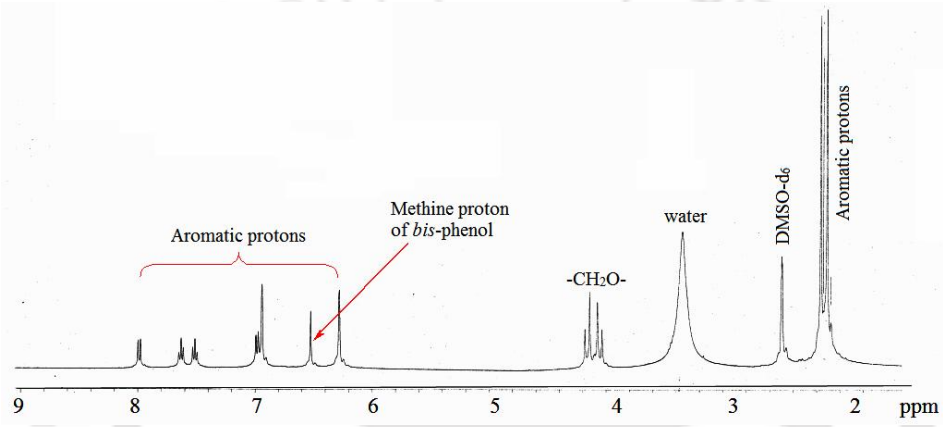

Figure 5.21: ^{1}H-NMR of the ligand **5.3** (DMSO-d_6, 400 MHz).

Synthesis of Complex $[K_2L^3(H_2O)]_n$ (5.3c): To a well stirred solution of ligand H_2L^1(0.9 g, 2 mmol) in dimethylformamide, potassium hydroxide (4 mmol) was added. The reaction mixture was stirred for another half an hour to dissolve it and then filtered to remove any solid impurity. The transparent liquid was kept for crystallization. After one week colorless block crystals of **5.3a** were obtained. Isolated yield: 60%. IR (KBr, cm^{-1}): 3442 (s), 2923 (w), 1624 (m), 1600 (s), 1536 (m), 1474 (m), 1412 (m), 1350 (m), 1322 (w), 1297 (w), 1239 (m), 1216 (m), 1143 (m), 1031 (s), 932 (w), 860 (m) 784 (w), 713 (w), 542 (w). Elemental analysis calculated for $[C_{27}H_{31}FCs_2O_9]_n$, Calculated: C, 51.91; H, 5.16. Found: C, 51.95; H, 5.07. ^{1}H-NMR (DMSO-d_6, 600 MHz): 7.91 (d, J= 7.8 Hz, 1H), 7.57 (t, J= 7.8 Hz, 1H), 7.46 (t, J= 7.8 Hz, 1H), 7.17 (d, J= 7.8 Hz), 6.93 (s, 1H), 6.91 (s, 2H), 6.37 (s, 2H), 3.26 (s, 4H), 2.20 (s, 6H), 2.12 (s, 6H).

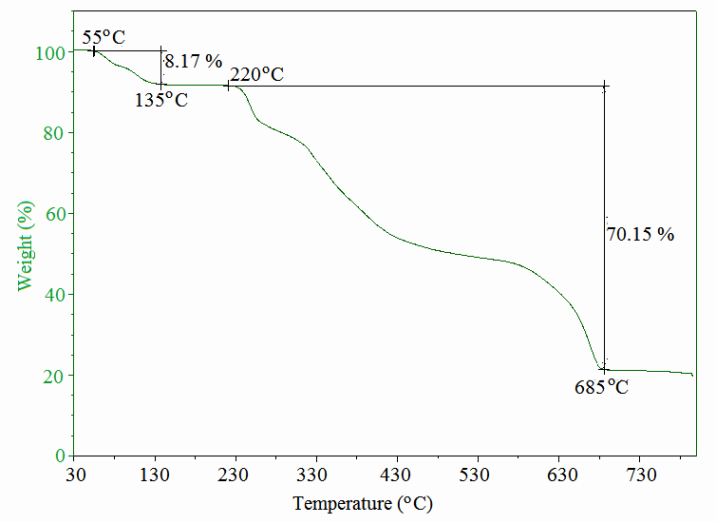

Figure 5.22: TG of the potassium complex **5.3c (**at 5°C per minute heating rate).

Synthesis of H_2L^4 (5.4): Ligand **5.4** was synthesized by a similar procedure adopted for ligand H_2L^1 **(5.1)** and H_2L^2 **(5.2)** and it was prepared starting from *bis*-phenol **5.4a** Isolated yield: 70%. IR (KBr, cm^{-1}): 3452 (s), 2921 (w), 2858 (w), 1735 (m), 1606 (s), 1522 (s), 1475 (s), 1429 (s), 1351 (s), 1209 (s), 1141 (s), 1034 (s), 947 (w), 833 (m), 713 (m); ^{1}H-NMR (DMSO-d_6, 400 MHz): 8.05 (s, J= 8 Hz, 1H), 7.77 (s, 1H), 7.54 (t, J= 8 Hz, 1H), 7.47 (d, J= 8 Hz, 1H), 6.93 (s, 1H), 6.89 (s, 2H), 6.44 (s, 2H), 3.89 (s, 2H), 3.86 (s, 2H), 2.16 (s, 6H), 2.12 (s, 6H), LCMS [M + Na^+]: 516.1430.

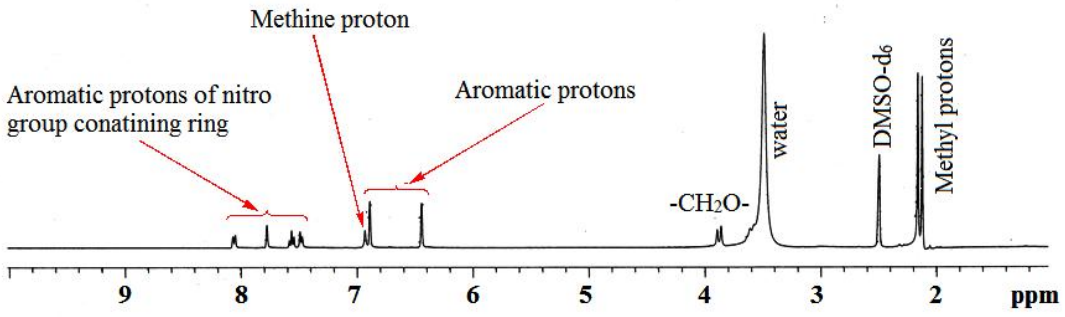

Figure 5.23: ^{1}H-NMR of the ligand **5.4** (DMSO-d6, 400 MHz).

References:

1. (a) D. Banerjee, J. B. Parise, *Cryst. Growth Des.*, 2011, **11**, 4704-4720; (b) K. M. Fromm, *Coord. Chem. Rev.*, 2008, **252**, 856-885.
2. (a) R. C. Lochan, M. Head-Gordon, *Phys. Chem. Chem. Phys.*, 2006, **8**, 1357-1370; (b) G. Ferey, F. Millange, M. Morcrette, C. Serre, M. -L. Doublet, J. -M. Greneche, J. -M. Tarascon, *Angew. Chem., Int. Ed.*, 2007, **46**, 3259-3263; (c) S. S. Han, W. A. Goddard, *J. Am. Chem. Soc.*, 2007, **129**, 8422-8423; (d) A. Blomqvist, C. M. Araujo, P. Srepusharawoot, R. Ahuja, *Proc. Nat. Acad. Sci. U. S. A.*, 2007, **104**, 20173-20176; (e) A. Mavrandonakis, E. Tylianakis, A. K. Stubos, G. E. Froudakis, *J. Phys. Chem. C*, 2008, **112**, 7290-7294; (f) P. Dalach, H. Frost, R. Q. Snurr, D. E. Ellis, *J. Phys. Chem. C*, 2008, **112**, 9278-9284; (g) E. Klontzas, A. Mavrandonakis, E. Tylianakis, G. E. Froudakis, *Nano Lett.*, 2008, **8**, 1572-1576; (h) A. Mavrandonakis, E. Klontzas, E. Tylianakis, G. E. Froudakis, *J. Am. Chem. Soc.*, 2009, **131**, 13410-13414.
3. J. D. Lee*, Concise Inorganic Chemistry;* Chapman & Hall: New York, 1991.
4. (a) A. Krief, A. Kremer, *Chem. Rev.*, 2010, **110**, 4772-4819; (b) E. Katsoulkou, K. F. Konidaris, A. Terzis, C. P. Raptopoulou, S. P. Perleps, E. Manessi-Zoupa, C. E. Kostakis, *Polyhedron*, 2011, **30**, 397-404; (c) G. Peng, L. Ma, J. Cai, L. Liang, D. Hong, G. E. Kostakis, *Cryst. Growth Des.*, 2011, **11**, 2485-2492; (d) R. Vaidhyanathan, S. Natarajan, C. N. R. Rao, *J. Solid State Chem.*, 2001, **162**, 150-157; (e) S. C. Chen, Z. H. Zhang, Y. S. Zhou, W. Y. Zhou, Y. Z. Li, M. Y. He, Q. Chen, M. Du, *Cryst. Growth Des.*, 2011, **11**, 4190-4197; (f) G. Swiderski, S. Wojtulewski, M. Kalinowska, R. Swislocka, W. Lewandowski, *J. Mol. Struct.*, 2011, **993**, 448-458; (g) A. Hazra, S. Gupta, S. Roy, T. N. Mandal, K. Das, S. Konar, A. Jana, S. Ray, R. J. Butcher, S. K. Kar, *Polyhedron*, 2011, **30**, 187-194; (h) S. M. Humphrey, R. A. Mole, R. I. Thompson, P. T. Wood, *Inorg. Chem.*, 2010, **49**, 3441-3448; (i) B. Murugesapandian, P. W. Roesky, *Dalton Trans.*, 2010, **39**, 9598-9603; (j) K. Rosenlehner, B. Schade, C. Boettcher, C. M. Jaeger, T. Clark, F. W. Heinemann, A. Hirsch, *Chem. Eur. J.*, 2010, **16**, 9544-9554; (k) O. Zech, M. Kellermeier, S. Thomaier, E. Maurer, R. Klein, C. Schreiner, W. Kunz, *Chem. Eur. J.*, 2009, **15**, 1341-1345; (l) J. Y. Wu, M. T. Ding, Y. S. Wen, Y. H. Liu,

K. L. Lu, *Chem. Eur. J.*, 2009, **15**, 3604-3614; (m) D. Huang, X. Zhang, C. Ma, H. Chen, C. Chen, Q. Liu, C. Zhang, D. Liao, L. Li, *Dalton Trans.*, 2007, **6**, 680-688; (n) G.S. Nichol, W. Clegg, *Polyhedron*, 2006, **25**, 1043-1056.

5. (a) Z. -H. Zhou, J. -M. Yang, H. -L. Wan, *Cryst. Growth Des.*, 2005, **5**, 1825-1830; (b) S. L. Childs, L. J. Chyall, J. T. Dunlap, V. N. Smolenskaya, B. C. Stahly, G. P. Stahly, *J. Am. Chem. Soc.*, 2004, **126**, 13335-13342; (c) P. Vishweshwar, A. Nangia, V. M. Lynch, *Cryst. Growth Des.*, 2003, **3**, 783-790; (d) C. Livage, C. Egger, G. Ferey, *Chem. Mater.*, 1999, **11**, 1546-1550; (e) A. Dimos, D. Tsaousis, A. Michaelides, S. Skoulika, S. Golhen, L. Ouahab, C. Didierjean, A. Aubry, *Chem. Mater.*, 2002, **14**, 2616-2622; (f) D. T. de Lill, N. S. Gunning, C. L. Cahill, *Inorg. Chem.*, 2005, **44**, 258-266. (g) L. A. Borkowski, C. L. Cahill, *Inorg. Chem.*, 2003, **42**, 7041-7045.
6. (a) M. -L. Tong, X. -M. Chen, B. -H. Ye, S. -W. Ng, *Inorg. Chem.*, 1998, **37**, 5278-5281; (b) S. -Q. Zang, Y. Su, Y. -Z. Li, H. -Z. Zhu, Q. -J. Meng, *Inorg. Chem.*, 2006, **45**, 2972-2978; (c) L. Pan, M. B. Sander, X. -Y. Huang, J. Li, M. Smith, E. Bittner, B. Bockrath, J. K. Johnson, *J. Am. Chem. Soc.*, 2004, **126**, 1308-1309; (d) X. -L. Wang, C. Qin, E. -B. Wang, Y. -G. Li, Z. -M. Su, *Chem. Commun.*, 2005, 5450-5452; (e) X. -L. Wang, C. Qin, E. -B. Wang, Y. -G. Li, Z. -M. Su, L. Xu, L. Carlucci, *Angew. Chem., Int. Ed.*, 2005, **44**, 5824-5827; (f) X. -L. Wang, C. Qin, E. -B. Wang, Z. -M. Su, *Chem. -Eur. J.*, 2006, **12**, 2680-2691; (g) J. Tao, J. -X. Shi, M. -L. Tong, X. -X. Zhang, X. -M. Chen, *Inorg. Chem.*, 2001, **40**, 6328-6330; (h) X. -M. Chen, G. -F. Liu, *Chem. -Eur. J.*, 2002, **8**, 4811-4817; (i) D. F. Sun, R. Cao, Y. -Q. Sun, W. -H. Bi, X. -J. Li, Y. -Q. Wang, Q. Shi, X. Li, *Inorg. Chem.*, 2003, **42**, 7512-7518.
7. D. S. Sagatys, C. Dahlgren, G. Smith, R. C. Bott, J. M. White, *Dalton Trans.*, 2000, 3404-3410.
8. D. Kalita, J. B. Baruah, *J. Chem. Sci.*, 2013, **125**, 267-273.
9. (a) Z. -B. Zheng, R. -T. Wu, J. -K. Li, Y. -F. Sun, Y. -F. Han, *J. Mol. Struct.*, 2010, **964**, 109-118; (b) A. R. Katritzky, P. J. steel, S. N. Denisenko, *Tetrahedron*, 2001, **57**, 3309-3314.
10. R. J. Sarma, J. B. Baruah, *Cryst. Growth Des.,* 2007, **7**, 989-1000.
11. (a) K. D. Demadis, E. Barouda, N. Stavgianoudaki, Hong Zhao, *Cryst. Growth Des.,* 2009, **9**, 1250-1253; (b) C. Barthes, C. Lepetit, Y. Canac, C. Duhayon, D.

Zargarian, R. Chauvin, *Inorg. Chem.*, 2013, **52**, 48-58; (c) B. L. Dietrich, J. Egbert, A. M. Morris, M. Wicholas, O. P. Anderson, S. M. Miller, *Inorg. Chem.*, 2005, **44**, 6476-6481; (d) S. Kumar, G. Mani, S. Mondal, P. K. Chattaraj, *Inorg. Chem.*, 2012, **51**, 12527-12539; (e) J. Hu, H. Xu, M.-H. Nguyen, J. H. K. Yip, *Inorg. Chem.*, 2009, **48**, 9684-9692.

12. A. Karmakar, J. B. Baruah, R. B. Shankar, *CrystEngComm*, 2009, **11**, 832-840.
13. S. Santra, B. Das, J. B. Baruah, J. *Chem. Crystallogr.*, 2011, **41**, 1981-1987.
14. A. Karmakar, J. B. Baruah, *Inorg. Chem. Comm.*. 2009, **12**, 140-144.
15. A. Misiolek, R. Huang, B. Kahr, J. E. Jackson, *Chem. Commun.*, 1996, 2119-2120.
16. J. A. Kaduk, *Acta Crystallogr.*, 2000, **56B**, 474-485.
17. (a) P. Thuery, B. Masci, *Cryst. Growth Des.*, 2010, **10**, 4109-4117; (b) R. -H. Zeng, Z. -Q. Fang, F. Sun, L. -S. Jiang, Y. -W. Tang, *Acta Cryst.*, 2007, **E 63,** m1813- m1814; (c) G. B. Li, S. H. Yang, M. Xiong, J. H. Lin, *Acta Cryst. C*, 2004, **60**, m612- m614; (d) N. C. Kasuga, M. Umeda, H. Kidokoro, K. Ueda, K. Hattori, K. Yamaguchi, *Cryst. Growth Des.*, 2009, **9**, 1494-1498; (e) P. Thuery, *Cryst. Growth Des.*, 2011, **11**, 3282-3294; (f) D. S. Sagatys, C. Dahlgren, G. Smith, R. C. Bott, J. M. White, *J. Chem. Soc., Dalton Trans.*, 2000, 3404-3410.
18. R. D. Bergougnant, A. Y. Robin, K. M. Fromm, *Cryst. Growth Des.*, 2005, **5**, 1691-1694.
19. (a) W. Huang, H. Qian, S. Gou, C. Yao, *J. Mol. Struct.*, 2005, **743**, 183-190; (b) M. Inosako, C. Shimokawa, H. Sugimoto, N. Kihara, T. Takata, S. Itoh, *Chem. Lett.*, 2007, **36**, 1306-1307; (c) J. Xu, Y. -H. Lai, *Tetrahedron Lett.*, 2002, **43**, 9199-9202.
20. D. C. Luehrs, K. Bowman-James, *J. Mol. Struct.*, 1994, **321**, 251-254.
21. (a) L. Torun, T. W. Robison, J. Krzykawski, D. W. Purkiss, R. A. Bartsch, *Tetrahedron*, 2005, **61**, 8345-8350; (b) A. Karmakar, J. B. Baruah, R. Boomi Shankar, *CrystEngComm*, 2009, **11**, 832-840.
22. (a) K. V. Domasevitch, J. A. Rusanova, O. Y. Vassilyeva, V. N. Kokozay, P. J. Squattrito, J. Sieler, P. R. Raithby, *J. Chem. Soc., Dalton Trans.*, 1999, 3087-3093; (b) C. M. Means, N. C. Means, S. G. Bott, J. L. Atwood, *J. Am. Chem. Soc.*, 1984, **106**, 7627-7628.

23. (a) J. M. Harrowfield, N. Lugan, G. H. Shahverdizadeh, A. A. Soudi, P. Thuery, *Eur. J. Inorg. Chem.*, 2006, 389-396; (b) H. Plenio, *ChemBioChem*, 2004, **5**, 650-655; (c) H. Takemura, N. Kon, M. Kotoku, S. Nakashima, K. Otsuka, M. Yasutake, T. Shinmyozu, T. Inazu, *J. Org. Chem.*, 2001, **66**, 2778-2783; (d) H. Takemura, S. Nakashima, N. Kon, M. Yasutake, T. Shinmyozu, T. Inazu, *J. Am. Chem. Soc*., 2001, **123**, 9293-9298; (e) H. Takemura, T. Iwanaga, T. Shinmyozu, *Tetrahedron Lett.,* 2006, **47**, 8989-8991.
24. (a) T. Katagiri, M. Duan, M. Mukae, K. Uneyama, *J. Fluor.*, 2003, **120**, 165-172; (b) T. Katagiri, M. Duan, M. Mukae, K. Uneyama, *J. Fluor. Chem.*, 2011, **132**, 587-595.
25. (a) H. Plenio, R. Diodone, *Angew. Chem. Int. Ed. Eng.*, 1994, **33**, 2175-2177; (b) H. Plenio, *Chem. Rev.*, 1997, **97**, 3363-3384; (c) H. Plenio, R. Diodone, *J. Am. Chem. Soc.*, 1996, **118**, 356-367; (d) H. Takemura, N. Kon, M. Yasutake, H. Kariyazono, T. Shinmyozu, T. Inazu, *Angew. Chem. Int. Ed. Eng.*, 1999, **38**, 959-961; (e) H. Takemura, H. Kariyazono, M. Yasutake, N. Kon, K. Tani, K. Sako, T. Shinmyozu, T. Inazu, *Eur. J. Org. Chem.*, 2000, 141-148.
26. B. R Srinivasan, S. Y. Shetgaonkar, P. Raghavalah, *J. Chem. Sci.*, 2008, **120**, 249-257.
27. H. Chen, T. Zhang, J. Zhang, C. Chen, *Prop. Explos. Pyrotechnol.,* 2006, **31**, 285-289.
28. R. Chutia, S. Dey, G. Das, *CrystEngComm*, 2013, **15**, 9641-9647.

Conclusion

Versatile scaffolds in host-guest chemistry to design the crystals of specific molecular arrangements using *bis*-phenols have been shown in this thesis. The two hydroxy groups present in *bis*-phenol having V-shaped geometry can form strong intermolecular hydrogen bonds. Interplay of such principal interactions with other weak interactions provides directional properties to *bis*-phenols to form various supramolecular architectures. Based on the V-shaped geometry of *bis*-phenols, various macrocyclic and polymeric architectures are designed by functionalizing the two hydroxy groups. It has been shown that N,N-dimethylaminobenzene unit attached to *bis*-phenol provides avenue to make series of solvates. Several of such solvates are isostructural. On the other hand, based on the types of interaction of the guest solvent molecules to O-H···O bond of the host molecule, three different classes of hydrogen bond motifs could be identified. These motifs bear the signatures of particular isostructural series of structures. The analysis of these structural motifs has helped in understanding the interplay between weak interactions in their formation.

The findings on the porous and non-porous polymorphs of a fluoro substituted *bis*-phenol have helped us to clearly understand the conversion of a porous structure to a non-porous structure. Two concomitant polymorphic solvates formed in the case of dioxane solvate of a fluoro substituted *bis*-phenol, is a very rare phenomenon. This has established the fact that the fine control by interplay of weak interactions of *bis*-phenol molecules with solvent led to the variations of self-assemblies, which resulted in simultaneous crystallisation of two polymorphs. The C-H···F-C interactions are responsible for formation of the particular concomitant polymorphic solvates is an exceptional observation. It has been also shown that a higher amount of solvent uptake by a *bis*-phenol at solvothermal condition compared to ambient condition is due to change in packing patterns. Namely, the host-guest ratio of a fluoro *bis*-phenol was manipulated by changing the crystallisation process. The caesium-π interactions in a fluoro-substituted *bis*-phenol with short bond length have been shown as a consequence of coordination effect of the *bis*-phenol to maximise its stability in a particular packing pattern.

In case of imidazole based *bis*-phenols we have been able to obtain two distinguishable self assembling of *bis*-phenols through O-H···N and N-H···π interactions leading to polymorphs. In this case also the polymorphs with porous and non porous structure were isolated and characterised. Generally a porous frameworks formed during desolvation have tendency to collapse, but one of the porous polymorph of imidazole based *bis*-phenol we reported is stable. Reversible acetone binding, i.e. the desolvate of acetone as well as in solvated form with acetone has been shown for the first time in *bis*-phenol chemistry. Moreover, nitrogen atom of these imidazole *bis*-phenols can interacts with different anions to give new charge assisted assemblies with interesting structures. One of the imizaole based *bis*-phenol forms circular assembly through O-H···O interaction in presence of sulphate anion. On the other hand, the disproportionation reaction of magnesium sulphate by sulphuric acid had enabled to stabilise bisulphate anion in a self-assembly of imidazole based *bis*-phenol, which may be considered as a novel information on dispropotionation of alkaline earth metal salt in acid.

The functioanlization of hydroxy groups of *bis*-phenol by flexible tethers ($-CH_2CO_2$) is utilized to generate pincer type of lignads. The coordination chemistry of these pincer types of lignads and the substituent effecting such coordination with alkali metal ions have been shown. The structural units of such complexes are highly dependent on the coordinated water molecules and the lattice water. The water molecules influence the packing patterns and control the dimensions of the complexes. While studying the substituent effect of the ligands, it has been observed that covalently linked nitro-group or fluoro-group can highly influence the structures of alkali metal complexes. It could also be shown that the covalently linked fluoro-group can be used as binding site under specific condition for caesium metal ion.

A series of mono-nuclear, cyclic dimer or dinuclear cadmium complexes were synthesised from dicarboxylic acids tethered through *bis*-phenol unit. The important finding was the selective synthesis of such complexes from particular solvent under similar reaction condition. The inter-conversion by solvent among dimers at ambient conditions has been shown and such systems may have applications in solvent mediated crystal to crystal transformations. Moreover, we have also able to show the closure of metallacycle to form binuclear complexes by changing solvents and the substituent in the ligands. Thus, rigid *bis*-phenol molecules can be converted to semi-

rigid molecules by functionalizing the hydoxy groups with flexible arms which can be further used in coordination chemistry to generate metal complexes of various dimensions. The substituent and solvents were found to change the course of crystallisation of particular complex, making new avenues for solvent assisted selective synthesis.

Appendix

Details of the analytical instruments:

X-ray crystallography

X-ray diffraction data were collected on Bruker 3-circle diffractometer with CCD area detectors ProteumM APEX or SMART 6000 or Bruker Nonius Apex 2, using graphite-monochromated Mo- Kα radiation (λ= 0.71073Å) from a 60W micro-focus Bede Microsourse® with glass polycapillary optics or sealed tube.

X-ray diffraction data for all crystals were collected using Bruker SMART software. This software is also used for indexing and determination of the unit cell parameters. The structures were solved by direct method and refined by full-matrix least squares against F^2 of all data, using SHELXTL software. The CIF of all the compounds synthesized and characterised are included in the soft copy.

All the non H-atoms were refined by full-matrix least squares in anisotropic, all H-atoms in isotropic approximation, against F^2 of all reflections. All non H-atoms were refined by full matrix least squares in anisotropic approximation and the hydrogen atoms attached to these atoms were treated as 'riding' in calculated positions and in some of the cases the hydrogen atoms have been located on the difference Fourier maps. In all the cases the H-atoms attached to the polar atoms such as O and N were located on the difference Fourier maps and refined in the final structure in isotropic approximation. The crystallographic tables for all the compounds are given at the end of this section, which includes the crystal parameters and the refinement factor.

Powder X-ray Diffraction data were collected on a Bruker D8 diffractometer in Bragg- Brentano θ-θ geometry with Cu K_α radiation (λ=1.5418Å) on a glass surface of an air dried sample using a secondary curved graphite monochromator. Diffraction patterns were collected over a 2θ range of 5-45°C at a scan rate of 2° per minute.

UV-visible Spectroscopy:

The UV-absorption spectra were recorded using Perkin-Elmer Lambda 750 spectrometer equipped with double cell compartments. All the chemicals and solvents used were as obtained from the standard suppliers such as E. Merck Germany, Sigma Aldrich USA, Ranbaxy India. The solvents for optical spectroscopy were of HPLC

grade (Aldirich or Merck) and used as obtained. The FT-IR spectra were recorded on Perkin-Elmer spectrum one spectrometer in the range of 4000-450 cm^{-1}.

NMR Spectroscopy:

The NMR spectra were recorded in a Bruker 400 MHz spectrometer. The chemical shifts in the NMR spectra are all given in ppm and tetramethylsilane as the internal standard.

Thermogravimetric Studies and Elemental Analysis:

The thermogravimetric studies were performed using a Mettlar Toledo TGA/ STDA 851^e and Mettlar Toledo DSC^e thermal analyser. Typically about 4-6 mg of the samples were mounted on platinum crucibles and the TG/ DSC profiles recorded at the heating rate of 5 ˚C/min and under nitrogen atmosphere. Elemental analyses were done on a Parkin-Elmer PE 2400 II CHN analyser 2400.

Crystallographic data and refinement parameters for the compounds:

Compound No.	**2.2**	**2.3**	**2.4**
Formulae	$C_{28}H_{35}NO_3$	$C_{27}H_{35}NO_3S$	$C_{29}H_{38}N_2O_3$
CCDC No.	893023	893024	893025
Mol. wt.	433.57	453.62	462.61
Space group	$P2_{1/c}$	$P2_{1/c}$	$P2_{1/c}$
a (Å)	12.1540(7)	12.3180(11)	12.606(10)
b (Å)	11.8231(8)	11.3498(11)	11.689(11)
c (Å)	17.9886(12)	18.4829(18)	18.529(16)
α (°)	90.00	90.00	90.00
β (°)	101.881(3)	98.544(6)	105.15(3)
γ (°)	90.00	90.00	90.00
V ($Å^3$)	2529.5(3)	2555.4(4)	2636(4)
Density (Mgm^{-3})	1.138	1.179	1.166
Abs. Coeff. (mm^{-1})	0.073	0.154	0.075
F(000)	936	976	1000
Total no. of reflections	4525	4592	4720
Reflections, $I > 2\sigma(I)$	2557	1603	1255
Max. θ (°)	25.25	25.25	25.25
Ranges (h, k, l)	$-14 \le h \le 13$ $-14 \le k \le 14$ $-21 \le l \le 21$	$-14 \le h \le 9$ $-13 \le k \le 8$ $-12 \le l \le 22$	$-15 \le h \le 10$ $-13 \le k \le 13$ $-22 \le l \le 21$
Complete to 2θ (%)	98.6	99.2	99.0
Data/ Restraints/Parameters	4525 / 0/ 299	4592 / 5/ 302	4720 / 2/ 318
Goof (F^2)	0.975	1.088	0.853

R indices [$I > 2\sigma(I)$]	0.0658	0.1154	0.0568
R indices (all data)	0.1010	0.2645	0.2238

Compound No.	**2.5**	**2.6**	**2.7**
Formulae	$C_{29}H_{37}NO_5$	$C_{29}H_{38}N_2O_3$	$C_{30}H_{40}N_2O_2$
CCDC No.	893026	893027	893028
Mol. wt.	479.60	462.61	460.64
Space group	P-1	$P2_{1/c}$	$P2_{1/c}$
a (Å)	9.8237(11)	12.3499(11)	12.4222(8)
b (Å)	11.8361(13)	12.7854(12)	12.7119(8)
c (Å)	13.2385(14)	17.0726(15)	17.3961(12)
α (°)	68.077(4)	90.00	90.00
β (°)	88.819(4)	101.913(5)	102.160(4)
γ (°)	68.848(4)	90.00	90.00
V ($Å^3$)	1320.1(2)	2637.7(4)	2685.4(3)
Density (Mgm^{-3})	1.207	1.165	1.139
Abs. Coeff. (mm^{-1})	0.082	0.075	0.071
F(000)	516	1000	1000
Total no. of reflections	4704	4727	4798
Reflections, $I > 2\sigma(I)$	2031	3116	2365
Max. θ (°)	25.2	25.25	25.25
Ranges (h, k, l)	$-11 \le h \le 11$ $-14 \le k \le 11$ $-15 \le l \le 15$	$-14 \le h \le 14$ $-15 \le k \le 15$ $-19 \le l \le 20$	$-14 \le h \le 14$ $-14 \le k \le 14$ $-20 \le l \le 20$
Complete to 2θ (%)	98.5	98.7	98.7
Data/ Restraints/Parameters	4704/ 0/ 324	4727/ 0/ 319	4798/ 2/ 326
Goof (F^2)	1.040	1.161	0.906
R indices [$I > 2\sigma(I)$]	0.0757	0.0558	0.0555
R indices (all data)	0.1827	0.0859	0.1121

Compound No.	**2.8**	**2.9**	**3.1a**
Formulae	$C_{34}H_{45}N_3O_2$	$C_{56}H_{76}N_4O_7$	$C_{23}H_{23}FO_2$
CCDC No.	893029	893030	937981
Mol. wt.	527.73	917.21	350.41
Space group	P-1	P-1	Pbca
a (Å)	8.6308(9)	12.988(2)	4.9312(3)
b (Å)	11.6990(12)	14.491(2)	19.1560(13)
c (Å)	15.9227(17)	15.156(3)	41.744(2)
α (°)	107.295(6)	88.529(14)	90.00
β (°)	105.133(6)	70.482(11)	90.00
γ (°)	92.092(6)	88.285(11)	90.00
V ($Å^3$)	1470.4(3)	2687.0(8)	3943.2(4)
Density (Mgm^{-3})	1.192	1.134	1.181
Abs. Coeff. (mm^{-1})	0.074	0.074	0.080
F(000)	572	992	1488
Total no. of reflections	5140	9682	3636
Reflections, $I > 2\sigma(I)$	2571	2614	1870

Max. θ (°)	25.25	25.25	25.49
Ranges (h, k, l)	$-10 \le h \le 10$ $-13 \le k \le 14$ $-18 \le l \le 19$	$-15 \le h \le 14$ $-17 \le k \le 17$ $-17 \le l \le 18$	$-5 \le h \le 5$ $-23 \le k \le 15$ $-44 \le l \le 50$
Complete to 2θ (%)	96.5	99.5	99.80
Data/ Restraints/Parameters	5140/ 2/ 360	9682/ 34/ 644	3636/ 0/ 247
Goof (F^2)	1.030	1.176	1.087
R indices [$I > 2\sigma(I)$]	0.0613	0.0659	0.0708
R indices (all data)	0.1370	0.2011	0.1407

Compound No.	**3.1b**	**3.1c**	**3.2a**
Formulae	$C_{23}\ H_{23}\ F\ O_2$	$C_{26}\ H_{30}\ F\ N\ O_3$	$C_{23}\ H_{23}\ F\ O_2$
CCDC No.	937982	937983	937984
Mol. wt.	350.41	423.51	350.41
Space group	$P2_{1/c}$	$P\ na2_1$	$P2_1/n$
a (Å)	16.2856(6)	12.006(2)	10.1891(3)
b (Å)	8.4173(4)	23.510(4)	12.1484(4)
c (Å)	14.5989(6)	8.2207(13)	15.5039(4)
α (°)	90.00	90.00	90.00
β (°)	110.232(2)	90.00	92.864(3)
γ (°)	90.00	90.00	90.00
V ($Å^3$)	1877.75(14)	2320.4(6)	1916.69(10)
Density (Mgm^{-3})	1.240	1.212	1.214
Abs. Coeff. (mm^{-1})	0.084	0.084	0.083
F(000)	744	904	744
Total no. of reflections	3502	3880	3469
Reflections, $I > 2\sigma(I)$	2366	1656	2533
Max. θ (°)	25.49	25.25	25.25
Ranges (h, k, l)	$-19 \le h \le 19$ $-8 \le k \le 10$ $-17 \le l \le 15$	$-14 \le h \le 14$ $-27 \le k \le 27$ $-9 \le l \le 9$	$-6 \le h \le 12$ $-14 \le k \le 13$ $-18 \le l \le 18$
Complete to 2θ (%)	1.00	97.60	99.90
Data/ Restraints/Parameters	3502/ 0/ 241	3880/ 1/ 288	3469/ 6/ 247
Goof (F^2)	0.875	1.103	0.964
R indices [$I > 2\sigma(I)$]	0.0435	0.0962	0.0520
R indices (all data)	0.0718	0.2205	0.0721

Compound No.	**3.2b**	**3.2c**	**3.2d**
Formulae	$C_{48}\ H_{52}\ F_2\ O_5\ S$	$C_{25}\ H_{29}\ F\ O_3\ S$	$C_{25}\ H_{27}\ F\ O_3$
CCDC No.	937985	937986	9439393
Mol. wt.	778.96	428.54	394.47
Space group	Pbcn	$P2_{1/c}$	P-1
a (Å)	12.0576(9)	8.3850(2)	9.0463(5)
b (Å)	18.7488(11)	29.3923(8)	9.5339(6)
c (Å)	18.9159(14)	19.4179(6)	13.1106(8)
α (°)	90.00	90.00	98.763(4)
β (°)	90.00	93.876(2)	103.988(4)
γ (°)	90.00	90.00	96.474(4)
V ($Å^3$)	4276.2(5)	4774.7(2)	1071.13(11)

Density (Mgm^{-3})	1.210	1.192	1.223
Abs. Coeff. (mm^{-1})	0.129	0.165	0.085
F(000)	1656	1824	420
Total no. of reflections	3873	8555	3850
Reflections, $I > 2\sigma(I)$	2777	4814	2642
Max. θ (°)	25.25	25.25	25.25
Ranges (h, k, l)	-7 ≤ h ≤ 14 -22 ≤ k ≤21 -9 ≤ l ≤22	-10 ≤ h ≤ 9 -35 ≤ k ≤33 -23 ≤ l ≤22	-10 ≤ h ≤ 10 -11 ≤ k ≤11 -15 ≤ l ≤15
Complete to 2θ (%)	99.80	99.20	99.00
Data/ Restraints/Parameters	3873 / 2/ 276	8555 / 0/ 557	3850/2/ 274
Goof (F^2)	1.185	1.011	1.084
R indices [$I > 2\sigma(I)$]	0.0509	0.0529	0.0448
R indices (all data)	0.0747	0.1328	0.0650

Compound No.	**3.2e**	**3.2f**	**4.1a**
Formulae	C_{25} H_{27} F O_3	C_{46} H_{45} F_2 O_4 Cs	$C_{21}H_{24}N_2O_2$
CCDC No.	937987	937988	904126
Mol. wt.	394.47	832.73	336.42
Space group	$P2_1/n$	P-1	$P2_1/c$
a (Å)	10.1337(9)	10.3787(9)	8.1858(8)
b (Å)	11.8820(7)	13.5980(9)	10.6531(12)
c (Å)	18.8355(16)	15.7691(8)	20.967(2)
α (°)	90.00	102.404(5)	90.00
β (°)	104.929(8)	102.068(6)	92.684(7)
γ (°)	90.00	106.190(7)	90.00
V ($Å^3$)	2191.4(3)	1999.7(2)	1826.4(3)
Density (Mgm^{-3})	1.196	1.383	1.223
Abs. Coeff. (mm^{-1})	0.083	0.977	0.079
F(000)	840	852	720
Total no. of reflections	3966	7249	3387
Reflections, $I > 2\sigma(I)$	1664	4236	1697
Max. θ (°)	25.25	25.25	25.50
Ranges (h, k, l)	-12 ≤ h ≤7 -14 ≤ k ≤10 -22 ≤ l ≤22	-12 ≤ h ≤12 -16 ≤ k ≤10 -18 ≤ l ≤18	-9≤ h ≤9 -12≤ k ≤12 -25 ≤ l ≤25
Complete to 2θ (%)	99.80	99.80	99.70
Data/ Restraints/Parameters	3966 / 0/ 268	7249 / 16/ 478	3387/ 0/ 237
Goof (F^2)	1.124	1.023	1.049
R indices [$I > 2\sigma(I)$]	0.0730	0.0621	0.0536
R indices (all data)	0.1860	0.1215	0.1232

Compound No.	**4.1b**	**4.1c**	**4.1d**
Formulae	C_{21} $H_{24}N_2O_2$	C_{45} $H_{54}N_4O_5$	$C_{23}H_{32}N_2O_4S$
CCDC No.	904127	904125	904123
Mol. wt.	336.42	730.92	432.57
Space group	C2/c	C2/c	$P2_1/c$
a (Å)	21.5904(13)	21.9667(7)	8.2791(6)

b (Å)	13.6380(8)	13.4559(7)	10.4599(7)
c (Å)	16.9958(17)	17.1405(7)	26.664(2)
α (°)	90.00	90.00	90.00
β (°)	123.947(3)	124.165(4)	96.212(7)
γ (°)	90.00	90.00	90.00
V ($Å^3$)	4151.4(5)	4192.1(3)	2295.5(3)
Density (Mgm^{-3})	1.077	1.158	1.252
Abs. Coeff. (mm^{-1})	0.070	0.076	0.172
F(000)	1440	1568	928
Total no. of reflections	3865	3902	4141
Reflections, $I > 2\sigma(I)$	1799	2766	3126
Max. θ (°)	25.50	25.50	25.25
Ranges (h, k, l)	-26≤ h ≤26 -16≤ k ≤16 -20 ≤ l ≤20	-26≤ h ≤26 -16≤ k ≤16 -20 ≤ l ≤20	-9≤ h ≤8 -11≤ k ≤12 -25 ≤ l ≤32
Complete to 2θ (%)	100.00	99.80	99.80
Data/ Restraints/Parameters	3865/ 1/ 237	3902/ 0/ 257	4141/ 5/ 298
Goof (F^2)	0.997	1.076	1.006
R indices [$I > 2\sigma(I)$]	0.0818	0.0689	0.0885
R indices (all data)	0.1690	0.0929	0.1085

Compound No.	**4.1e**	**4.1f**	**4.2a**
Formulae	C21 H25 Cl N2 O6	C_{42} H_{50} F_6 N_4 O_4 Si	$C_{20}H_{22}N_2O_2$
CCDC No.			859874
Mol. wt.	436.88	816.95	322.14
Space group	P-1	C2/c	$P2_1/n$
a (Å)	7.9643(3)	21.6442(13)	13.7298(6)
b (Å)	8.5995(3)	16.3879(10)	9.1144(4)
c (Å)	15.7931(7)	14.7429(9)	14.9435(6)
α (°)	99.561(2)	90.00	90.00
β (°)	96.346(2)	126.4750(10)	90.00
γ (°)	100.409(2)	90.00	90.00
V ($Å^3$)	1038.00(7)	4205.0(4)	1747.40(13)
Density (Mgm^{-3})	1.398	1.290	1.225
Abs. Coeff. (mm^{-1})	0.225	0.128	0.080
F(000)	460	1720	688
Total no. of reflections	3736	3761	2910
Reflections, $I > 2\sigma(I)$	2882	2920	2407
Max. θ (°)	25.25	25.25	24.99
Ranges (h, k, l)	-9 ≤ h ≤ 9 -10 ≤ k ≤10 -18 ≤ l ≤ 18	-25 ≤ h ≤ 25 -19 ≤ k ≤18 -15 ≤ l ≤ 17	-15 ≤ h ≤ 15 -10 ≤ k ≤ 10 -16 ≤ l ≤ 16
Complete to 2θ (%)	99.30	98.50	95.0
Data/ Restraints/Parameters	3736 /2/ 360	3761/0/ 273	2910/0/227
Goof (F^2)	0.970	1.069	0.993
R indices [$I > 2\sigma(I)$]	0.0533	0.0483	0.0577
R indices (all data)	0.0647	0.0619	0.0678

Compound No.	**4.2b**	**4.2c**	**4.2d**
Formulae	$C_{21}H_{26}N_2O_3$	$C_{24}H_{28}N_2O_7$	$C_{22}H_{24}N_2O_4$
CCDC No.	859875	859878	859877
Mol. wt.	354.14	456.48	380.43
Space group	P-1	$P2_1/c$	P-1
a (Å)	8.7555(8)	15.7164(10)	8.0009(3)
b (Å)	10.3506(10)	9.2068(5)	9.2227(3)
c (Å)	11.3880(12)	16.0795(10)	13.6691(5)
α (°)	79.478(7)	90.00	90.928(2)
β (°)	70.873(6)	90.744(4)	102.486(2)
γ (°)	79.682(6)	90.00	103.478(2)
V ($Å^3$)	950.73(16)	2326.5(2)	955.31(6)
Density (Mgm^{-3})	1.238	1.303	1.323
Abs. Coeff. (mm^{-1})	0.083	0.096	0.092
F(000)	380	968	404
Total no. of reflections	3416	4484	3424
Reflections, $I > 2\sigma(I)$	2790	2945	2943
Max. θ (°)	25.50	26.00	25.50
Ranges (h, k, l)	$-10 \le h \le 10$ $-12 \le k \le 12$ $-13 \le l \le 13$	$-18 \le h \le 19$ $-11 \le k \le 8$ $-19 \le l \le 18$	$-9 \le h \le 9$ $-11 \le k \le 11$ $-16 \le l \le 16$
Complete to 2θ (%)	96.3	98.0	96.2
Data/ Restraints/Parameters	3416/0/247	4484/0/316	3424/0/267
Goof (F^2)	1.053	0.706	0.926
R indices [$I > 2\sigma(I)$]	0.0518	0.0505	0.0420
R indices (all data)	0.0621	0.0723	0.0490

Compound No.	**4.2e**	**4.2f**	**4.2g**
Formulae	$C_{20}H_{23}ClN_2O_6$	$C_{40}H_{46}N_4O_8S$	$C_{20}H_{24}N_2O_6S$
CCDC No.	859879	859883	859881
Mol. wt.	422.85	742.87	420.47
Space group	$P2_1/c$	$R3_2$	P-1
a (Å)	15.309(3)	15.094(8)	8.0024(6)
b (Å)	8.9162(19)	15.094(8)	10.0959(8)
c (Å)	15.951(4)	48.91(5)	13.6380(10)
α (°)	90.00	90.00	81.435(4)
β (°)	110.878(13)	90.00	77.635(4)
γ (°)	90.00	120.00	70.938(4)
V ($Å^3$)	2034.4(7)	9650(12)	1013.53(13)
Density (Mgm^{-3})	1.381	1.150	1.378
Abs. Coeff. (mm^{-1})	0.227	0.127	0.200
F(000)	888	3546	3546
Total no. of reflections	3675	4002	3546
Reflections, $I > 2\sigma(I)$	1838	3309	2974
Max. θ (°)	25.50	25.48	25.25
Ranges (h, k, l)	$-18 \le h \le 17$ $-10 \le k \le 10$ $-19 \le l \le 18$	$-15 \le h \le 18$ $-18 \le k \le 18$ $-50 \le l \le 59$	$-9 \le h \le 9$ $-12 \le k \le 12$ $-16 \le l \le 14$
Complete to 2θ (%)	97.1	99.5	96.6

Data/ Restraints/Parameters	3675/0/279	4002/0/246	3546/0/277
Goof (F^2)	0.983	1.055	1.050
R indices [$I > 2\sigma(I)$]	0.0730	0.0741	0.0373
R indices (all data)	0.1557	0.0863	0.0457

Compound No.	**4.2h**	**4.2i**	**5.1**
Formulae	$C_{20}H_{25}BF_4N_2O_3$	$C_{20}H_{23}N_3O_5$	$C_{28}H_{31}O_8$
CCDC No.	859880	859882	804435
Mol. wt.	428.23	385.41	495.53
Space group	P-1	$P2_1/c$	$P2_1/c$
a (Å)	8.1285(5)	8.0447(12)	14.9498(13)
b (Å)	10.9801(7)	26.422(5)	14.8055(12)
c (Å)	11.9948(7)	11.2878(18)	12.5249(10)
α (°)	96.789(4)	90.00	90.00
β (°)	95.608(4)	126.488(10)	97.545(3)
γ (°)	99.124(4)	90.00	90.00
V ($Å^3$)	1042.17(11)	1929.0(6)	2748.3(4),
Density (Mgm^{-3})	1.365	1.327	1.198
Abs. Coeff. (mm^{-1})	0.114	0.097	0.088
F(000)	448	816	1052
Total no. of reflections	3700	3215	4960
Reflections, $I > 2\sigma(I)$	2552	1694	2689
Max. θ (°)	25.49	25.25	25.25
Ranges (h, k, l)	$-9 \le h \le 9$ $-12 \le k \le 12$ $-16 \le l \le 14$	$-9 \le h \le 9$ $-13 \le k \le 11$ $-14 \le l \le 14$	$-17 \le h \le 17$ $-17 \le k \le 17$ $-15 \le l \le 14$
Complete to 2θ (%)	95.0	92.0	99.7
Data/ Restraints/Parameters	3546/0/277	3215/0/266	4960/5/335
Goof (F^2)	0.928	1.083	1.224
R indices [$I > 2\sigma(I)$]	0.0635	0.1063	0.0819
R indices (all data)	0.0895	0.1774	0.1237

Compound No.	**5.3**	**5.1c**	**5.1d**
Formulae	$C_{27}H_{27}NO_2$	$C_{27}H_{36}Na_2O_{11}$	$C_{27}H_{30}K_2O_{11}$
CCDC No.	840829	851818	851819
Mol. wt.	493.50	582.54	608.71
Space group	$P2_1/n$	$P2_1/c$	$P2_1/c$
a (Å)	16.297(3)	17.6717(12)	17.4531(15)
b (Å)	9.222(2)	14.1935(9)	14.4853(15)
c (Å)	16.374(4)	11.5938(8)	11.8689(10)
α (°)	90.00	90.00	90.00
β (°)	94.019(15)	101.479(4)	78.186(4)
γ (°)	90.00	90.00	90.00
V ($Å^3$)	2454.8(9)	2849.8(3)	2937.1(4)
Density (Mgm^{-3})	1.335	1.358	1.377
Abs. Coeff. (mm^{-1})	0.099	0.129	0.380
F(000)	1040	1232	1272
Total no. of reflections	4427	5073	7250

Reflections, $I > 2\sigma(I)$	2439	3484	5475
Max. θ (°)	25.50	25.25	28.29
Ranges (h, k, l)	-16 ≤ h ≤ 19 -11 ≤ k ≤11 -19 ≤ l ≤ 19	-21≤ h ≤ 21 -17 ≤ k ≤17 -12 ≤ l ≤ 13	-23 ≤ h ≤ 23 -16 ≤ k ≤ 19 -15 ≤ l ≤ 15
Complete to 2θ (%)	97.00	98.60	99.50
Data/ Restraints/Parameters	4427/0/331	5073/3/396	7250//4/381
Goof (F^2)	1.040	1.227	1.027
R indices [$I > 2\sigma(I)$]	0.0658	0.0638	0.0957
R indices (all data)	0.1216	0.094	0.1154

Compound No.	**5.1e**	**5.2c**	**5.2d**
Formulae	$C_{54}H_{52}Cs_2O_{15}$	$C_{27}H_{35}FNa_2O_{11}$	$C_{27}H_{25}Cs_2FO_9$
CCDC No.	851821	931636	931637
Mol. wt.	1216.86	600.53	778.29
Space group	C2/c	$P2_1/a$	$P2_1/a$
a (Å)	31.862(3)	11.5752(7)	11.7311(7)
b (Å)	14.3653(14)	14.2375(8)	14.2417(9)
c (Å)	11.8638(12)	17.5742(15)	17.7909(11)
α (°)	90.00	90.00	90.00
β (°)	92.336	101.423(7)	92.802(6)
γ (°)	90.00	90.00	90.00
V ($Å^3$)	5425.7(9)	2838.9(3)	2968.8(3)
Density (Mgm^{-3})	1.490	1.400	1.741
Abs. Coeff. (mm^{-1})	1.409	0.137	2.510
F(000)	2464	1256	1512
Total no. of reflections	5340	5112	5357
Reflections, $I > 2\sigma(I)$	3149	2595	3424
Max. θ (°)	28.51	25.25	25.25
Ranges (h, k, l)	-39 ≤ h ≤ 39 -17 ≤ k ≤ 17 -14 ≤ l ≤ 14	-12 ≤ h ≤ 13 -17 ≤ k ≤ 15 -21 ≤ l ≤ 11	-10 ≤ h ≤ 14 -17 ≤ k ≤ 15 -21 ≤ l ≤ 13
Complete to 2θ (%)	99.90	99.60	99.90
Data/ Restraints/Parameters	5340/0/326	5112/9/400	5357/0/356
Goof (F^2)	1.178	1.105	1.068
R indices [$I > 2\sigma(I)$]	0.0556	0.0815	0.0701
R indices (all data)	0.1025	0.1506	0.1085

Compound No.	**5.3c**	**6.1a**	**6.2a**
Formulae	$C_{27}H_{27}K_2NO_{11}$	$C_{42}H_{41}CdN_3O_9$	$C_{37}H_{37}FN_2O_7Cd$
CCDC No.	851820	806671	941258
Mol. wt.	619.70	844.18	753.09
Space group	Pbca	$P2_1/c$	P-1
a (Å)	13.8855(4)	16.3357(5)	9.5955(6)
b (Å)	12.4867(3)	14.1196(5)	10.1247(7)
c (Å)	33.5892(10)	18.3475(6)	18.8961(12)
α (°)	90.00	90.00	79.787(4)
β (°)	90.00	104.841(2)	79.330(4)
γ (°)	90.00	90.00	71.632(4)

V (Å^3)	5823.8(3)	4090.7(2)	1698.15(19)
Density (Mgm^{-3})	1.414	1.371	1.481
Abs. Coeff. (mm^{-1})	0.385	0.591	0.700
F(000)	2576	1736	772
Total no. of reflections	7251	7341	6217
Reflections, $I > 2\sigma(I)$	5245	4341	4408
Max. θ (°)	28.34	25.25	25.50
Ranges (h, k, l)	-9 ≤ h ≤ 9 -13 ≤ k ≤ 11 -14 ≤ l ≤ 14	-19 ≤ h ≤ 19 -16≤ k ≤ 16 -22 ≤ l ≤ 22	-11 ≤ h ≤ 11 -12 ≤ k ≤ 12 -22 ≤ l ≤ 22
Complete to 2θ (%)	99.6	99.1	98.20
Data/ Restraints/Parameters	7251/2/382	7341/0/500	6217/ 2/ 445
Goof (F^2)	1.098	0.820	0.976
R indices [$I > 2\sigma(I)$]	0.0646	0.0366	0.0417
R indices (all data)	0.0882	0.0715	0.0690

Compound No.	**6.2b**	**6.2c**	**6.3a**
Formulae	$C_{68}H_{72}F_2N_2O_{14}S_2Cd_2$	$C_{86}H_{92}F_2N_6O_{16}Cd_2$	$C_{68}H_{74}Cd_2N_4O_{22}$
CCDC No.	941259	941260	837719
Mol. wt.	1468.20	1728.46	1524.11
Space group	P-1	P-1	$P2_1/c$
a (Å)	8.9073(5)	10.1146(4)	17.4571(11)
b (Å)	10.3960(5)	11.5411(4)	21.0538(12)
c (Å)	19.1286(9)	19.1631(6)	9.2040(5)
α (°)	92.139(4)	90.606(3)	90.00
β (°)	98.135(4)	101.112(3)	93.921(4)
γ (°)	109.480(4)	105.444(3)	90.00
V (Å^3)	1646.32(14)	2111.24(12)	3374.9(3)
Density (Mgm^{-3})	1.481	1.348	1.500
Abs. Coeff. (mm^{-1})	0.780	0.575	0.710
F(000)	752	878	1564
Total no. of reflections	6117	7833	5843
Reflections, $I > 2\sigma(I)$	4894	6763	3876
Max. θ (°)	25.50	25.50	25.50
Ranges (h, k, l)	-10 ≤ h ≤ 10 -11 ≤ k ≤ 12 -23 ≤ l ≤ 22	-12 ≤ h ≤ 11 -13 ≤ k ≤ 13 -22 ≤ l ≤ 23	-19 ≤ h ≤ 20 -24 ≤ k ≤ 25 -10 ≤ l ≤ 10
Complete to 2θ (%)	99.80	99.80	93.0
Data/ Restraints/Parameters	6117/0/412	7833/0/535	5843/0/440
Goof (F^2)	1.059	1.326	1.259
R indices [$I > 2\sigma(I)$]	0.0469	0.0407	0.0789
R indices (all data)	0.0654	0.0489	0.1242

Compound No.	**6.3b**	**6.3c**	**6.4a**
Formulae	$C_{74}H_{74}Cd_2N_6O_2$	$C_{86}H_{96}Hg_2N_{10}O_{20}$	$C_{74}H_{70}Cd_2N_6O_{26}$
CCDC No.	844623	837718	837730
Mol. wt.	1592.19	1990.91	1684.16
Space group	$P2_1/c$	P-1	P-1

a (Å)	12.5560(10)	9.7843(3)	11.7715(8)
b (Å)	25.231(2)	12.7257(4)	12.4713(9)
c (Å)	12.2248(10)	19.1614(6)	15.3045(11)
α (°)	90.00	90.829(2	80.416(3)
β (°)	101.953(4)	97.845(2)	80.098(3)
γ (°)	90.00	111.982(2)	67.749(3)
V ($Å^3$)	3788.8(5)	2186.08(12)	2035.8(2)
Density (Mgm^{-3})	1.396	1.512	1.374
Abs. Coeff. (mm^{-1})	0.635	3.582	0.600
F(000)	1632	1002	860
Total no. of reflections	9492	7501	7252
Reflections, $I > 2\sigma(I)$	6870	5716	6287
Max. θ (°)	28.48	25.50	25.50
Ranges (h, k, l)	$-16 \leq h \leq 16$ $-32 \leq k \leq 33$ $-15 \leq l \leq 16$	$-11 \leq h \leq 11$ $-15 \leq k \leq 15$ $-23 \leq l \leq 23$	$-14 \leq h \leq 14$ $-15 \leq k \leq 15$ $-18 \leq l \leq 18$
Complete to 2θ (%)	99.0	92.1	95.60
Data/ Restraints/Parameters	9492/0/460	7501/0/539	7252/0/491
Goof (F^2)	1.294	0.995	1.079
R indices [$I > 2\sigma(I)$]	0.0867	0.0341	0.0384
R indices (all data)	0.1088	0.0503	0.0449